DIGITAL IMAGES ASSESSMENT OF POSTERIOR CAPSULE OPACIFICATION

A Thesis submitted by

Haya M. AL-Farhan

For the degree of

Doctor of Philosophy

ADVISORS

Dr. C C Hull, Senior lecturer in clinical and visual optics, Department of Optometry and Visual Science, City University, London, UK.

Professor E G Woodward, Professor of Optometry and Visual Science, Department of Optometry and Visual Science, City University, London, UK.

Applied Vision Research Centre, City University, London, UK.

Table of Contents

List of Tables

List of Figures

Acknowledgements

I gratefully acknowledge my advisors Dr. Chris Hull and Professor Geoffrey Woodward. I would particularly like to thank Chris for his continuous assistance, enthusiasm, and expertise in various aspects of computer vision which without this project would never see the light. Also, Professor Geoffrey for his advice and vast knowledge particularly in clinical aspects which without this project would not be complete.

I also wish to thank all members of the academic and technical staff within the Optometry Department of City University.

I am very grateful to both Mr. Horgan and Dr. Hameed for their support, and giving me the opportunity to collect the project data through their clinics. I also wish to thank all members of the Royal Eye Unit at Kingston Hospital for their kindness and cooperation.

Finally, would like to thank my mother for her endless love, care and encouragement, and my father for giving me the freedom to pursue my dream. Also, I would like to thank all my family members for their support all the time.

Abstract

A digital imaging system has been developed for the objective assessment of severity and morphology of posterior capsule opacification (PCO). The system is based on a Nikon FS-2 photo slit-lamp and a Kodak DCS 100 digital camera system. The slit-lamp was used with conventional (forward) illumination and studies were carried out to determine the best combination of slit-lamp and camera parameters to optimize the images. These were found to be a slit beam width of 3.5mm, slit angle of 45°, film speed (ISO) of 1600 for the camera and 800 for the digital storage unit (DSU), exposure compensation 0, flash intensity 2 and a magnification of 25x. A fixation stimulus was developed since it was shown to decrease the variability of the images and reduce the possibility of unwanted reflexes affecting the area of interest. In all cases a central 3mm x 3mm area of the posterior capsule, centred on the pupil, was analysed. The image processing software used throughout the work was Image Pro+ v4.51 (Media Cybernetics, Silver Spring, MD).

For validating the system, subjects who had previously had uncomplicated cataract surgery were recruited from the Nd:YAG capsulotomy clinics of the Royal Eye Unit at Kingston. Intra-observer repeatability was assessed by taking 6 repeat images for each of 10 subjects. The coefficient of variation for total spectral power in the image, a measure of the severity of opacification, was 1.5%. Inter-observer repeatability was tested for 3 observers, an ophthalmologist, an optometrist and a non-clinician, by recording 2 images for each observer for each of 9 subjects. There was a 6 fold increase in the limits of agreement when the non-clinician was involved indicating that suitable training is required to use the system in a repeatable fashion.

Severity of opacification was measured by calculating the log of the total spectral power in the Fourier Transform image of the area of interest. Results on 45 eyes correlated well with subjective grading of PCO by an experienced ophthalmologist: Within the 3 morphological groups, fibrotic, mixed and pearl, correlation coefficients of 0.909, 0.864 and 0.713 were found, which were all statistically significant.

Morphological classification was carried out by developing a simple expert system. The rules in the knowledge base were derived from known histological features of PCO and clinically observed changes. The weighted kappa score for agreement between the objective classifier and an experienced ophthalmologist was 0.61 indicating a good level of agreement. However 14 out of 45 cases did not exhibit agreement. It may be possible with further work to improve the classification rules to reduce this number.

New methods have been presented for objectively measuring the severity and morphologically classifying PCO. The system developed in this work shows distinct potential for use within primary care environments since it uses techniques and instruments whose operation is familiar to all practitioners involved. The validation studies presented here demonstrate variability in the measurements that is largely in agreement with previously published systems.

Declaration

I grant the power of discretion to the University Librarian to allow this thesis to be copied in whole in part without further to me. This permission covers only single copies made for study purposes, subject to normal conditions of acknowledgement.

CHAPTER ONE

1. Introduction

The crystalline lens is the second transparent, avascular and refractive component in the eye. Its primary purpose is to focus an image on to the retina. The function of lens metabolism is to maintain transparency, which is essential to permit light to pass through the eye. However, the breakdown of lens crystalline, in part an age related process, leads to cataract formation which can be corrected with surgery.

During the last decade cataract surgery techniques and instruments have advanced rapidly. This has led to an improvement in the outcome of the surgery; it is now considered a safe procedure used to restore patients' vision and consequently improve their quality of life. Extracapsular cataract extraction (ECCE) with continuous curvilinear capsulorhexis (CCC) and phacoemulsification with CCC are the commonly used surgical techniques with phacoemulsification the method of choice. In the UK over 200,000 cataract operations are performed annually (Johnston, 2003). However, even with the use of advanced technology, posterior capsule opacification (PCO), or secondary cataract, remains a major complication following cataract surgery. PCO is caused by lens epithelial cell (LEC) migration and proliferation across the posterior capsule, ultimately blocking the visual axis and causing a reduction in vision. Twenty percent of cases occur within five years following cataract surgery (http://www.doh.gov.uk). The current treatment for PCO is Nd:YAG laser capsulotomy, which can restore visual function.

However, the high prevalence of PCO and the concomitant cost of Nd:YAG laser capsulotomy have led researchers to find ways of inhibiting PCO. These have included physical inhibition using techniques such as capsule polishing and modifications to the intraocular lens (fixation methods, materials, size, and surface properties) and pharmacological methods. These methods will be reviewed in chapter 3.

Currently optometrists are reliant on subjective techniques to assess PCO. These include visual acuity (Tan et al. 1998), slit lamp grading (Sellman & Lindstrom 1988, Kruger et al 2000) or fundus visibility (Prajna et al. 2000). However, these techniques are, on the whole, considered to be unreliable (Chylack et al. 1987, Tetz et al. 1997, Aslam et al. 2002, ASCRS meeting 2001). Several attempts have been made to develop systems that quantify PCO, either objectively or with the help of user intervention. However, the assessment and classification of PCO is usually an outpatient procedure performed by general practitioners and optometrists, who then refer the patient for treatment. The main drawback of these systems is that they use specialised techniques or equipment, such as purpose designed retroillumination cameras, thus these systems are not really appropriate for use in a primary care setting.

The aim of this study was therefore to develop an objective digital imaging system that can accurately quantify the severity and morphologically classify PCO. The system should not require specialised instrumentation or sophisticated techniques to analyse the images. We believe that such a system would help general practitioners (GP) and optometrists to document and objectively quantify the severity of PCO. This in turn will facilitate the decision of referral for a YAG capsulotomy procedure. Results could be used in combination with a database containing patient case history such as

cataract extraction procedure and type of IOLs implanted, to study either the effect of various surgical techniques or IOL materials and designs on the prevalence of PCO.

CHAPTER TWO

2. Crystalline lens

2.1 Anatomy of the crystalline lens

The lens is one of the principal refractive components of the eye. It is a transparent, elastic, avascular, elliptical, biconvex body surrounded completely by a transparent capsule. The lens lies between the iris and the vitreous. Anteriorly it contacts with the free border of the iris, yet retreats from the periphery to form the posterior chamber. Posteriorly it touches the hyaloid fossa of the vitreous body. The posterior lens pole is more convex than the anterior lens pole. The area where the anterior surface meets the posterior surface is known as the equator (equator lentis). Laterally, the equatorial area of the lens extends into the posterior chamber and is attached by the zonules to the ciliary epithelium. The ciliary epithelium functions are to hold the lens suspended between the iris and the vitreous, and through contraction the ciliary epithelium allows the shape of the lens to change and focus images on the retina (Bron, Tripathi, 1997).

The equatorial diameter of the adult lens is 9-10mm. The lens axial sagittal width is 3.5-4.0mm at birth, 4mm at 40 years and at extreme old age increases slowly to 4.75-5.0. At birth the accommodative power is 15-16 diopters decreasing to 7.5 diopters at about 25 years and to 2 diopters at 50 years. The crystalline lens consists of three main structures: the lens capsule, the lens epithelium, and the lens fibres (Bron, Tripathi, 1997).

2.1.2 The lens capsule

The lens capsule is formed by the accumulation of thin hyaline at the edge of the lens. Later, it develops and progressively increases in thickness such that by the fifth month the capsule completely covers the entire lens. It is transparent, homogeneous, highly elastic, and a PAS-positive membrane. Its major functions are to reshape the lens during accommodation and to act as a metabolic barrier (Bron, Tripathi, 1997, Fisher, 1971) has reported that 90% of the age related loss in accommodation is due to changes in elasticity of the capsule. Weale (1982) has reported that it may be due to lamellae loss. Several studies have shown that the capsule is freely permeable to water ions and other small molecules and offers a barrier to protein molecules the size of albumin and haemoglobin (Fisher, 1969, Hockwin et al. 1973).

The lens capsule is the thickest basement membrane in the body, with the anterior portion thicker than the posterior portion (Bron, Tripathi, 1997). Fisher (1969) found that the anterior lens capsule increases in thickness with age, although there is little change at the posterior pole. Rafferty and Goosens, (1978) reported that the lens capsule increase in thickness by deposition of new lamellae either on the inside of new lamella, or added at the inner surface and pushed through towards the outer surface. The capsule is rich in type IV collagen and also contains types I and III collagens, and a number of extracellular matrix components such as laminin, fibronectin, heparin sulphate, proteoglycan and entactin. The zonular fibres insert on the outermost surface of the equatorial lens capsule. The posterior border of insertion of the zonular fibres onto the lens coincides with the insertion of the anterior face of the vitreous. Contraction of the ciliary muscle during accommodation results in relaxation of the zonular fibres, the lens capsule

relaxes and the lens becomes more spherical increasing its refractive power (Bron, Tripathi, 1997).

2.1.3 The lens epithelium

The lens epithelium is made up of a single row of cuboidal cells. These cells overlay the anterior surface of the lens and continue outwards to the equator. There are no epithelial cells on the posterior surface because the posterior epithelial cells of the embryonic lens are involved in the formation of the primary lens fibres that lie in the centre of the lens nucleus. The lens epithelium is divided biologically into three regions: The central region consists of stable polygonal epithelial cells, their nuclei rounded and located slightly apically as seen in figure (2.1). The cell numbers decline slowly with age (Bron, Tripathi, 1997). These cells have minimal mitotic activity, yet when there is inflammation or trauma, the primary response of the anterior epithelial cells is to proliferate and form fibrous tissue by undergoing a fibrous metaplasia (Apple et al. 1992). The intermediate region is peripheral to the central region. Its epithelial cells are small, more cylindrical with central nuclei and occasionally mitose. The germinative region is the most peripheral. The cell nuclei are flattened and lie in the plane of the cell axis. The cells of this region are very active and proliferate rapidly, since it is rich with enzymes and has extensive protein metabolism. This region is therefore responsible not only for continuously producing new lens fibres, but also, for the migration of the new cells posteriorly to become lens fibres. Some cells may migrate forwards into the intermediate region (Bron, Tripathi, 1997).

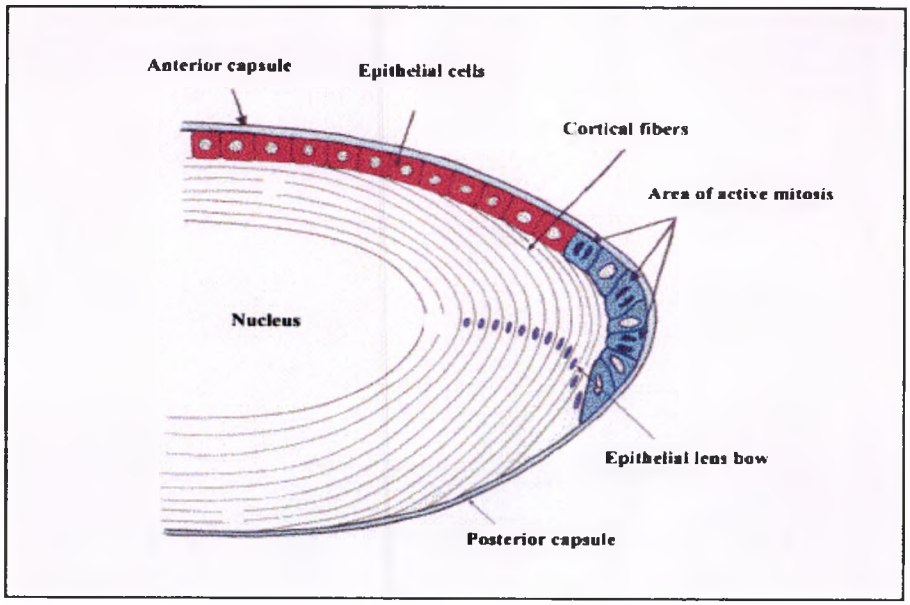

Figure 2.1 Major components of the adult crystalline lens: the lens capsule, the lens epithelium, and the lens fibres. The figure also shows the types of lens cells and their location that are responsible for posterior capsule opacification formation (Apple et al. 2000a).

2.1.4 The lens fibres

The lens fibres are strap-like or spindle-shaped cells that arch over the lens in concentric layers from front to back, in which the outermost represent the cortex and the innermost represent the nucleus of the lens. In the adult lens, the lens fibres' average width is 10-12 μm and average thickness 1.5-2 μm. Kuszak et al. (1989) reported that the asymmetrical shape of the lens in sagittal section and the greater thickness of the anterior cortex are due to thin posterior lens fibres. The tips of the lens fibres meet those of other fibres to form sutures; this arrangement becomes increasingly complex with the growth of the lens (Bron, Tripathi, 1997).

2.2 Cataract

Cataract is a major and frequent disorder of the lens because it is predominantly an age related disease. This term describes any localized or complete lens opacification. It can be classified as either primary such as senile cataract (age related), or secondary such as congenital, traumatic, metabolic (diabetes mellitus) or nutritional defects, radiation or toxic cataract (Apple et al. 1989). In fact, according to the World Health Organization, cataract is the main cause of global blindness. Age related cataract accounts for about 16 million cases of blind people around the world, in which Africa and Asia represent approximately half of all blindness. This could be due to an increase in population and life expectancy, and inadequate eye care services (WHO, 1997).

The prevalence of cataract according to the Department of Health data in the United Kingdom (UK) for the period 1998-2002 ranges from 22% to 29% with age related cataract accounting for approximately 92% of all cataract types. Comparing the prevalence of cataract for the four age groups (0-14, 15-59, 60-74, and age 75+) for the period 1998-2002 (fig. 2.2) shows an increase in the prevalence of cataract especially for the age groups 15-59, 60-74 and age 75+. The increase in the aging population in UK, and in the world in general, is considered one of the main causes for the increase in blindness in the world (Brian and Taylor 2001). In contrast, the low prevalence in the younger group 0-14 could be explained since the main causes of cataract in this group are congenital or trauma.

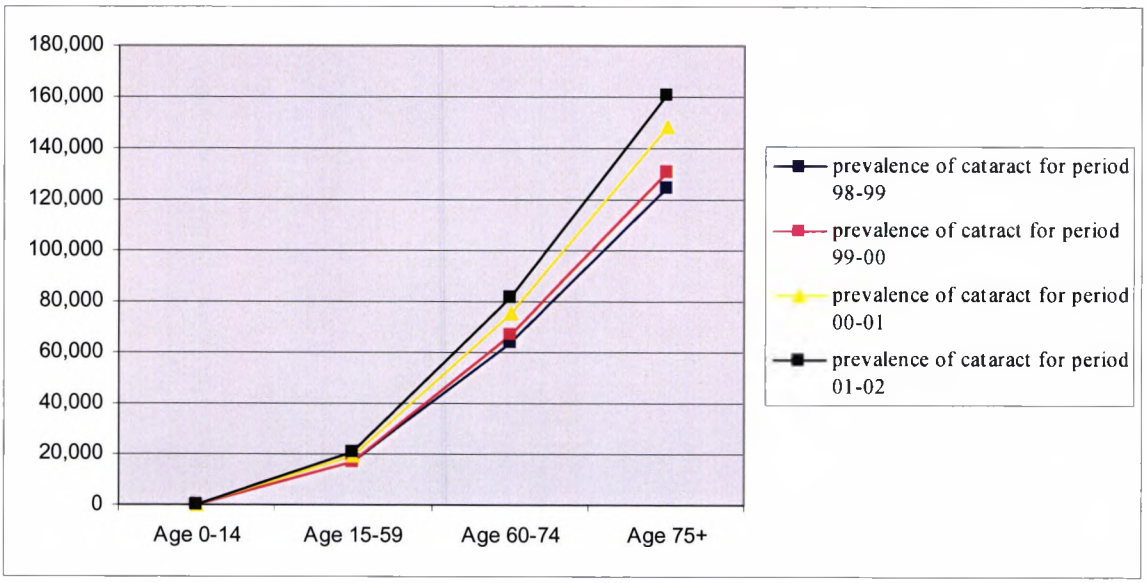

Figure 2.2 Prevalence of cataract in the UK for the period between 1998-2002.

The risk factors that have been identified in the pathogenesis of age related cataract are genetic factors (Bloemendal et al. 1996), diabetes mellitus (prevalence of cataract is increased three to four times with diabetic patients under the age of 60 years compared with non diabetic patients (Caird, 1973, Ederer et al. 1981, Klein et al. 1998), smoking (two to three fold increased risk of developing cataract (West et al. 1995, Hiller et al. 1997)), ultraviolet (UV) radiation exposure (Hollows & Moran, 1981, Burton et al. 1997), and medication such as thyroid hormones (AREDS, 2001a).

Senile cataract is subdivided morphologically into three types: cortical, nuclear and subcapsular (anterior or posterior). Cortical cataract (soft cataract) involves the anterior and posterior or equatorial cortex. It is clinically recognized as a cuneiform shaped opacity in the periphery of the cortex, punctate perinuclear opacities in the cortex or cupuliform shaped opacity in the posterior cortex. The histological changes that may occur in

cortical cataract are clefts that consist of diffuse water or eosinophilic material representing altered cell proteins. The cell fragments are pieces of broken-up lens cortical cells and Morgagnian globules (small or large fragments of cortical cells), crystals of calcium oxalate, cholesterol, and cystine that may be deposited in long standing cataract (Christmas tree cataract), and calcium salt that may impregnate long standing cataract (cataract calcarea). A break in the anterior capsule may lead to cortical material trapped in the equatorial region of the lens forming a Soemmering's ring cataract (Yanoff et al. 1996).

Nuclear cataract (hard cataract) is caused by increasing density of the lens due to accumulation of lens cells on lens cells, breakdown of intercellular membranes within the lens nucleus, and dehydration with accumulation of pigment. Accumulation of pigment in the nucleus leads to a variation in the lens colour from light yellow through darker shades of yellow and even in some cases to dark brown (cataract brunescens) and rarely black (cataract nigra). Posterior subcapsular cataract lies in front of the posterior capsule and is associated with abnormal behaviour of the lens epithelial cells that proliferate and migrate posteriorly reaching the posterior pole of the lens. Anterior subcapsular cataract lies directly under the lens capsule and is associated with fibrous metaplasia of the anterior epithelial cells of the lens (Yanoff et al. 1996).

2.3 Modern Cataract Surgery

2.3.1 Introduction

There are several surgical techniques used to extract cataract yet all fall under three main categories: intracapsular cataract extraction (ICCE), extracapsular cataract extraction (ECCE: automated or manual), and phacoemulsification (phaco). Intracapsular cataract extraction was developed by Henry Smith in 1903. Since that time ICCE has been through many phases of development (Smith, 1926). Until 1980 intracapsular cataract extraction was the commonest method used to extract cataract. It involved creating a large 180 degree incision and removing the entire lens and capsule. A cryoprobe is used to freeze tissue of the lens, permitting removal of the entire lens by squeezing it out of the eye by pressure on the limbus or sclera after the appropriate limbal incision. For instance, the best-known manoeuvre that was introduced by Smith is a muscle hook used to apply pressure at the inferior limbus to expel the cataractous lens through a superior incision; later other instruments were used to apply suitable pressure such as spoons and forceps. The main undeniable advantage of ICCE is the complete absence of posterior capsule opacification (Natchiar, 1998); yet one of the major disadvantages of ICCE is unsatisfactory visual results due to spectacle correction. ICCE is still performed these days especially in rural areas with aphakic spectacles prescribed mostly due to financial reasons (Apple et al. 2000b). In industrial and developing countries ICCE is performed under certain circumstances such as crystalline lens dislocation into the anterior chamber or the risk of phacodonesis. The complications that are associated with ICCE technique were the risk of capsule rupture and vitreous loss, retinal detachment (RD), cystoid macular edema CME), and aphakic bullous keratopathy (ABK)

(Albert et al. 1999).

In 1748 Jacques Daviel published an article explaining a new method to extract cataract which became the foundation for modern ECCE. ECCE involves removing the lens, leaving behind the posterior capsular bag (Daviel, 1967). Between the period 1977-2000 the ECCE technique went through several modifications such as (1) the use of viscoelastic to create or maintain space in the anterior chamber and capsular bag or dispersive viscoelastic to isolate particular intraocular areas such as the corneal endothelium, capsular tear, or a prolapsing iris, (2) continuous curvilinear capsulorhexis to reduce radial tears and increase the stability of IOL haptics, (3) the introduction of hydrodissection to improve cortical clean-up and (4) small incision (Apple et al. 2000c).

Kelman (1967) introduced the phacoemulsification technique, which involves removing the nucleus by emulsifying it with ultrasound. Since then many modifications have taken place to improve phaco surgical instrumentation and surgical techniques such as "divide and conquer" or "phaco chop". These help to reduce the time of surgery thus decreasing trauma. In addition incision construction can achieve small size self sealing wounds (Apple et al. 2000c).

2.3.2 Anterior capsulotomy techniques

Performing an anterior capsulotomy opening is a very important step that facilitates nucleus and cortex removal for uncomplicated ECCE or phacoemulsification. A poor capsulotomy may result in capsule rupture and vitreous loss possibly leading to retinal detachment. There are three major anterior capsulotomy techniques: In the can-opener technique a series of zig-zag incisions are connected to create a large, central opening approximately 5 to 6mm in diameter as seen in figure (2.3.A). This technique is easy to learn and perform on all types of cataract including hypermature ones, but tends to produce numerous radial tears emanating from the incisions that compromise the capsule integrity (Jaffe et al. 1997). This makes hydrodissection difficult to perform and less effective because the force of fluid injected may cause extension of radial tears. The radial tears also increase the prevalence of asymmetrical fixation (Apple et al. 1992). An attempt was made to minimize the ragged edge of the can-opener capsulotomy technique by prolapsing the nucleus into the iris plane for subsequent phacoemulsification. However, the use of a high-energy phacoemulsification tip in the iris plane carried greater risk of corneal endothelial damage and iris trauma.

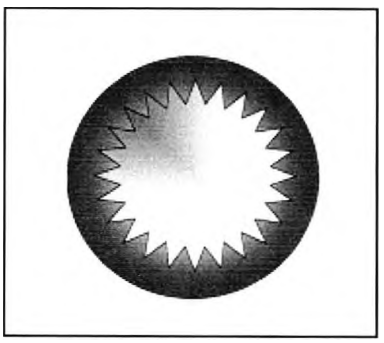

Figure 2.3.A The can-opener capsulotomy that creates zig-zag edged circular opening (Apple et al. 2000c).

Envelope or linear capsulotomy was a very well known technique in the 1980s. It involves creating a horizontal, slightly curved capsulotomy slit as seen in figure (2.3.B). This technique maintains the capsule integrity, protects the corneal epithelium, and facilitates removal of the lens substance and subsequent posterior chamber intraocular lens implantation (Assia et al. 1991). However, experimental studies reported that the envelope capsulotomy technique was associated with IOL dislocation in postoperative period due to marked asymmetry of the capsule and high occurrence of radial anterior capsule tears (Caballero et al. 1995).

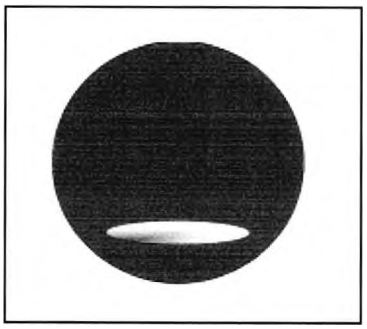

Figure 2.3.B The envelope capsulotomy (Apple et al. 2000c).

Gimble and Neuhann (1990) introduced a new technique known as the continuous curvilinear capsulorhexis technique (CCC). It involves tearing the lens anterior capsule with bent forceps to create a smooth edged circular opening without serrations leaving the bag intact as seen in figure (2.3.C). It is difficult to perform this technique with a heavily fibrosed and shrunken capsule as in the case of congenital or traumatic cataract, yet this obstacle could be overcome by performing a small size rhexis then use the forceps to bring the peripheral extension of the rhexis toward the centre.

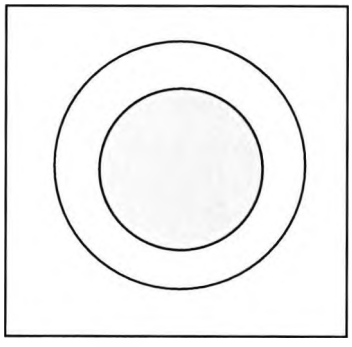

Figure 2.3.C The most commonly used continuous curvilinear capsulotomy that creates a smooth edged circular opening (Apple et al. 2000c).

In the past it was difficult to distinguish the anterior capsule from the underlying cortex especially in the case of mature white cataract combined with a pigmented fundus or vitreous diseases where the usual red reflex is absent. This increases the risk of radial tear toward the lens equator and subsequent posterior capsule rupture and vitreous loss. Yet, recently with the introduction of various capsule dyes such as fluorescein, indocyanine green and trypan blue to improve visualization of the anterior lens capsule (fig. 2.4), a CCC can be safely performed (Pandey et al. 2000). Advantages of the continuous curvilinear capsulorhexis technique are no radial tears, maintaining capsule integrity thus hydrodissection is more effective and the capsulorhexis edge is extremely smooth and resistant. The reported prevalence of posterior capsule rupture with vitreous loss with can-opener, linear, and continuous curvilinear techniques was 4.1%, 4.3%, and 2.1% respectively (Chitkara et al. 1997).

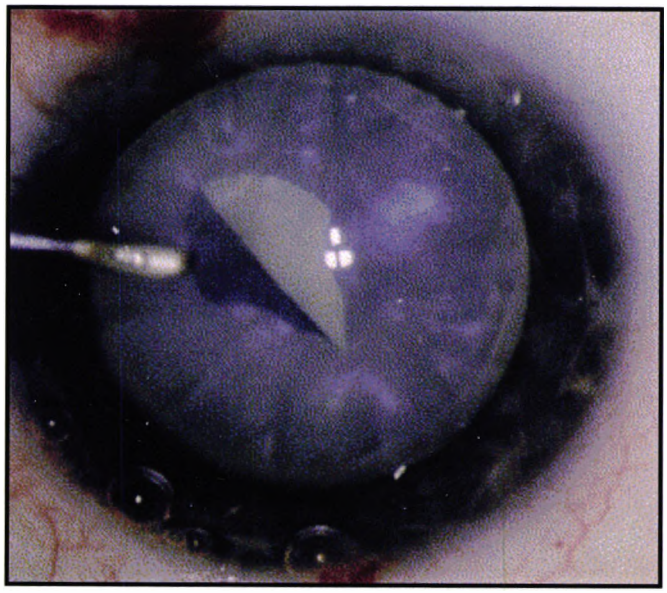

Figure 2.4 Trypan blue staining of the anterior capsule used to facilitate visualization with a dense white cataract (Pandey et al. 2000).

The CCC technique is compatible with other advanced surgical techniques, such as small incision surgery, in the bag implantation of foldable IOLs, and hydrodissection all of which are used in phacoemulsification or ECCE. Landau et al. (1999) concluded that phacoemulsification with continuous curvilinear capsulorhexis is a more reliable technique than ECCE with linear capsulotomy. However, the CCC technique is associated with a number of complications such as retention of large numbers of the anterior lens epithelial cells resulting in PCO, optic decentration or excessive distortion of loops, and Soemmering's ring (Masket et al. 1993a, Gillies et al. 1998).

2.3.3 Hydrodissection technique

The hydrodissection technique reached full potential with the introduction of the CCC which provides a stable and intact capsule. It is an essential procedure performed during ECCE and phacoemulsification techniques. Hydrodissection's main functions are to facilitate the removal of the lens substance through a small incision without damaging the posterior capsule and to reduce the time of the operation, hence enhancing the overall safety of cataract surgery. Another long term advantage of efficient removal of the cortex and LECs is reduction of PCO prevalence (Peng et al. 2000). Hydrodissection involves a 26 or 27 gauge polished round cannula and balanced salt solution injected under the anterior capsular rim until a fluid wave is seen to pass beneath the entire width of the nucleus. This procedure is continued until the three distinct stages are completed: hydrodelineation to free the nucleus from the epinucleus, classic hydrodissection to separate the epinucleus from the cortex, and cortical cleavage to separate the cortex from the lens capsule (Apple et al. 1992, Gimbel et al. 1994).

2.3.4 Extracapsular cataract extraction

Extracapsular cataract extraction is subdivided into two basic types: manual or automated. Manual ECCE is mainly performed without expensive machinery and is used only in some rural areas of Asia. Automatic ECCE involves nuclear extraction followed by removal of lens substance by irrigation/aspiration. This technique provides a high degree of visual rehabilitation with intraocular lens implantation and is mainly used in developed countries (Jaffe et al. 1997, Apple et al. 2000c).

There are various ways to perform extracapsular cataract extraction depending on the patient's eye, medical conditions and the surgeon's preference. However, ECCE can be divided into five main steps: First, the incision size and location is chosen according to the size of the removed nucleus and implanted IOL. For example, implanting a rigid IOL requires a larger incision (e.g.11mm), than that required for a foldable IOL (e.g.3.2mm). The most recent development is a self sealing incision that can be left without sutures. However the incision must not exceed certain dimensions. For instance, scleral incision; the wound must not exceed 2mm in length, and a corneal incision must not exceed 4mm or 5mm in length.

The second step is to perform an anterior capsule capsulotomy in order to facilitate nucleus and cortex removal. Nowadays, the most frequently used technique is CCC. The third step involves nucleus extraction which can be achieved by various techniques, for example, small incision intracapsular washout with hydrosonic hydrodelineation technique. In this case balanced salt solution is hydrosonically injected into the nucleus causing the nucleus to fracture into small pieces, followed by washout of the eye with a special irrigation gutter spatula. Alternatively manual expression where the nucleus is expressed either with pressure superiorly just behind the incision site or within the limbus inferiorly can be used. The fourth step is removal of the epinucleus and cortex of the lens. First, the epinucleus needs to be removed either by irrigation into the anterior chamber forcing the epinucleus out through the incision, or by aspirating the epinucleus with a cannula through an incision which is at least 4mm. This is then followed by cortex removal through the automated irrigation-aspiration system. The final stage is implantation of an intraocular lens, which will differ depending on the IOL material. For example, a rigid IOL such as PMMA is grasped with insertion forceps as seen in figure (2.5.A). First generation foldable IOLs are folded

and inserted with special forceps in the lens capsule as seen in figure (2.5.B). The new generation of foldable the IOLs are inserted in the lens capsule by a cartridge injector system as seen in figure (2.5.C). The advantages of the cartridge injector system are sterility, ease of folding, insertion, and implantation of IOL through a smaller incision. For example, an IOL with a 6mm optic and foldable PMMA haptics can be implanted through a 3.5mm incision.

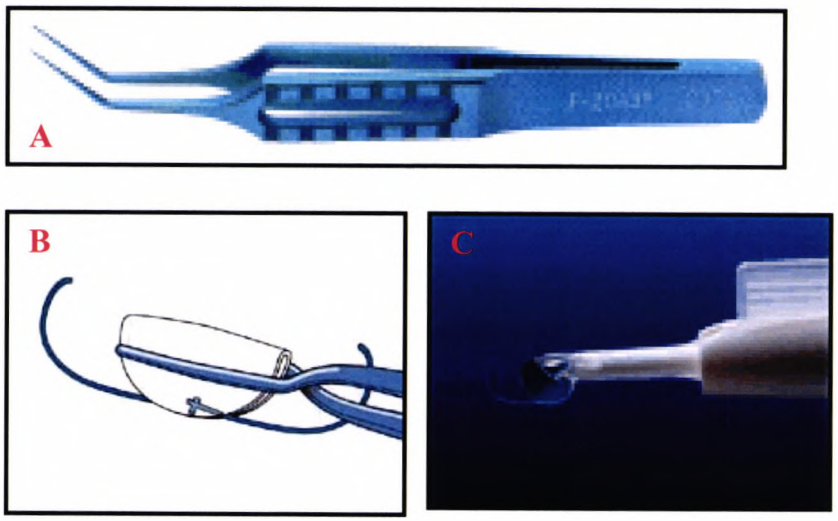

Figure 2.5 (A) The forceps used for rigid IOL, (B) the forceps were used before to fold and insert a foldable IOL, and (C) a cartridge injector system developed for the new generation of foldable IOL used to insert a foldable IOL into the lens capsule (http://www.ophtec.com).

2.3.5 Phacoemuslification

Nowadays, phacoemulsification is the most frequently used technique, especially with the recent development of surgical instruments that allow cataract removal through small incisions. There has been a consequent escalation in the development of foldable intraocular lenses that make it possible to implant a 6mm optic through a 3mm incision (Shepherd et al. 1994). The phacoemulsification system consists of two main components: an ultrasound energy system used to emulsify the nucleus, and an irrigation/aspiration system used to remove the emulsified part of the nucleus through a small incision (e.g. 2.8mm). This circuit is supplied by an elevated irrigating bottle that provides fluid volume and pressure to maintain the anterior chamber hydrodynamically and hydrostatically. Phacoemulsification can be either performed in the anterior chamber or the posterior chamber. In the former case it is less likely cause rupture of the posterior capsule but can cause endothelial cell loss and nuclear prolapse into the anterior chamber. Phacoemulsification in posterior chamber is less likely to cause endothelial cell loss (Jaffe et al. 1997).

Basically, the phacoemulsification technique is performed after opening the anterior capsule with a continuous curvilinear capsulorhexis (CCC). The best anterior capsule opening diameter is about 4.5 to 5mm. Hydrodissection is performed to break adhesion between the lens nucleus and epinucleus and the cortex, allowing the lens nucleus to freely rotate within the capsule. This facilitates removal of the lens nucleus using one of a variety of techniques. For example "crater divide and conquer" involves forming a large central crater in the nucleus, leaving a dense peripheral rim to fracture into multiple sections that are then emulsified one by one (Jaffe et al. 1997). Alternatively, in the phaco chop technique, the phaco tip is

buried into the nucleus superiorly and a chopper is introduced into the eye through a side port incision and is buried into the nucleus at 6 o'clock position. The chopper is then pulled towards the phaco tip, which holds the nucleus in place. In spite of the approaches used, the main goal is to minimize phacoemulsification power, time, and intraocular manipulation. This helps to reduce corneal endothelial cell loss and maintain lens capsule integrity. Following the removal of the lens nucleus the cortex often lines the inner surface of the lens capsule. The cortex is removed by engaging the free end of the cortical sheet under the anterior capsule with moderate levels of vacuum and peeling the cortex anteriorly to posteriorly as the I/A tip is moved toward the centre of the pupil. To improve further the surgical result of cataract extraction a capsular polishing is performed. It is involves using a manual scratcher instrument to loosen cortical remnants from the posterior capsule.

There is growing evidence from the literature that the phacoemulsification technique is taking over from ECCE. For example, (Leaming 1986, 1998), reported that the use of phacoemulsification has increased from 12% to 97% between 1985 and 1997. In the United Kingdom, (Courtney 1992) conducted a prospective cross-sectional survey to access delivery and outcome of cataract surgery for age related cataract within the NHS hospitals in the United Kingdom. He reported that the prevalence of performed conventional ECCE, ICCE, and phacoemulsification was 92%, 4%, and 4% respectively. In 1997 Desai et al. performed a survey of over 100 NHS hospitals in the United Kingdom to collect routine clinical information on the outcomes of cataract surgery. They found that the numbers of performed ECCE and phacoemulsification procedures were 23% and 77% respectively (Desai et al. 1999). In addition, the analysis of Department of Health data for NHS hospitals in the United Kingdom over

the period between 1998 to 2002 showed that the numbers of phacoemulsification and (ICCE + ECCE) procedures were 81.5% and 18.5% for the year 1998-1999 respectively, 88.9% and 11.1% for the year 1999-2000, 93.5% and 6.5%, for the year 2000-2001, and 95.1% and 4.9% for the year 2000-2002 respectively. This shows that phacoemulsification is the primary technique used in the UK for cataract extraction and eclipses other types of cataract surgery (fig. 2.6). It appears that ECCE & ICCE are used only under certain medical conditions.

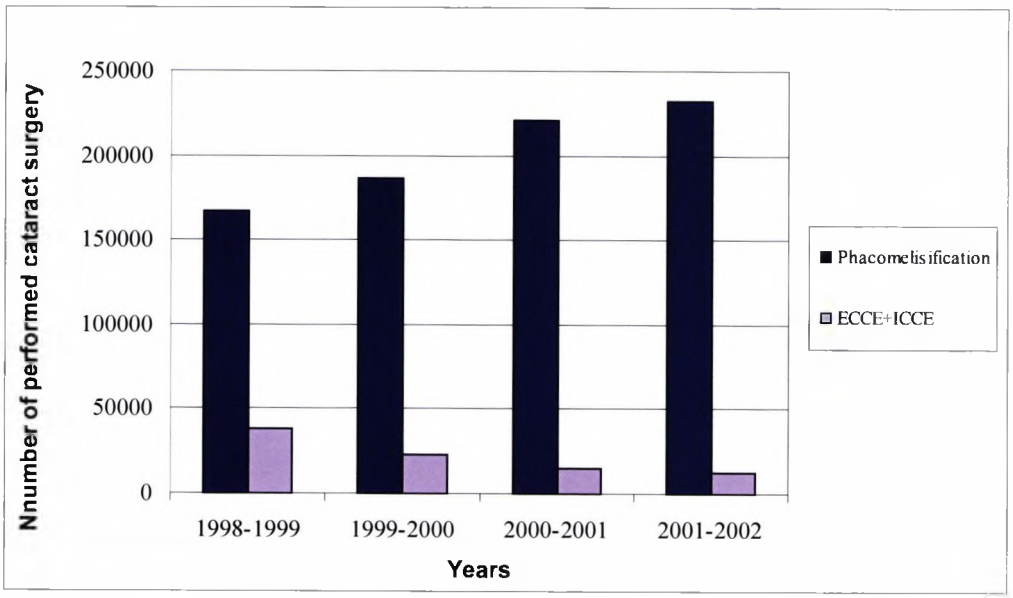

Figure 2.6 Phacoemulsification and other cataract extraction surgery (ECCE + ICCE) performed in NHS hospitals for period between 1998-1999, 1999-2000, 2000-2001 and 2000-2002.

Figure (2.7) shows the numbers of phacoemulsification and other cataract surgery (ECCE + ICCE) procedures performed for four age groups for the past four years. It reveals an increasing use of phacoemulsification and a concomitant decrease in other types of cataract surgery. This means that phacoemulsification is also considered to be a safe and reliable procedure to extract cataract for younger patients, a finding consistent with other studies (Apple et al. 2000c, Yun & Shi 2001, O'Keefe et al. 2000).

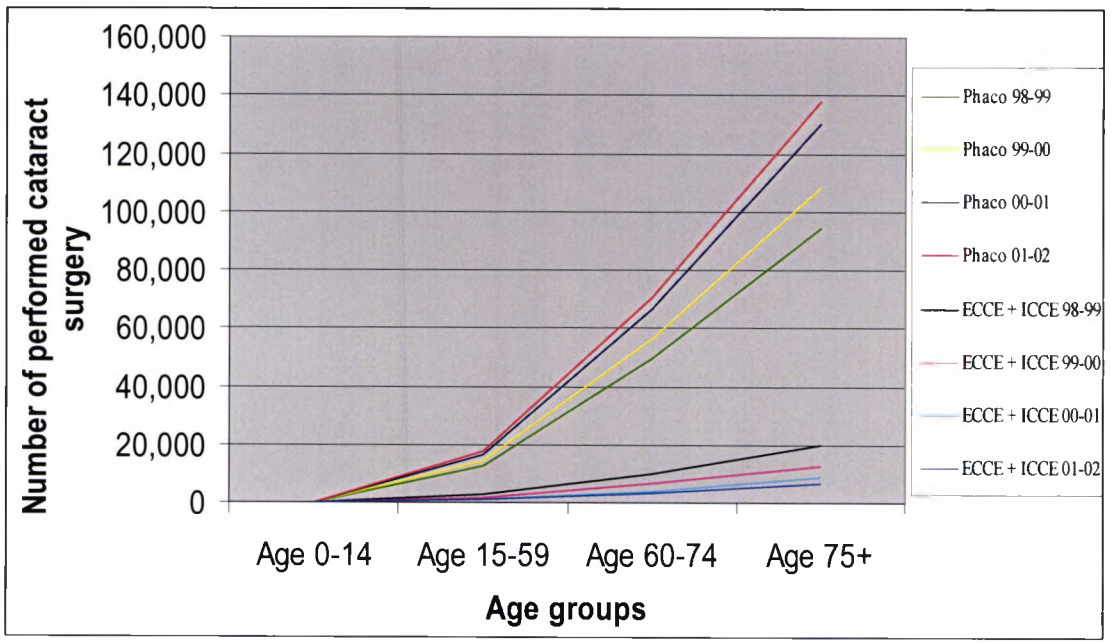

Figure 2.7 Trends in cataract surgery within the UK for the period 1998-1999 to 2000-2002.

The trend is not surprising due to the advantages of the phaco technique over ECCE. This includes the cost of performing phacoemulsification surgery which is less than ECCE (Minassian et al. 2001), small incision size (e.g. 1.4mm to 3.4mm) that eradicates large incision related complications, less tissue damage, less induced astigmatism (Drews et al.

2000, He et al. 2000), less inflammation (Laurell et al. 1997) and reduced overall time of the surgery decreasing the trauma (Dowler et al. 2000). ECCE is now usually only performed under certain conditions such as for very dense mature cataract and zonular weakness to reduce the risk of lens dislocation, capsule rupture and vitreous loss. However, there are some disadvantages that prevent phacoemulsification from spreading world wide. The technology used with phaco requires training; the cost of the machinery used for phaco is greater than for ECCE and proper maintenance of the phaco system is required to prevent complications such as thermal wound injury (Linebarger et al. 1999).

2.3.6 Methods used for Phakic corrections

The removal of the lens induces hypermetropia and to restore useful vision, there are four methods of correction: spectacle correction, contact lenses, intraocular lens implantation, and refractive corneal surgery. Table 2.1 summarizes the advantages and disadvantages of these methods (Apple et al 2000d & g).

Type of corrections	Advantages	Disadvantages
Spectacle	1. Simple to dispense and adjustable	1. Heavy lenses 2. Unsatisfactory visual outcome due to: - Not suitable for unilateral aphakic subjects (causes diplopia) - The spectacle lens is far in front of the nodal Point of the eye induces 25% magnification. - Limited visual field and form physiological ring scotoma
Contact lens	1. Eliminates disadvantages of spectacles	1. Difficult to wear especially by elderly or bilateral aphakic subjects 2. Causes infection and corneal vascularization 3. Requires regular sterilization 4. In certain conditions contact lenses are not suitable
Intraocular lens implantation	1. Best way to correct aphakia 2. Permits restoration of visual functions: 3. Full visual field and minimum optical aberration	Required advanced surgical techniques, induced astigmatism, corneal endothelial damage
Refractive corneal surgery such as: keratomileusis (LASIK), photorefractive keratectomy (PRK), laser subepithelial keratomileusis (LASEK)	1. Mostly for subject with very high myopia	1. There is no potential reversibility or adjustability in corneorefractive procedures 2. Expensive 3. Complications such as ectasia, haze, diffuse lamella keratitis, regression, or even infection

Table 2.1 The advantages and disadvantages of the four methods used for correcting hypermetropia following cataract extraction surgery.

2.4 Intraocular lens

2.4.1 History of the intraocular lens

The intraocular lens was first used by a British ophthalmologist, Harold Ridley, at St Thomas' hospital in 1949. Ridley implanted a disc shaped lens made of polymethylmethacrylate (PMMA) with a rimmed edge, which was placed into the capsular sac after extracapsular cataract extraction. However, this lens was large, heavy (106mg) and caused many complications such as iritis due to residual lens material in the eye or inadequate removal of implant sterilizing solution. Other complications, included occlusion of the pupil by a dense inflammatory membrane due to badly finished IOLs, posterior capsule opacification especially in young patients, secondary glaucoma, iris atrophy caused by pressure exerted by the PMMA optic, and IOL dislocation in a large number of cases. Therefore, it became necessary to design a different shape of lens (Ridley, 1956).

The second generation of intraocular lenses was first introduced and designed by Baron in 1952 and were all supported in the anterior chamber to minimize the risk of dislocation. In addition, the IOL could be implanted after ICCE and extracapsular cataract extraction. However, the major disadvantage of the anterior chamber lens was corneal decompensation; therefore they failed to find wide favour (Apple et al. 2000d).

The third generation of IOL introduced by Binkhorst, was supported by the stroma of the iris and known as the `Binkhorst clip lens` (Binkhorst 1959). It was intended to overcome the main complications of the first and second generations of IOLs. However, this lens caused atrophy and erosion of ocular tissue, corneal decompensation, oedema and pseudophakic bullous keratopathy, cystoid macular edema (CME), inflammation, uveitis-glaucoma-hyphema (UGH) syndrome, cellular proliferative reaction, subluxation or dislocation, and complications related to biomaterials (nylon and metal loops).

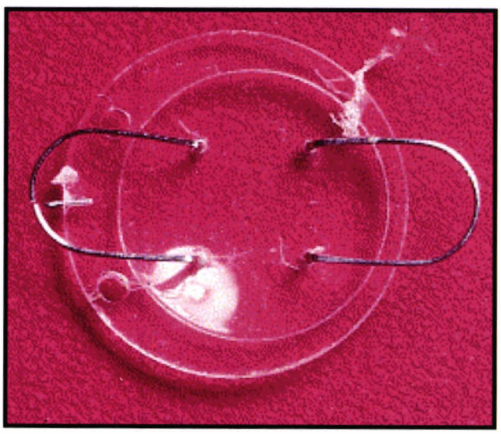

Figure 2.8 A third generation iris–fixated IOL with two metal loops (Apple et al. 2000e).

In England in 1975 John Pearce, developed a small rigid tripod posterior chamber IOL (PC-IOL). The lens had a central optic disc 4mm in diameter and the total diameter of the lens was 8.5mm with the lens made totally of PMMA (Pearce, 1984). In 1977 Shearing expanded the role of the PC-IOL with development of a lens that had an optical disc of 5mm with two flexible J-shaped loops of polypropylene attached to the optic on one end. Its total diameter was almost 13mm and the loop was designed to fit in the

ciliary sulcus. This gave rise to a whole new generation of lenses with flexible haptics all supported by the structure of the posterior chamber behind the iris (Shearing et al. 1984).

2.4.2 Modern generation of intraocular lenses

Evolution of IOL design and materials continues especially with the introduction of small incision cataract surgery. This is drive by the need to develop intraocular lenses that have high biocompatibility to prevent lens epithelial cell adhesion, eradicate visual aberrations and discoloration, decentration, therefore improving the outcomes of cataract surgery.

2.4.2.1 Anterior chamber IOL

The new generation of open-loop AC-IOL designs is considered one of the four main achievements along the pathway of IOL development. The main advantages of the new generation of AC-IOL are a remarkably well-made, well polished, no-hole haptic and a three or four-point fixation open loop. Use of AC-IOLs must be accompanied by high surgical expertise and proper patient selection. Even so the main disadvantage of an AC-IOL is still defective design (Apple et al. 2000e).

Nowadays, although anterior chamber IOLs are not the preferred option, they are used in certain conditions such as when ECCE is unavailable, secondary or exchange implantation, or medical conditions such as lens displacement. Their use may also, depend on the preoperative condition of the eye. For example, an AC-IOL is used in cases of uveal bleeding disorders and severe scleroconjunctival scarring following trauma.

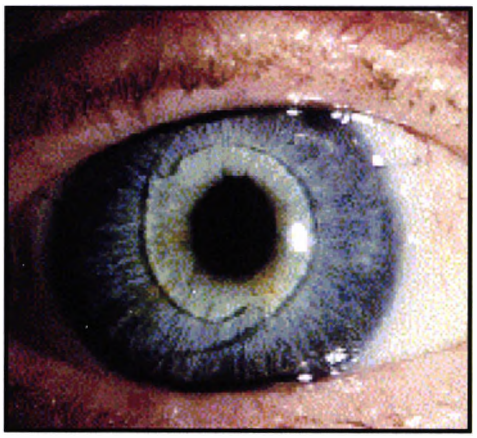

Figure 2.9 An example of an anterior chamber IOL (Apple et al. 2000e).

Leaming (2000) found that 87% of cataract surgeons preferred the use of an AC IOL for secondary implantation because it is safer with a lower risk of eye threatening complications compared to a sutured PC-IOL. Several clinical studies documented a significantly positive outcome of the new generation of open loop AC-IOL designs especially in the 1990s (Bellucci et al.1996, Hassan et al. 1991, Leaming, 1998, Lois et al 1997). Clemente conducted the largest clinical series of primary AC-IOL implantation (one with four point fixation as seen in figure 2.9, and the second one with three point fixation) between 1994 and 1997 with a mean follow up of 21 months. At the annual meeting of Deutsche Gesellschaft für Intraoklären-Linsen Implantation (DGII), Frankfurt, Germany, March 1999, he reported that the patients can do very well after high quality implantation of modern AC-IOLs performed by a skilled surgeon. Furthermore, a comparative study reported that the prevalence of endothelial cell loss in an eye with an AC-IOL and an eye with aphakic spectacles was 5.3% and 4.1% respectively. These results suggest that the advanced development of AC-IOL implantation has reduced endothelial cell loss, which was a major complication of early AC-IOLs (Snellingen et al. 2000).

2.4.2.2 Posterior chamber IOL

The posterior chamber (PC) is the primary implant location used with both ECCE and phacoemulsification. The main advantage of posterior chamber intraocular lenses (PC-IOLs) is that they are implanted behind the pupil thus eradicating optical aberrations, haloes and glare caused by the edge of the IOL. The new generation of three piece rigid IOLs made of PMMA show excellent results. However, the one piece IOL produced a lower prevalence of PCO and Nd:YAG laser posterior capsulotomy compared to three piece PMMA lenses (26% versus 33%) (Apple et al. 2000c). Conversely, the new generation of foldable IOLs result in a prevalence of PCO of 30.2% with a one-piece silicone lens and 39.1% with a three-piece silicone IOL. Although, the difference was insignificant, this may be due to the altered amount of capsule stretching and adherence of the optic to the posterior capsule (Mamalis et al. 1996). The prevalence of PCO as well as anterior capsule opacification (ACO) was low for three pieces, sharp edge, hydrophobic, foldable, acrylic IOLs even though patients complain from glare and visual aberrations (Doan et al. 2002). In the case of one piece, hydrophobic, foldable, acrylic IOLs, so far only one preliminary report has been recently published demonstrating good results (Caporossi et al. 2002).

2.4.3 Intraocular lens material

2.4.3.1 Introduction

The ideal material used for implantation must be biocompatible, durable, adapt to the desired shape and be able to be sterilized without affecting its properties. Furthermore, the materials used for the intraocular lens must remain optically transparent and have a high resolving power (Christ et al. 1995). Intraocular lens materials are divided into two categories: rigid materials and foldable or soft IOL materials (fig. 2.12). Common rigid and soft intraocular lens materials will be considered in the following sections.

2.4.3.2 Polymethylmethacrylate (PMMA)

The quality of modern polymethylmethacrylate IOLs has been perfected during the past two decades. It sets a standard for other IOL materials. PMMA is a rigid, glassy material that is chemically stable. Therefore, it is an ideal material for an IOL where inertness, stability, excellent optical clarity, a low water diffusion constant and high resistance to the effects of light, oxygen, and hydrolysis are all required (Christ et al. 1995).

The main drawback of rigid PMMA IOLs is that they require a large incision length and therefore suturing is needed. This can induce postoperative astigmatism and slower visual rehabilitation (Talamo et al. 1991. In addition PMMA IOLs have been correlated with increased postoperative blood aqueous barrier breakdown (Oshika et al. 1994), optical side effects such as halos or ghost images (Masket et al. 1993b), and can compromise the view of the fundus periphery (Levy et al. 1994).

2.4.3.3 Hydrogel

Hydrogel refers to a broad class of polymeric materials that have a water content of at least 20% when hydrated. They are formed from a cross-linked hydrophilic polymer network incorporating a bonded benzotriazole-type UV absorber (Martin et al. 1993). When the polymerization process is altered, the optical properties, elasticity and gas permeability can be varied (Shimizul et al. 1987). Intraocular lenses made of hydrogel such as the Iogel 1103-hydrogel, and Hydroview H60M, have high biocompatibility thus causing minimal disruption of the blood aqueous barrier. However, these IOLs have demonstrated a high incidence of regeneratory PCO due to the lack of adhesion between the IOL and lens capsule (Menapace et al. 1996, Hollick et al. 2000).

2.4.3.4. Silicone

Silicone elastomers are synthetic polymers having a generalized structure of a polysiloxane. The polymer contains a repeating silicon-oxygen backbone containing organic groups R, attached to a significant number of the silicon atoms by silicon-carbon bonds (fig. 2.10). Industrial silicones have R groups that are mostly methyl. Silicone elastomer does not contain organic additives, ultraviolet chromophores, dyes, accelerators and plasticizers (Allarakhia et al. 1987).

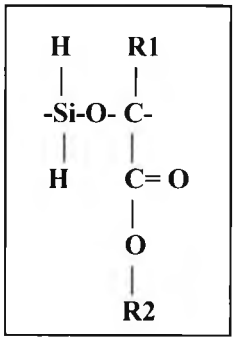

Figure 2.10 The chemical structure of a Soflex2 IOL developed by IOLAB (Masket & Crandall, 1999).

Polydimethylsiloxane is primarily an elastomer prepared for use in biomedical applications. Most medical grade elastomers are especially designed and evaluated to provide a high level of safety and efficacy for medical uses (Christ et al. 1995). Many studies have reported that silicone IOLs are safe, show no toxicity either clinically or histologically and have effective performance during long term follow-up (Christ et al. 1989, Buchen et al. 1989, Steinert et al. 1997). A clinical study has also reported that there is less protein and cellular debris accumulated on a SILM-2IUV silicone lens than on a PMMA IOL (Steinert et al. 1997). Olson et al. 1998 reported that PCO was less with silicone IOLs than with PMMA IOLs with the rate of capsulotomy 24% and 33% respectively. However, Kim et al. (1999) reported that the silicone IOLs induced PCO faster than PMMA IOLs. This was attributed to the fact that a silicone IOL is extremely slippery when wet or dry and can easily tear increasing the prevalence of unstable fixation (Chehade et al. 1997).

2.4.3.5 Acrylic

The Acrylic IOL is one of most recent intraocular lens materials. Although acrylic IOLs are more fragile than silicone (Milazzo et al. 1996), its optical quality is not easily affected except by applying extreme nonphysiological manipulations (Oshika et al. 1996). It is chemically stable, inert and optically transparent.

Acrylic IOLs are made from phenylethylacrylate or phenylethylmethacrylate co-polymers cross-linked with butanediol acrylate (fig. 2.11) (Christ et al. 1995). The high refractive index (1.55) is the key property that allows a thin intraocular lens design. The centre thickness of a 24D acrylic IOL ranges from 0.72mm to 0.9mm, while the silicone and PMMA IOLs have thickness of 1.0mm and 1.1mm respectively. This means that acrylic lenses can be adapted for multiple in the bag lens implantation in cases of high hyperopia (Shugar et al. 1996).

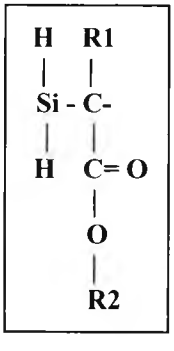

Figure 2.11 The basic chemical structure of acrylic lens materials (Masket & Crandall, 1999).

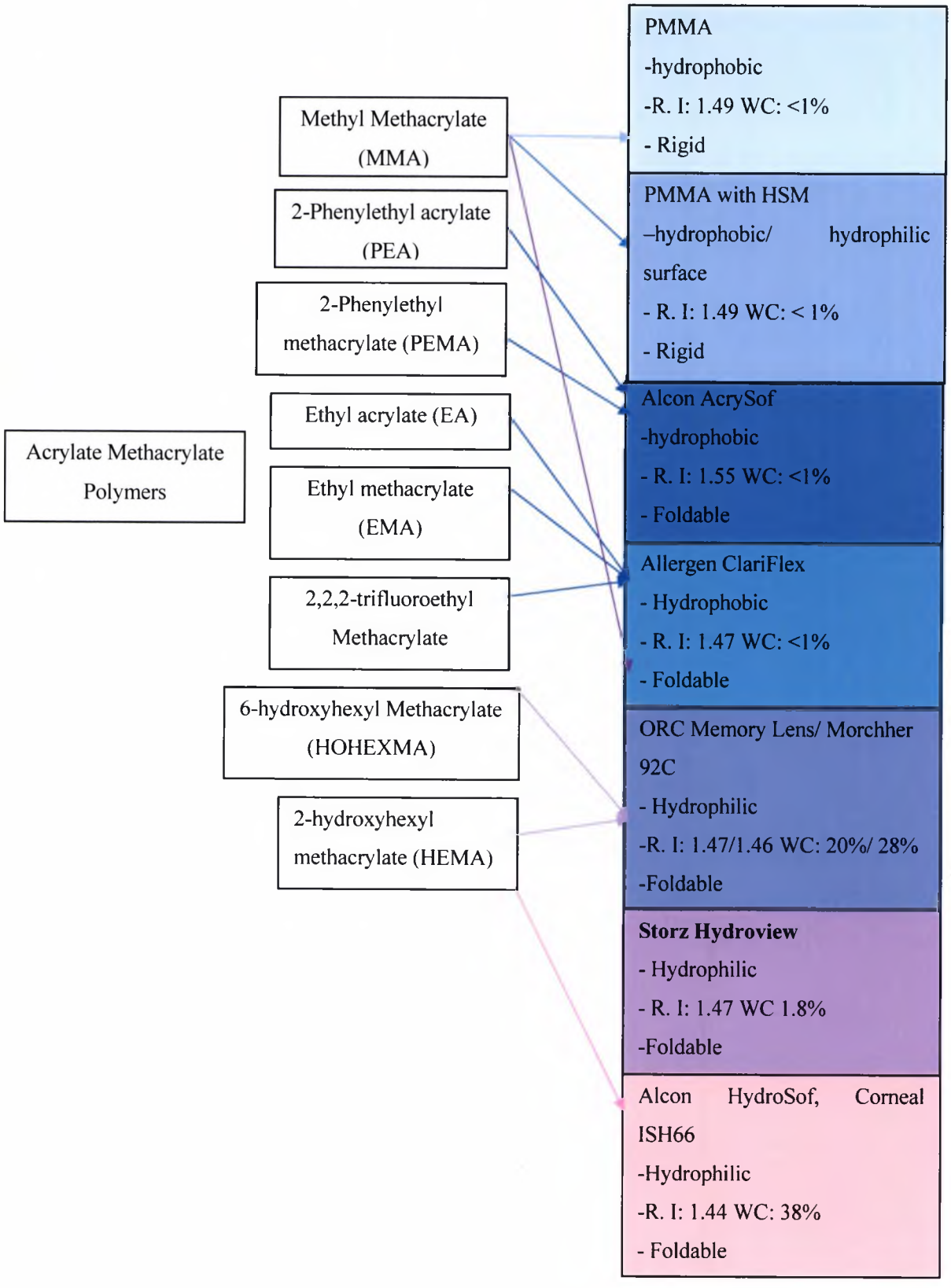
Acrylate Methacrylate Polymers
Methyl Methacrylate (MMA)
2-Phenylethyl acrylate (PEA)
2-Phenylethyl methacrylate (PEMA)
Ethyl acrylate (EA)
Ethyl methacrylate (EMA)
2,2,2-trifluoroethyl Methacrylate
6-hydroxyhexyl Methacrylate (HOHEXMA)
2-hydroxyhexyl methacrylate (HEMA)
PMMA
-hydrophobic
-R. I: 1.49 WC: <1%
- Rigid
PMMA with HSM
–hydrophobic/ hydrophilic surface
- R. I: 1.49 WC: < 1%
- Rigid
Alcon AcrySof
-hydrophobic
- R. I: 1.55 WC: <1%
- Foldable
Allergen ClariFlex
- Hydrophobic
- R. I: 1.47 WC: <1%
- Foldable
ORC Memory Lens/ Morchher 92C
- Hydrophilic
-R. I: 1.47/1.46 WC: 20%/ 28%
-Foldable
Storz Hydroview
- Hydrophilic
- R. I: 1.47 WC 1.8%
-Foldable
Alcon HydroSof, Corneal ISH66
-Hydrophilic
-R. I: 1.44 WC: 38%
- Foldable

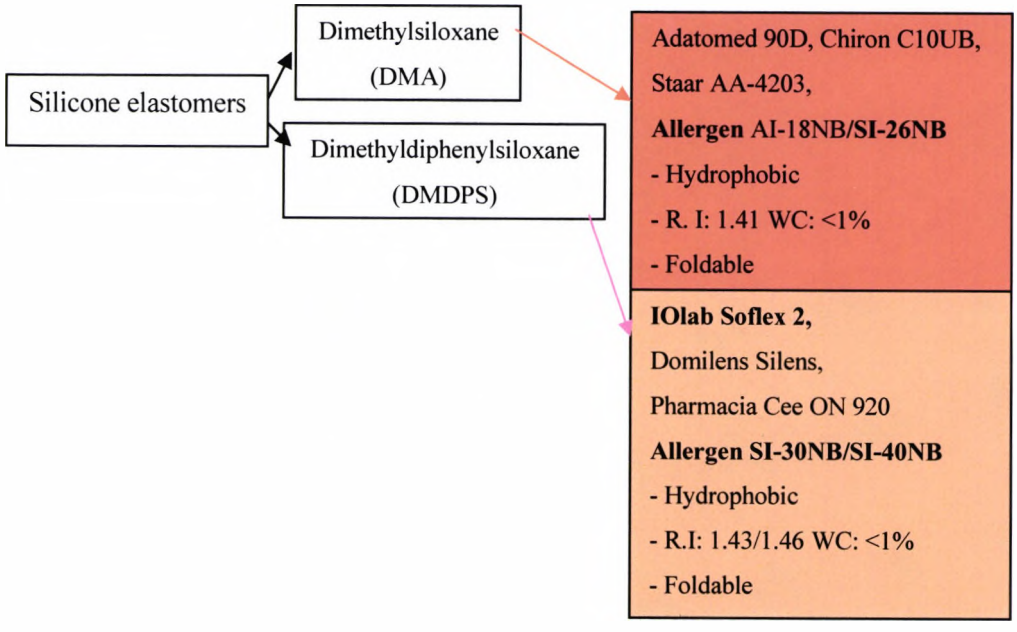

Figure 2.12 The major components of rigid and foldable IOL optic; PMMA (rigid), hydrogel (foldable) and acrylic (foldable) IOLs. Some of these IOLs were implanted for recruited subjects in this study (Bold letters). The hydrophicilty of the IOL depends on the water contact wetting angle in air; the lower this value the more hydrophilic the IOL surface. PMMA, polymethyl methacrylate; HSM, heparin surface modification; RI, refractive index; WC, water content (Kohnen, 1996).

2.4.4 Intraocular lens surface properties

2.4.4.1 Introduction

Intraocular lens surface properties are fundamental to determining biocompatibility and biostability. This is because the lens surface comes into contact with the lens debris and cells and mediators from the various phases of the inflammatory response. In particular hydrophilicity/hydrophobicity will influence cellular adhesion and postoperative cell reaction.

2.4.4.2 Hydrophilic or hydrophobic surfaces properties

A hydrophilic material has a higher biocompatibility than hydrophobic or oleophobic surfaces. A foreign body reaction on a hydrophilic IOL surface is lower than on a hydrophobic surface (Amon et al, 1994, 1996). Also, hydrophilic materials support less or no LEC proliferation and metaplasia resulting in less opacification and thickening of the capsule rim (Abela-Formanek et al. 2002). However, Schauersberger et al. (1999) reported that there is no clinically significant difference in laser flare-cell measurements between the hydrophobic IOLs (silicone and acrylate) and the hydrophilic lenses (hydrogel and polyHEMA) in the postoperative inflammation period, and the only difference was that acrylic IOLs on the first postoperative day had significantly higher flare values than silicone and polyHEMA IOLs.

2.4.4.3 Biocompatibility

Biocompatibility of an IOL is the ability to inhibit stimulation of lens epithelial cell proliferation and remain as a clear refractive element in a pseudophakic eye (Apple et al. 1992, Pande et al. 1996a). It can be evaluated before introducing it for human use either by laboratory testing using cell culture or by injecting extract of the material into an animal such as mouse, rabbit, or guinea pig to test systemic toxicity, irritation and sensitizing reactions. In vivo, studies are conducted to assess and compare biocompatibility of various IOL materials within the lens capsule, which is the actual habitat of IOL, by using specular microscopy or slit-lamp biomicroscopy to examine various types of cells (e.g. epithelioid-like cells, giant cells, and lens epithelial cells) on the IOL at different times after implantation (Amon 1994, Mulluer-Eidenböck et al. 2001, Schauersberger et al. 2001).

Although, the biocompatibility of PMMA posterior chamber IOLs has been verified, they still have a higher prevalence of PCO than hydrophobic acrylic and some silicone IOLs (Apple et al. 2000f, Ursell et al. 1998). Furthermore, Khan et al. (1999) who conducted a long-term prospective trial for 12 years, reported that the P-HEMA IOL group biocompatibility was better than the PMMA group.

2.4.4.4 Biostability

Biostability is the material's ability to resist the effects of agents of the intraocular media such as aqueous, enzymes, and inflammatory mediators (complement system and arachidonic acid cycle), ultraviolet radiation and stress either from contraction of the haptics or fibrosis within the capsular bag (Christ et al. 1995). There are two methods used to evaluate intraocular lens material biostability: In the first method the IOL material is implanted subcutaneously or within muscle since these two sites provide easy visualization of the IOL's reaction with surrounding tissue. The second method uses a species whose eye reasonably mimics that of the human, such as cat or rabbit. Following implantation, the intraocular tissue and IOL is examined for signs of inflammation. A complete histological evaluation of the cornea, iris and the retina is carried out for signs of abnormality and a microscopic examination of the IOL is used to detect any changes (Christ et al. 1995).

Recently, studies reported vacuoles or opacification occurring on or within the IOL optics of modern foldable IOLs. For example, glistenings have been observed on Acrysof IOLs, calcification within the optics of SC60B-OUV IOLs, and surprisingly "Snowflake" or crystalline opacification of a PMMA IOLs. Glistening of an IOL is defined as acute onset of intralenticular small refractile fluid-filled vacuoles present inside the optic of Alcon Acrysof IOLs. This usually occurs in the early stages following cataract surgery and implantation. The mechanism of glistening is unknown, yet studies report that this may be related to the package-associated microenviroment (Omar et al. 1998, Christiansen et al. 2001) and variation in the temperature (Omar et al. 1998, Kato et al. 2001, Apple et al. 2001). Glistening causes a decrease of contrast sensitivity yet has only minor impact on visual acuity (Trivedi et al.

2002). Tognetto et al. (2002) conducted a comparison study using seven types of foldable IOLs (CeeOn Edge 911A, ACR6D, AcrySof, SI-40NB, Hydroview H60M and Stabiba). They reported that the Acrysof had a higher percentage and a greater number of glistenings compared to other types of IOLs.

Calcification or opacification within the optics of SC60B-OUV IOLs which appear as a nuclear cataract (fig. 2.13) (Werner et al. 2001, Trivedi et al. 2002), often occur as a late postoperative complication (approximately 24 months). This occurs especially within the optic substance of some IOLs manufactured from at least one source of hydrophilic acrylic biomaterial (Macky et al. 2001, Werner et al. 2001). The light microscopic and scanning electron microscopy (SEM) of cut section and sagittal views of explanted IOLs respectively reveals that the granules are deposit within the optic of the IOLs, are in part composed of calcium and have various sizes. These granules are in the intermediate region beneath the anterior and posterior surfaces and not in the central area. The mechanism of formation is not fully understood. Although, Frohn et al. (2000) suggested that it may be related to the presence of unbound ultraviolet (UV) absorbers. Opacification within the optic of the IOL causes glare and significant decreases visual acuity and glare (Trivedi et al. 2002).

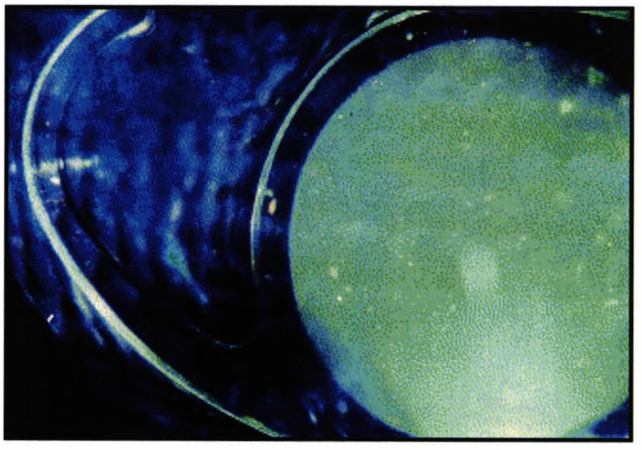

Figure 2.13 Calcification within the optics of SC60B-OUV IOLs (Forhan et al. 2001).

Opacification of PMMA IOL appears as white-brown crystalline deposits within the IOL optic (fig. 2.14). It is a late postoperative complication progressing slowly approximate 8-15 years following implantation. The Snowflake usually appears in the central and mid-peripheral portion of the IOL optics. SEM analysis reveals that the opacifications are all within the substance of the IOL. The possible explanation that some IOLs made from the 1980s to the early 1990s particularly with moulding processes (injection, compression, and cast) may be responsible for opacification. It does not have a significant impact on visual acuity initially yet as the opacification progresses the vision deteriorate (Trivedi et al. 2002).

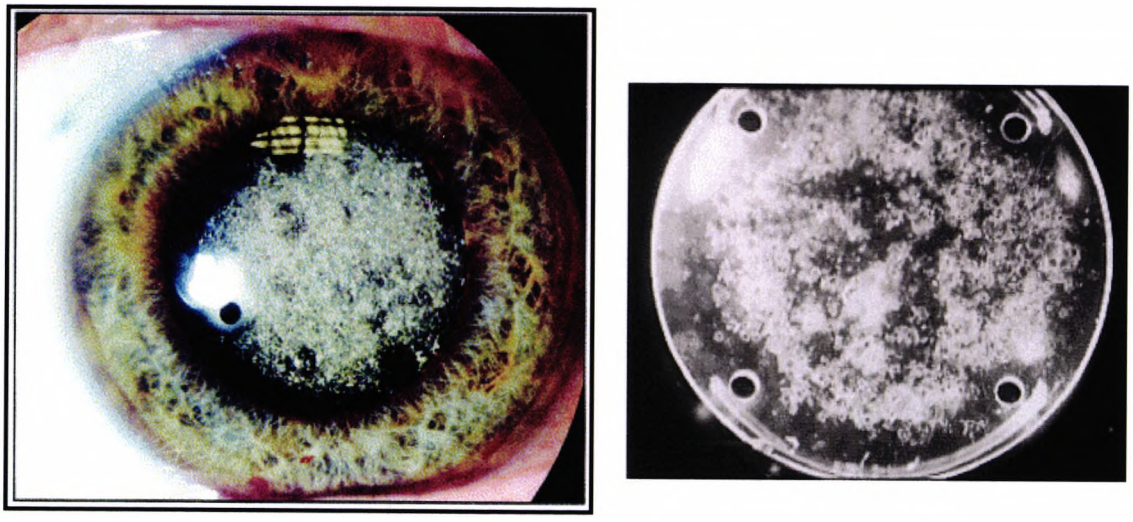

Figure 2.14 Opacification of PMMA IOL optic appears as white-brown crystalline deposits (Apple et al. 2002).

CHAPTER THREE

3. Posterior capsule opacification

3.1 Prevalence and Management of PCO

The incidence of PCO is difficult to state with certainty. It has been reported by many studies to vary from 10% to 50% within five years following cataract surgery (Apple et al. 1992, Schaumberg et al. 1998). In the United Kingdom, data collected by the Department of Health on posterior capsule opacification showed that between 21% to 26% of patients developed PCO within four years following cataract surgery. The variability in these figures is due to many factors such as the varying interval between surgery and opacification or follow up. In addition, Nd:YAG laser capsulotomy rate is often used as an indicator for the incidence of PCO. However, this measure is affected by availability or accessibility to this treatment (Apple et al. 1992, Ram et al. 2001). The age of the patient is a primary factor that influences PCO formation. Other factors include surgical technique, intraocular lens material (Apple et al. 2001), design (Caporossi et al. 2002), surface properties (Schauersberger et al. 2001), size of IOL (Meacock et al. 2001a), and methods of implantation (Ram et al. 2001). Tawab & Tassignon (1995) reported that certain ocular or systemic diseases such as uveitis, and diabetes mellitus, increase the incidence of PCO due to the increased inflammatory reaction, which stimulates lens epithelial cells proliferation, results confirmed these results by Dana et al. (1997).

The age of the patient is the most important risk factor for the development of posterior capsule opacification. The older the patient, the lower the incidence of PCO. A possible explanation is that younger patients may have a large number of juvenile lens epithelial cells that have a great potential to proliferate and migrate (Mackool, 1991). Nd:YAG laser capsulotomy rate for patients younger than 40 years was 20% and for those older than 66 years was 7% (Frezzotti and Caporossi, 1990). This was supported later by (McPherson et al. 1995) who reported that the incidence of re-opacification after successful Nd:YAG capsulotomy was 0.7% when patients were younger than 50 years at the time of cataract surgery as seen in figure (3.1).

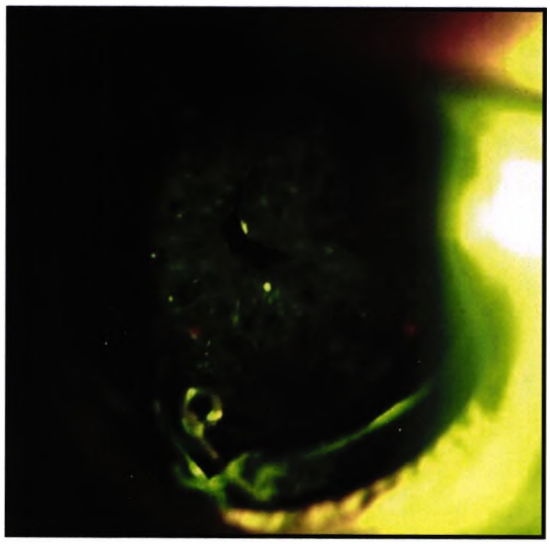

Figure 3.1 Pearl-type posterior capsule re-opacification subsequent to Nd:YAG laser capsulotomy.

Some studies have also demonstrated that the type of cataract may influence the incidence of PCO. In particular, senile complete cataract had a lower tendency to produce PCO (Frezzotti & Caporossi, 1990, Argento et al. 1992). Recent studies have reported that the incidence of PCO was higher among female patients than male patients after cataract surgery (Ninn et al. 1997,

Sundelin et al. 1999). However, Westling et al. (1991) reported that there was no association between age or sex of the patients, different surgeons or complications during and after surgery and the risk of getting posterior capsule opacification.

3.2 Pathogenesis of posterior capsule opacification

3.2.1 Introduction

Early studies have documented that posterior capsule opacification is due to proliferation and migration of lens epithelial cells and their derivatives following ECCE (Duke Elder, 1969, Apple et al. 1989, 1992). Indirect evidence also reveals that inflammation and stimulation by the immune system plays a role in cell proliferation providing a possible explanation for the increased incidence of PCO in infants (Naumann, 1980). Recently many studies have documented that posterior capsular opacification is a result of the postoperative inflammatory reaction (Miyake et al. 1990, Nishi et al. 1992).

Factors that influence metaplasia of the lens epithelial cells in the human are the patients' age and inflammation (Tan et al. 1993, Jamal et al. 1993, Alió et al. 1997). Age has a significant effect on the onset of PCO formation, because the growth rate of LECs is age dependent with patients younger than 50 years demonstrating a two-fold higher risk of developing pearling than patients older than 50 (Jamal et al. 1993, Wormstone et al. 1997). Inflammation following surgical procedures is inevitable yet controlling or reducing this factor is important because the release of inflammatory mediators, complement activation, and some cytokines, such as interleukin-1 and-6,

stimulate proliferation of LECs (Nishi et al. 1992).

3.2.2 Origin of cells involved in PCO

There are three possible cell types that have the ability to produce significant opacification:

1. Anterior epithelial cells, which have the ability to grow slowly toward the equator, to form the equatorial lens bow and have a high level of mitotic activity. Also they have the ability either to grow along the posterior capsule to form bladder cells during cataract formation or to form epithelial pearls following ECCE (Apple et al. 1989). Cells of the germinal zone of the equatorial region of the lens are the primary cells of origin in the most cases of pearl-type PCO, while the anterior epithelial cells are the primary cells of origin for fibrotic PCO.

2. Cuboidal epithelial cells that line the anterior capsule. These cells can often transform into fibrous cells. However, these cells do not have the ability to migrate. Therefore, it is possible that these cells are responsible for the pathogenesis of the fibrotic form of PCO (Apple et al. 1989).

3. Residual cortical fibres from the equatorial lens bow that become dislodged and float freely within the capsule following ECCE. These LECs either migrate centrally toward posterior capsule and undergo pseudofibrous metaplasia or remain localized and organize in the equatorial region to form the outer bulk of a Soemmerring's ring as seen in figure (3.2). The Soemmerring's ring occurs due to either planned anterior capsulotomy or partial removal of lens substance after ECCE (Apple et al. 1989). Therefore, implanting an IOL in the bag alone cannot inhibit the formation of a

Soemmerring's ring. Good cortical clean-up is the best way to prevent it (Ram et al.2001).

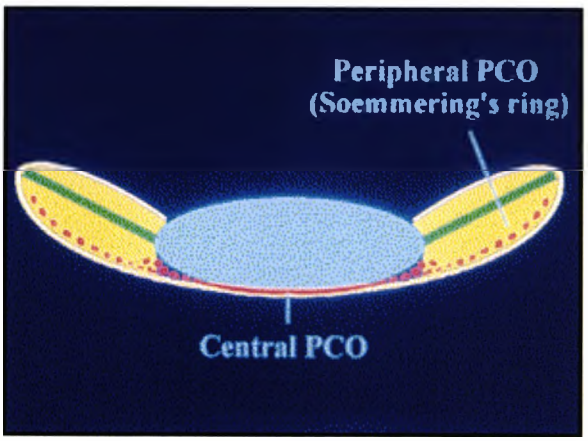

Figure 3.2 The formation of a Soemmerring's ring is due to the remnants of LECs (Apple et al. 2000a).

3.3 Morphological forms of PCO

3.3.1 Elschnig Pearls

The classic clinical use of the term "Hirschberg-Elschnig pearls" refers to a process caused by rupture of the anterior lens capsule after accidental or surgical trauma. This releases highly mitotic lens epithelial cells that then cause opacification. Lens epithelial cells from the germinative region at the equator are responsible for pearl PCO formation, because these cells are actively mitotic and have the ability to migrate posteriorly across the lens capsule. Also, these epithelial cells are capable of undergoing fibrous metaplasia forming a fibrous encapsulation around the IOL loop as part of the healing process (Apple et al. 1992). Clinically, the development of pearl-type PCO requires several months to several years whereas fibrotic PCO develops

within a period of 2 to 6 months following cataract extraction surgery (Kim et al. 1999).

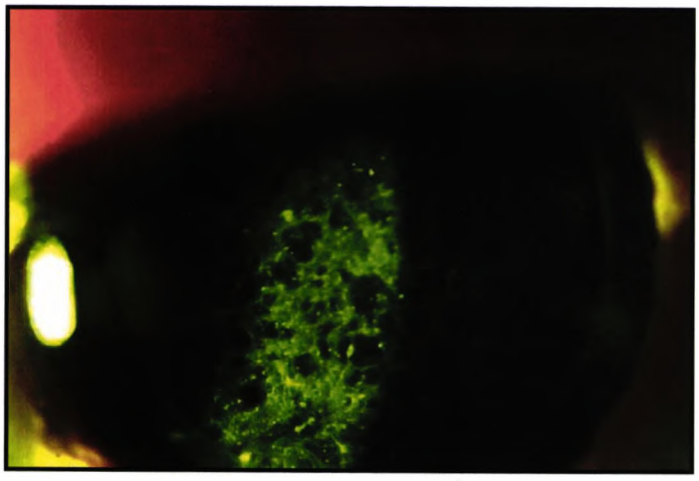

Figure 3.3 Slit-lamp image of pearl-type posterior capsule opacification

3.3.2 Fibrosis

Fibrosis is morphologically subdivided into two forms (Tan et al, 1993): diffuse, Non-Specific Fibrosis (NSF), and Early Central Posterior Capsule Fibrosis (ECPCF). It appears as well defined morphological pattern with a fine radial bundles extending from the capsulorhexis edge as seen in figure (3.4). The former develops as a result of central opacity contraction and the latter probably by myofibroblastic changes.

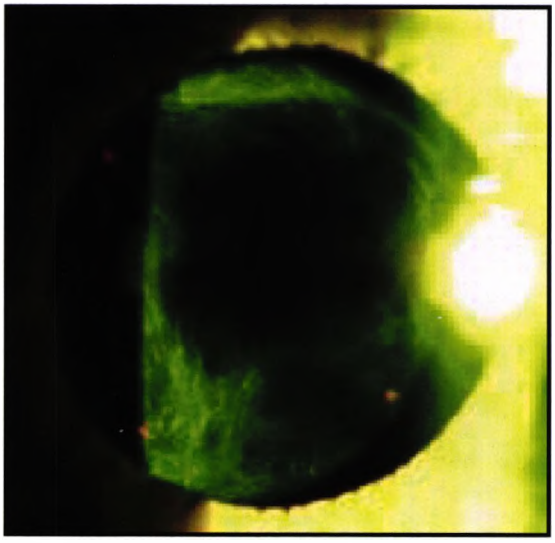

Figure 3.4 Early posterior capsule fibrosis with fine radial bundles extending from the capsulorhexis edge toward the centre.

Ishibashi et al. (1994) reported that the extracellular matrix, which is the main component of PCO, consisted essentially of collagen fibrils and basal lamina-like material. The collagen fibrils were found to be types I and III collagen. The basal lamina that surrounded the spindle cells and the basal lamina-like material in the extracellular matrix was found to consist of type IV collagen. This suggests that basal lamina-like material corresponds to a true basal lamina. It also suggests that lens epithelial cells in PCO secrete collagen fibrils and that the collagen types may play a role in the formation of PCO.

McDonnell et al. (1983) reported that the anterior epithelium at the cut edge of the anterior capsule underwent a fibrous metaplasia that caused wrinkling of the adjacent posterior capsule. Also, wrinkling of the posterior capsule possibly occurs due to the contractile nature of the newly formed fibrocytes as seen in figure (3.5). These may cause traction and resultant folds and wrinkles of the posterior capsule, which could cause visual distortion such as

a Maddox rod effect, and glare. The thicker the membrane, the greater the chance for visual aberration and the more difficult the Nd:YAG laser capsulotomy (Apple et al. 1989).

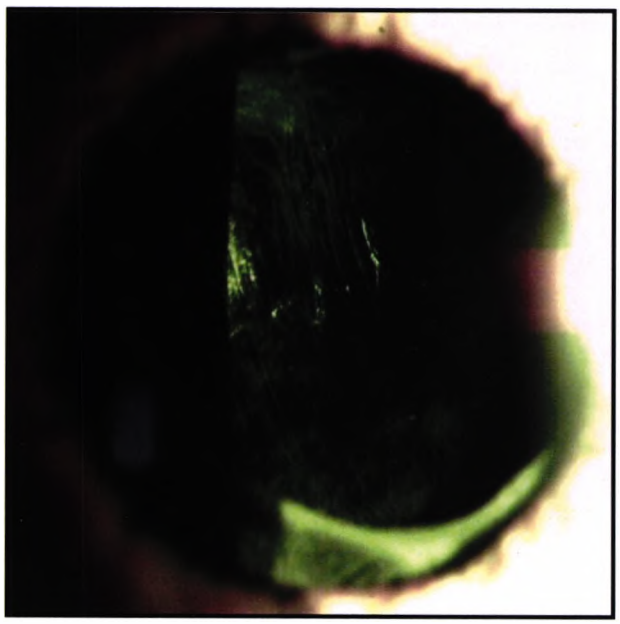

Figure 3.5 An image showing folds or wrinkles of the posterior capsule caused by contraction of the newly formed fibrocytes.

3.3.3 Less common causes of clinical PCO

The surgical techniques and the various manipulations of cataract extraction and IOL implantation always cause a breakdown of the blood aqueous barrier (BAB). Surgical trauma and BAB breakdown cause the release of free-floating materials such as LECs, inflammatory cells and mediators, protein fibrin, pigment, and erythrocytes, which circulate through the aqueous humor during and after the operation (Apple et al. 1989). A transient fibrin reaction is clinically common and harmless and occurs immediately in the postoperative period after ECCE (Nishi et al. 1988). Saika et al. (1996)

reported that lens epithelial cells are involved not only in the eye's cellular reaction to the IOLs but also in the formation of extracellular matrix on the IOLs. Furthermore, Nagamoto et al. (1996) reported that LECs proliferate onto the IOL optic by three different routes (1) from the anterior capsulotomy margin, (2) from the inner surface of the anterior capsule, and (3), from the posterior capsule. This is further evidence supporting the hypothesis that membranes observed on the IOL are LEC sheets. These membranes would be classified as a fibrosis-type of PCO and clinically they are insignificant. However, their density and location may cause visual decline requiring Nd:YAG laser capsulotomy (Apple et al. 1992).

Peripseudophakic membranes are known as "cocoon membranes", and are formed by fibrous metaplasia of dispersed cells. It is the result of inflammatory debris and blood breakdown products after haemorrhage, which organizes to create retrocorneal fibrous membranes in front of, on, or around the IOL. Haemorrhage is a common cause of clinical PCO and opacification of the media in general and is largely due to direct trauma to the iris caused by surgical instrument manipulation and chafing from either the IOL optic or loops (Apple et al. 1989).

3.4 Prevention or Containment of PCO

3.4.1 Introduction

Over the past years, several methods have been introduced and investigated to reduce or eliminate posterior capsule opacification. The medical reasons are to avoid the possible complications of Nd:YAG laser capsulotomy. There are also strong financial reasons given the cost of equipment and the increased number of cataract cases (250,000 pa predicted by 2003 in the UK).

3.4.2 Surgical technique

The techniques of cataract surgery continue to improve making the operation easier and safer. Postoperative inflammation is minimized intra-operatively by careful, gentle manipulation of the eye at all stages of surgery (Alio et al. 1996). Studies have reported that phacoemulsification induced less inflammation than ECCE in both non-diabetic and diabetic patients (Chee et al. 1999, Dowler et al. 2000). This can be explained by the development of phaco-machines that reduce the duration of the surgical procedures consequently leading to a reduction of trauma (Kruger et al. 2001). Also, many studies have documented that the incision size plays a major role in reducing inflammation and producing better visual results (Gills et al. 1991, Oshika et al. 1992). Pande et al. (1996b) compared two groups: The first group were given a 7.0 mm optic diameter PMMA IOL following ECCE, and a second group had a 5.0 × 6.0 mm optic diameter PMMA IOL following phacoemulsification. They reported a significant difference in the mean flare measurement at day 1, one week and one month postoperatively, and concluded that phacoemulsification with CCC induced less inflammation than ECCE with envelope capsulotomy and a large incision.

The incision location also affects the degree of the BAB breakdown. Dick et al. (2000) reported that postoperative flare values with a clear corneal incision were significantly lower than with a sclerocorneal tunnel incision for the same incision length and silicone IOL implantation. However, after 5 months no statistically significant difference was found. Conversely, limbus incisions in the vascular region resulted in a fibroblastic response that enhanced incision stability and allowed rapid incision healing within 7 days compared to corneal incisions that required 60 days for healing (Ernest et al. 1998).

Since the uveal tract is the most vascular tissue in the eye, direct or indirect trauma to the iris and ciliary body plays a more important role than incision size in postoperative breakdown of BAB. The extent of BAB breakdown depends on the technique used to expel the lens nucleus. For instance, with ECCE, manual nucleus expression is used by applying pressure on the limbus inferiorly which could cause injury to the iris and ciliary body. In contrast, with phacoemulsification the lens nucleus is fractured into small pieces in the capsular bag before removing it, thus there is less risk of injury to the iris and ciliary body. This may explain why phacoemulsification induces less inflammation than ECCE (Pande et al. 1996a, Chee et al. 1999).

An intact CCC also reduces inflammation since radial tears of the lens capsule disrupt the zonular fibres resulting in an unstable capsular bag that could increase surgical trauma during cataract extraction. Also, an intact CCC decreases the foreign body reaction since it effectively isolates the IOL from vascular uveal tissue by shielding the IOL in the intact capsular bag. This theory is supported by the fact that the reported incidence of giant and epithelioid cells and pigmented cells following extracapsular cataract

extraction with an intact CCC were 12% and 4% respectively. For a CCC with rim tears these values were 33% and 33% respectively (Pande et al. 1996b).

A recent study compared two anterior capsulotomy techniques, continuous curvilinear capsulorhexis (CCC) and envelope capsulotomy. Results revealed that the anterior capsulotomy techniques and IOL type influence the incidence of PCO. Because the absence of capsular tears preserves the capsular bag, and allows stable in the bag IOL fixation, this allows the lens posterior capsule to stretch over the IOL. The result is an increased area of contact and adhesion between the IOL and the lens posterior capsule preventing the migration and growth of retained LECs into the visual axis. Using subjective grading, Brinci et al. (1999) reported that PCO occurred at a significantly lower rate with CCC 11.5% than with envelope capsulotomy 24.5%.

3.4.3 Thorough removal of lens material

The risk of posterior capsule opacification can be decreased through cortical clean up (McDonnell et al. 1988, Apple et al. 1992, 2001, Dahan et al. 1991). Also, phacoanaphylactic endophthalmitis is a late postoperative inflammation that occurs due to lens epithelial cells (LECs) remaining after cataract surgery (Naumann, 1980). Therefore, removal of lens epithelial cells and cortical remnants in the equatorial region during cataract surgery is as important as avoiding excessive tissue damage or capsular rupture during irrigation /aspiration of the lens.

Studies have documented that in-the-bag phacoemulsification through a miniature capsulorhexis allows extensive polishing (Hara et al. 1984, Michelson, 1991, Nishi O et al. 1991a). Recently, further studies have indicated that hydrodissection of the lens capsule is the most efficient method to remove cortical material. However, this technique is best achieved with a CCC that provides an intact, stable capsular bag. An unstable capsule may be subject to capsular rupture during the removal of LECs (Apple et al. 1989, 1992, 2001, Gimble, 1994, Peng et al. 2000). Nishi et al. (1991b) found that meticulous capsule polishing using ultrasound during endocapsular cataract surgery significantly reduced the number of patients requiring laser capsulotomy from 10.8% to 3.7%.

In a comparative study for five different mechanical polishing instruments, Mathey et al. (1994) concluded that satisfactory results were obtained only with an ultrasound irrigation/aspiration system. In the ultrasound I/A technique eight out of nine specimens had no epithelium left and the remaining specimen showed 0.2% residual cells of which 99.2% were lytic. The capsular stress was acceptable and no lesions occurred that would cause a capsular tear. The result with I/A phaco tip showed 2% of cells left in place (83% healthy, 17% lytic). The conclusion was that ultrasound I/A was more effective than I/A alone. However, the equatorial region is less accessible to the available polishing instruments. Also, this technique needs additional surgical time, increasing surgical trauma and hence disruption of the BAB.

Davidson et al. (2000) reported that phacoemulsification with and without anterior and equatorial vacuuming led to less initial LEC density in the capsular bag than ECCE. Phacoemulsification and cortical I/A leads to less residual LEC concentration on the internal capsule surfaces than ECCE with manual nuclear expression. However, Quinlan et al. (1997) reported that there was no significant difference between phacoemulsification and ECCE surgery on the rate of survival and growth of the LECs because the LECs are dependent on the donor rather than the surgical technique performed. Khalifa et al. (1992) reported that polishing the posterior capsule had no effect on the long term development of PCO.

3.4.4 Intraocular Lens

3.4.4.1 Intraocular Lens Fixation

Implantation of the intraocular lens in the capsular bag following extracapsular cataract extraction is considered the ideal site since it provides good centration and consistent, secure implantation. Capsular fixation helps to minimize the blood aqueous barrier breakdown and increases the IOL biocompatibility, barrier effect and radial stretch of the posterior capsule (Tana et al. 1996, Alio et al. 1997, Ram et al. 1999a & b). Many clinical and experimental studies have confirmed that implantation in the capsular bag reduces the incidence of PCO minimising the space for LEC proliferation behind the IOL optic as seen in figure (3.6) (Apple et al. 1992, 2001, Martin et al. 1992, Ram et al. 1999b). Ram et al. (2001) reported that the incidence of PCO with in the bag implantation following ECCE and phacoemulsification were 14.67% and 11.9% respectively. Conversely the incidence of PCO with sulcus fixation following ECCE and phacoemulsification were 51.16% and 50% respectively.

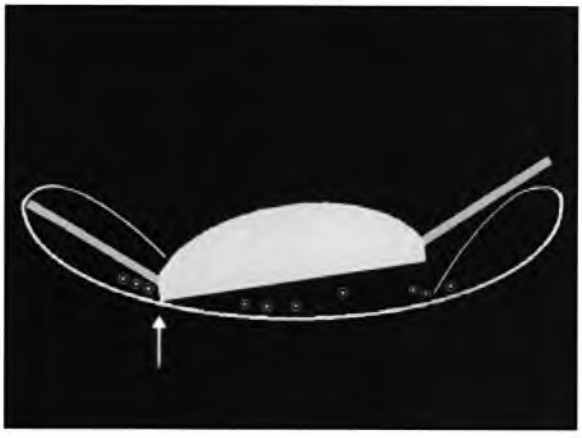

Figure 3.6 Asymmetric fixation, where one of the loops is outside the capsular sac, causing a separation between the anterior capsular flap and the adjacent posterior capsule. This facilitates LEC migration hence increasing the incidence of PCO (Apple et al. 2000a).

Optimal, safe and stable in-the-bag placement became possible with the development of the continuous curvilinear capsulorhexis (CCC) technique as the anterior capsulotomy of choice in cataract extraction (Lee, 1990, Pandey et al. 2000). The CCC produces an intact lens capsule that is best suited for stable and centred in the bag implantation (Apple et al. 1992, 2001). Moreover, there is a large body of evidence indicating that the size of CCC opening compared to the IOLs optic diameter plays an important role in reducing posterior capsule opacification. A CCC with a diameter slightly smaller than the IOL optic diameter increases adhesion between the edge of the anterior capsule and the anterior surface of the IOL optic. This enhances IOL fixation and centration and isolates the interior compartment of the capsule containing the IOL optic from the surrounding aqueous humour. Thus the incidence of PCO with a CCC smaller than IOL optic diameter is lower than for a larger CCC (Apple et al. 1992, 2001, Ravalico et al. 1996). However, a comparative study reported that the incidence of PCO with a

CCC opening larger than the optic diameter of an AcrySof IOL with a sharp edge is less than for a PMMA lens with a round edge. This could be due to the IOL material and sharp edge (Meacock et al. 2001b).

3.4.4.2 Intraocular lens materials

Foreign-body reactions occur commonly after cataract surgery and intraocular lens implantaion. The amount of cell reaction is affected by the IOL's material, and fixation (Amon et al, 1994). These reactions lie between subjectively asymptomatic with a mild short-term cell adhesion on the lens surface, to dense, chronic cell membranes along with severe uveitis and cystoid macular oedema (Wenzel et al. 1988).

The main contents of this reaction are macrophages in the form of small cells and giant cells (Saika et al. 1995), which is similar to the granulomatous reaction against foreign-bodies implanted subcutaneously in animals (Ishibashi et al. 1994). Tamura et al. (1990) reported that these macrophages adhere to the IOL surface even when the lens is implanted in the anterior chamber with an intact crystalline lens. This suggests that the removal of the crystalline lens has little influence on the induction of macrophages. Postoperative inflammation and metaplasia of LECs demonstrate the IOLs biocompatibility to inflammatory mediators in postoperative aphakic and pseudoaphakic eyes (Apple et al. 1989, Miyake et al. 1991).

The properties of IOLs and atraumatic surgery are important factors in reducing inflammation during and after cataract surgery (Pande et al. 1996 a). Prevention of PCO formation does not only depend on the intraocular lens design (posterior convexity, haptic angulation, and sharp rectangular edges), but also on the IOL material's biocompatibility, stability and adhesiveness

(Apple et al. 1992, 2001, Amon et al. 1996). Santos et al. (1986) found that a PMMA IOL inhibited LEC migration and LEC metaplasia stops when the cells came into contact with the IOL.

Recently, studies have introduced two new concepts: First, adhesion between the lens capsule and various intraocular lens materials and second that lens epithelial cells, small cells, epithelioid cells, and giant cells adhere to various intraocular lens surfaces differently (Ravalico et al. 1997, Versura et al. 1999, Majima, 1996). The adhesive force between different intraocular lens materials and the capsule varies significantly. For example, silicone, due to its slippery nature when wet, causes a lack of adhesion to the lens capsule (Oshiko et al. 1998). Hydrogel IOLs are also nonadhesive and fail to establish a firm and extensive contact with the posterior capsule allowing the LECs to migrate from the equatorial zone to the posterior capsule. In addition, permeability of the hydrogel material allows a continuous translental supply of nutrients to the lens epithelial cells (Menapace et al. 1996, Scaramuzza et al. 2001).

Acrylic IOLs adhere to the lens capsule more strongly than PMMA IOLs. This could be due to their sticky surface increasing adhesion between the lens and the capsule. This results in encapsulation of lens epithelial cells from the immunologically active postoperative aqueous humor. A very thin optic also leaves less space between the anterior and the posterior capsule reducing LEC proliferation. These factors may explain the reduced incidence of PCO, (6.2% with AcrySof IOLs and 22.2% with PMMA IOLs), during a 3-year follow-up (Sundelin et al. 2001).

Many studies have reported that lens epithelial cells, small cells, epithelioid cells, and giant cells adhere to various intraocular lens surfaces differently (Ravalico et al. 1997, Ursell et al. 1998, Versura et al. 1999, Mullner-Eidenbock et al. 2001, Scaramuzza et al. 2001). For example, the LEC density on IOL surfaces of HSM-PMMA, polyHEMA and silicone is less than on a PMMA IOL surface (Versura et al. 1999). Cunanan et al. (1991) found that silicone and hydrogels exhibit a lower cell adhesion than PMMA. This finding has been supported by Ravalico et al. (1997) who reported that the poly-hydroxyethylmethacrylate (polyHEMA) and silicone IOLs showed fewer epithelioid cells than PMMA.

Mullner-Eidenbock et al. (2001) concluded that AcrySof had the highest incidence of epithelioid cells and giant cells but lowest incidence of LECs whereas hydroview (hydrogel) IOLs had the lowest incidence of epithelioid cells and giant cells but the highest incidence of LECs. However, Ursell et al. (1998) found that the giant cell counts were significantly lower with acrylic IOLs than PMMA and silicone IOLs, and hence that blood-aqueous barrier breakdown was lower with acrylic IOLs. Thus, implantation of silicone IOLs should be avoided in eyes with pre-existing BAB damage such as patients with uveitis, and diabetes. This may explain the high incidence of visually significant PCO and LEC layer formation on the anterior surface of hydroview IOLs compared to AcrySof IOLs (Scaramuzza et al. 2001).

3.4.4.3 Surface modification and coating of the intraocular lens

Surface modification has been developed to improve the biocompatibility of IOL materials. Surface modification can be divided into two types: (1) Surface passivation where the surface is made smooth, to avoid cellular debris adhering to the IOL surface, and (2) Heparin surface coating used to transform a hydrophobic surface into a hydrophilic surface resulting in less molecular interactions between the lens surface and the biological environment of cells. A comparative study used four types of surfaces hydrophobic, oleophilic, surface passivated (SP), and heparin surface modified (HSM). It reported that there was no significant difference in the prevalence of cell reactions on the unmodified IOL surface (hydrophobic and oleophilic) and SP IOL surface. However the incidence of cell reactions on the HSM IOL surface was significantly lower than on the hydrophobic IOL surface (Amon. et al. 1996).

Heparin surface modification decreases cellular deposits on the IOLs indicating a reduced foreign body reaction (Harfstrand et al. 1990, Nishi et al. 1996, Tognetto et al. 2001, Borgioli et al. 1992). Therefore, heparin surface modification could be used for eyes with a high risk of blood-aqueous barrier breakdown to reduce inflammation and postoperative intraocular reaction (Mester et al. 1998).

In a double blind study comparing heparin surface modified (HSM) IOLs with PMMA IOLs in patients with diabetes mellitus or inactive uveitis, the results showed no statistically significant difference in the number of cellular deposits on the anterior IOL surface of the HSM IOL and PMMA IOL. There was no difference in the number of LECs on the IOL or in the incidence of capsular opacification (Tabbara et al. 1998). Also, comparing soft

hydrophobic acrylic lenses and HSM PMMA lenses, shows that these IOLs induce the same degree of BAB disruption after phacoemulsification (Gatinel et al. 2001). Teflon modification has been used recently to reduce cell adhesion (Legeais et al. 1998, Werner et al. 1999).

3.4.5 Intraocular lens design

The effect of IOL design on the PCO is well-documented (Menapace et al. 1996, Apple et al. 2001). Experimental and clinical studies have examined various features of optic design including: edge shape, IOL optic size, IOL overall size and haptic angulation on the postoperative outcome (Hansen et al. 1988, Jamal et al. 1993, Tan et al. 1993, Tana et al. 1996, Hashizoe et al. 1998). Randomized clinical trials have also been conducted to determine the significance of these design differences in inhibiting or reducing the incidence of PCO (Martin et al. 1992).

3.4.5.1 Barrier effect and "No space No cells"

During the past 25 years, several IOL designs have been investigated (Simcoe, 1978, Pearce, 1984, Sterling et al. 1986, Santos et al. 1986, Apple et al. 1992, Nagamoto, 1997). Early in their development, posterior convexity of the IOL optic was considered the primary design factor that inhibits LEC migration by maximizing contact between the IOL optic and the lens posterior capsule (fig. 3.8.A) (Apple et al.1992). Many studies have investigated the effect of biconvex and plano-convex IOLs on PCO. Santos et al. (1987) and Nagamoto et al. (1997) concluded that placing plano side against the posterior capsule is superior to a biconvex IOL, because a plano-convex design blocks the LECs at the sharp optic edge as seen in figure (3.7).

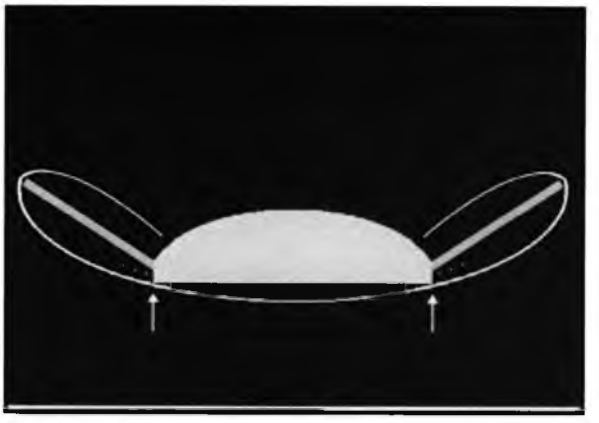

Figure 3.7 The sharp edge of a convex-plano IOL hindered migration of LECs from the lens capsule equator toward the centre of the posterior lens capsule (Apple et al. 2000a).

Conversely, Jamal et al. (1993), Lindstorm and Harris (1980), Sellman et al. (1988) all reported that a plano-convex IOL with the convex surface placed against the posterior capsule increased the area of contact between the IOL and the capsule enhancing the barrier effect and reducing the incidence of pearl PCO. Martin et al. (1992), Bron et al. (1990) and Assia et al. (1992) reported that the biconvex IOLs had better optical quality and reduced PCO more than plano convex IOLs as seen in figure (3.8.A). Hansen et al. (1988) has reported that contact between the posterior capsule and the PMMA optic might promote fibrosis formation since the contact between the cells made them more likely to undergo metaplasia to myofibroblastic forms and induce fibrotic capsular opacification.

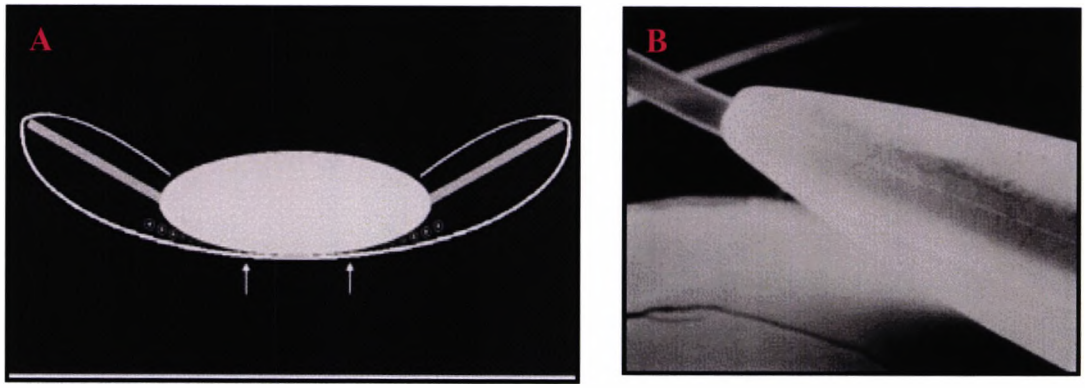

Figure 3.8 (A) A biconvex IOL with round edge implanted in the lens capsule, showing that contact between the IOL optic and the lens capsule hindered LEC migration toward the centre part of the posterior capsule. (B) An image of the biconvex IOL with round edge (Apple et al. 2000a).

Recently, there has been an increasing body of evidence indicating that not only maximizing contact between the IOL optic and the lens posterior capsule reduces the incidence of PCO, but also that the sharp edge of the IOL optic helps too (Apple et al. 2001, Nishi et al. 1998a). The new concept states that the convexity of the IOL optic and the sharp edge both play a major role in inhibiting PCO (Nishi et al. 1998b, Oshika et al. 1998, Nagamoto et al. 1997). This conclusion is based on previous experimental studies that have reported that the LECs were severely inhibited at the posterior capsule bend created by a plano-convex edge of an IOL (Nagata et al.1993) as seen in figure (3.7). The LECs trapped in this well did not grow and climb along the rectangular wall of the well after they became confluent, although the cells could grow and climb along the wall of wells with a U-shaped bottom. This means that the LECs may not grow and migrate over an abruptly discontinuous bend in the capsule (Nishi et al. 1998b). However, Bhermi et al. (2002) reported that the sharp discontinuous bend did not appear to induce contact inhibition of

migrating LECs nor did it significantly hinder the rate at which LECs migrated. Therefore, a discontinuous bend in the lens capsule in isolation is unlikely to be responsible for the observed reduction in posterior capsule opacification associated with the use of square-edged IOLs.

The concept was further documented by clinical studies that reported that the sharpness of the IOL optic edge is an important factor in impeding posterior capsule opacification by creating high pressure on the posterior capsule and also acting as a barrier by blocking and accumulating LECs at the sharp edge as seen in figure (3.9.A) (Nagamoto et al. 1997). The incidence of PCO with sharp-edged biconvex (BC) IOLs, sharp-edged convex-plano (CP) IOLs, round-edged BC IOLs, and round-edged CP IOL were 2%, 6%, 31%, and 21% respectively (Nagata & Watanabe 1996). However, Hollick et al. (1999) reported that it is unlikely that relatively minor differences in the lens edge design would be sufficient to account for such dramatic differences in PCO rates.

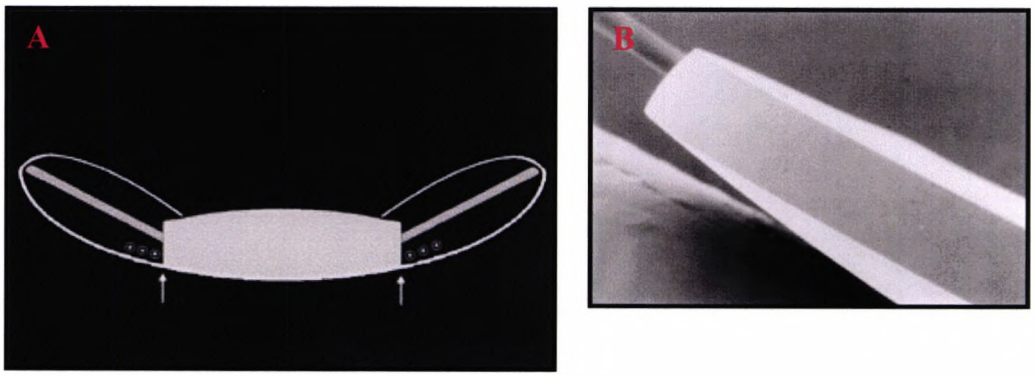

Figure 3.9 (A) A biconvex IOL with sharp edge implanted in the lens capsule, showing the convex part of the IOL increasing the area of contact between the IOL optic and the lens capsule. The sharp edge blocks LEC migration toward the centre part of the posterior capsule and haptic angulation provides more pressure to stretch the lens capsule over the IOL preventing formation of folds. (B) An image of a square or truncated edge, such as seen on the Alcon AcrySof biconvex IOL, that blocks the cell growth toward the visual axis (Apple et al. 2000a).

Recently, Tassignon et al. (2002) introduced a new design of IOL called "Bag-in-the-lens". It is shaped like a biconvex lens with a central round optic and circular equatorial groove in. The circumferential haptic consists of both anterior and posterior lips, defining a grove between them (fig. 3.10 A & B). It was made of foldable hydrophilic poly HEMA, where the largest diameter is 8.5mm, the smallest is 6.5mm, the optic size is 6.5mm, the total thickness of the haptic is 0.90mm, and each lip is 0.25mm. To implant the IOL, a calibrated CCC was performed on both the anterior and posterior capsules, so that the two capsules are placed in the grove of the IOL. The IOL was implanted in 10 human eyes 2 of them children and 8 adult. They reported that the bag-in-the-lens prevents PCO particularly in high risk patients such as those with congenital cataract, uveitis and diabetes.

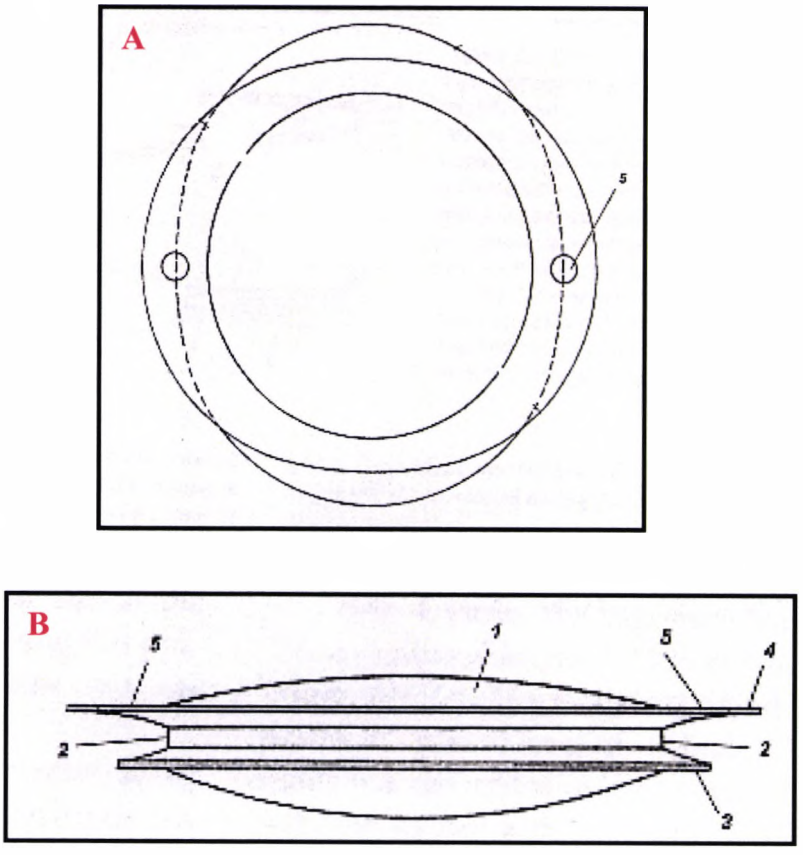

Figure 3.10 (A) Diagram illustrate the design of "bag-in-the-lens" IOL. (B) A side view showing the characteristics of the IOL (1) optic, (2) groove into which anterior and posterior capsules will settle, (3, 4) oval-shape of both anterior and posterior haptic, (5) positioning holes (Tassignon et al. 2002).

3.4.5.2 Radial Stretch of the Posterior Capsule

Radial stretch of the posterior capsule is a second step to secure further the barrier effect established by the optical design convexity plus sharp edge. It is created by IOL haptic angulation, bending–shaped loop IOL or a capsular tension ring. Radial stretch improves the barrier effect by stretching the capsule over the IOL optic posterior surface preventing the formation of folds

and increasing the adhesion and area of contact between the IOL and the lens posterior capsule (Lindstrom et al.1980, Downing et al. 1986, Tetz et al. 1988).

The configuration and dimension of the capsular bag are affected by the IOL optic size, IOL overall size, and haptic angulation, as well as by capsular tears (Assia et al. 1995). A comparative study used two IOLs with similar material and design apart from their optic diameter (5.5mm and 6mm) and haptic angulation. The authors of this study reported that PCO is influenced by IOL optic size being less with the 6mm optic than 5.5mm optic. This may be due to an increased haptic angulation with a large optic diameter IOL and hence a greater backward force against the lens capsule leading to increased area of contact and adhesion with the IOL (Meacock et al. 2001). However, Schmidbauer et al. (2002) conducted a comparative study to evaluate the influence of various haptic angulations of IOLs (0, 5, 10, and 15 degrees) to prevent PCO. They concluded that the angulation did not seem to be a significant factor in reducing PCO yet it may be due to (1) the barrier effect of the truncated optic edge, (2) the relative thickness of the IOL optic, which creates a tight fit between the posterior optic surface and the anterior surface of the IOL, and (3) the relatively thick haptic, which helps achieve tight capsule optic contact.

Many studies reported that suitable intraocular lens overall size inhibits PCO formation since implanting an IOL with overall size smaller than 12.5 mm in a large capsular bag can result in unstable fixation, and facilitate LEC migration and proliferation. Implanting an IOL larger than 12.5 mm in a small capsular bag can result in excessive stretching and distortion forming folds that permit LEC migration as seen in figure (3.11.B) (Apple et al. 1992, Lim et al. 1998). Tana and Belmonte (1996) reported that IOLs with a, 12mm

overall length, a 6.5mm optic diameter and an optic-haptic junction angled at about 90 degrees, are most suitable for in the bag implantation, because a larger arc of contact with the equator prevents LECs migrating across the posterior capsule. Another, comparative study concluded that PMMA IOLs with a large overall size such as 13.5mm significantly decreased the incidence of Nd:YAG capsulotomy to 16% whereas PMMA IOLs with an overall size more than 13.5mm had an incidence of Nd:YAG capsulotomy of 38% (Mamalis et al. 1995).

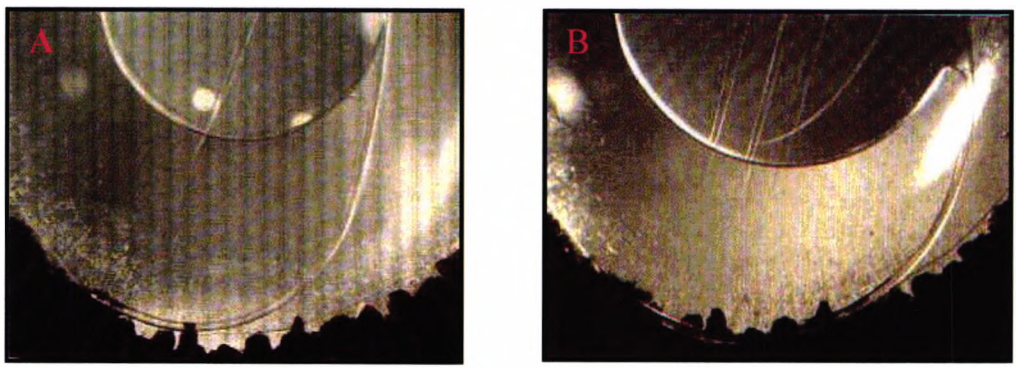

Figure 3.11 Images showing the effect of overall IOL size on the lens capsule (A) 11mm IOL (B) 13mm IOL (Mamalis et al. 1995).

A new design of IOL has been introduced recently known as capsular bending haptic IOL. This IOL has a capsular bending ring, which is made of PMMA and has a sharp edge as seen in figure (3.12, A, B). It is inserted into the capsular fornix before insertion of the IOL, creating a sharp bend in the capsule. Histopathological observation shows that the equator ring effectively inhibited LEC migration from the equator of the lens capsule toward the central area of the lens posterior capsule as seen in figure (3.12.C) (Hara et al. 1995).

Experimental studies have also revealed that the capsule bending haptic and capsule bending ring significantly inhibited migration of LECs (Nishi et al. 1998b & c). Support for these results comes from a series of clinical studies conducted by the same group. They concluded that a discontinuous bend created by the sharp, square optic edge of a PC IOL may prevent LEC migration hence reducing PCO (Nishi et al. 1998a) as well as anterior capsule fibrosis and shrinkage (Nishi et al. 2001). The main drawback of a bending haptic or a capsule-bending ring is their size requiring a large incision for implantation. However, lately, a capsular tension ring inserter has been developed that allows implanting a capsular tension ring through small incision.

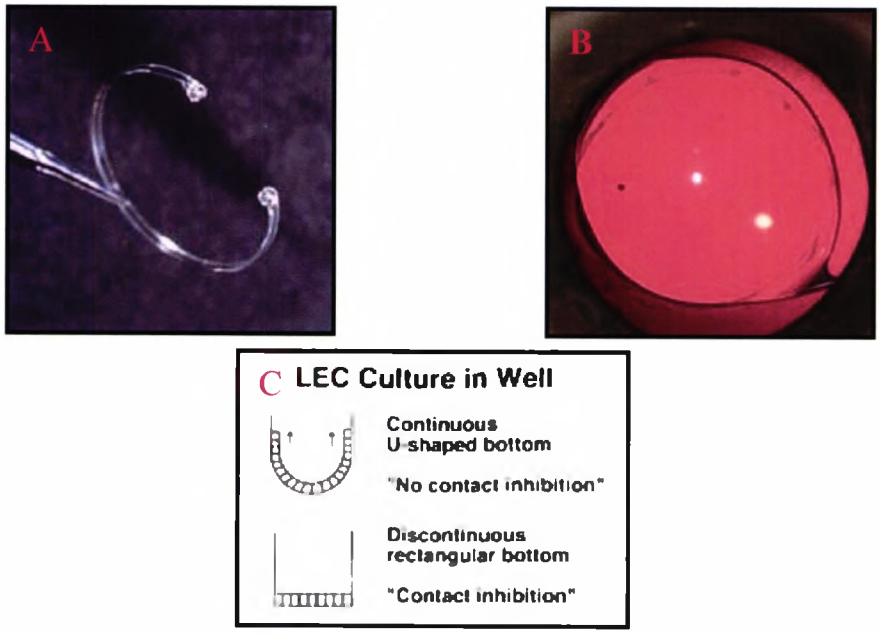

Figure 3.12 (A) An image of the first human implanted capsular bending ring, implanted before the IOL, which effectively inhibited the LECs. (B) An image of implanted capsular bending haptic IOL. (C) A discontinuous or rectangular bend created by the sharp, square edge may induce contact inhibition that prevent LECs migrating hence reducing PCO

(http://www.akh-wien.ac.at/iol).

Finally, Apple et al. (2001) concluded that implementation of all these key points will minimise intraoperative and post-operative breakdown of the blood aqueous barrier and hence decrease the rate of Nd:YAG capsulotomy to single figures: (1) Phacoemulsification with a CCC diameter slightly smaller than the IOL, (2) Performing hydrodissection to facilitate removal of lens fibres and epithelial cells, (3) placement of an IOL that has a high biocompatibility, (4) IOL with a sharp truncated edge optic and angulated haptics to provide a radial stretching of the posterior capsule.

3.5 Pharmacologic and Immunologic approaches for PCO inhibitation

There is a growing body of pharmacological strategies to reduce PCO by using three categories of pharmaceutical agents: antimetabolites designed to inhibit LEC proliferation and differentiation, immunotoxins used to inhibit the LEC adhesion and anti-inflammatory and immunomodulating drugs (Bertelmann & Kojentinsky, 2001). The cells that are responsible for PCO formation are: (1) LECs present on the anterior capsule and in the equatorial lens bow (2) retained cortical fibres (elongated lens epithelial cells), (3) bladder cells (Wedl cells, their histopathologic correlate with clinical Hirschberg-Elshnig pearls), (4) fibrocyte-like cells derived from metaplasia of lens epithelial cells (pseudofibrous metaplasia), and (5) myoepithelial cells (contractile smooth muscle-containing cells derived from transformed lens epithelial cells) (Apple & Rabb 1998). This means that complete blocking of cell migration by physical means is difficult to achieve thus pharmacological methods may be a better approach (Nagamoto et al. 1996). There are enormous numbers of pharmacological experimental studies investigating various drugs with different techniques to determine which drug and delivery

system could be used to inhibit PCO with minimal side-effects to the surrounding tissue in the eye. Therefore, the next sections will only highlight the main drug groups used and give examples of their subgroups.

3.5.1 Antimetabolites

There are several experimental studies reporting the use of antimetabolite derivatives such as 5-fluorouracil (Ruiz et al. 1990), and mitomycin C (Ismail et al. 1996). Both 5-fluorouracil and mitomycin C have been used in irrigation of the capsular bag during extracapsular cataract extraction in rabbits. 5-fluorouracil significantly inhibited proliferation of the anterior capsular epithelium yet it required 10 minutes application during the operation (Ruiz et al. 1990). The mitomycin C results show that it can prevent PCO without causing ocular toxicity (Ismail et al. 1996, Chung et al. 2000). In a pilot study conducted by (Tetz, 1994), Daunorubicin was used with a sustained drug delivery system (SDDS). The results show a complete destruction of LECs. However, the major disadvantage of antimetabolites is severe toxicity to ocular structures such as the corneal endothelium and retinal cells.

3.5.2 Immunotoxins and lens epithelial cell adhesion molecules as blocking agents

Lens epithelial cell adhesion molecule blocking agents, such as antitransferrin receptor immunotoxin (Goins et al. 1994) and ethylenediaminetetra-acetic acid (Nishi et al. 1996a), have been used in experimental studies to inhibit LEC adhesion to the IOLs. Ethylenediamine tetra-acetic acid EDTA has been used previously to loosen the junctional complexes between LECs and the

lens capsule permitting easier LEC removal with a low level of aspiration (Nishi et al. 1993). Recently, Nishi et al. (1996b) used EDTA in a sustained release system to disrupt interaction between the capsule and LEC migration onto the posterior capsule. The result revealed a significant reduction in the migration of LECs onto the posterior capsule. This suggests that Ca++ depletion inhibits the adhesion of integrins expressed by migrating LECs, and disrupts the interactions between the posterior capsule and migrating LECs.

Nishi et al. (1997) reported that the use of a combination of both arginine-glycine-aspartic acid sequence peptide (RGD) and EDTA had a more significant inhibitory effect on LEC migration than RGD peptide, or EDTA alone. This may be due to the combination of RGD and EDTA, or a higher total amount of EDTA present. However, the disadvantages of sustained release disks are disk opacification, weight of the disk (the EDTA and RGD peptide disk weight is 40mg) and the IOL weight. Also, there is a risk of significant damage to the corneal endothelium and ciliary bodies by the disk. On the positive side, EDTA and RGD peptide are generally less harmful and non-toxic to the other ocular tissues than antimetabolites such as daunimycin, 5-fluorouacil and colchine (Legler et al. 1993).

3.5.3 Anti-inflammatory and immunomodulating drugs

Indomethacin and diclofenac sodium are examples of anti-inflammatory drugs tested to inhibit LEC proliferation (Nishi et al. 1995, 1996b, Cortina et al. 1997). Nishi et al. (1995) reported that an Indomethacin-coated IOL significantly reduced postoperative inflammation and PCO. However, later (Nishi et al. 1996b) concluded that sustained release of Indomethacin significantly decreases inflammation but does not reduce PCO. This suggests that exposure to a higher Indomethacin concentration for a short period is

more effective than exposure to a lower concentration for a long period in inhibiting LEC proliferation.

3.5.4 Heparin

Gallenga et al. (1986) introduced the use of topical heparin therapy in pseudophakia. Later Gallenga et al. (1990) reported the pharmacological activity of heparin on the IOL and its mechanism for preventing the formation of cellular membranes. Mastropasqua et al. (1997) reported that topical heparin eye drops were effective in reducing fibrotic PCO in the long-term. There are two possible mechanisms to explain this effect: either by inhibiting proliferation of anterior epithelial cells, or by preventing the formation of cellular membranes on both the IOL and surrounding structures (Gallenga et al. 1990).

3.6 Treatment of PCO

3.6.1 Surgical discission

In the past, posterior capsule opacification was treated by discission and polishing. The posterior capsule is opened using a needle which is inserted into the eye via the pars plana and an opening is made into the fibrotic posterior capsule to polish the posterior capsule. However, the complications associated with this method are retinal detachments 3% and cystoid macular oedema 2%. With Nd:YAG laser capsulotomy the complication rates were retinal detachments 0.17% and cystoid macular oedema 0.68% (Shah et al. 1986).

3.6.2 Nd:YAG laser capsulotomy

Nd:YAG laser capsulotomy is an excellent modality for treating PCO (Apple et al. 1992). The principle of Nd:YAG laser capsulotomy is to cause photodisruption thereby making holes in the posterior capsule (Aron-Rosa et al. 1981, Ficker & Steele 1985). However, Nd:YAG laser therapy is associated with a number of complications such as: increased intraocular pressure that can be transient (Shah et al. 1986) or long-term (Fourman & Apisson 1991, Steinert et al. 1991b, Jahn & Emke, 1996). The risk for worsening of pre-existing glaucoma was 0.56% (Steinert et al. 1991b). The incidence of retinal detachment after ECCE, IOL implantation and Nd:YAG laser capsulotomy varied from 0.89% to 1.64% (Ambler & Constable, 1988, Dardenne et al. 1989, Steinert et al. 1991b). Yet, the incidence of retinal detachment after phacoemulsification, IOL implantation, and Nd:YAG laser capsulotomy was from 0.85% to 1.59% (Dardenne et al. 1989, Powell & Olson, 1995) although, Olsen & Olson (2000) found no detachments after phacoemulsification, IOL implantation and Nd:YAG capsulotomy.

The incidence of cystoid macular oedema (CME) ranges from 0.68% to 1.23% (Steinert et al.1991b). IOL luxation into the vitreous cavity after Nd: YAG laser capsulotomy has been reported with hydrogel and silicone plate haptic IOLs (Schneiderman et al. 1997, Dahlhauser et al. 1998, Dick et al. 1998). This may be due to IOL backward movement after Nd:YAG capsulotomy, which occurs more frequently with plate haptic silicone IOLs rather than with PMMA, 3-piece silicone, polyHEMA (MemoryLens®), or soft, hydrophobic acrylate IOLs (AcrySof®) (Findl et al. 1999).

IOL pitting is one of Nd:YAG laser treatment drawbacks. (Mamalis et al. 1996) have subdivided the IOL damage following Nd:YAG laser capsulotomy into three categories; mild with small pits with raised smooth edges, moderate, with deeper, large pits and small cracks and severe damage characterized by cracking with a focal area of crevice formation deep into the optic. (Dick et al. 1997) reported that the silicone, polyHEMA, and acrylic IOLs containing HEMA had a high resistance to Nd:YAG laser, with only small pits to the posterior surface in comparison to PMMA IOLs. However, a comparative study by Newland et al. (1999) using PMMA, silicone and soft, hydrophobic acrylate IOLs, reported that the silicone IOL had the lowest threshold for laser and was more likely to form a pit, or linear extension after exposure than PMMA and acrylic polymers. Furthermore, silicone IOLs had the lowest resistance to Nd:YAG laser. Acrylic had a high resistance to Nd:YAG laser damage, similar to PMMA. This also has been supported by an electron microscopic study which has shown that the Nd:YAG laser damage of soft acrylic is equivalent to or less than that of PMMA (Martin et al. 1993).

Kurosaka et al. (2002) found that after Nd:YAG posterior capsulotomy a string of pearls was formed. They suggested that intraocular lens implantation with CCC may promote its formation. The incidence of a string of pearls one year after Nd:YAG capsulotomy was 75% and the incidence of a string of pearls with CCC and IOL implantation was 61.1%. However, a clinical study by Caballero et al. (1997) reported the disappearance of Elschnig pearls after several years following Nd:YAG laser posterior capsulotomy. They suggested that this might be due to three possibilities: After the first year the lens epithelial cells at the equatorial region lose their ability to proliferate and die, macrophages possibly from the vitreous engulf and absorb the pearls or destruction and softening of the pearl cells by enzymes.

3.7 Monitoring Progression

3.7.1 Introduction

Methods used to evaluate posterior capsule opacification can be divided into subjective and objective techniques. Subjective methods cover not only visual acuity (Goble et al. 1994), contrast sensitivity and glare sensitivity (Magno et al. 1997, Westheimer et al. 1994) but also the slit-lamp-grading (Kruger et al. 2000, Sellman et al. 1988, Odrich et al.1985), fundus visibility (Legler et al. 1993, Prajna et al. 2000), the lens opacity meter (Olson et al. 1998) and often Nd:YAG-laser capsulotomy rates (Nishi et al. 1991, Scaramuzza et al. 2001, Apple et al. 2001). However, results using such methods are affected by a wide range of bias such as the mood of the patient and the examiner, and their levels of fatigue, patience and enthusiasm (Lasa et al. 1995). Even when the Nd:YAG laser capsulotomy rate is used as an index of PCO, the validity of any conclusion is limited by the variable criteria for capsulotomy among physicians, financial factors and access to equipment (Pande et al. 1997). Most of the extraneous variables in subjective methods are difficult to control. In fact, in 2001 the american society of cataract and refractive surgery (ASCRS) meeting considered the analysis of visual acuity, glare, contrast sensitivity and Nd:YAG laser capsulotomy rates as unreliable methods of assessing the amount of PCO (Auffarth, 2001). Therefore the development of an objective and quantitative direct measurement of LEC proliferation on the posterior capsule is essential if accurate assessment of mechanical and pharmacological methods to inhibit PCO is sought. Recently several studies have highlighted the development of computerised systems used for objective and quantitative assessment of posterior capsule opacification (Pande et al. 1997, Friedman et al. 1999, Hayashi et al. 1998a). These systems will be discussed following an introduction to slit-lamp

photography.

3.8 Development of Slit-lamp Photography

The primary application of slit-lamp microscopy is as a standard instrument for the examination of the anterior segment of the eye and adnexa. It not only allows the examiner to view the structures of the anterior segment of the eye under high magnification, but also has the potential for a stereoscopic view (Benliner, 1943). Many efforts were originally made to capture and document these findings. However, they were unsuccessful, because the image of the slit beam was unfocused at the film plane and the depth of field was insufficient (Brown et al. 1972, 1988).

Several attempts were made to overcome these obstacles. For instance, the use of a small aperture was suggested, although this degraded the images by diffraction (Brown et al. 1972). Goldmann (1939) created a camera capable of changing focus during exposure. The focusing mechanism was synchronised to the focal plane in such a way that the film exposed the sharp section of the image only, thereby bringing a different part of the subject into focus step-by-step. Although this technique worked it was time consuming and not widely adopted.

3.8.1 Scheimpflug method

In 1960 Anjou and Krakau introduced the first application of the Scheimpflug principle to ophthalmic photography. The Scheimpflug principle, introduced by Thomas Scheimpflug an Austrian Naval Officer in 1906, allows a focused sagittal section of the eye to be photographed by careful tilting of the camera

and image plane. Normal slit-lamp photography of such a section does not permit an in-focus image from the cornea to the posterior capsule of the lens to be obtained.

The Scheimpflug principle was implemented on a modified slit-lamp by Drews in 1964. Niesel & Bachmann (1974) subsequently showed that Scheimpflug photographs could be subjected to densitometric and geometric evaluations. Later in 1978 Dragomirescu developed new equipment that could obtain Scheimpflug photographs of the anterior segment at different slit angles and could also eliminate the corneal reflex. The latter is important when densitometric evaluation is required. These developments and modifications opened the door for several studies using the Scheimpflug principle, such as the monitoring of cataracts (Edwards et al. 1990).

3.8.2 Retro-Illumination method

This method is used to observe either normal or pathologic structures of the eye where light is reflected from tissues situated posteriorly to the structure of interest. For example, to examine the posterior capsule, light reflected from the fundus is used (Benliner, 1943). Retro-illumination is subdivided into two types' direct retroillumination and indirect retroillumination. Direct retroillumination is obtained when the slit beam is directed obliquely through the cornea and the microscope is positioned in the direction of the reflected light. In this case the object of regard is viewed against a bright background. In indirect retro-illumination the microscope is not in the specular direction of the reflected light hence the object of regard is viewed against a dark non-illuminated background. This method is used to examine epithelial oedema, vacuoles, and capsular and subcapsular changes, as well as lenticular opacities (Benliner, 1943). The main advantage of the retro-illumination

method is that the whole image of the lens is displayed. It is therefore useful for long-term observation of lens pathology and for the evaluation of drugs (Miyauchi et al. 1990). However, the major obstacle of the retro-illumination technique is variation in illumination and uneven background illumination of the images. This is not only due to photographic variability and variation in flash intensity, but is also caused by the differing amounts of light entering the eye through different pupil sizes and variation in the amount of light reflected from the fundus. In fact, these variations have been measured and documented by (Chylack et al. 1987).

The main source of variation of illumination results from minor changes in the eye's alignment. To overcome this problem a fixation target is used. Image processing techniques have also been applied to compensate for uneven illumination. Sparrow et al. (1990) suggested performing a digital transform on the frequency distribution of the gray levels within the area of interest since this standardises the frequency distribution and improves the repeatability. Chylack et al. (1990) & Miyauchi et al. (1990) have adopted a different approach by dividing the lens into small regions of a grid network. This permitted regional identification that was relatively immune to uneven illumination. Vivino et al. (1995) and Harris et al. (1993) have subsequently described new image segmentation methods applied to retro-illumination images.

Other sources of uneven illumination in retro-illumination systems are the Purkinje images, the strongest of which is the corneal reflex. These could be eliminated by using a polarisation filter (Sparrow et al. 1990), but the polarised light creates a dark cross (Maltese cross) which is primarily due to corneal birefringence. The Maltese cross has a strong influence on any quantitative analysis (Miyauchi et al. 1990). In addition, Pande et al. (1997)

reported that the use of a polarised filter could not completely eliminate the Purkinje images due to a variation in IOL centration and tilt. An alternative technique used to remove the unwanted reflections involves placing an obstruction adjacent to the slit beam to eliminate the specular reflection (Brown et al. 1972, Harris et al. 1993 and Friedman et al. 1999). Reduction of the room illumination also helps, as does reducing the diameter of the slit beam to approximate that of the dilated pupil (Friedman et al. 1999). Image segmentation techniques can also help eliminate the effect of the Purkinje images (Barman et al. 2000).

3.9 Imaging systems used to evaluate posterior capsule opacification

3.9.1 Standard film photographic Systems

Tetz et al. (1997) developed the Evaluation of Posterior Capsule Opacification (EPCO) non-automated system. It uses retroillumination colour photographs taken with a Zeiss® photoslit-lamp (model 40 SL/P) to score PCO based on a morphological densitometric assessment. The individual PCO score is calculated by multiplying the density of the opacification, graded from 0 to 4 (0= none, 1 = minimal, 2 = mild, 3 = moderate, 4 = severe), by the area of the posterior optic involved, calculated between 0 and 1. The systems evaluate a larger area of the posterior capsule than does visual acuity testing therefore it is possible to obtain correlation between PCO and other visual problems such as perception of glare and halos, and the system shows reliability and insignificant inter-investigator variation.

Currently, EPCO is available and allows the computer user to outline boundaries of different levels of PCO of digital images and the software calculates the value of PCO using the original method. The EPCO system used to quantify PCO is not expensive and is accessible. However, it is not fully objective because it requires a skilled user using computer graphics to assess and outline levels of PCO on colour images (Aslam et al. 2002).

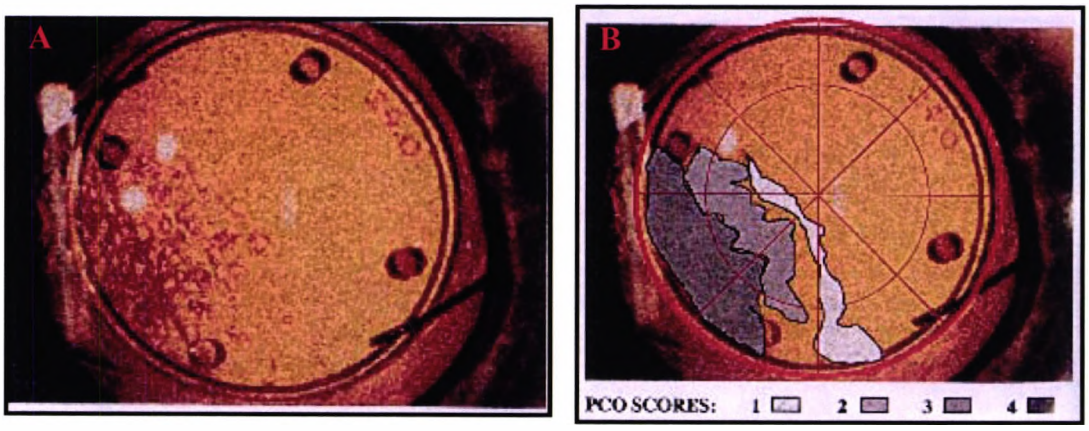

Figure 3.13 Two images captured using the EPCO system (A) retroillumination image of the posterior capsule. (B) The same image with the areas of opacity outlined, and evaluated then scored into different areas according to PCO density (Tetz et al 1997).

Camprini et al. (2000) introduced a system utilising reflected light images, using a Topcon SL-7E film camera. The images were subjectively assessed and graded using the same grid system used to grade cortical and posterior capsular opacities according to the AREDS cataract grading system. However, the film based camera produced an image artefact, and subjective grading does not eliminate the element of subjective bias, which has been documented by previous studies (Haris et al. 1993, Pandel et al. 997).

3.9.2 Digital imaging systems

3.9.2.1 Scheimpflug systems

Vivin et al. (1993) introduced a computerised video system that used Scheimpflug images for quantitative measurement of lens opacities. The system consisted of a Scheimpflug slit-lamp and video camera connected to a Macintosh computer. The method used Beer's law to derive the concentration of scatterers, because an increase in optical density should correlate directly with an increase in cataract. After capturing an image of the lens opacity with the camera and video frame grabber, each pixel is converted into a corresponding optical density using a calibration look-up table. Lasa et al. (1995) modified the EAS-1000 system and developed special software that expressed the measurement of PCO in optical density units and dimensions in millimetres. However, this system measures the average density of a central 1mm portion of the posterior capsule, which did not correlate with patients' visual acuity (Hayashi et al. 1998a).

The anterior eye segment analysis system EAS-1000 is capable of taking both Scheimpflug and retro-illumination photographs. The system has been through many phases of development to improve its reliability and reproducibility for applications such as cataract detection and classification (Edwards et al. 1988, Sakamoto et al. 1992, Magno et al. 1994, Sasaki et al. 1990, Nakaizumi 1992). Recently, Hayashi et al. (1997) modified the EAS-1000 by adding a CCD camera and on-line image analysis system to calculate the various areas in the anterior segment of the eye. Hayashi et al. (1998a) and Hayashi et al. (1998b) developed the Anterior Eye Segment Analysis System (EAS-1000; Nidek, Gamagori, Japan) to take Scheimpflug photographs. The central 3mm portion of the posterior capsule is quantified

by means of area densitometry. Scheimpflug slit images of the implanted IOL are taken at 0°, 60°, 120° meridians after full dilatation. The highest quality image of each meridian is selected and then transferred to an online computer. Axial densitometry is used to calculate the scatter light density of the central 3-mm area of the posterior capsule and an identical area of the IOL. The density value is expressed in computer-compatible tape steps (CCT). The density value of one section is determined by subtracting the scatter light density in the IOL from the measured value of the posterior capsule. The averaged density values of the 3 meridians are considered to be the PCO value.

The EAS-1000 is objective and straightforward to operate. Yet, it is not currently available, and there is scope for missing areas of opacity if they do not lie within the slit sections. This may explain why the measured meridian are changing from 0°, 60°, 120° (Hayashi et al. 1998a) to 0°, 45°, 90° and 135° from one study to another (Hayashi et al. 1998b & c)

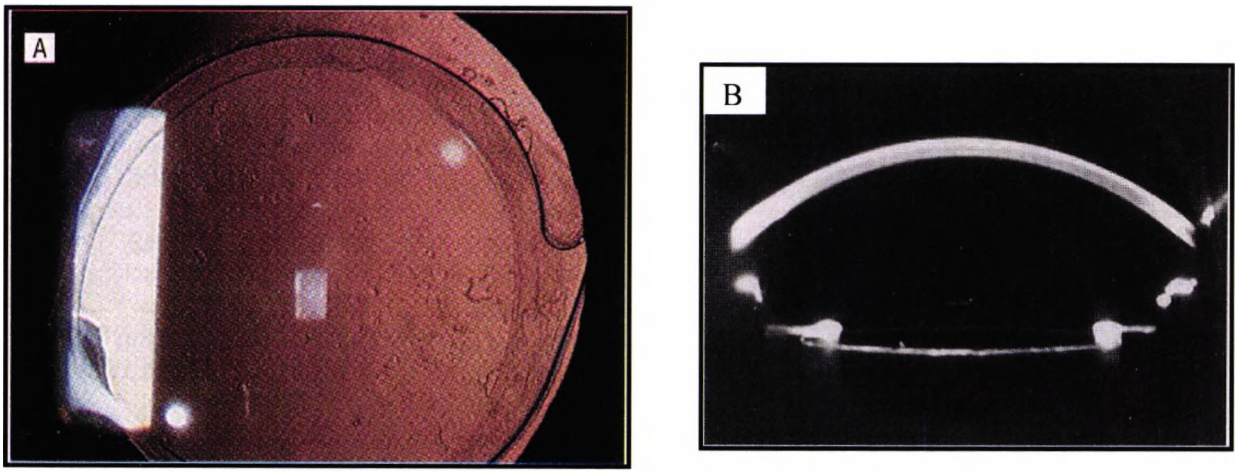

Figure 3.14 Two images captured using the EAS-1000 system, (A) retro-illumination image of the posterior capsule (B) Scheimpflug image (Hayashi et al. 1998b).

3.9.2.2 Retro-Illumination systems

Pande et al. (1997) developed a high-resolution digital retroillumination imaging system. It uses coaxial illumination and imaging based on Zeiss® components with a digital camera directly linked to a computer for online image verification and image analysis. The system produces high-resolution digital retro-illumination images of the posterior capsule; 8-bit image (256 shades of gray) at a resolution of 1512 × 1024 pixels. These images provide objective documentation of PCO and allow quantitative measurements. However, the system produces digital images that are inevitably affected by the central Purkinje reflection as seen in figure (3.15) that cannot be removed by a filter, and which prevents analysis of the central area of the posterior capsule. Recently, the system was modified by installing image processing software to blank off Purkinje reflections prior to enhancing the image contrast by "mean filtering". In this method smooth area that might still be opaque (such as fibrosis) could end up with a texture similar to transparent

areas since texture is the main feature used to define PCO. Secondly, the image is classified into areas that are either opaque or transparent. Finally, algorithms are used to group together classes that correspond to opaque areas and classes that correspond to transparent areas of the image, and calculate the percentage area of PCO based on the number of opaque pixels (Barman et al. 2000).

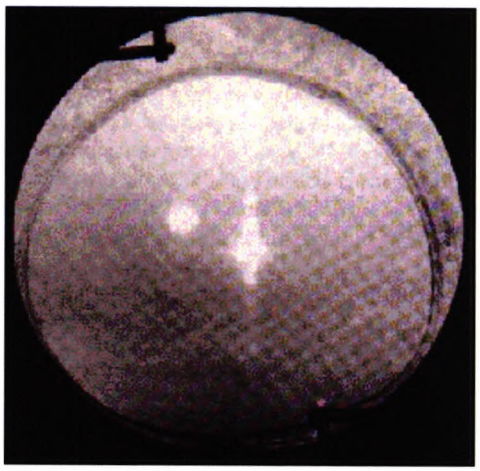

Figure 3.15 An image of posterior capsule opacification captured by a high-resolution digital retro-illumination system. This image shows that the central area of the posterior capsule is inevitably affected by a central Purkinje reflection (Pande et al. 1997).

This system is objective. Nevertheless it requires a specialised digital retroillumination system, and extensive image processing and manipulation. To remove the Purkinje reflections obstacle image segmentation software was used based on intensity values of the image. However, data beneath these central Purkinje reflections are lost (Aslam et al. 2002).

Friedman et al. (1999) developed and validated an automated digital retroillumination system that used a digital camera mounted on a slit lamp incorporating cross-polarised illumination to suppress the corneal reflex. The system uses an automated analysis algorithm to calculate the percentage of area covered by opacity and assigns a gray level for each unit of areas. The gray levels are weighted by the area covered at each level and an average is calculated. The areas of opacification are identified by a threshold. However, the cross-polarisation produces a distinct Maltese cross illumination artefact in the image.

Wang et al. (2000) used the anterior eye segment analysis system EAS-1000 to capture retro-illumination images of PCO. The system uses the brightness of different points on the digital image and graded it from 0 to 255 brightness units. The computer threshold is set to 167 and the percentage level of transparency in a particular area is calculated thus any pixel above this value is considered transparent area and any value below it is considered opaque. The system is objective considering that there is no subjective grading of posterior capsule. Nevertheless, using a fixed, discrete point indicates that there are some areas of dense fibrosis or pearling formation which are not covered by the analysis, and using a fixed threshold for analysis might not be appropriate for use with images having different luminance.

Buehl et al. (2001) developed the Automated Quantification of After-Cataract system using digital coaxial retroillumination photography (DCRP). It consists of a Zeiss 30 slitlamp, a Zeiss retrolux illumination module and digital camera (Kodak NC2000). The AQUA software is used to assess PCO using texture analysis. It calculates the inhomogeneity of the texture of the PCO image using the gray level co-occurrence matrix (GLCM) of the bitmap. Recently Buehl et al. introduced fusion software to overcome the Purkinje

reflections of digital retroillumination images by taking a series of images for the same eye for different directions of fixation. This allows the area covered by the Purkinje reflections to be replaced by the corresponding Purkinje reflection free area from another image. The system is objective; however the fusion process is less reliable when the Purkinje reflections are large in size (Findl et al. 2003).

The most recently developed system is POCO-Man by Bender, (2001). This system was developed at St. Thomas' Hospital and Kings' College in London. It uses software that places a grid over the digital image and the user can identify the areas of PCO and software automatically calculates the percentage of area of opacity. The system is not complicated, but not objective. Camparini et al. (2000) found that the use of only retroillumination images may significantly underestimate the presence and severity of PCO when compared to reflected light images.

Findl et al. (2003) conducted a comparison of three quantitative methods: Automated Quantification of After-Cataract (AQUA), Evaluation of Posterior Capsule Opacification (EPCO), POCO-Man, and subjective grading performed by four experienced and four inexperienced student examiners. To grade all the images that are displayed on a computer screen using a score of 0 to 10 in 0.5 steps at one session. The images were taken by the high resolution digital coaxial retroillumination system similar to the system reported by Pande et al. (1997) and Buehl et al. (2002). Results demonstrated that the objective automated AQUA score correlated well with subjective scoring and the EPCO technique. The POCO technique did not adequately describe PCO intensity since it results in a percentage of the pupil area. The subjective grading results showed no significant differences between experienced and in experienced examiners.

CHAPTER FOUR

4. Standardization of the digital imaging system

4.1 Introduction

The main aim of this study is to create a digital imaging system to document, identify and quantify posterior capsule opacification objectively. This involves capturing digital images of the lens posterior capsule using a modified slit lamp then processing and analysing the area of interest, to derive objective measures of PCO.

Several attempts have been made to develop a digital, fully automated, objective system to measure and quantify PCO. These systems have either used the Scheimpflug or the retroillumination techniques. Methods require custom built or modified equipment and commonly use computationally expensive software that requires considerable manual input either to enhance the image or to remove unavoidable Purkinje reflexes. A full review of these techniques has been given in chapter 3.

4.2 Optimal digital images of posterior capsule opacification

4.2.1 Introduction

In order to achieve the main goal of this research there were several variables that needed to be investigated in order to demonstrate that such a system could be established. The system had to be capable of producing repeatable and reproducible high quality digital images of the posterior capsule to enable objective documentation, identification and quantification of posterior

capsule opacification.

4.3 Experimental setup

4.3.1 Digital imaging system

The system consists of a digital camera module (Kodak DCS100), which uses a Nikon F3 body and back with a CCD array of 1.3 million pixels. The array measures 16.4 × 20.5mm, and is 1280 pixels wide by 1024 pixels high. These pixels are sensitive to red, green and blue wavelengths, where the green pixels amount to 75% of the total array, and both blue and red 12.5% each. The arrangement of red, green and blue pixels on the CCD array of the Kodak DCS 100 camera is shown in figure (4.1). Note that the pixel arrangement used on the DCS 100 has been superseded by a 'Bayer' pixel arrangement on newer Kodak digital cameras (Owen, 1998).

The DCS100 was mounted on a Nikon FS-2 photo slit-lamp without modification and was attached by an umbilical cable to a digital storage unit (DSU) in order to save the captured images. The DSU is a 200 megabytes (MB) recorder capable of storing 156 uncompressed images. It contains a monochrome liquid crystal display (LCD) allowing immediate viewing of the images. However, the image quality on the LCD was very poor, so the digital storage unit was connected to an external video monitor, thereby allowing the images to be screened and then deleted if required.

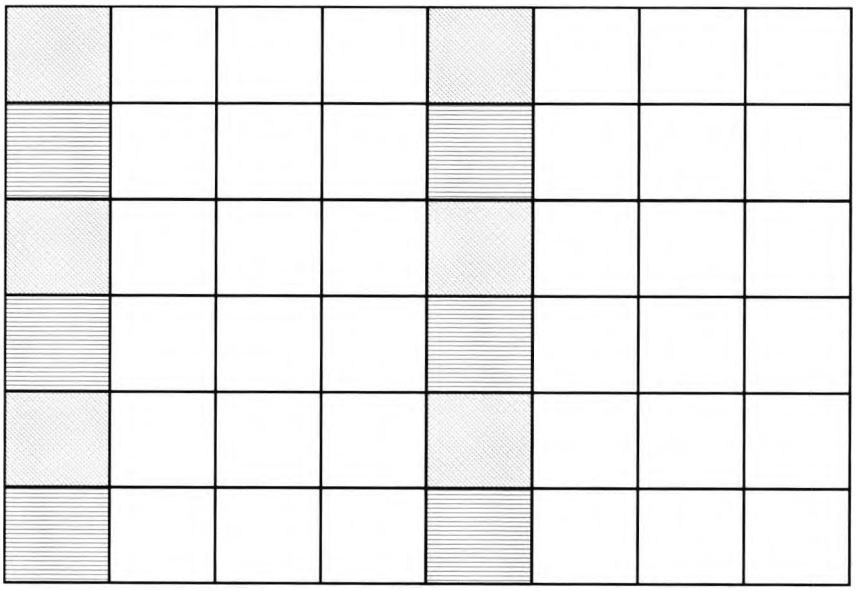

Figure 4.1 Spatial arrangement of red, green and blue pixels in the CCD array of the DCS 100 camera. Green pixels (unfilled squares) occupy 75% of the array, red pixels (diagonal lines) and blue pixels (horizontal lines) both occupy 12.5% of the array respectively.

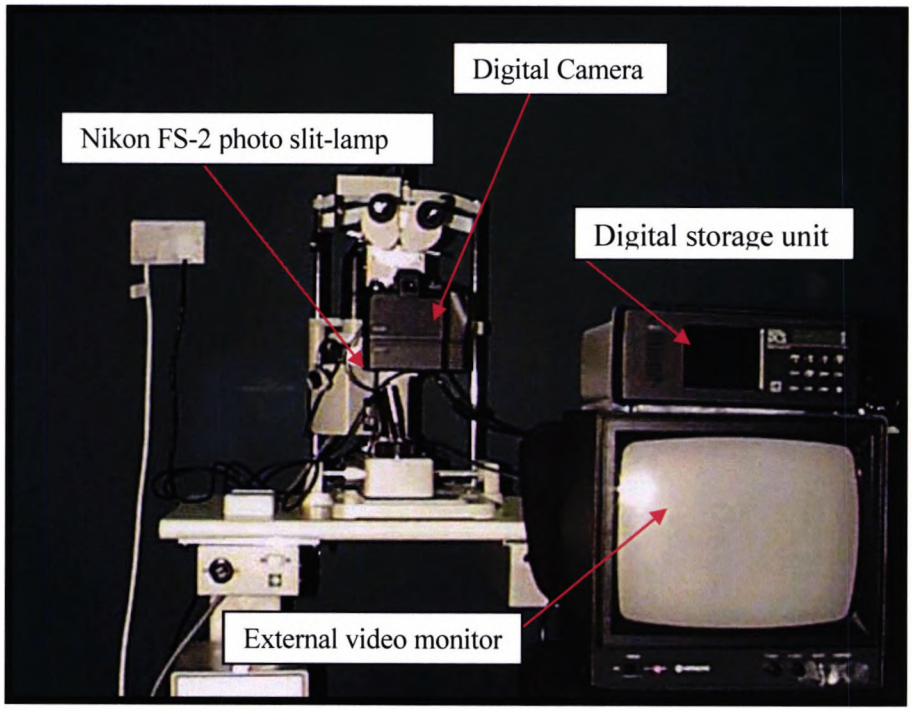

Figure 4.2 Major components of the digital imaging system developed in this study.

The slit lamp height and the chin rest were adjusted until the subject was seated comfortably behind the slit lamp with their chin placed firmly on the chin rest and forehead against the headrest. Before the images were taken, all the procedures were explained to the subject, and the subject was instructed to look straight ahead. The examination room's lighting was reduced to minimize any corneal reflex artefacts. The examiner then adjusted the slit lamp to focus on the posterior capsule by placing the slit lamp illumination at the edge of the dilated pupil. This avoids any excessive illumination of the iris, as recommended in a previous study by (Freidman et al. 1999).

4.3.2 Subjects

The subjects were volunteers recruited from the Royal Eye Unit at Kingston Hospital, following uncomplicated cataract surgery for age-related cataract with posterior chamber intraocular lens implants. All subjects were healthy and attending a clinic prior to Nd:YAG laser capsulotomy. The images of PCO were captured through a dilated pupil (one drop of tropicamide 1%). In addition, systemic and ocular histories were taken to exclude diabetic and glaucoma subjects from the study. All sections of this study have been subject to a review by Research and Ethical Committee. Informed consent was obtained from all patients included in the trial. All procedures followed the tenets of the Declaration of Helsinki.

4.3.3 Camera exposure settings

The user's manual supplied with the Kodak digital camera (DCS100) recommended that for a high quality image the film speed (ISO) should be set to 200 for both the camera and DSU. This setting has also been recommended in a previous study (Tetz et al. 1997). However if the lighting level is low it is recommended that the camera film speed be set to 1600 and the DSU film speed be set to 800. Therefore, the following settings were tested for the camera and the DSU respectively: 200/200, and 1600/800. For each setting the camera exposure compensation was varied from 0, +1, and +2 whilst keeping the other parameters constant to determine the optimal exposure settings.

4.3.4 Slit-Lamp Settings

The slit beam widths tested were 2mm, 2.50mm, 3mm and 3.50mm, in order to determine which covered the largest area of the posterior capsule without getting unwanted reflexes in the area of interest. Furthermore, the angle of the slit beam was tested at angles of; 30°, 35°, 40°, 45°, 50° and 60°, with the angle of the microscope system locked on zero. This was to determine which angle provided a better view of the central area of the posterior capsule, without introducing a corneal reflex into the measurement area. For all measurements the magnification of the slit lamp was fixed at 25X. A lower magnification, such as 16X, produces a smaller image of the opacity at lower resolution; whereas at a higher magnification, 48X, the edge of the pupil was not visible. The edge of the pupil was used to determine the pupil centre and hence this was an important consideration. The flash intensity was tested using three settings: level 1, 2, and 3.

4.4 Results

4.4.1 Subjects

Fourteen eyes of fourteen patients with posterior capsule opacification following uncomplicated cataract extraction with posterior chamber intraocular lens implants were included. The mean age was 80.71 ± 7.17 years (mean ± SD) for all subjects, with a range of 63 to 90 years, and the subjects included 5 men and 9 women. Table (4.1) shows the subjects' demographic details, according to posterior capsule opacification morphological types.

Characteristic of Subjects	Posterior capsule opacification Types		
	Fibrotic (n=8)	Pearl (n=4)	Mixed (n=2)
Age of subjects (Mean ± SD)	81.63 ± 4.21	82.25 ± 8.1	74 ± 15.56
Gender (F / M)	6 / 2	3 / 1	0 / 2

Table 4.1 Subjects' details.

A form was given to an experienced ophthalmologist that contained two visual analogue scales (VAS) (5cm long) for each presented image of PCO shown on the computer screen. The first VAS scale was used to grade severity, and the second used to grade the confidence of morphological classification of PCO within the central area of interest of all the images according to their three basic types. Table 4.2 shows the subjective classification of PCO morphologically, confidence and severity grading for each subject.

Subjects	Morphological classification	Morphological confidence grading (1-5)	Severity grading (1-5)
1	Fibrotic	2	1.2
2	Fibrotic	3.5	3
3	Fibrotic	4	3.8
4	Fibrotic	3.5	3.3
5	Pearl	4	3.8
6	Pearl	3	2.5
7	Pearl	4	3
8	Mixed	2.5	2.8
9	Fibrotic	3	3
10	Mixed	2.5	2.3
11	Fibrotic	3	2.4
12	Pearl	3.5	3
13	Fibrotic	4.3	4.5
14	Fibrotic	4	3.7

Table 4.2 Subjective classification of PCO morphology with associated confidence level and severity of posterior capsule opacification.

The subjects had received the following intraocular lens implants in the capsular bag: Allergen Medical Optic (AMO) IOL types S130NB silicone (2 out of 14 eyes; 14.3%), S140NB (2 out of 14 eyes; 14.3%), PS53ANB (3 out of 14 eyes 21.4%), PS26TB (1 out of 14 eyes 7.1%), and Bausch & Lomb silicone Soflex2 (5 out of 14 eyes; 35.7%), Storz (1 out of 14 eyes 7.1%).

The details of the IOLs received by the subjects recruited in this study are summarized in table 4.4. Table 4.3 shows the time interval between cataract surgery and Nd:YAG laser capsulotomy according to implanted IOL types.

IOLs	PS53ANB (N=3)	SI30NB (N=2)	S140NB (N=2)	Sofles2 (N=5)	PS26TB (N=1)	Storz (N=1)
Interval between surgery and Nd:YAG laser capsulotomy (months)	46 ± 12.49	42 ± 8.48	25.5± 14.85	15.4± 11.76	36 months	84 months

Table 4.3 The time Interval between cataract surgery and Nd:YAG laser capsulotomy in months (Mean ± standard deviation (SD)).

IOL Characteristic	Allergen medical optic (AMO)				Bausch & Lomb	Storz
Model	SI-30NB	SI-40NB	PS53NB	PS26TB	SOFLEX2	----------
OM	3piece Silicone	3piece Silicone	*	3piece Silicone	3piece Silicone	1 piece Hydrogel
RI	1.46	1.46	*	*	1.43	1.475
OC	Biconvex	Biconvex	*	*	Biconvex	Biconvex
OD (mm)	6mm	6mm	5mm	7mm	6mm	6mm
OL (mm)	12.5-13mm	12.5-13mm	12.5mm	14mm	12.5-13mm	12mm
WC	<1%	<1%	<1%	*	<1%	17.8%
HM	Polypropylene	PMMA	*	*	PMMA, blue	PMMA
HC	10degree	10degree	*	Modified C	0 angulation	10° Modified C

Table 4.4 Characteristics of the intraocular lenses (IOLs) that have been implanted in the subjects' eyes; (OM) optic material, (RI) refractive index, (OC) optic configuration, (OD) optic diameter, (OL) overall length, (WC) Water content, (HM) haptic material, and (HC) haptic configuration. (* data not available) (Apple et al. 2000h).

4.4.2 Exposure Settings

4.4.3 Setting the angle of illumination of the system

Images with different angles of illumination, such as 30°, and 35° reveal that the central area of the posterior capsule lies between two reflexes produced by the cornea and the IOL (highlighted by a red circle at the nine o'clock position) (fig. 4.3 A & B). The central area is clearly affected by the two reflections producing uneven background illumination. Increasing the illumination angle by 5° the distance between the two reflexes increases hence reducing the effect of the reflexes on the central area of interest as seen in figure (4.3 C & D).

Comparing the images produced with a 40° and 45° slit angle shows that the corneal reflex lies far from the central area of interest of the posterior capsule, producing an image with a uniform illumination as seen in figure (4.3.C & D). These images also illustrate that the width of the illuminated central area of the posterior capsule is larger with a 45° slit angle than 40°. The width of the illuminated area produced by 45° is 4.95mm, whilst the width of illuminated area produce by 40° is 4.3mm. This is due to the angle of illumination because the width of illuminated area is equal to the beam width / cos θ° as illustrated in figure (4.4).

Images produced with a 50° and 60° slit beam angle demonstrate that the central area of the posterior capsule is not affected by corneal reflexes. However, the images appear very dim and fine details are lost, especially in the central area of the posterior capsule. This is because most of the light reflected back by the iris, thus the amount of light is entering the eye is not sufficient to illuminate the central area of the posterior capsule (fig. 4.5); the

temporal and central area appear in shadow whilst the nasal side of the image is illuminated as seen in figure (4.3 E & F). Our findings are supported by other studies (Brown et al. 1972, 1988, Kawara et al. 1980, AREDS 2001b, Camparini et al. 2000).

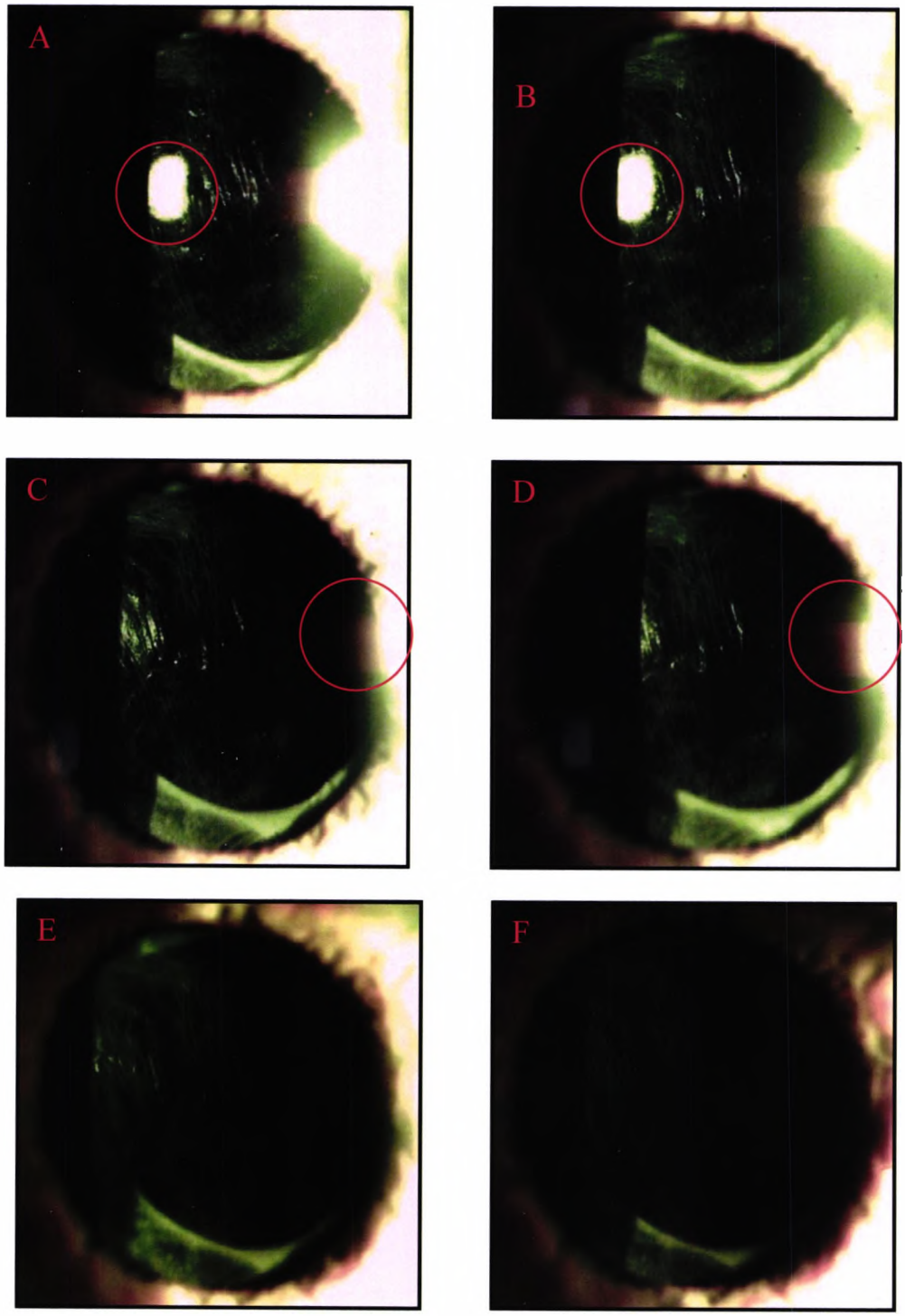

Figure 4.3 Images captured with different illumination angles (A) 30°, (B) 35°, (C) 40°, (D) 45°, (E) 50°, and (F) 60°. Other settings were a slit beam width of 3.50mm, film speed for camera 1600 and DSU 800, exposure compensation 0, flash intensity 2, and magnification 25X.

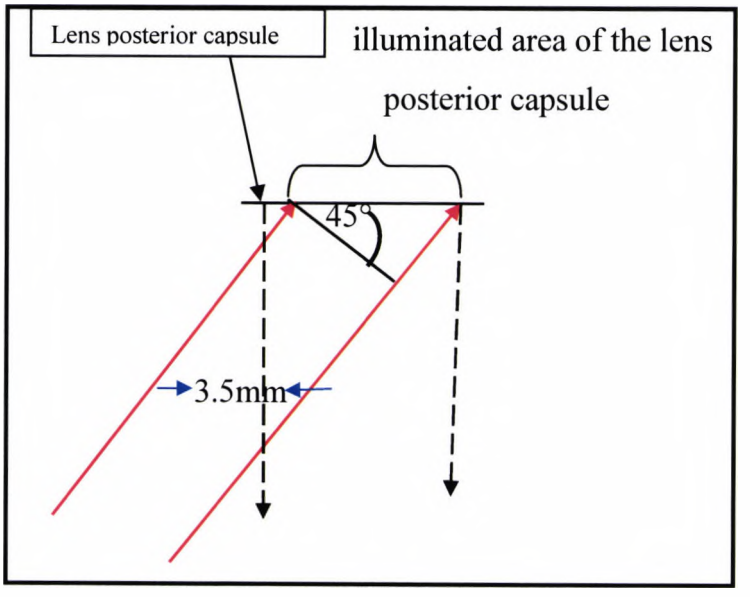

Figure 4.4 Optical diagram illustrating that a larger area of the lens posterior capsule is illuminated at oblique slit angles.

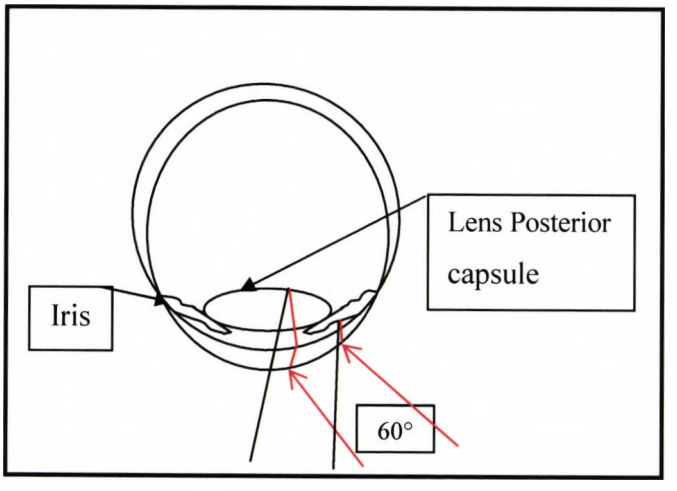

Figure 4.5 Optical diagram illustrating why the central area of the posterior capsule appears very dim resulting in the loss of the fine detail of the opacity at slit angles greater than 45°. This is because most of the light that enters the eye is reflected by the iris thus producing a poor quality image of the lens posterior capsule.

4.4.5 Setting the slit beam width

Images were captured with beam widths varying from 2mm to 3.50mm in 0.5mm steps. These images reveal that the 2mm beam width covers a relatively narrow region of the posterior capsule 2.8mm wide figure (4.6.A). Images captured with beam widths of 2.50mm and 3mm produce wider illuminated regions of 3.50mm and 4.24mm width respectively (fig. 4.6. B & C). Comparing these images to the 2.5mm beam width image reveals that although opacity could be seen within a central area of interest (3mm diameter circle) especially with severe PCO where the central area of the posterior capsule is affected by the opacity, there was less information about peripheral areas (fig. 4.7). Also, for mild opacification a 2.5mm beam width provides less information about PCO types and progress as seen in (fig. 4.6.B). Since posterior capsule opacification normally starts to develop at the periphery and progressess towards the centre, the largest extent possible of the posterior capsule should be imaged to detect changes at the earliest time as seen in figure (4.6.D). The ideal beam width is therefore 3.50mm since it covers the largest area of the posterior capsule and therefore provides information about the progress and type of opacity on the posterior capsule as seen in figure (4.6.D).

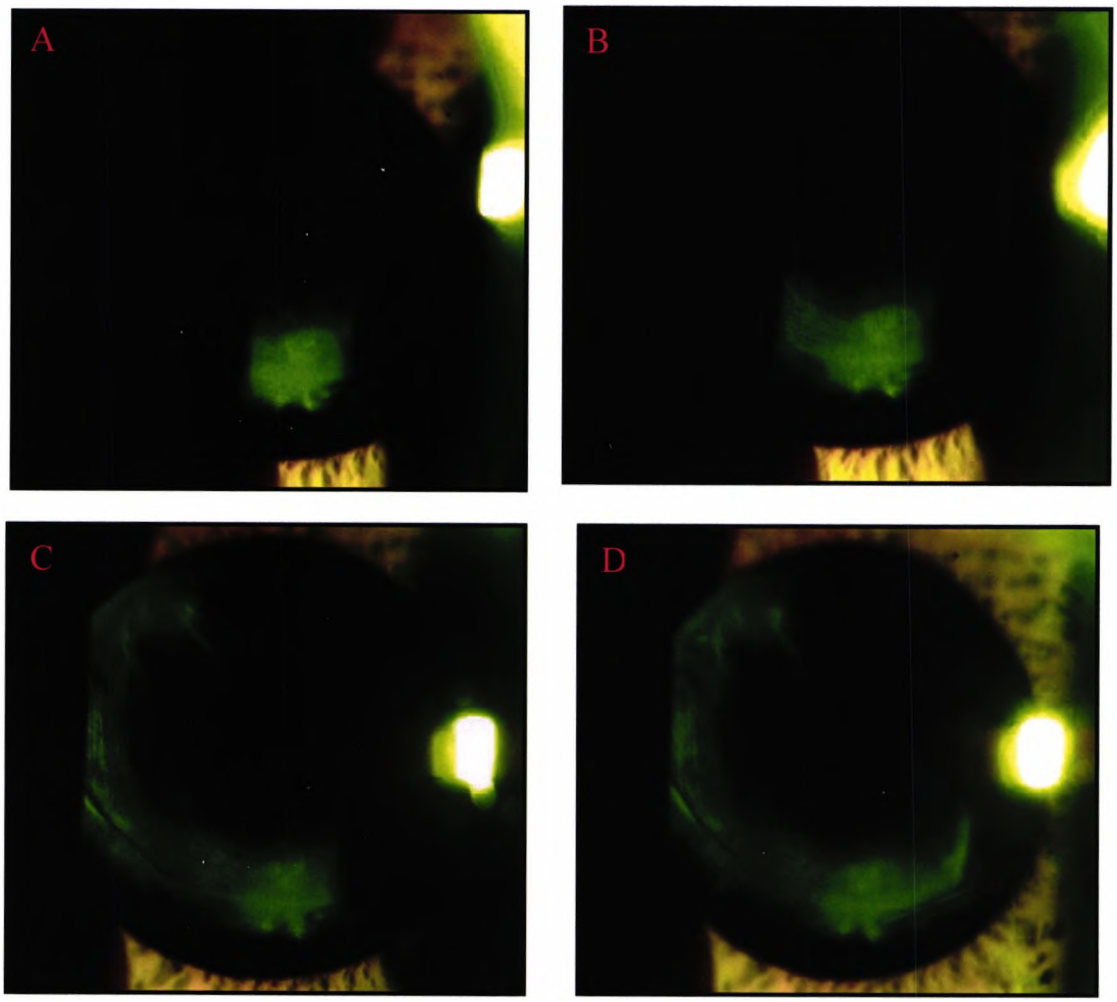

Figure 4.6 Variations in slit beam width (A) 2mm, (B) 2.50mm, (C) 3mm, and (D) 3.50mm. The resulting images, A to D, are images from the same subject. Other settings were: angle of illumination at 45°, film speed for camera 1600 and DSU 800, flash intensity 2, exposure compensation 0, and magnification 25X.

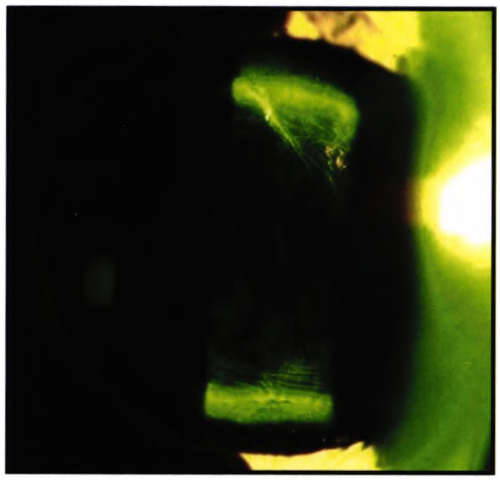

Figure 4.7 Image shows that the 2.5mm slit beam width could cover the AOI and provide information about the type of PCO but only in the central area of the capsule. Other settings were: angle of illumination at 45°, film speed for camera 1600 and DSU 800, flash intensity 2, exposure compensation 0, and magnification 25X.

4.4.6 Setting the digital camera exposure compensation and slit lamp flash intensity

Images were captured using slit lamp flash intensities of 1, 2 and 3 with digital camera exposure compensation values of 0, +1 and +2. The other parameters were kept constant (slit beam width 3.50mm, angle of illumination 45°, film speed for both camera 1600 and DSU 800, and magnification 25X). In an initial study images were captured with the following settings: camera exposure compensation values 0, +1 and +2 while the other parameters were kept constant (2.5mm beam width, angle of illumination 45°, film speed for cameras 1600 and DSU 800, flash intensity 2, and magnification 25X). Comparing these images reveals that exposure compensation 0 produced clear and fine details of the opacity compared to images captured with exposure compensation values of +1 and +2 especially

at the six o'clock position. Also, the quality of the images and fine details decreases as the exposure compensation increases as seen in (fig. 4.8. A, B & C).

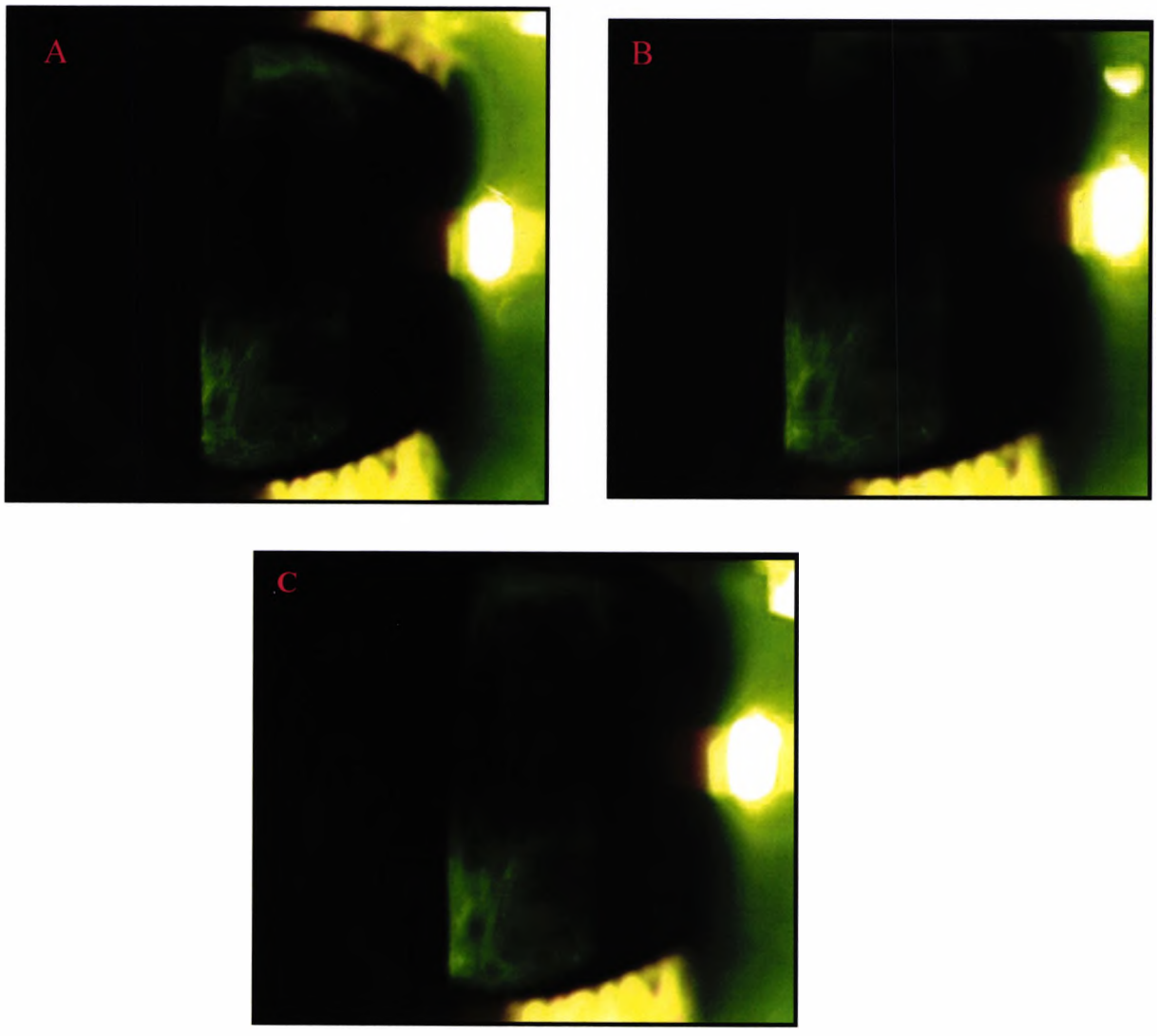

Figure 4.8 (A, B and C) Images captured from the same subject using slit lamp flash intensity 2 with exposure compensation settings (A) 0, (B) +1, (C) +2. (Slit beam width 3mm, angle of illumination 45°, film speed for camera 1600 and the DSU 800, and magnification 25X).

In subsequent work images were captured with the following settings to test this effect: slit lamp flash intensity 1, 2 and 3 with different camera exposure compensation values of 0, +1 and +2 while the other parameters were kept constant (3.5mm beam width, angle of illumination 45°, film speed for cameras 1600 and DSU 800, flash intensity 2, and magnification 25X). Figure 4.9. A, B, and C reveal dim, poor quality images and loss of fine details of all images due to the low level of flash intensity compare to those images that were captured using flash intensities 2 and 3. Comparison of the images captured using flash intensity 2 and 3 with exposure compensation values of +1, and +2 (fig. 4.10 A & B and fig. 4.10 C & D respectively) reveal that as the exposure compensation value increases the quality of the images is degraded.

Furthermore, comparing images captured using flash intensity 2 and 3 with exposure compensation 0 reveals that there is no significant difference between the images as seen in figure (4.11 A & B). Therefore the best exposure compensation for the camera is 0 with the flash intensity 2 for different types of PCO as documented in previous studies (Brown et al. 1988, Tetz et al. 1997, Camparini et al. 2000).

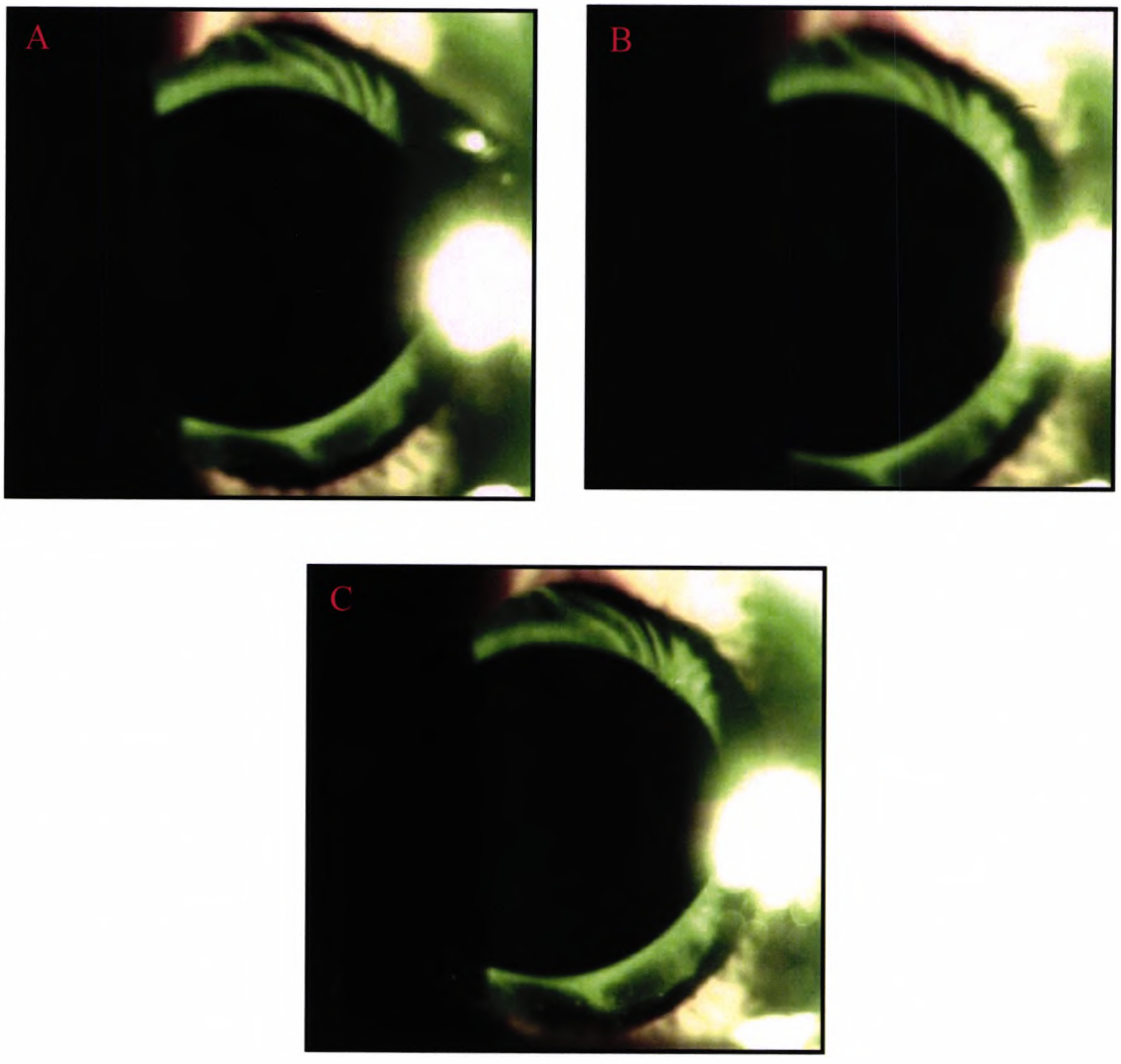

Figure 4.9 (A, B and C) Images captured from the same subject using slit lamp flash intensity 1 with digital camera exposure compensation settings of (A) 0, (B) +1 and (C) +2. (Slit beam width 3.50mm, angle of illumination 45°, film speed for camera 1600 and DSU 800, and magnification 25X).

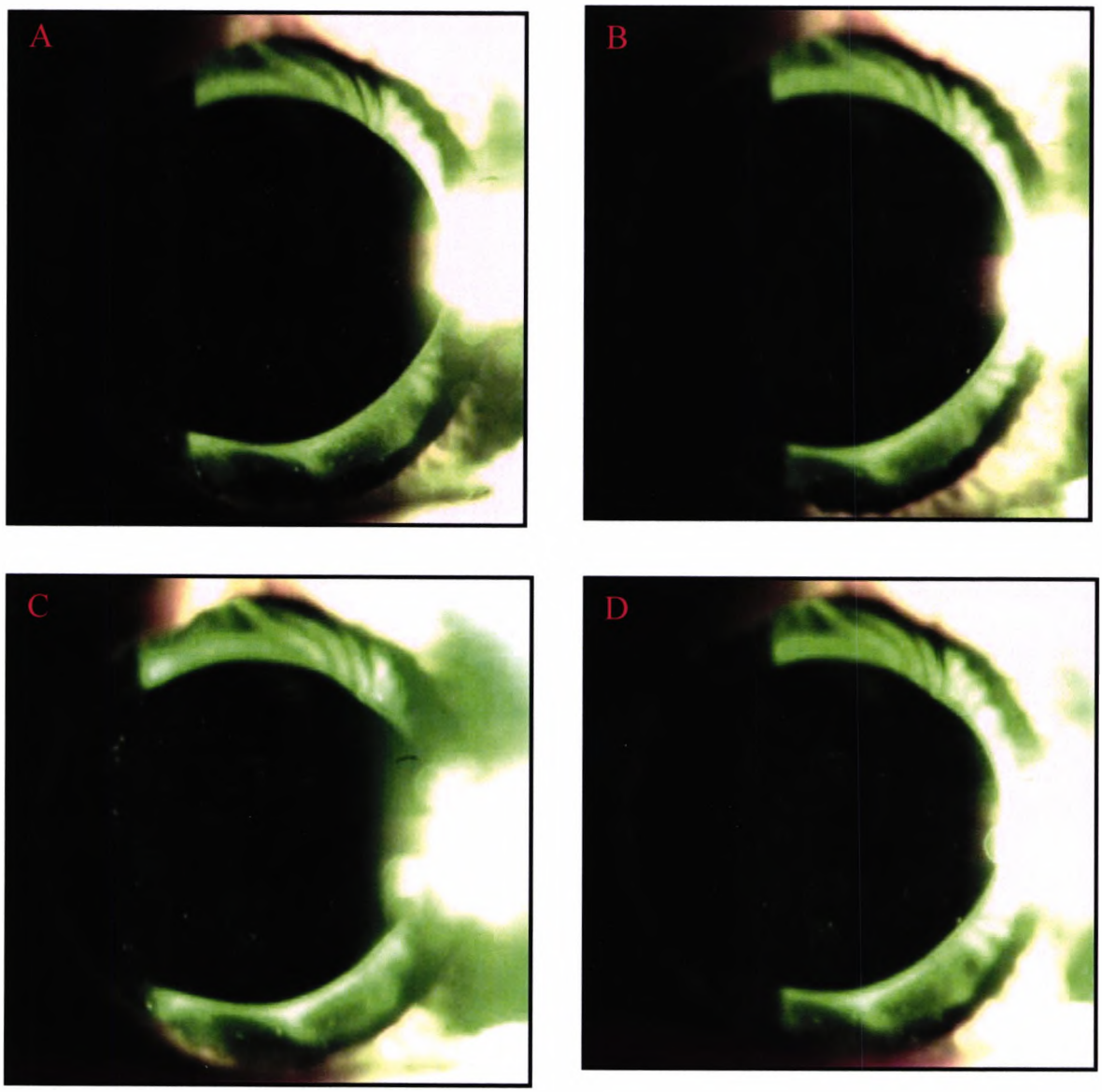

Figure 4.10 Images captured from the same subject using slit lamp flash intensity 2 with digital camera exposure compensation settings of (A) +1, (B) +2. Images using flash intensity 3 with digital camera exposure compensation settings of (C) +1, (D) +2 (slit beam width 3.50mm, angle of illumination 45°, film speed for camera 1600 and DSU 800, and magnification 25x).

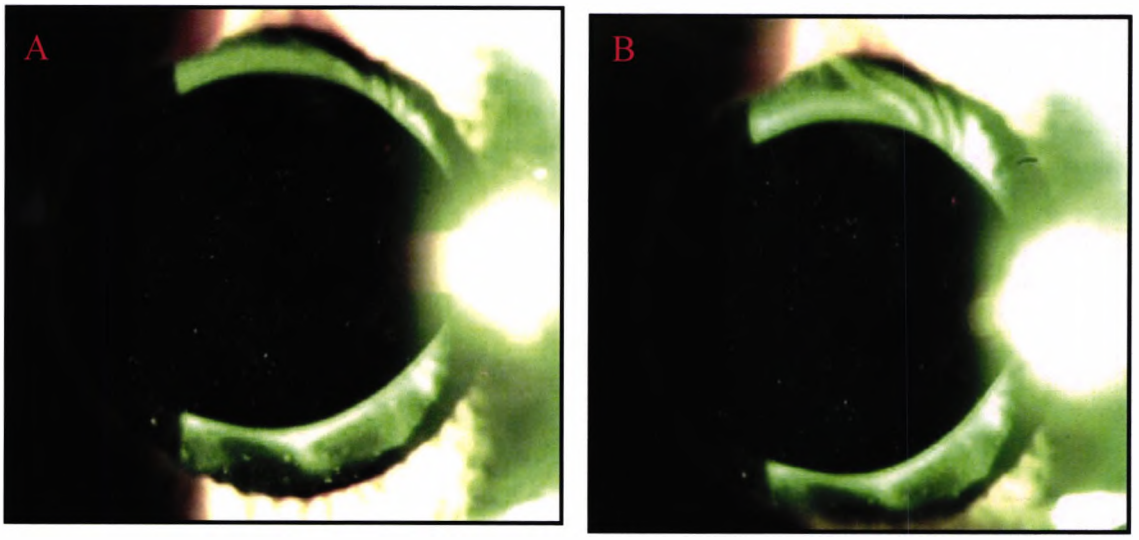

Figure 4.11 Images captured from the same subject using two different slit lamp flash intensities: (A) flash intensity 2 and camera exposure compensation 0. (B) flash intensity 3 and camera exposure compensation 0 (The slit beam width 3.50mm, angle of illumination 45°, film speed for camera 1600 and DSU 800, and magnification 25X).

4.5 The digital camera film speed settings and morphology of PCO types

4.5.1 Fibrotic PCO

Images of different types and severity of PCO were captured with two different film speed settings: (200/200 and 1600/800), while standardizing all the other settings: (Slit beam width 3.50mm, angle of illumination at 45°, flash intensity 2, exposure compensation 0, magnification 25X). Comparing the images captured for the same subjects revealed that for the images captured with film speed setting 200/200 the opacity appears dim and fine details are lost figure (4.12. A). Images captured with ISO 1600/800 appear

good quality, correctly exposed, and with uniform background illumination. The opacity appears as a white, homogeneous, thick sheet at six o'clock position, whilst at position 2 to 4 o'clock white fibrous filaments appear with fine details as seen in figure (4.12. B).

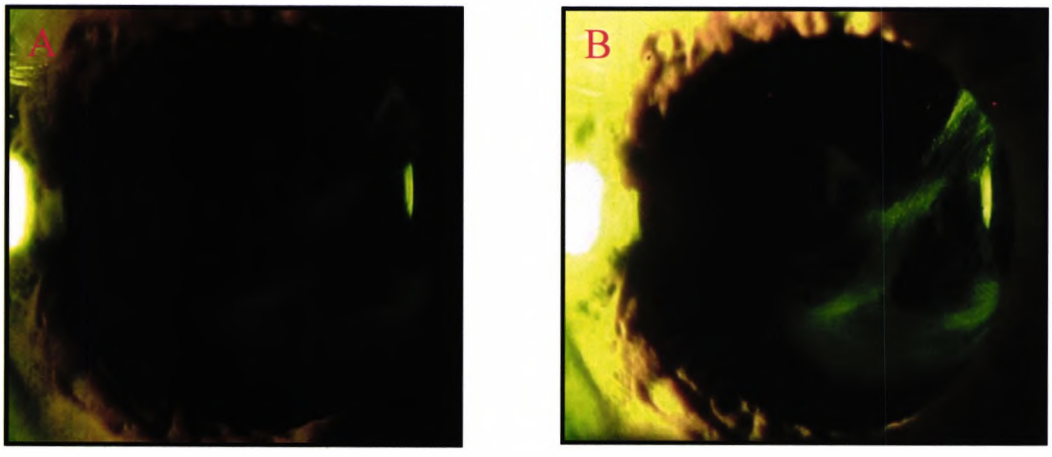

Figure 4.12 Images of fibrotic PCO for the same subject (severity graded as 3.5) with two different film speed settings: (A) film speed 200 for the camera and the DSU and (B) film speed for the camera of 1600 and 800 for the DSU. (Other settings were a slit beam width of 3mm, angle of illumination 45°, exposure compensation 0, flash intensity 2, and magnification 25X).

4.5.2 Pearl PCO

Pearl-type appears as heterogeneous, globular areas of mottling as seen in figure (4.13). Images show that the film speed setting for the camera 1600 and the DSU 800 produces optimal images with correct exposure compensation, uniform background illumination and reveal fine details of the heterogeneous textured opacity without being over-exposed as seen in figure (4.14. B). In comparison images captured with film speed 200 for the camera and the DSU do not show any fine detail of pearling PCO microstructure and

the opacity appears dim as seen in figure (4.14. A). This also applied to mixed PCO which is a combination of both fibrotic and pearl PCO as seen in figures (4.15 A & B).

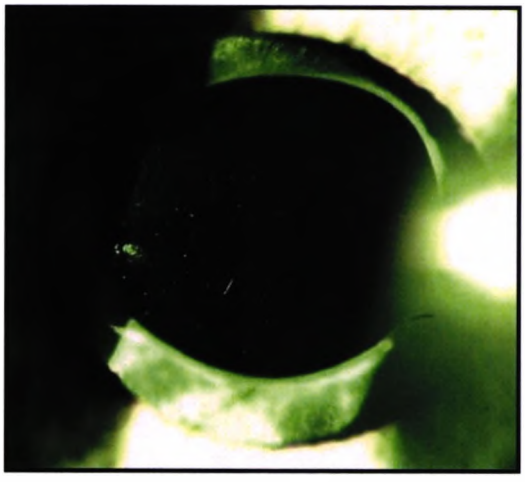

Figure 4.13 Image of pearl PCO (severity graded as 2.7). (Settings were slit beam width 3.50mm, angle of illumination 45°, film speed for the camera 1600 and the DSU 800 exposure compensation 0, flash intensity 2, and magnification 25X).

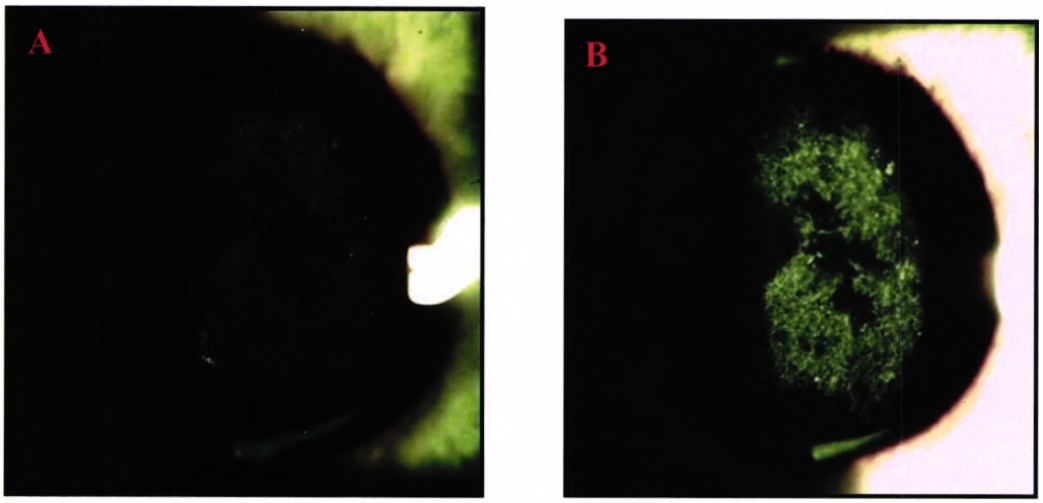

Figure 4.14 Images show pearl PCO for the same subject (severity graded as 4.2) with two different film speed settings: (A) film speed 200 for the camera and the DSU and (B) film speed for the camera 1600 and the DSU 800. (Other settings were a slit beam width 3mm, angle of illumination 45°, exposure compensation 0, flash intensity 2, and magnification 25X).

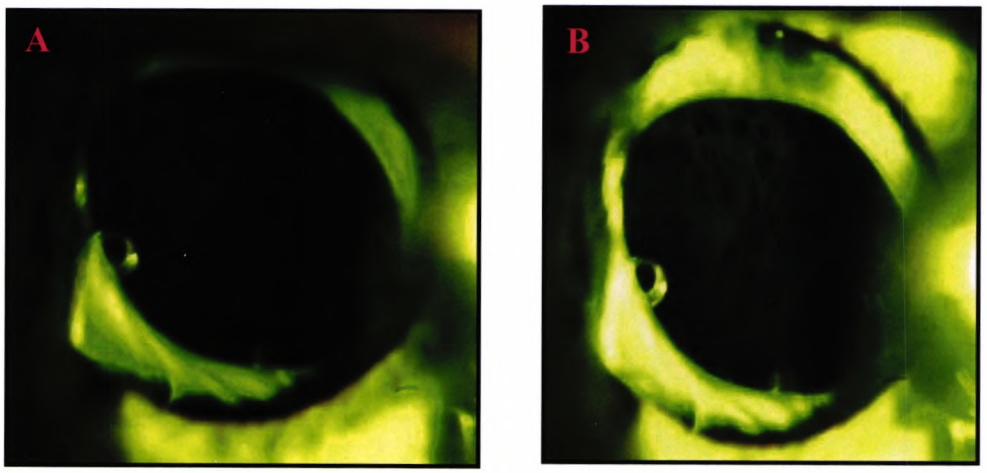

Figure 4.15 Images show mixed PCO for the same subject (severity graded as 2.8) with two different film speed settings: (A) film speed 200 for the camera and the DSU and (B) film speed for the camera of 1600 and the DSU 800. (Other settings were a slit beam width 3mm, angle of illumination 45°, exposure compensation 0, flash intensity 2, and magnification 25X).

4.6 Subject exclusion criteria

There are factors that may affect the quality of the images, such as diabetes mellitus due to uveitis, corneal scarring figure (4.16.A), vitreous clouding figure (4.16.B) and glaucoma as seen in figure (4.17). A dislocated IOL affects the images as seen in figure (4.18.A) as does a tilted IOL as seen in figure (4.18.B). Therefore subjects with such complications were excluded from this study. These exclusion criteria have been documented in previous studies (Pande et al. 1997, Camparini et al. 2000).

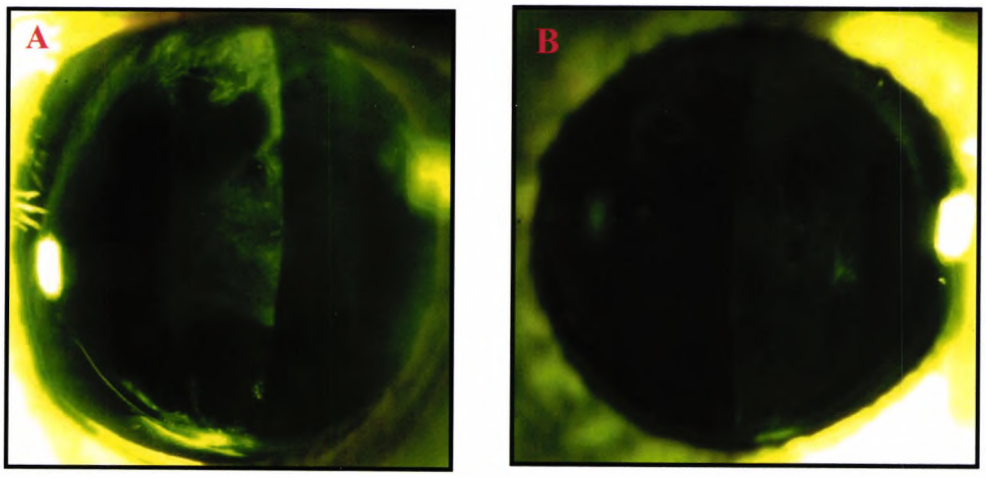

Figure 4.16 Images demonstrate that ocular media diseases such as (A) corneal opacity or scarring; and (B) vitreous clouding affect the quality of digital image.

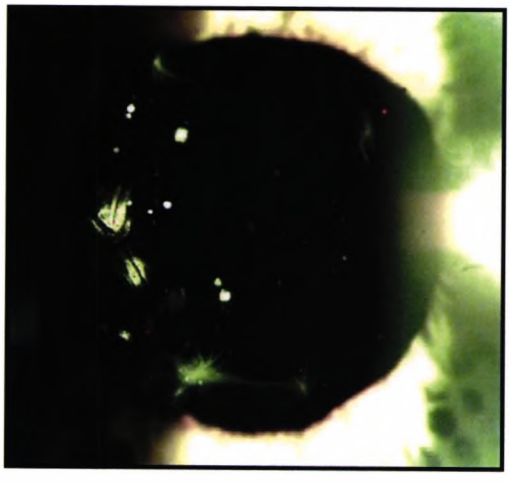

Figure 4.17 Image demonstrates that glaucoma affects the quality of the digital image.

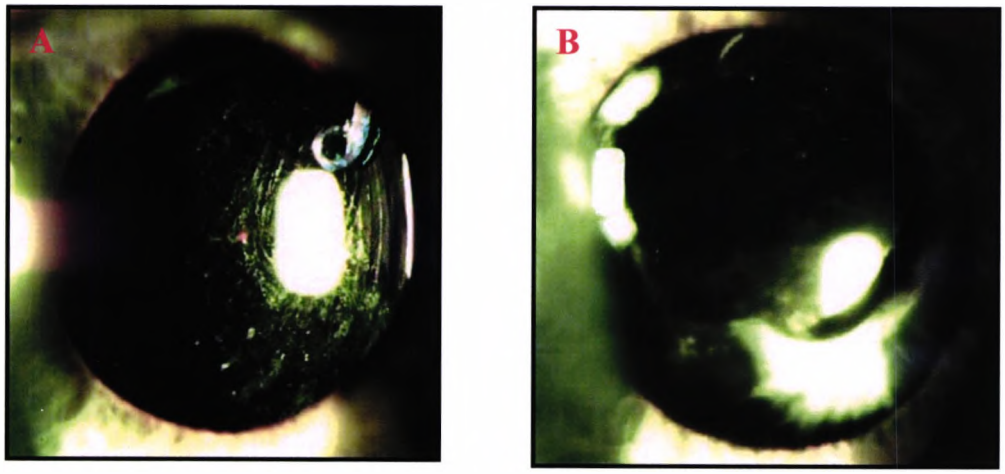

Figure 4.18 Images reveal that complications of IOLs such as (A) tilted IOL, and (B) dislocated IOL affect the quality of the digital image.

4.7 Discussion

The system is capable of consistently producing high quality images for different types of PCO using the following settings: 3.50mm beam width, angle of illumination 45°, film speed for camera 1600 and DSU 800, flash intensity 2, exposure compensation 0, and magnification 25X. This exposure setting is capable of detecting the presence of the three main types of PCO at different levels of severity according to subjective morphological classification, morphological confidence grading, and severity grading that was performed by an experienced ophthalmologist. The developed system is easy to setup, and does not require slit lamp modification or expensive software to enhance the images or remove inherited Purkinje reflections that affect the area to be analysed.

The results demonstrate that the ideal angle of illumination for the conventional technique is 45° between the illumination system and the microscope. At angles greater than 45° the iris obstructs most of the illumination that is required to illuminate the posterior capsule, thus images captured with 50° or 60° slit angles are degraded. This finding is supported by other studies (Kawara et al. 1980, Brown et al. 1972, 1988, AREDS, 2001b, Camparini et al. 2000). Also, our results demonstrated that at an angle of 45° a larger area of the posterior capsule is captured than those captured with angles at less than 45°. This is because images captured at angles of less than 45° produce a smaller central area lying between two specular reflections. The best beam width is 3.50mm because it allows the capturing of a larger area of the capsule hence providing more information about the PCO type and status of progress. This is important since PCO originates from the anterior capsule and equatorial lens bow. Our findings are supported by Camparini et al. (2000), although, AREDS (2001b) recommended using a 3mm beam.

The area of interest was defined as a 3mm central circle that coincides with the pupil centre. Previous studies have used the same size area to analyse their results (Camparini et al. 2000, Wang et al 2000). Camparini et al. (2000) reported that the magnification is best set at 16X. However our study shows that this magnification produces a smaller image of the opacity at a lower resolution. We conclude that the magnification is best set at 25X. Our results show that the camera exposure compensation is best set to zero, in order to produce consistent high quality images with fine details. Also, the flash intensity is best set at 2, again supported by previous studies (Brown et al. 1988, Tetz et al. 1997, Camparini et al. 2000).

The film speed of 1600 for the camera and 800 for the DSU results in optimal images showing good detail of the microstructures seen for different types of PCO at different levels of severity. For example, pearl type PCO is known for its heterogeneous, globular areas of mottling, whereas fibrotic PCO manifests itself in the early stages as white fibrous filaments, then progresses to a white, homogeneous, thick sheet of tissue. Mixed PCO is a combination of the two.

We believe that the settings of the slitlamp used in this study such as beam width, angle of illumination, flash intensity, and magnification could be used with another slitlamp. In support of this claim we note that the magnification used by Camparini et al is the only setting that is different from those found in this study although they subsequently magnify the photographic images (Camparini et al (2000)). However, the parameters of the camera such as film speed and exposure compensation may require modification.

Chapter Five

5. Fixation stimulus and imaging system validity

5.1 Introduction

Images that have been produced with the digital imaging system described in this thesis reveal that some are affected by Purkinje reflexes and this could be due to poor fixation. These Purkinje reflexes often encroach on the area of interest (fig. 5.1) and lead to uneven background illumination, which enhancement software cannot compensate for. Providing a fixation stimulus for the subject during image acquisition can help to reduce these artefacts.

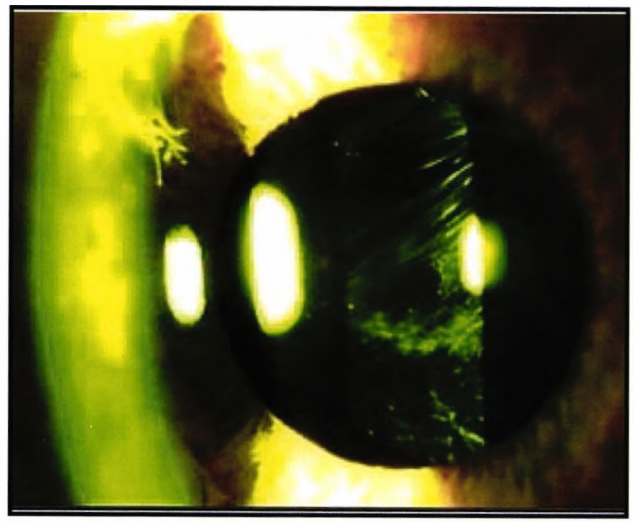

Figure 5.1 An image of the right eye captured in an earlier pilot study without a fixation stimulus using the following settings: slit beam width 2mm, 45° angle of illumination, film speed (ISO) for camera 1600 and DSU 800, exposure compensation 0, flash intensity 2, and magnification 25X.

Fixation stimuli currently in use can be divided into commercial fixation stimuli and those which are constructed purely to meet specific system designs. For example, the Eye Anterior System (EAS1000) (Hayashi et al. 1998 a, Wang et al. 2000, Saika et al. 2001) uses an internal fixation stimulus built into the system that coincides with the optical axis of the slit projection lens. This works by instructing the patient to fixate on the central LED while the observer moves the circle on the monitor screen into the red corneal reflex caused by the alignment light.

The most recently published study on subjective grading of photographic reflected light images of PCO used the AREDS fixation stimulus. This consists of two LEDs suspended through a ring that is fitted to the microscope system of the slit lamp. The LEDs are 1mm in diameter and the LED for the right eye is placed directly between the two viewing lenses whilst the LED for the left eye is mounted approximately 11mm to the right of the first LED (Camparini et al. 2000).

A pilot study was conducted to design a fixation stimulus for the digital imaging system that would help eliminate Purkinje reflexes caused by poor fixation. The pilot study went on to investigate the reliability of the fixation stimulus and repeatability of system acquisition.

5.2 Design of Fixation Stimulus - version (1)

A consideration when designing a fixation stimulus is the provision of simple, straight forward instructions for the subject to follow. This is particularly important here since all subjects are experiencing blurred vision due to mydriasis and the presence of PCO in one eye, whilst the other is occluded to avoid diplopia. Therefore, a central red light emitting diode (LED) was suspended by cable between the two viewing lenses of the slit lamp microscope system as documented in previous studies (Sparrow et al. 1990, AREDS, 2001b). In addition, four red light emitting diodes were fitted at the periphery of the ring and were tilted towards the centre of the fixation stimulus to produce a sharp specular reflection point on the cornea. This permits the examiner to assess subject fixation objectively through the position of the specular reflection of the four red LEDs, relative to the edge of the pupil (fig. 5.2).

The fifth central red light emitting diode measured 3.5mm in diameter and was mounted so that it lay directly between the two objective lenses of the slit lamp microscope. A control box allowed the LEDs to be switched on and off individually (fig. 5.3).

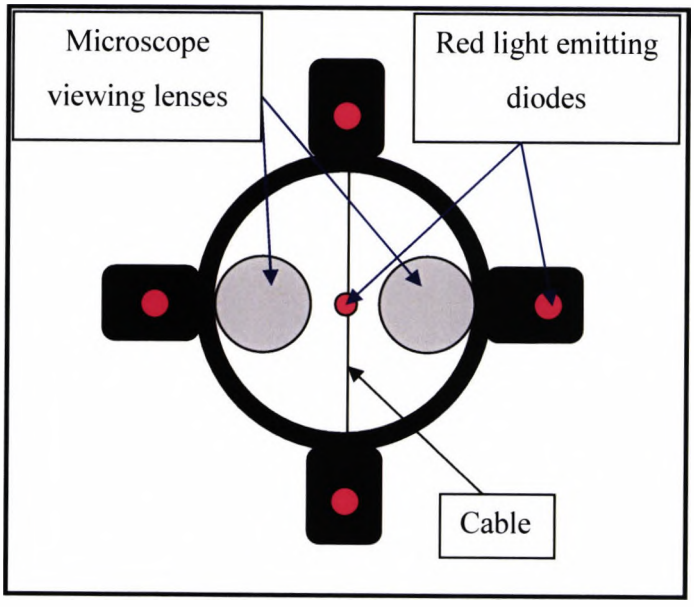

Figure 5.2 Design of the fixation stimulus version (1) consisting of four red LEDs at the periphery of the ring. The LEDs were tilted towards the centre, and a fifth LED was suspended by a cable between the two microscope objectives.

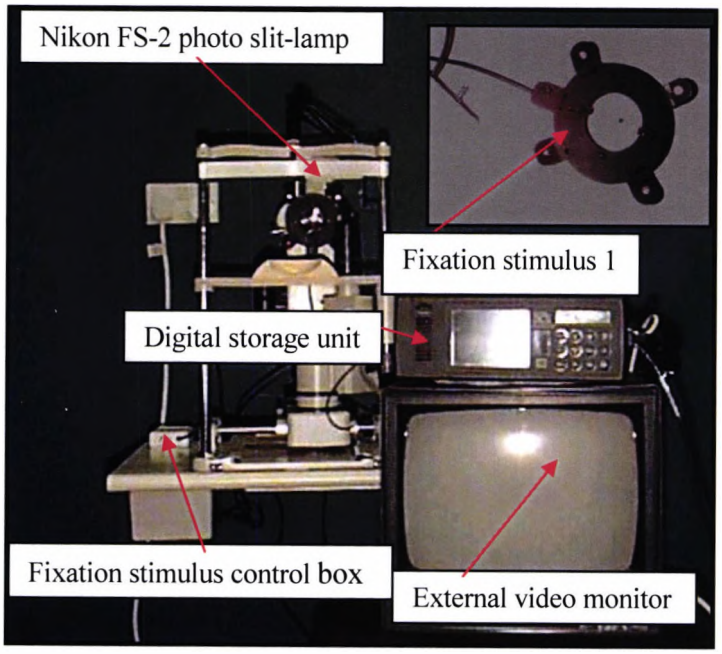

Figure 5.3 Image of the fixation stimulus version (1) insert, and attached to the slit lamp microscopic system with the control box to switch the LEDs on or off individually.

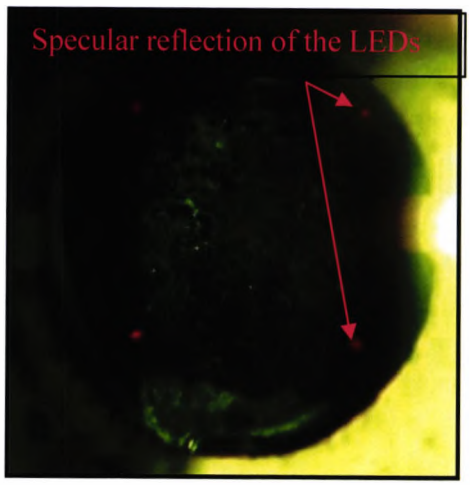

Figure 5.4 Image showing the specular reflection of four light emitting diodes on the border of the illuminated area of the posterior capsule, and the central fixation LED.

5.3 Materials and Methods

This part of the study comprised of 15 eyes of 15 subjects. Images of the posterior capsule of the eyes were taken using the Nikon FS-2 slit lamp with fixation stimulus version (1), and with the two following configurations: (1) slit beam width 3.5mm, 45° angle of illumination, film speed (ISO) for camera 1600 and DSU 800, exposure compensation 0, flash intensity 2, and magnification 25X; and (2) slit beam width 3.5mm, 45° angle of illumination, film speed for camera 200 and DSU 200, exposure compensation 0, flash intensity 2, and magnification 25X.

The subjects were all volunteers recruited from the Royal Eye Unit at Kingston Hospital. They had all had uncomplicated cataract surgery subsequent to age related cataract with posterior chamber intraocular lens implants. All subjects were healthy and attending a clinic prior to the Nd:YAG laser capsulotomy. The images of PCO were captured through a dilated pupil (one drop of tropicamide 1%).

The slit lamp height and the chin rest were adjusted until the subject was seated comfortably behind the slit lamp with their chin placed firmly on the chin rest and their forehead against the headrest. The fixation stimulus LED was on during image acquisition and the subject was instructed to fixate the central red LED and ignore the peripheral LEDs. The non-tested eye was occluded to avoid diplopia. The examination room lighting was reduced to minimise any further corneal reflex artefacts. To test the reliability of the fixation stimulus, the slit lamp microscope was focused on the posterior capsule plane. Four images were taken at the same session for each subject and with the same observer. The following two sets of settings were used for each subject: (1) slit beam width 3.5mm, 45° angle of illumination, film

speed for camera 1600 and DSU 800, exposure compensation 0, flash intensity 2, and magnification 25X; (2) slit beam width 3.5mm, 45° angle of illumination, film speed for camera 200 and DSU 200, exposure compensation 0, flash intensity 2, and magnification 25X.

The X and Y coordinates of the pupil centre and the specular reflection of the central LED were located using Image Pro+, and the distance between them ("the displacement") calculated. The values of the actual displacements for each subject should not differ widely if the fixation stimulus is maintaining subject fixation.

The *repeatability* of the image acquisition system was tested by taking 2 images at the same session with the same observer, and the same setting for each subject. The fixation stimulus version (1) was turned off just before the camera shutter was pressed in order to capture the image without the reflection of the central LED affecting the image. This has been documented in a previous study (Buehl et al. 2002). The following settings were used: slit beam width 3.5mm, 45° angle of illumination, film speed for camera 1600 and DSU 800, exposure compensation 0, flash intensity 2, and magnification 25X.

5.4 Image Processing

5.4.1 Spatial Scale Calibration

Images captured with the digital camera (DSC100) were saved to the digital storage unit (DSU) and then exported into the computer using a SCSI card and Aldus PhotoStyler version 1.1 (Aldus Corporation, Seattle, MD) software. The images were saved on the computer in a TIFF format. Image Pro+ version 4.5.1 (Media Cybernetic, Georgia Avenue, USA) software was then used for all image processing and analysis. The advantage of Image Pro+ software is that it has a spatial scale calibration option and is capable of expressing measurement of the image in a variety of terms such as millimetres or microns instead of pixels. However, for the purpose of this study the area of interest was defined in millimetres. Thus an image of a millimetre ruler was used with the same setting as the posterior capsule image to calibrate the measurement. The intensity calibration was set to grey levels ranging from 0 to 256 as recommended by Image Pro+ manual.

5.4.2 Defining the Area of Interest

The best-fit circle option in Image Pro+ was used to define the edge of the pupil. The number of point used to define a circle was set to 15 so that once the edge of the pupil is defined by 15 point a fixed circle defining the edge of the pupil is obtained. It is also possible to display in millimetres the measurements related to the best-fit circle such as the position of the central coordinate and the radius. Once the pupil has been defined, a circle is drawn by placing the cursor on the image and dragging it until it has a radius of 1.5mm. The centre of this circle is then adjusted, to coincide with the pupil centre. The measurements of all the features that have been defined on the

image are saved, so that they can be used again on the same image each time it is displayed. Finally, to isolate the area of interest (AOI) from the rest of the image, a circular AOI is superimposed on the 3mm diameter drawn circle. The circular AOI can be edited until it exactly fits the drawn circle. Defining the area of interest means that various image-processing commands such as histograms, save, etc will operate only upon the pixels within the AOI. The size of the AOI relates to the *image* of the posterior capsule viewed through the cornea and is not the actual anatomical dimension of the posterior capsule. In addition, the posterior capsule is curved. For typical parameters, the magnification is about 0.8x and the effect of the curvature is that an arc of length 3.004mm is projected on to a plane of length 3mm. This implies that the effects of corneal magnification and posterior capsule curvature are not large.

A review of the relevant literature reveals that different imaging systems have used various sizes of AOI. Hollick et al. (1999) used a 6mm diameter central area of the posterior capsule. This relatively large area was justified to compensate for the lost data caused by the inherited Purkinje reflection with the retroillumination technique. However, Hayashi et al. (1998a) used a 3mm central area of the posterior capsule, stating that this area corresponded to the visual function of the eye. The images captured with our system do have a high quality with uniform illumination and the central area of the posterior capsule is not affected by a Purkinje reflex, therefore, we decided to use a 3mm diameter circular area of the posterior capsule concentric with the pupil centre (fig. 5.5).

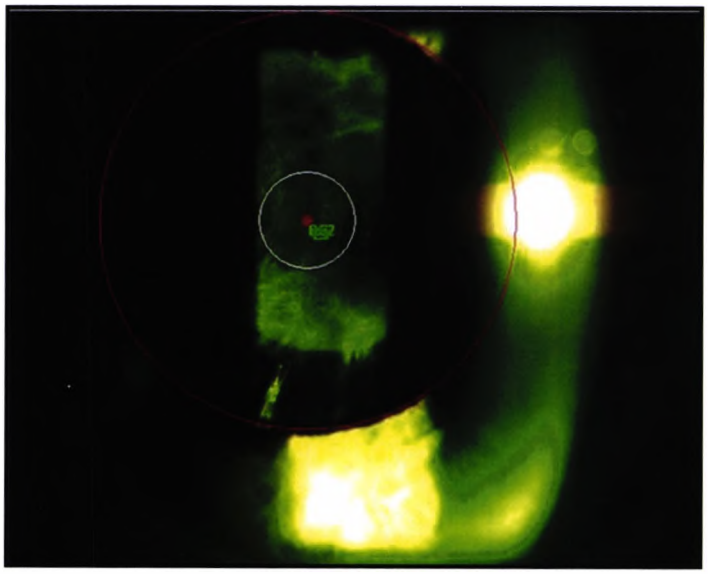

Figure 5.5 The central white circle represents a 3mm diameter AOI selected and fitted to the previously drawn circle. The red circle is fitted to the edge of the pupil.

5.4.3 Converting True Colour Image into a Grey Image

The colour image is a 24-bit (RGB) image, meaning that 8 bits or 256 (linear) levels of brightness are stored in the red, blue and green channels. This 24-bit colour image can be converted to a monochrome image by extracting the red, green and blue image channels to produce three 8-bit images, each one equal in size (~ 1.310 MB), (fig. 5.6 A, B, C). Both the blue and the red channel images are ignored in this study because the quality of these images is poor and dim. The green channel, however, produces an image of high quality that clearly shows details of the posterior capsular opacity. This may be due to the fact that green pixels account for 75% of the total array, whereas the blue and red amount to only 12.5% each. It was therefore decided to use the green plane image throughout the rest of this study.

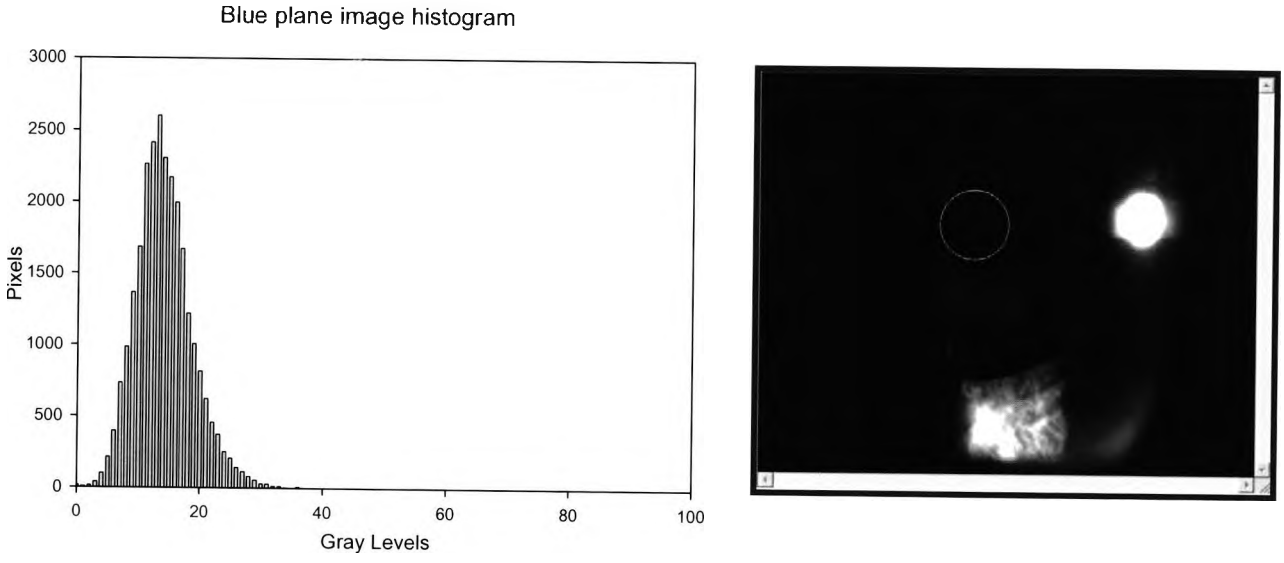

Figure 5.6.A The blue channel image is very dim, of poor quality, and even the capsular opacity is difficult to resolve against the background.

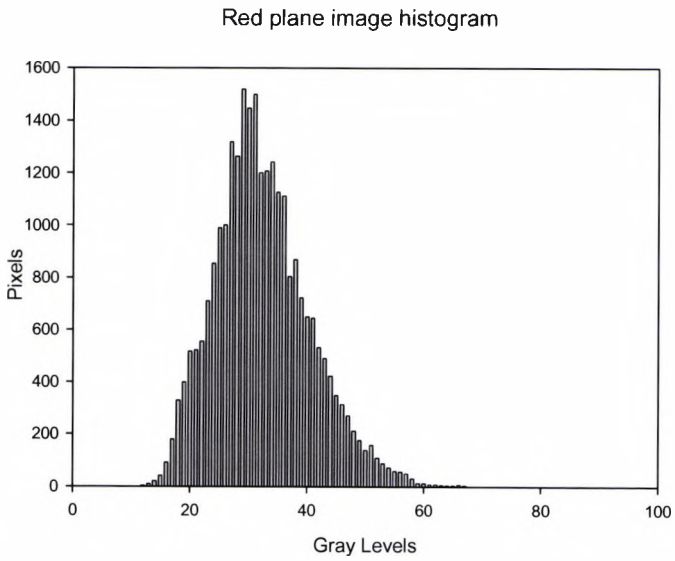

Figure 5.6.B The red channel image is also dim, but reveals more detail of the capsular opacity than revealed by the blue channel. Comparing the blue and the red image histograms shows that a greater range of grey levels are obtained with the red plane image. This may be due to the increased sensitivity of pixels in the red plane.

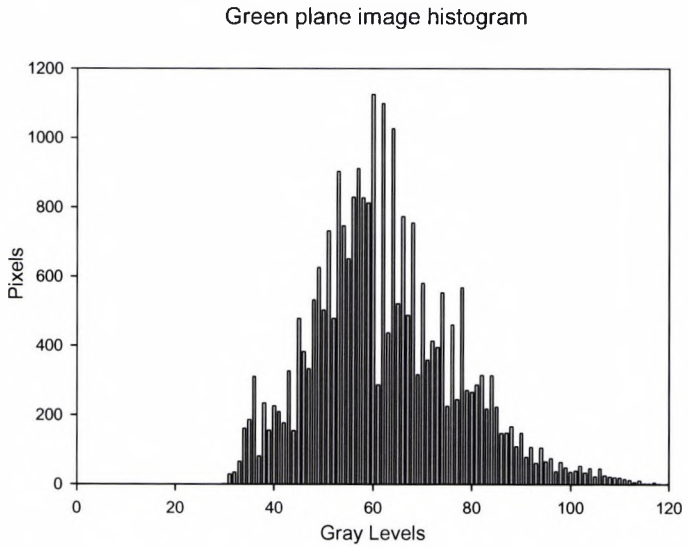

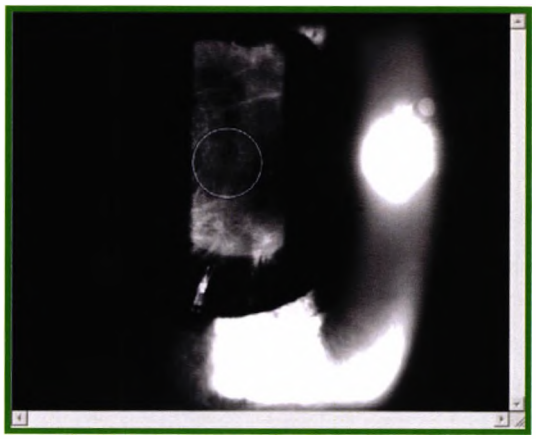

Figure 5.6.C reveals that the green plane image shows more fine detail of the capsular opacity. This detail is clearly reflected in the histogram.

5.4.4 Spectral Power in the image

The Fourier Transform is a commonly used tool in image processing applications. It allows the image to be viewed in the frequency domain as well as its more usual spatial domain. Fourier transformation is the process by which images are converted from the spatial domain, where each pixel represents the light level at a point in the image, to the frequency domain. In general, the Fourier transformed image in the frequency domain is complex in that it has both real and imaginary components. The real component is known as the amplitude spectrum, which gives the distribution of energy in the wave number, and the complex component, the phase image, carries information about the image structure (Bernd, 2002). Each point in the

amplitude spectrum image represents a different spatial frequency and the pixel value at that point determines how much light of that spatial frequency is in the original image. In general, the patterns in the amplitude spectrum image are centred and the central point represents the "d.c." or average light level in the original image. This can be seen in figure (5.7) where a set of black and white stripes form the original spatial image. The stripes describe a step-function and hence sine waves with a high spatial frequency are needed to reconstruct the stripes (Hecht, 1996). This can be seen from the points of light away from the centre of the amplitude spectrum.

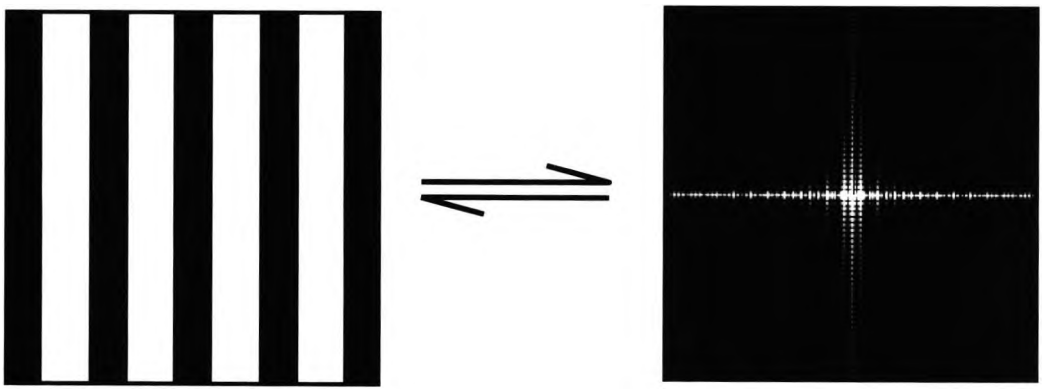

Figure 5.7 Example of the amplitude spectrum obtained from the Fourier Transform of the original image.

A good example of this approach is to note that the Fraunhofer diffraction patterns of apertures in optics are the Fourier Transforms of the aperture shape. Thus the amplitude spectrum of a white circle on a black background is an Airy pattern, a series of light a dark rings that rapidly fade centred on a bright disc (fig. 5.8). The fact that the amplitude spectrum is not a perfect Airy pattern is caused by pixelation and other "discrete" artefacts. This can occur because discrete Fast Fourier Transforms can only be applied to images of size 2^n x 2^n i.e. 128 x 128, 256 x 256 ...

Images that do not meet this requirement have black pixels added around them to make them up to the size needed. This can lead to Fourier components generated by the boundary between the image and black surround. Most of our images have black backgrounds and so this is a minor problem for our intended application.

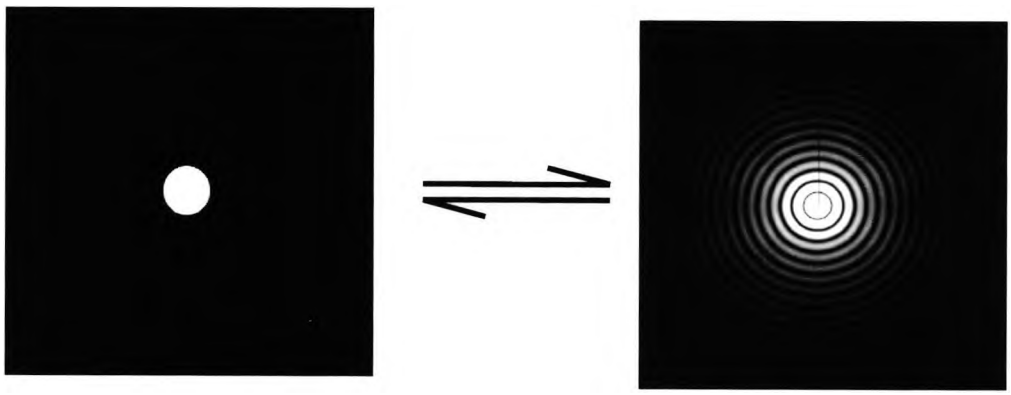

Figure 5.8. Fourier Transform image of a pinhole is an Airy pattern.

There are various applications of Fourier Transformed images (modifying the amplitude or phase spectrum) such as image enhancement, high pass or low pass filtering and image compression. Converting images from the spatial domain into the frequency domain also facilitates performing certain image measurement and processing operations that would require a significantly large computational effort in the spatial domain. With all of these applications it is not essential to deal deeply with mathematics to arrive at a practical working knowledge of the techniques (Russ, 2000).

In this study, we wished to develop an objective measure of the severity of PCO. The images captured are reflected light images in that any structure that is visible must reflect light out of the eye. Any opacification must therefore back scatter light to be visible. Unlike retro-illumination techniques that predominantly work on the area of the pupil covered, reflected image techniques work more on the amount of back scatter. It is possible to quantify this using the "total power" in the image. This can be calculated from the amplitude spectrum image since, from Parseval's theorem, the total power in the image in the spatial domain is the same as when calculated in the frequency domain (Press *et al*, 1992). In mathematical terms, for a 1-dimensional, real function *h(x)*, the total power is given by

$$Power = 2\int_{0}^{\infty} |H(u)|^2 \, du \qquad (5.1)$$

where *H(u)* is the Fourier Transform signal and *u* is spatial frequency. The reason for this approach was, in addition, to use the information in the frequency domain to develop a morphological classification system for PCO. This has not been presented in this thesis but helps explain the approach taken to evaluating severity of PCO. Further details extending this approach to images are given in section 6.2.

Practically, image processing software is used to compute the amplitude spectrum of a 3 x 3mm area of the posterior capsule centred on the pupil centre. Data from the histogram of the amplitude spectrum image (the one-sided power spectral density) is then transferred into Excel where the integration to find the total power has been programmed.

5.5 Results

5.5.1 Subjects

Fifteen eyes of fifteen subjects following uncomplicated cataract surgery, with posterior chamber intraocular lens implants, were included in this part of the study. The mean age was 76.33 ± 10.61 years (mean ± SD), with a range of 51 to 92 years. The subjects included 8 men and 7 women. Table (5.5) summarises the subjects' demographic details and posterior capsule opacification morphological types. For further details about subjective classification see chapter 4.

Characteristic of subjects	Posterior capsule Opacification Types		
	Fibrotic (n=5)	Pearl (n=5)	Mixed (n=5)
Age of subjects (Mean ± SD)	74.4 ± 13.41	75.4 ± 9.4	79.2 ± 10.47
Gender (F / M)	5 / 0	1 / 4	1 / 4

Table 5.1 Subjects' details.

The subjects had received the following intraocular lens implants in the capsular bag: Allergen Medical Optic (AMO) IOL types S130NB silicone (1 out of 15 eyes; 6.7%), PS53ANB (5 out of 15 eyes 33.3%) and PS26TB (1 out of 15 eyes; 6.7%), Bausch & Lomb silicone 3 piece SOFLX2 (7 out of 15 eyes; 46.6%), Chiron vision IOLab 6840B (1 out of 15 eyes; 6.7%). Further details of the IOLs can be found in table (4.4), chapter 4. Table 5.2 summarises the mean interval between surgery and Nd:YAG laser capsulotomy by IOL type.

IOLs	PS53ANB (N = 5)	SOFLX2 (N = 7)	SI30NB (N = 1)	PS26TB (N = 1)	IOLab 6840B (N = 1)
Interval between surgery and Nd:YAG laser capsulotomy (Mean ± SD)	43.6 ± 11.26	14.43 ± 10.37	36	24	14

Table 5.2 Time interval, in months, between cataract surgery and Nd:YAG laser capsulotomy (Mean ± standard deviation (SD)).

The central area of interest of all the images was morphologically classified subjectively according to PCO type (fibrotic, pearl, and mixed) by an experienced ophthalmologist. The confidence of morphological grading and the severity of the PCO were graded using a visual analogue scale as detailed in Chapter 4. Table (5.3) shows the subjective grading of PCO morphological group (fibrotic, mixed and pearl), the confidence attached to that grading and the severity of the PCO for each subject.

Subjects	PCO types	Morphological confidence grading (1-5)	Severity grading (1-5)
1	Pearl	3.9	2.4
2	Pearl	3.0	2.5
3	Mixed	2.5	2.8
4	Mixed	2.5	2.0
5	Fibrotic	3.0	1.0
6	Fibrotic	3.5	1.2
7	Fibrotic	2.7	1.2
8	Fibrotic	3.5	3.0
9	Fibrotic	2.0	0.5
10	Mixed	2.5	1.8
11	Pearl	4.0	3.0
12	Pearl	4.0	3.0
13	Pearl	3.5	2.5
14	Mixed	2.5	1.5
15	Mixed	2.5	3.0

Table 5.3 Subjective classification of PCO morphology with associated confidence level and severity of posterior capsule opacification.

5.5.2 Reliability of the Fixation Stimulus - Version (1)

The ability of fixation stimulus version (1) to control patient fixation was assessed by capturing four images of the posterior capsule of each of 14 subjects. The images were all taken by the same examiner (HA-F) and at the same session for each subject, with the fixation stimulus on. Image Pro+ software was used to detect the edge of the pupil and to locate the X and Y

coordinates of the centre of the pupil. The displacement between the pupil centre and the specular reflection of the central LED on the fixation stimulus was calculated using Pythagoras' theorem. The mean, SD, SE and 95% confidence intervals of the actual displacement for all fourteen subjects is given in Table 5.4.

Subject	Mean (mm)	SD (mm)	SE (mm)	CI+ (mm)	CI- (mm)
1	0.713	0.277	0.1385	1.26	0.169
2	0.504	0.149	0.0747	0.797	0.211
3	0.648	0.099	0.0497	0.843	0.453
4	1.23	0.404	0.0831	2.019	0.436
5	0.452	0.126	0.0631	0.699	0.205
6	0.431	0.098	0.0488	0.622	0.239
7	0.475	0.218	0.1092	0.903	0.047
8	0.889	0.060	0.0301	1.01	0.772
9	0.328	0.195	0.0973	0.709	-0.054
10	1.013	0.222	0.1109	1.45	0.577
11	0.988	0.277	0.1388	1.53	0.444
12	1.102	0.571	0.2853	2.22	-0.017
13	0.890	0.212	0.1061	1.31	0.475
14	0.487	0.166	0.2019	0.812	0.159

Table 5.4 Measurements of the actual displacements of the four images captured for each subject, including the mean, standard deviation (SD), standard error (SE) and 95% confidence interval (CI).

The variation of the mean values for the displacement between subjects is expected due to physiological differences (uneven pupil dilation, position of the corneal apex). However for any one subject the values of the displacement should not vary greatly if the target helps maintain patient fixation. Hence the standard deviation of each subject is considered as a measure of the variability in fixation. The mean SD was 0.220mm (95% confidence limits of <-0.045mm, 0.484mm>). Assessing the positive effect of a fixation target is difficult in this context because the reflection of the central LED has been used as a reference point. Images without a fixation target cannot therefore be assessed in the same way. This difficulty is resolved when a modified version of the fixation target is presented in section 5.8. For now it is simply noted that 66% of displacement values will lie on average within ±0.220mm. For 95% of subjects this value will be within the range -0.045mm to 0.484mm.

The displacements of both the X and Y coordinates of the pupil centre, and the specular reflection of the central LED of the fixation stimulus revealed that the subjects may lose their fixation vertically more than horizontally. Reasons for this could include the irregular shape of the pupil after dilation, subject fatigue, and/or cooperation. During image acquisition we noted that some subjects are very cooperative producing low SD values (subjects 6, 7, and 9). In comparison, subject 4's pupil was unevenly dilated resulting in the circle being used to define the edge of the pupil not fitting the pupil exactly. This may explain the higher SD for subject 4, which is close to the upper 95% confidence limit. Figure 5.9 revealed that there is a larger displacement on the vertical axis than on the horizontal axis for subject 4. However, subject 9's pupil is round and regular after dilation as shown in figure (5.10). Here the graph indicates that the displacement is smaller but still indicating a tendency for vertical shift. Although subjects will have a tendency to drift to

their primary gaze position if not fixating, we know of no explanation why this should be predominantly in the vertical plane in the absence of any neurological disorder.

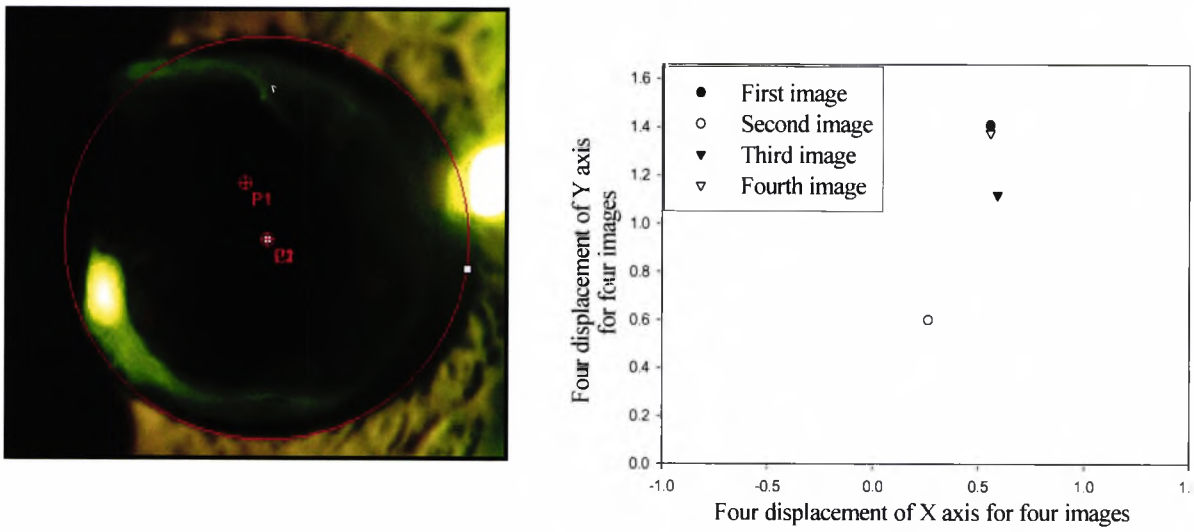

Figure 5.9 shows the variation in displacement for subject 4 where the best fit circle is a poor approximation to the pupil edge due to its irregular shape.

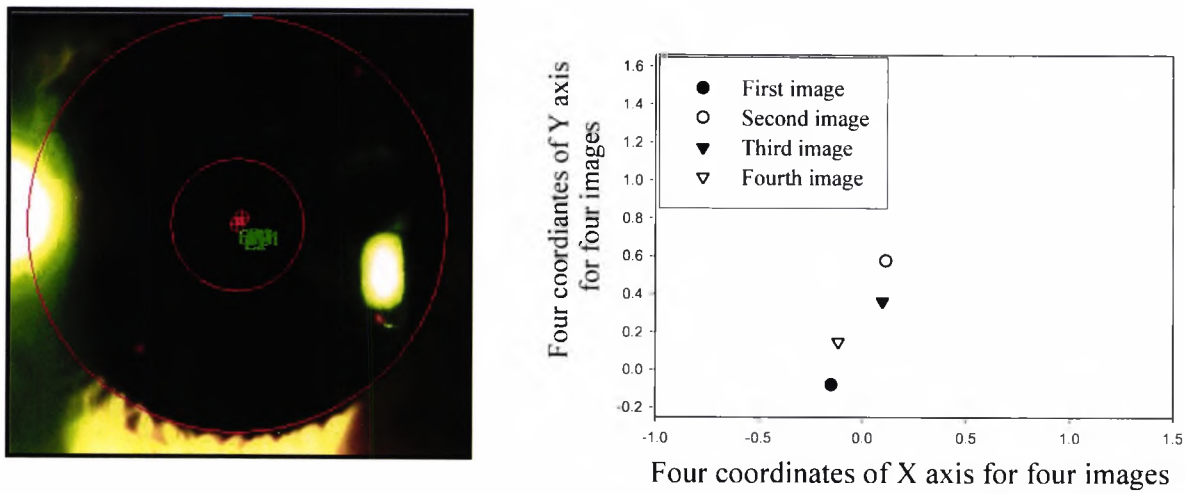

Figure 5.10 shows the variation in displacement for the four images of subject 9 where the best fit circle matches the pupil shape well.

5.5.3 Intra-observer Repeatability

The intra-observer repeatability of the image acquisition was tested by capturing 2 images of the posterior capsule of 13 subjects. All the images were taken by the same examiner with the same system settings and at the same session for each subject. Intra-observer repeatability was assessed using the Bland and Altman method (Bland and Altman, 1999). The spectral power of both images within the AOI, the mean, standard deviation, and the standard error of all 13 subjects are shown in the table 5.5.

Subject	First image	Second image	Mean	Difference
1	65.05	65.17	65.11	- 0.122
2	48.09	48.40	48.25	- 0.306
3	32.82	34.09	33.46	- 1.28
4	49.37	49.19	49.28	0.177
5	63.39	62.44	62.92	0.957
6	50.78	51.38	51.08	- 0.597
7	68.96	67.59	68.28	1.37
8	30.87	30.40	30.64	0.465
9	40.31	39.45	39.88	0.867
10	61.51	60.82	61.17	0.69
11	40.34	40.72	40.53	- 0.376
12	72.48	73.31	72.89	- 0.835
13	19.92	19.66	19.79	0.259

Table 5.5 The spectral power within the area of interest of first and second images, the mean and difference.

The mean of the differences of spectral power within the area of interest for the first and the second images provides an estimate of the bias, The mean of the difference of the spectral power of both images was 0.0976 indicating that there is little evidence of overall bias. To check that the difference is unrelated to the magnitude of the measurement a mean-difference plot was constructed (fig. 5.11). The plot revealed that there is no obvious trend (Pearson correlation coefficient of 0.254; P = 0.403). A one-way analysis of variance (ANOVA) gave the within subjects standard deviation to be 0.527 therefore the *within subjects coefficient of variation*, equal to the within subjects SD/ overall mean (49.481 in this case), is 0.011 or 1.1 %. This indicates that the within subject variability of total spectral power during image acquisition is small.

The 95% limits of agreement show how large the differences are likely to be between the first and second images. The limits of agreement were 1.61 to -1.42; we would expect 95% of the differences to lie between these limits of agreement provided that the differences are normally distributed.

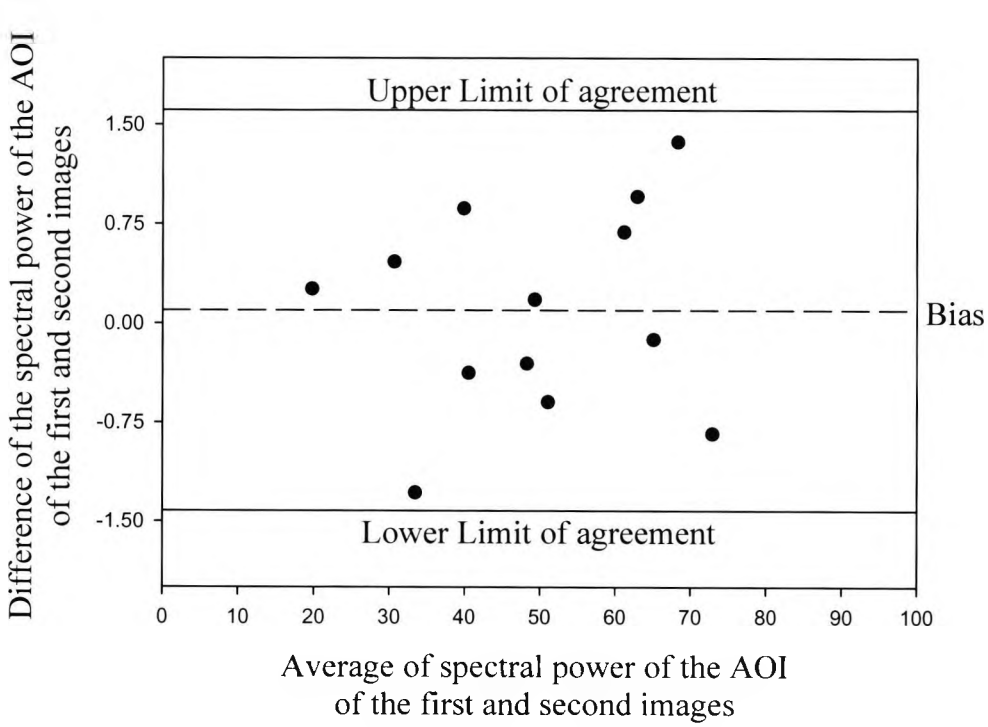

Figure 5.11 Altman-Bland mean-difference plot for the 13 subjects in this part of the study. The long dashed line represents the mean difference and the solid lines represent the 95% limits of agreement.

5.6 Summary

Images taken with the fixation stimulus version (1) revealed that it may help to maintain subject fixation because 66% of the displacement values lie on average within ± 0.22mm. The standard deviation of each subject indicated relatively low variability between the values of the displacement and hence the fixation target may contribute towards eliminating Purkinje reflections caused by poor fixation. Assessing the positive effect of a fixation target was difficult in this pilot study because the reflection of the central LED has been used as a reference point. Images without a fixation target cannot therefore be assessed in the same way.

The displacements of both the X and Y coordinates of the pupil centre, and the specular reflection of the central LED of the fixation stimulus revealed that the subjects tended to lose their fixation vertically more than horizontally. Reasons for loss of fixation could include the irregular shape of the pupil after dilation, subject fatigue, and/or cooperation and these factors have been documented in a previous study (Barman et al. 2000). However, we know of no explanation, in the absence of any neurological disorders why there is a tendency for the loss of fixation to be predominantly in the vertical plane. The variation of the mean values for the displacement between subjects is expected due to physiological differences (uneven pupil dilation, position of the corneal apex).

During this phase of the study a number of limitations were discovered: First, a lot of concentration was required by both the examiner and the subject because the fixation stimulus has to be turned off just before pressing the camera shutter. This can be difficult especially with those subjects that are suffering from some form of senility and those who experience blurred vision in one eye whilst the other is occluded to avoid diplopia. Hence the process of acquiring the images can be very time consuming. Secondly, the illumination system could not be swung from the temporal to the nasal side without removal of the fixation stimulus. This is because the peripheral LEDs obstruct the slit projection head. Thirdly, the consequent frequent removal of the fixation stimulus caused an unstable fitting to the microscopic system and hence a poor repeatability.

The intra observer repeatability demonstrated that there was good agreement between the first and second images produced by the digital imaging system. The coefficient variation for the 13 subjects was 1.1% indicating that there is small variability of image acquisition within any subject.

5.7 Fixation Stimulus Version (2)

5.7.1 Design of Fixation Stimulus

The main aim of this section of the study was to redesign the fixation stimulus, to investigate the reliability of this new fixation stimulus and to assess the intra and inter-observer repeatability of the digital imaging system.

The modified fixation stimulus consisted of a glass reinforced plastic copper laminated printed circuit board, five red LEDs and a control box for the fixation stimulus settings. The circuit board contains an electrical circuit that is connected to the control box via a cable to supply electricity to the LEDs. The five LEDs are fitted to the circuit board with specific distances between them. The distance between the horizontal peripheral LEDs was 76.1mm, the distance between the vertical peripheral LEDs was 76.3mm, and the distance between the fifth central LED and any one of the four peripheral LEDs was 54.2mm (fig. 5.12).

The diameter of the four peripheral LEDs was 4.85mm, and the diameter of the fifth central LED was 1.5mm. The four peripheral LEDs were modified by flattening their convex heads to provide a smaller and sharper specular reflection on the corneal surface. This avoided having to bend them towards the centre of the fixation stimulus as was necessary for the first version of the fixation target. The design of the new fixation stimulus provided sufficient space for the illumination system of the slit lamp to swing from the temporal side of the left eye to the right eye without having to remove it from the slit lamp. It was then screwed onto the microscope objective housing of the slit lamp thereby providing greater stability.

The control box had two switches. The first was used to switch the power on and off whereas the second switch had two settings: the first allowed all five LEDs to stay on until the examiner pressed the camera shutter, which then caused the central LED to be turned off for less than a second during image acquisition. This allowed the subject to maintain fixation and the examiner to obtain a good focused image hence accelerating the process of image acquisition. The second setting allowed all five LEDs to stay on even when the camera shutter was pressed. There were two cables connected to the control box; one was the camera shutter cable, which was attached to the joystick of the slit lamp. The second cable connected the control box of the modified fixation stimulus to the camera shutter socket on the DSU.

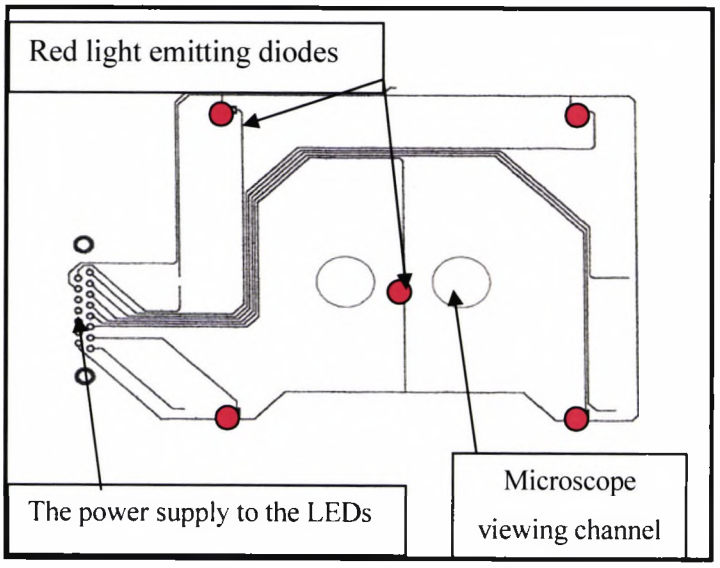

Figure 5.12 Diagram illustrating the design of the modified fixation stimulus.

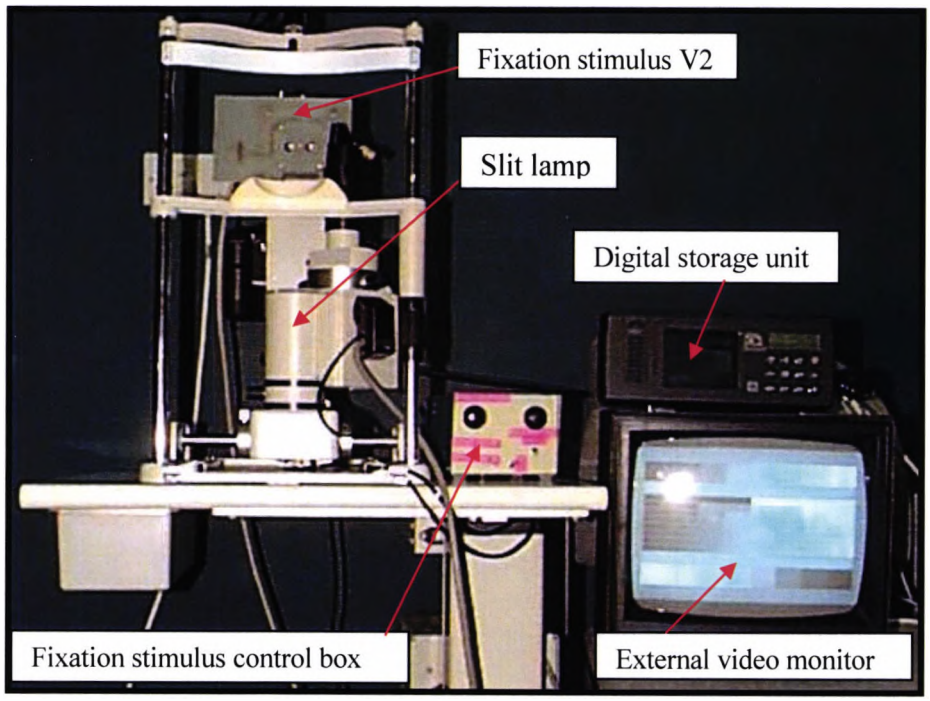

Figure 5.13 An image of the modified fixation stimulus fitted to the microscopic system of the slit lamp. The fixation stimulus is connected to the control box and DSU through a cable.

5.8 Materials and Methods

For this section of the study 25 eyes of 25 subjects were used. Images of the posterior capsule of the eyes were taken using a Nikon FS-2 slit lamp with the modified fixation stimulus and the following settings: (1) slit beam width 3.5mm, 45° angle of illumination, film speed (ISO) for camera 1600 and DSU 800, exposure compensation 0, flash intensity 2, and magnification 25X; (2) slit beam width 3.5mm, 45° angle of illumination, film speed for camera 200 and DSU 200, exposure compensation 0, flash intensity 2, and magnification 25X. All the procedures used to capture the images were the same as described in §5.4. All the subjects were volunteers recruited from the

Royal Eye Unit at Kingston Hospital, after having uncomplicated cataract surgery with posterior chamber intraocular lens implantation. They were attending a clinic prior to Nd:YAG laser capsulotomy. The images of PCO were captured through a dilated pupil (one drop of tropicamide 1%).

The *reliability* of the modified fixation stimulus was tested by taking 12 images for each of six subjects, at the same session, with the same setting and the same observer. Six images were taken without the modified fixation stimulus where the subject was asked to sit back between images. Then six more repeated images were taken with the modified fixation stimulus fitted to the slit lamp microscope system, where the subject was instructed to fixate on the central LED and with a 1 minute interval between images. The modified fixation stimulus was switched on, where all the LEDs were on but once the camera shutter was pressed to capture the image the central LED was turned off. The main reason for conducting the experiment in this way was because the fixation stimulus was fitted in front of the microscopic system of the slit lamp and hence the subject could fixate on the unlit central LED.

The *intra-observer repeatability* of the system was tested by taking 12 images for each of ten subjects at the same session, with the same setting, the same observer, and with the modified fixation stimulus. 12 repeated images were allocated randomly using table B13 (Altman, 1991) for each subject as illustrated in table (5.6). 6 repeated images were captured with the central LED switched on even when the camera shutter is pressed and 6 repeated images were captured with the central LED switched off once the camera shutter was pressed. The subject, in each case was instructed to sit back and wait for 1 minute between each image. Thus these images were taken over an approximate 24 minute period.

Time	1	3	5	7	9	11	13	15	17	19	21	23
Random allocations	O	O	O	W	O	W	O	W	W	W	O	W
Subject1(Images NO)												

Table 5.6 Random allocations and timing interval used for capturing the images with the modified fixation stimulus, central LED off (O) and central LED on (W).

The inter-observer repeatability of the system was tested by capturing 2 images for each of nine subjects by three observers: an ophthalmologist, an optometrist, and a non-clinician. Identical system settings were used and the images taken at the same session for each subject, and with modified fixation stimulus. The central LED of the fixation stimulus was switched off once the camera shutter was pressed to capture the image.

All the images obtained were first processed by detecting the edge of the pupil and defining the AOI, and by extracting the green channel. A 3mm × 3mm area centred on pupil was then Fourier transformed using the FFT algorithm in Image Pro+. The data from the amplitude spectrum was exported to the Excel and a purpose written macro used to calculate the total spectral power.

5.9 Results

5.9.1 Subjects

Twenty five eyes of 25 subjects following uncomplicated cataract surgery and posterior chamber intraocular lens implantation were included. The mean age was 79.21 ± 8.74 years (mean ± SD), with a range of 54 to 92 years, and the subjects included 13 men and 12 women. Table (5.7) shows the subjects' demographic details according to PCO type.

Characteristic of subjects	Posterior capsule Opacification Types		
	Fibrotic (n=9)	Pearl (n=12)	Mixed (n=4)
Age of subjects Mean ± SD	81.2 ± 5.43	75.5 ± 9.92	84.33 ± 5.86
Gender (F / M)	6 /3	5 / 7	1 / 3

Table 5.7 Subjects' details

All subjects had received intraocular lens implants in the capsular bag: Allergen Medical Optic (AMO) IOL types Bausch & Lomb silicone 3 piece SOFLX2 (17 of 24 eyes; 68 %), S130NB silicone (2 of 25 eyes; 8 %), S140NB silicone (2 of 25 eyes; 8 %), PS26TB (2 of 25 eyes; 8 %), PS53ANB (1 of 25 eyes 4 %), Storz (1 of 25 eyes; 4 %). For details of the IOLs see table (4.4) in chapter 4.

IOLs	Sofles2 (N=17)	SI30NB (N=2)	SI40NB (N=2)	PS26TB (N=2)	PS53ANB (N=1)	Storz (N=1)
Interval between surgery and Nd:YAG laser capsulotomy (Mean ± SD)	14.1 ± 8.76	42 ± 8.48	24 ± 0	36 ± 0	36 months	84 months

Table 5.8 The interval in months between cataract surgery and Nd:YAG laser capsulotomy (Mean ± standard deviation (SD)).

Any PCO within the central area of interest was morphologically classified by an experienced ophthalmologist. The confidence of morphological grading and the severity of the PCO was also graded using a visual analogue scale. Further details about subjective grading can be found in chapter 4. Table 5.9 shows the subjective grading of morphological type, morphological confidence and severity for each subject.

Subject	PCO Types	Morphological confidence grading (1-5)	Subjective severity grading (1-5)
1	Fibrotic	3.6	3.5
2	Fibrotic	3.0	2.0
3	Pearl	4	3.8
4	Fibrotic	3.3	3.0
5	Pearl	3.7	3.2
6	Pearl	3.5	2.3
7	Fibrotic	4.5	4.5
8	Fibrotic	2.4	2.6
9	Pearl	3.0	2.4
10	Pearl	3.1	2.1
11	Pearl	3.6	3.0
12	Pearl	2.8	1.9
13	Mixed	3.3	3.0
14	Pearl	3.1	3.0
15	Pearl	3.5	3.0
16	Mixed	2.5	2.7
17	Fibrotic	3.2	2.5
18	Pearl	3.0	2.3
19	Fibrotic	3.5	3.5
20	Fibrotic	3.5	3.3
21	Pearl	3.0	1.9
22	Fibrotic	3.0	3.0
23	Mixed	2.5	2.6
24	Mixed	1.3	2.5
25	Pearl	3.3	2.4

Table 5.9 Subjective classification of PCO morphology with confidence level and severity of posterior capsule opacification.

5.9.2 Reliability of the modified Fixation Stimulus

The reliability of the modified fixation stimulus was tested using the spectral power of the area of interest for each subject with and without the modified fixation stimulus as our metric. The variances were calculated to perform Levene's test, which does not necessarily require data with a normal distribution. The result for Levene's test showed that there is no significant difference between those images captured with and without the modified fixation stimulus (P= 0.298). Although the standard deviation with the modified fixation stimulus is less than the standard deviation without the modified fixation stimulus (fig. 5.14). This suggests that, although the modified fixation stimulus is capable of reducing intra-subject variation, the difference is not statistically significant. Table (5.10) shows the mean spectral power, the standard deviation, the satandard error, and the 95% confidence intervals for each subject with and without the modified fixation stimulus.

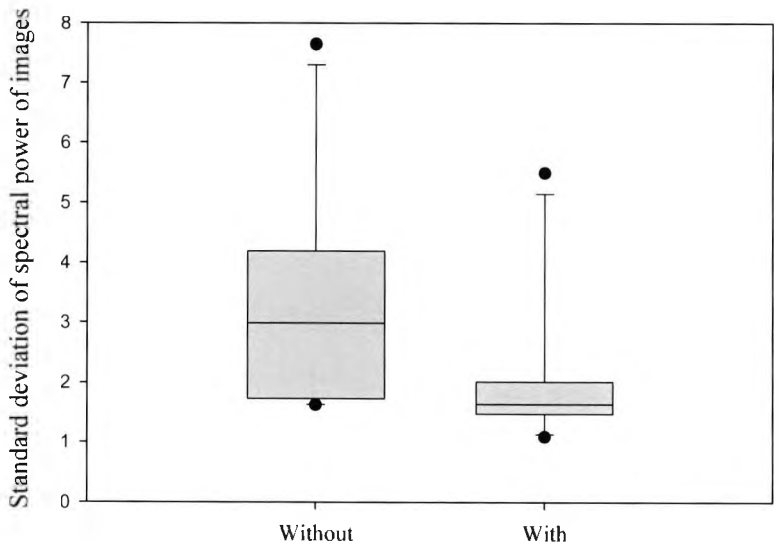

Figure 5.14 Comparison of the standard deviation between the images captured with and without the modified fixation stimulus.

Subject	Fixation	Mean	SD	SE	CI-	CI+
1	Without	25.89	1.73	0.707	24.51	27.28
1	With	30.36	1.55	0.631	29.12	31.59
2	Without	49.29	4.19	1.71	45.94	52.65
2	With	51.26	1.74	0.709	49.87	52.65
3	Without	42.70	1.63	0.665	41.40	44.01
3	With	32.06	2.02	0.823	30.44	33.67
4	Without	55.82	1.91	0.781	54.29	57.35
4	With	61.63	1.48	0.603	60.44	62.80
5	Without	72.15	7.65	3.12	66.02	78.26
5	With	77.95	5.49	2.24	73.55	82.35
6	Without	22.88	4.07	1.66	19.62	26.14
6	With	20.32	1.09	0.444	19.45	21.19

Table 5.10 The spectral power of the AOI with and without the modified fixation stimulus, the standard deviation (SD), standard error (SE), and confidence interval (CI) for each subject.

5.9.3 Inter Observer Repeatability

Inter-observer repeatability was calculated based on the Bland and Altman method (Bland & Altman, 1999). The spectral power within the area of interest of the amplitude spectrum of the first and the second images and the mean of the two replicates for each of the three observers was calculated. The table 5.11 shows the spectral power of the first and the second images within the AOI for each observer with their mean.

Subject	Observer 1			Observer 2			Observer 3		
Replicate	1	2	Mean	1	2	Mean	1	2	mean
1	55.22	55.77	55.49	55.28	54.61	54.945	44.26	43.18	43.72
2	101.21	101.49	101.35	101.43	100.11	100.77	101.49	99.73	100.61
3	70.57	71.42	70.99	70.71	68.37	69.54	70.59	69.19	69.89
4	30.44	32.88	31.66	30.98	32.62	31.8	30.76	31.1	30.93
5	59.33	58.32	58.83	59.25	55.54	57.395	50.43	49.25	49.84
6	65.65	66.15	65.9	65.12	65.17	65.145	64.18	68.42	66.3
7	45.1	45.57	45.335	45.3	46.11	45.705	38.34	34.48	36.41
8	30.86	33.26	32.06	30.47	34.63	32.55	29.1	36.28	32.69
9	54.26	51.79	53.03	54.45	52.17	53.31	53.14	51.77	52.455

Table 5.11 The spectral power of the AOI of the first and second images captured by three observers and the corresponding mean for each subject and for each observer.

The mean difference gives the estimate of bias for each pair of observers. These were 0.387 (observer 1 and 2), 3.53 (observer 1 and 3), and 3.15 (observer 2 and 3). This indicates that there is little evidence of overall bias between observers 1 and 2 but a relatively large bias for observer 3 (non-clinician) when compared to observers 1 and 2. The limits of agreement indicate how far the differences are likely to be between each pair observers. For observers 1 and 2, 1 and 3, and 2 and 3, these were 1.86 to - 1.1, 13.1 to - 6.02 and 12.54 to- 6.24 respectively (fig. 5.15, 5.16, and 5.17). This could be due to many factors such as patient fixation, observer focusing techniques or a naive observer.

To indicate the accuracy of the measurement over the range of measured values; a mean-difference plot was constructed for each pair of observers (fig. 5.15, 5.16 and 5.17).

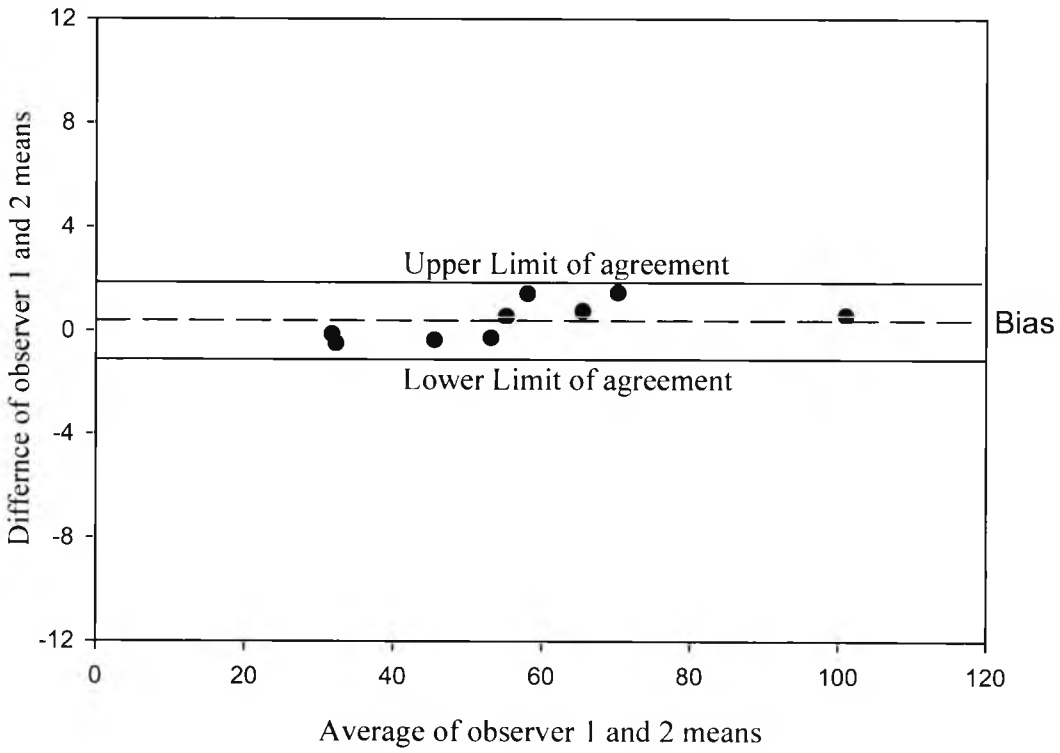

Figure 5.15 The difference of observer 1 and observer 2 plotted against the average of observer 1 and observer 2 (n=9). The long dash line represents the mean difference and the solid lines represent the limits of agreement.

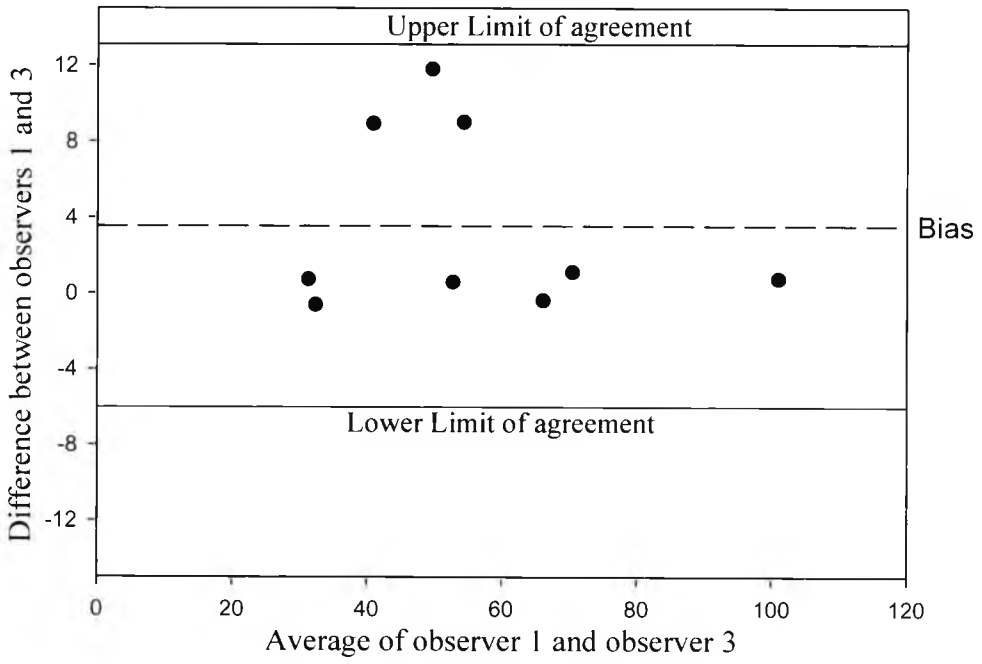

Figure 5.16 The difference of observer 1 and observer 3 plotted against the average of observer 1 and observer 3 (n=9). The long dash line represents the mean difference and the solid lines represent the limits of agreement.

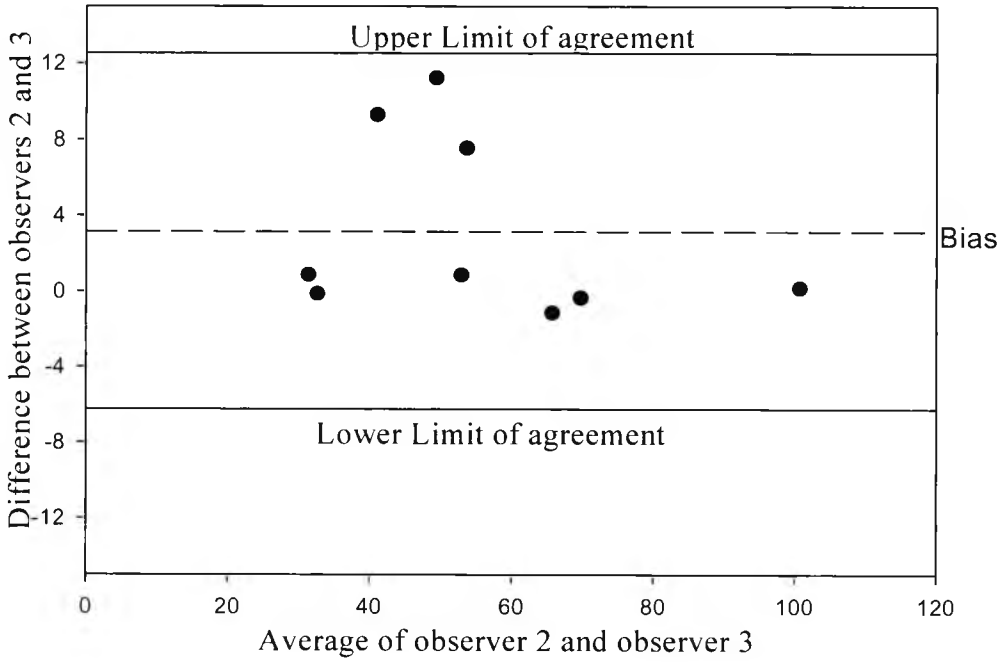

Figure 5.17 The difference of observer 2 and observer 3 plotted against the average of observer 2 and observer 3 (n=9). The long dash line represents the mean difference and the solid lines represent the limits of agreement.

5.9.4 Intra Observer Repeatability

Intra-observer repeatability was calculated based on the Bland and Altman method (Bland & Altman, 1999). The images were obtained using the same instrument settings, with the same observer and at the same session for each subject randomly according to table (5.6). The spectral power within the area of interest of the amplitude spectrum images of the six replicates, the mean, and the standard deviation for each subject was calculated.

Subject	Image 1	Image 2	Image 3	Image 4	Image 5	Image 6	Mean	SD
1	141.40	139.67	140.99	140.84	141.69	141.25	140.97	0.706
2	45.02	46.20	46.15	43.86	43.21	43.68	44.69	1.298
3	61.95	61.56	60.19	61.56	60.55	57.79	60.60	1.529
4	25.14	24.58	25.57	25.28	24.01	25.39	24.99	0.591
5	91.16	91.73	91.20	91.32	91.39	91.33	91.36	0.202
6	63.31	63.67	64.05	63.01	63.81	62.68	63.42	0.514
7	39.48	40.01	39.24	38.52	39.74	39.65	39.44	0.517
8	31.66	30.93	31.70	31.69	30.67	31.29	31.33	0.442
9	30.16	30.79	29.27	29.61	30.80	30.19	30.14	0.618
10	343.78	342.83	343.09	344.01	340.96	335.79	341.75	3.111

Table 5.12 The spectral power of the AOI of the six replicates images captured by one observer, the mean and SD for each subject.

A one-way analysis of variance (ANOVA) gave the within subject standard deviation to be 1.26. However, since there is genuine variation in the within-subject variability, the pooled within-subject SD will be an indication of typical variability. The within-subject coefficient of variation, equal to within subject SD/overall mean (86.87 in this case), is 0.015 or 1.5%.

To check that the error is unrelated to the magnitude of the measurement the mean values of the six replicates is plotted against their SD values (fig. 5.18). The plot revealed that there is no obvious trend (Spearman's correlation coefficient of 0.273; P = 0.446).

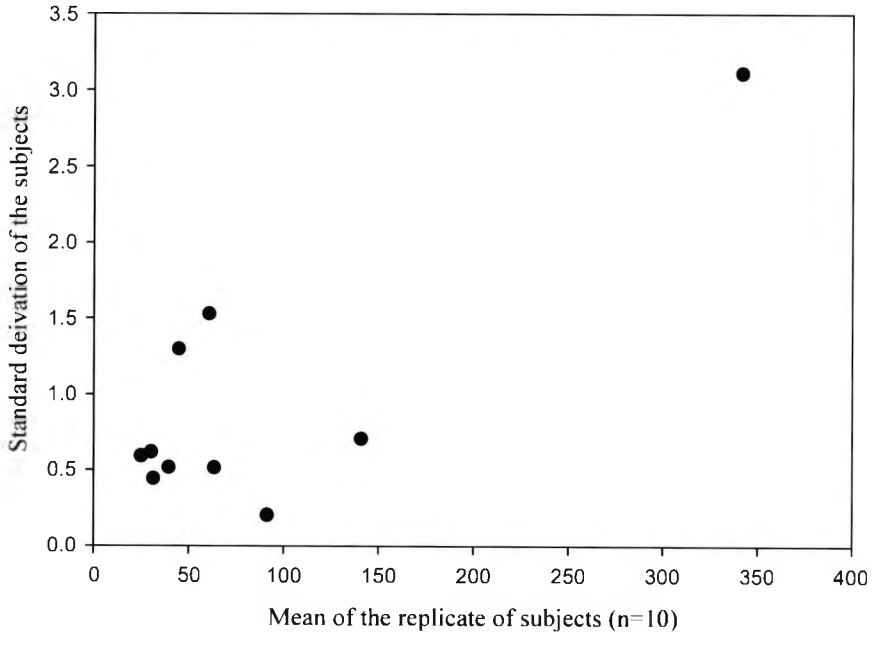

Figure 5.18 the mean of the replicates of each subject plotted against their standard deviation (n=10).

To test that the residuals are normally distributed a normality plot of the residual values was constructed of ten subjects (fig. 5.19). The result of the Kolmogrowv-Smirnov normality test of the residual values was ($P < 0.01$) this suggests that there is significant difference from normal distribution, which may be due to two specious values for subjects 3 and 10 from table (5.12).

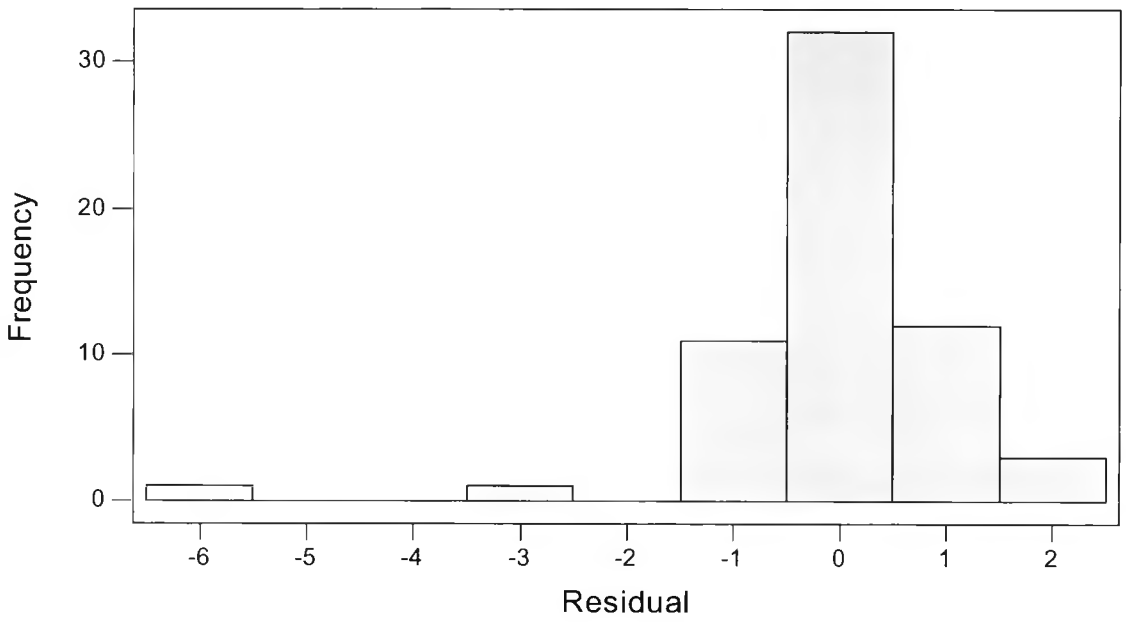

Figure 5.19 Normal plot of the residual from analysis of variance of the intra observer repeatability (n=10).

The specious values for subjects 3 and 10 in this data are more than three standard deviations away from the mean. This indicates that the specious values are particularly important because they can have a considerable influence on the results of statistical analysis. Therefore, if we exclude the two specious values for subjects 3 and 10 (57.79 and 335.79) and repeat the analysis ANOVA gives the within subject standard deviation to be 0.743. The within-subject coefficient of variation, equal to within subject SD/overall mean (80.31 in this case), is 0.0093 or 0.93%.

A normality plot of the residual values was constructed for ten subjects excluding the two specious values for subjects 3 and 10 (fig. 5. 20). The Kolmogrowv-Smirnov normality test of the residual values gave P= 0.091. Although the residuals pass the Kolmogrowv-Smirnov normality test, (fig. 5.20) shows that the distribution is still slightly skewed.

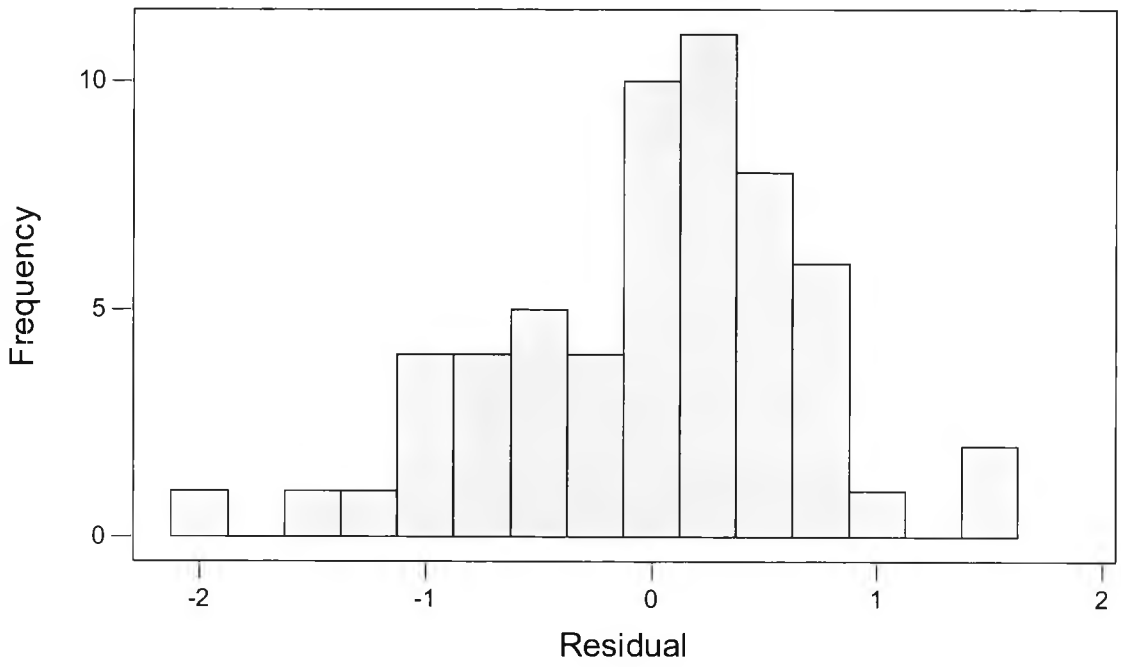

Figure 5.20 Normal plot of the residuals from analysis of variance of the intra observer repeatability (n=10) without the two specious values for subjects 3 and 10.

5.10 Discussion

The design of the modified fixation stimulus demonstrates that the limitations found for fixation stimulus version (1) have been rectified. This helps to accelerate image acquisition and hence the subjects would suffer less fatigue. The standard deviation value for the subjects with the modified fixation stimulus is smaller than the standard deviation value without the modified fixation stimulus, which suggests that the modified fixation stimulus is helpful in reducing variation in results. However the result for Levene's test demonstrated that this reduction is not statistically significant.

The inter-observer repeatability for the three pairs of observers (observers 1 and 2, 1 and 3, and 2 and 3) revealed good agreement between observers 1and 2. However, the agreement between observers 1 and 3, and 2 and 3 was poor. This may indicate that a non-clinician without training would be inappropriate for taking these images. A previous study by Friedman et al. (1999) reported that there are many factors that can affect reproducibility during image capturing such as patient fixation, and operator focusing techniques.

The intra-observer repeatability results revealed that that there is genuine variation in the within-subject variability thus the pooled within-subject SD is used as an indication of typical variability. The within-subject coefficient variation was 1.5%. A Spearman's correlation of coefficient of 0.273 (P = 0.446) indicated that the error is unrelated to the magnitude of the measurement. The P-value of the Kolmogrowv-Smirnov normality test of the residual values with and without the two specious values for subjects 3 and 10 were 0.01 and 0.091 respectively. This indicates that the residual values without the two specious values pass the normality although the distribution is still slightly skewed. Excluding the two specious values for subjects 3 and 10 reveals that the within subject standard deviation was 0.743. The associated within-subject coefficient of variation was 0.93%.

Chapter Six

6. Spectral power as an objective measure of PCO severity

6.1 Introduction

PCO is most commonly seen first by primary care practitioners and typically optometrists. If symptoms are significant then patients are referred back to the ophthalmology department for a YAG capsulotomy procedure. As discussed in chapter 3, different systems have been developed to analyse and quantify PCO either objectively or with the help of user intervention. However, most of these techniques use specialised methods or equipment, such as purpose designed retro-illumination cameras, and are therefore not appropriate for primary care settings. Therefore, the aim of this section of the study is to develop an objective measure to quantify the severity of posterior capsule opacification that can be used by optometrists within a primary care practice. The equipment and methods of analysis should therefore be widely available to meet this requirement.

6.2 Objective measure to quantify PCO

Subjective grading of PCO at the slit lamp typically involves looking at the posterior capsule and assessing the amount of white light scatter returned from the opacification as well as the area of the capsule involved figure (6.1A & B). Measures of area would seem to be only one limited aspect of opacification since it is well known that a small, localised opacity can cause

significant visual disturbance. Also, as the severity of the opacification increases, it doesn't have to spread to new areas as seen in figure (6.2. B) but may also increase in "density". The latter will appear as an increase in the backscatter from the opacity as seen in figure (6.2. A)

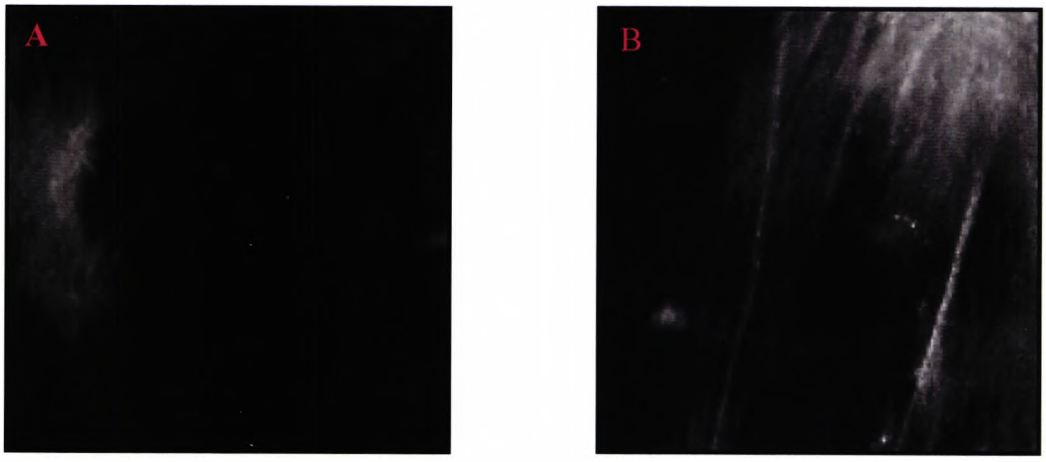

Figure 6.1 Images of AOI for subjects 34 (A) and 5 (B). Both have fibrotic PCO and are subjectively graded as 3.2 and 3.6 respectively. It is clear that the back scatter varies with opacification severity.

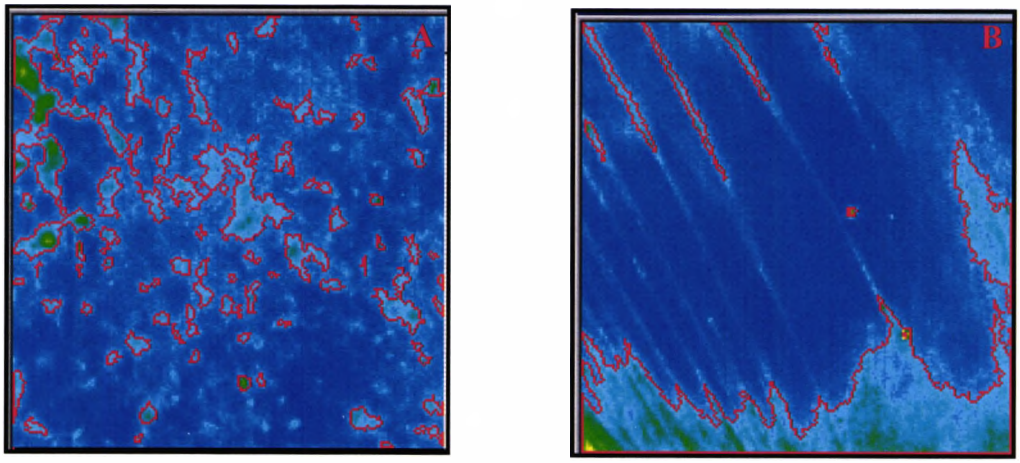

Figure 6.2 Images of AOI, (A) subject 13 subjectively classified as pearl PCO, and (B) subject 10 subjectively classified as fibrotic PCO. The dark yellowish green colour represents high density in both images, both subjective graded as 3.0 and 2.6 respectively.

The total power in an image is a concept derived from Fourier Transform techniques. If the image is represented by $h(x,y)$ where the function contains the gray level values at each spatial location in the image, then its Fourier Transform is given by

$$H(u,v) = \int_{-\infty}^{\infty}\int_{-\infty}^{\infty} h(x,y)e^{-2\pi i(ux+vy)}dxdy$$

where (u,v) represent spatial frequency. The Fourier Transform of a signal therefore contains real and imaginary components. Images provide discrete data and hence to calculate the Fourier Transform the two-dimensional discrete Fourier Transform must be used. For an $N \times N$ image, represented by the discrete function $h(a,b)$, where $a = 0,1,\ldots N$ and $b = 0,1,\ldots N$, its discrete Fourier Transform is given by

$$H(c,d)=\frac{1}{N^2}\sum_{a=0}^{N}\sum_{b=0}^{N}h(a,b)e^{2\pi i\left(\frac{ac}{N}+\frac{bd}{N}\right)}.$$

The real component of $H(c,d)$, represented by the amplitude spectrum, has information about the magnitude of each frequency present in the image. The imaginary component is known as the phase spectrum and contains information about where features are. This can best be seen from figure 6.3 where an original image has been reconstructed using an inverse Fourier Transform without amplitude and phase information respectively. To derive information about the severity of the PCO it is therefore the amplitude spectrum that needs to be considered. The one-sided power spectrum of a real function is given by

$$P(c,d)=2|H(c,d)|^2$$

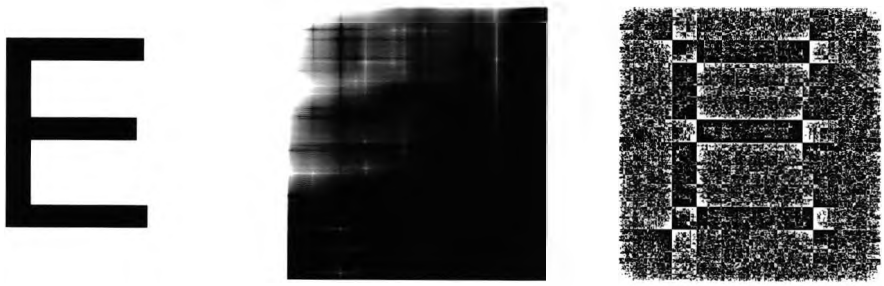

(a) (b) (c)

Figure 6.3 (a) original image (b) reconstructed using an inverse Fourier Transform and only amplitude information and (c) reconstructed with an inverse Fourier Transform and only phase information.

However, images already provide an intensity representation of the function and so it is not necessary to take the magnitude and square its value. A histogram of the amplitude spectrum image following Fourier Transformation will therefore plot the one-sided power spectral density for all spatial frequencies in the original image. The total power in the image is then calculated as the area under this curve, which can be mathematically expressed as

$$Power = \sum_{c=0} \sum_{d=0} P(c,d)$$

Such an approach combines the amount of back scatter and the area covered by the opacification. This is demonstrated in figure (6. 4 A & B, 6.5 A & B). Here the image is a black square with a round white circle. For an 8-bit image the gray level of all pixels within the white circle was 255. The power spectral density was calculated as described above and found to be 640.7. A second image was created but this time the area of the circle was doubled and the gray level of the pixels in the circle reduced to 128. The power spectral density was again calculated and found to be 645.3. The discrepancy in the readings was most likely caused by the fact that a gray level of 128 is just over 50% of 255 and the diameter of the circle had to be specified to the nearest pixel leading to rounding error. Ostensibly the results are the same to within numerical accuracy and therefore confirm that a change in total power assesses both changes in area covered and intensity of the backscattered light within the image.

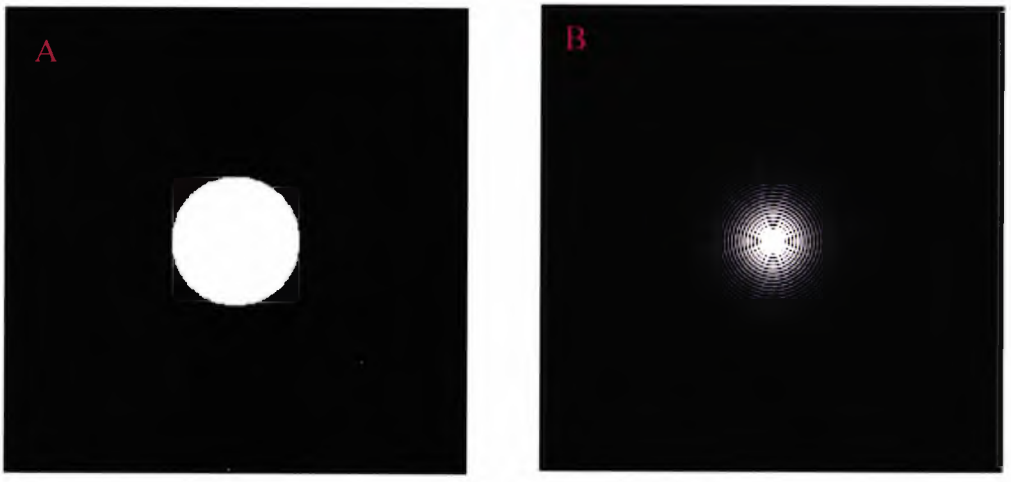

Figure 6.4 (A) The gray level of all pixels within the white circle was 255 and (B) amplitude spectrum following Fourier transformation.

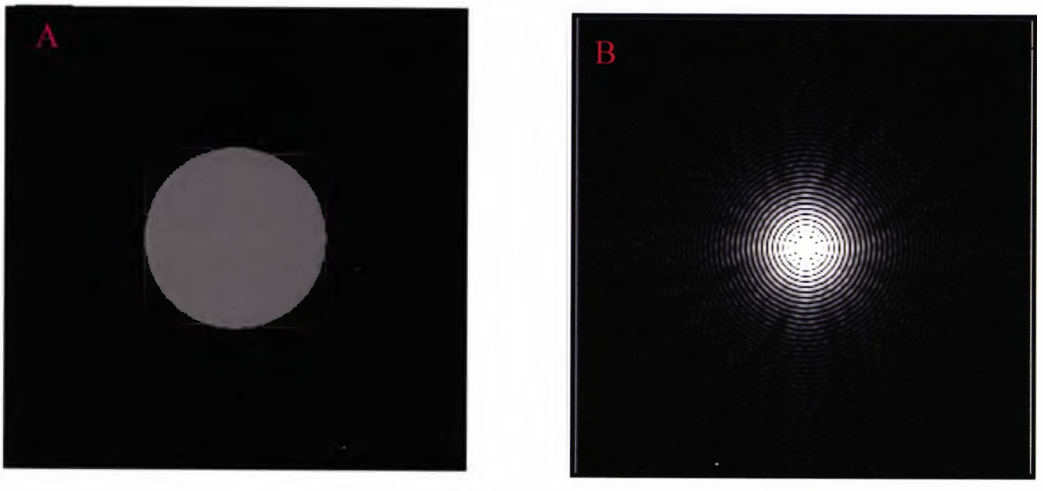

Figure 6.5 (A) Image with the area of the circle doubled and the gray level of the pixels in the circle reduced to 128 and (B) amplitude spectrum following Fourier transformation.

In this study, Image Pro+ version 4.5.1 was used to calculate the Fourier Transform of the area of interest of an image. The data from a histogram of the amplitude spectrum was transferred into Excel and the trapezoidal rule implemented to find the one-sided power spectral density for all spatial frequencies in the image. This calculates the area under the one-sided power spectral density function, which is simply the histogram of the amplitude spectrum.

6.4 Method and materials

This section of the study comprised 45 eyes of 45 subjects. Images of the posterior capsule of the eyes were taken using a Nikon FS-2 slit lamp with a fixation stimulus and with the following settings: slit beam width 3.5mm, 45° angle of illumination, film speed (ISO) for the camera 1600 and DSU 800, exposure compensation 0, flash intensity 2, and magnification 25X. All the images were obtained at the same session for each subject and with the same observer. The subjects were all volunteers recruited from the Royal Eye Unit at Kingston Hospital. They had all received uncomplicated cataract surgery with posterior chamber intraocular lens implants due to age related cataract. They were attending a clinic prior to Nd:YAG laser capsulotomy. The images of PCO were captured through a dilated pupil (one drop of tropicamide 1%). All the procedures used to capture the images were the same as described in section 5.4.

6.4.1 Procedure to obtain objective measure to quantify PCO

The following steps are used to quantify PCO objectively after image processing. Firstly, the gray level of the AOI image of PCO is transformed from the spatial domain into an amplitude spectrum image (fig. 6.6). Secondly, a histogram is obtained from this newly acquired image, and finally two sections of data from the histogram are transferred to an Excel spreadsheet: The pixels, which are transferred onto a specific column of the spreadsheet utilizing the Image Pro+ dynamic data exchange (DDE) command, and the histogram frequency scaling factor of X axis was copied and transferred onto the frequency scaling factor column of the spreadsheet (fig. 6.7).

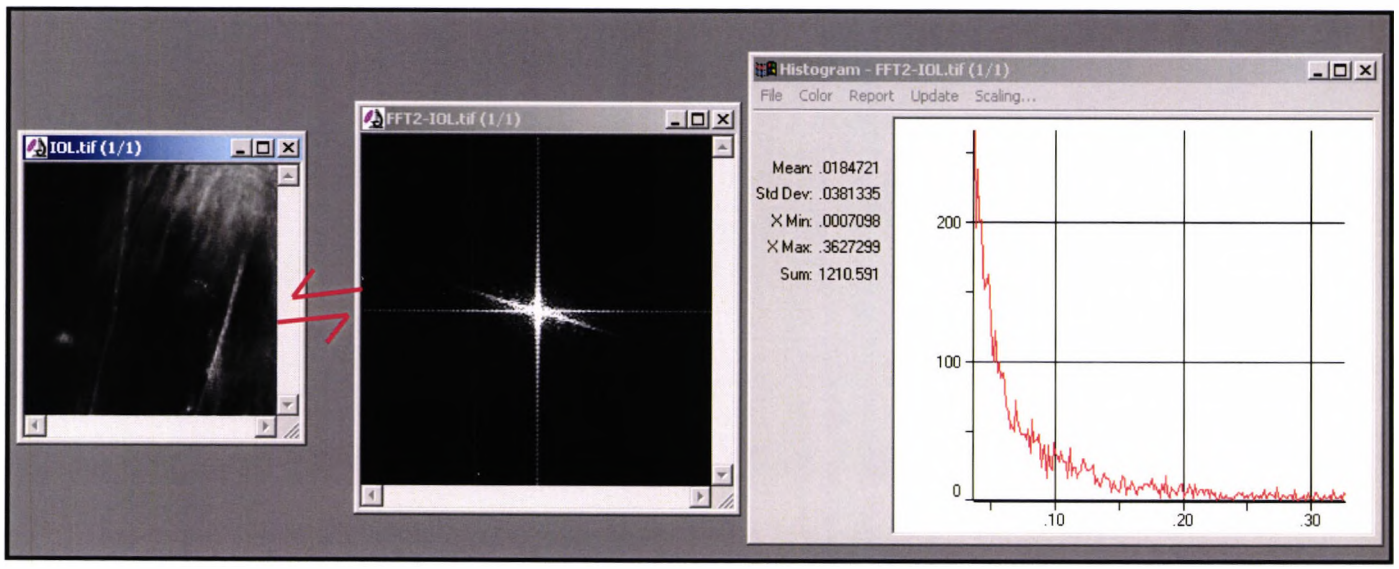

Figure 6.6 Shows the image of the AOI for subject 5, taken from table (6.3) in the spatial domain, which has then been Fourier transformed into an amplitude spectrum image and a histogram of amplitude spectrum produced of the intensities.

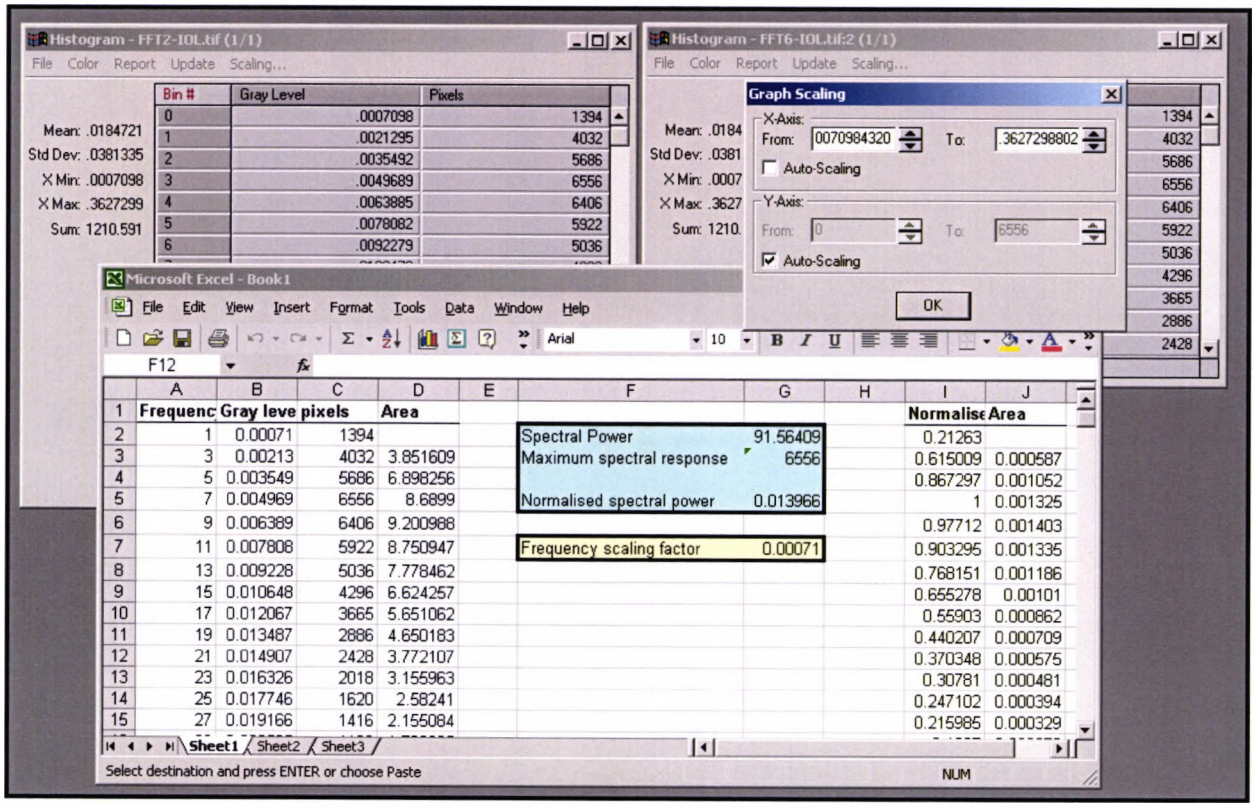

	A	B	C	D	E	F	G	H	I	J
1	Frequenc	Gray leve	pixels	Area					Normalise	Area
2	1	0.00071	1394			Spectral Power	91.56409		0.21263	
3	3	0.00213	4032	3.851609		Maximum spectral response	6556		0.615009	0.000587
4	5	0.003549	5686	6.898256					0.867297	0.001052
5	7	0.004969	6556	8.6899		Normalised spectral power	0.013966		1	0.001325
6	9	0.006389	6406	9.200988					0.97712	0.001403
7	11	0.007808	5922	8.750947		Frequency scaling factor	0.00071		0.903295	0.001335
8	13	0.009228	5036	7.778462					0.768151	0.001186
9	15	0.010648	4296	6.624257					0.655278	0.00101
10	17	0.012067	3665	5.651062					0.55903	0.000862
11	19	0.013487	2886	4.650183					0.440207	0.000709
12	21	0.014907	2428	3.772107					0.370348	0.000575
13	23	0.016326	2018	3.155963					0.30781	0.000481
14	25	0.017746	1620	2.58241					0.247102	0.000394
15	27	0.019166	1416	2.155084					0.215985	0.000329

Figure 6.7 The table of values for the histogram of amplitude spectrum image for subject 5. The data is transferred into a spreadsheet via DDE, and the graph-scaling factor for the X axis, also input into the spreadsheet.

6.5 Results

6.5.1 Subjects

Fourty five eyes of fourty five patients with posterior capsule opacification following uncomplicated cataract surgery with posterior chamber intraocular lens implants were included in this pilot study. The mean age was 78.39 ± 9.39 years (mean ± SD) for all subjects, with a range of 51 to 92 years, and the subjects included men 23 and 22 women. Table (6.1) shows the subjects' demographic details, according to posterior capsule opacification morphological types.

Characteristic of Subjects	Posterior capsule opacification Types		
	Fibrotic (n= 17)	Pearl (n= 18)	Mixed (n= 10)
Age of subjects (Mean ± SD)	79.44 ± 8.95	75.76 ± 9.65	81.88 ± 9.25
Gender (F / M)	8 / 9	9 / 9	5 / 5

Table 6.1 Subjects' details.

The subjects had received the following intraocular lens implants in the capsular bag: Allergen Medical Optic (AMO) IOL types S130NB silicone (3 out of 45 eyes; 6.6%), S140NB (2 out of 45 eyes; 4.4 %), PS53ANB (6 out of 45 eyes 13.3 %), PS26TB (4 out of 45 eyes 8.8 %), Bausch & Lomb silicone Soflex2 (28 out of 45 eyes; 62 %), Storz (1 out of 45 eyes 2.2%) and Chiron (1 out of 45 eyes 2.2 %). For details of the IOLs see table (4.4). Table 6.3 shows the time interval between cataract surgery and Nd:YAG laser capsulotomy according to implanted IOL types.

IOLs	PS53ANB	SI30NB	S140NB	Sofles2	PS26TB	Storz	Chiron
Interval between surgery and Nd:YAG laser capsulotomy (months)	42. 3± 10.5	40 ± 6.93	30 ± 8.5	14.3 ± 9.24	33 ± 6	84 months	14 months

Table 6.2 The time Interval between cataract surgery and Nd:YAG laser capsulotomy in months (Mean ± standard deviation (SD)).

The central area of interest of all images were morphologically and subjectively classified according to PCO types (fibrotic, pearl, and mixed). The severity of the PCO was also graded using a VAS, (for further details see chapter 4). The spectral power of the AOI of the amplitude spectrum images was calculated as previously described.

Subjects	Subjective morphological classification of PCO Types	Spectral Power	Subjective severity grading (1-5)
1	Fibrotic	51.1509	3.3
2	Fibrotic	34.0041	1.5
3	Fibrotic	19.5717	0.5
4	Mixed	40.2364	2.5
5	Fibrotic	91.3235	3.5
6	Mixed	50.7564	2.5
7	Pearl	49.1412	2.7
8	Pearl	51.9428	2.5
9	Fibrotic	55.5289	2.7
10	Fibrotic	65.001	2.6
11	Fibrotic	48.095	2.0
12	Fibrotic	25.5723	2.0
13	Pearl	67.4099	3.0
14	Pearl	30.4012	2.2
15	Fibrotic	82.1023	3.3
16	Pearl	139.44	3.8
17	Fibrotic	63.8064	3.0
18	Pearl	61.9743	3.2
19	Pearl	30.1568	2.3
20	Fibrotic	69.8374	3.5
21	Fibrotic	343.779	4.5
22	Pearl	65.6482	3.0
23	Pearl	73.2705	3.4
24	pearl	28.0338	2.3
25	Pearl	31.8222	1.9
26	Fibrotic	62.1536	3.0
27	Mixed	33.525	2.6
28	Mixed	61.7563	2.8
29	Fibrotic	39.653	2.6

30	Fibrotic	79.0854	3.5
31	Mixed	62.5558	3.0
32	Pearl	46.2043	2.4
33	Mixed	39.3896	2.2
34	Fibrotic	45.2612	2.5
35	Pearl	30.9114	2.3
36	Pearl	33.3342	1.9
37	Pearl	54.2583	3.0
38	Pearl	72.3124	3.0
39	Pearl	59.332	3.0
40	pearl	31.5414	2.1
41	Mixed	40.931	2.0
42	Mixed	55.2191	2.7
43	Fibrotic	101.211	3.5
44	Mixed	22.6654	1.3
45	Mixed	63.3664	2.6

Table 6.3 Subjective classification of PCO morphology grading of severity together with the spectral power of the amplitude spectrum for each image.

To assess the degree of association between subjective grading and the spectral power, scatter plots of subjective grading within the area of interest against the spectral power of the amplitude image within the area of interest was constructed for fibrotic PCO (fig. 6.8), pearl PCO (fig. 6.10), and mixed PCO (fig. 6.12). However, the scatter plot reveals that there is no linear correlation between subjective grading and the spectral power. This could be due to the fact that the human eye responds logarithmically to light level (Gonzalez & Woods, 1992) and the grading was performed subjectively by an ophthalmologist. Therefore, scatter plots of subjective grading within the area of interest against the Log of spectral power were constructed for fibrotic PCO (fig. 6.9), pearl PCO (fig. 6.11), and mixed PCO (fig. 6.13), these plots

demonstrate a linear relationship between the two variables for all types of PCO.

Spearman's rank correlation coefficient was used to calculate the correlation coefficient because the variables are nonparametric and use different units of measurements. Spearman's rank correlation coefficients for fibrotic, pearl and mixed PCO were 0.909, 0.864, and 0.713. This indicates that there is a good correlation between subjective grading and Log spectral power for the three types of PCO. We conclude that spectral power could be used as an objective measure for PCO severity.

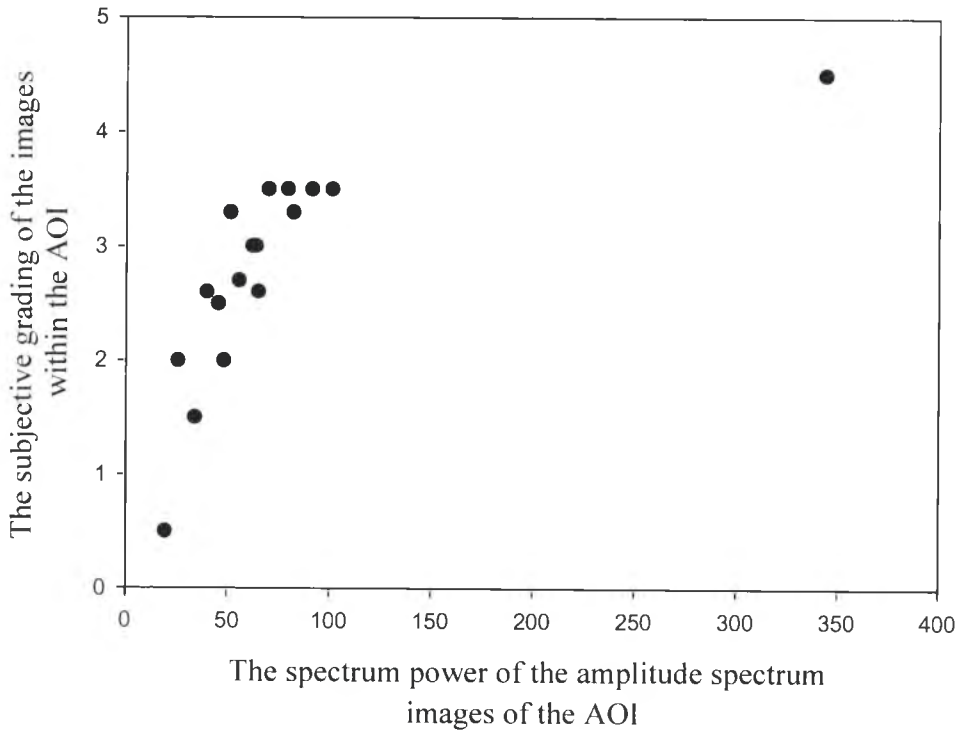

Figure 6.8 Subjective grading of fibrotic PCO plotted against the spectral power of amplitude spectrum images. There is no linear relationship between the two variables.

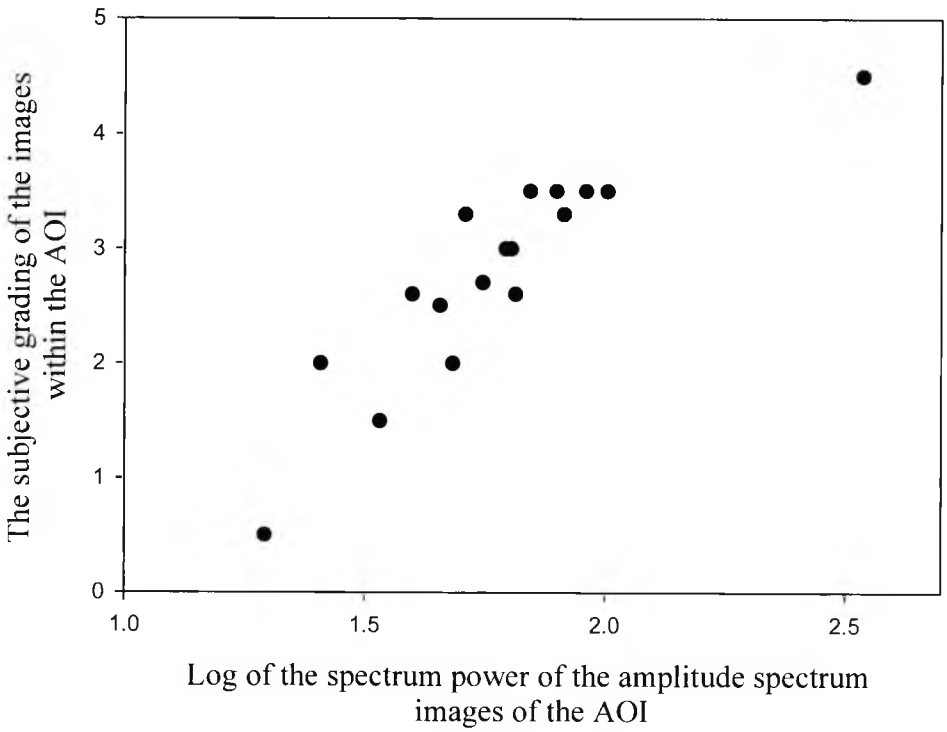

Figure 6.9 Subjective grading of fibrotic PCO plotted against the Log of the spectral power. There is linear relationship between the two variables.

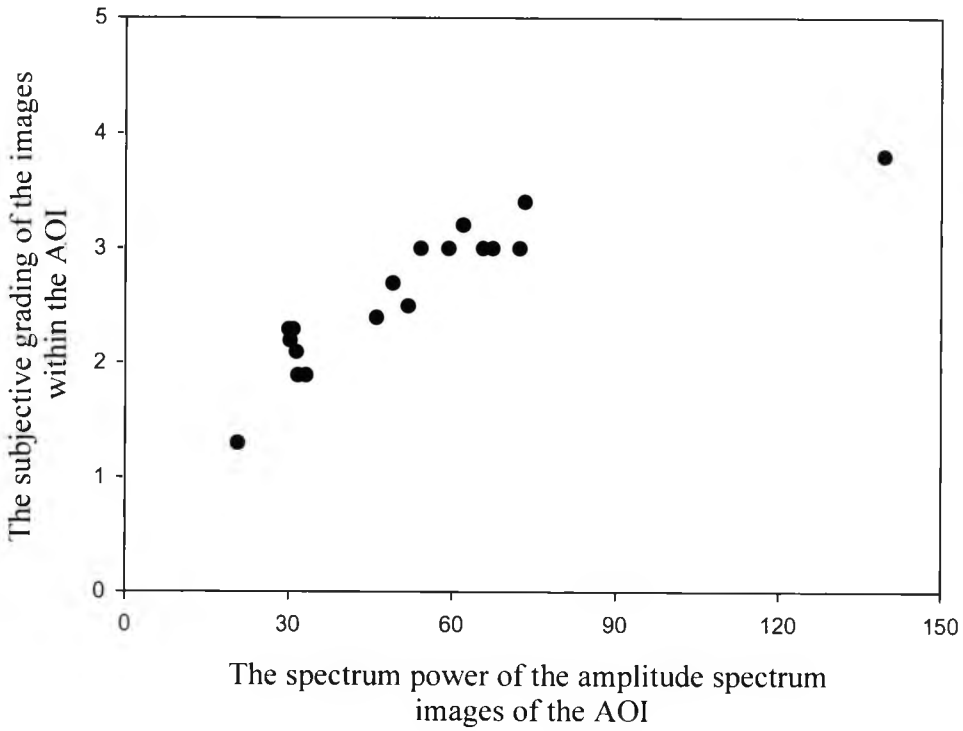

Figure 6.10 Subjective grading of pearl PCO plotted against the spectral power. There is no linear relationship between the two variables.

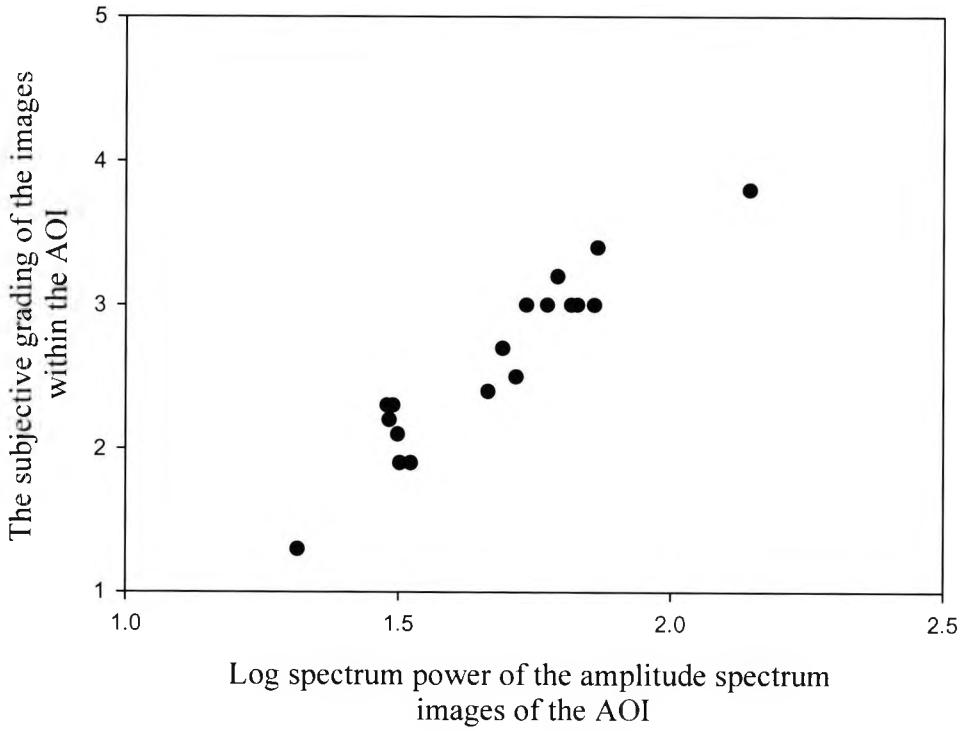

Figure 6.11 Subjective grading of pearl PCO plotted against the Log spectral power. There is linear relationship between the two variables.

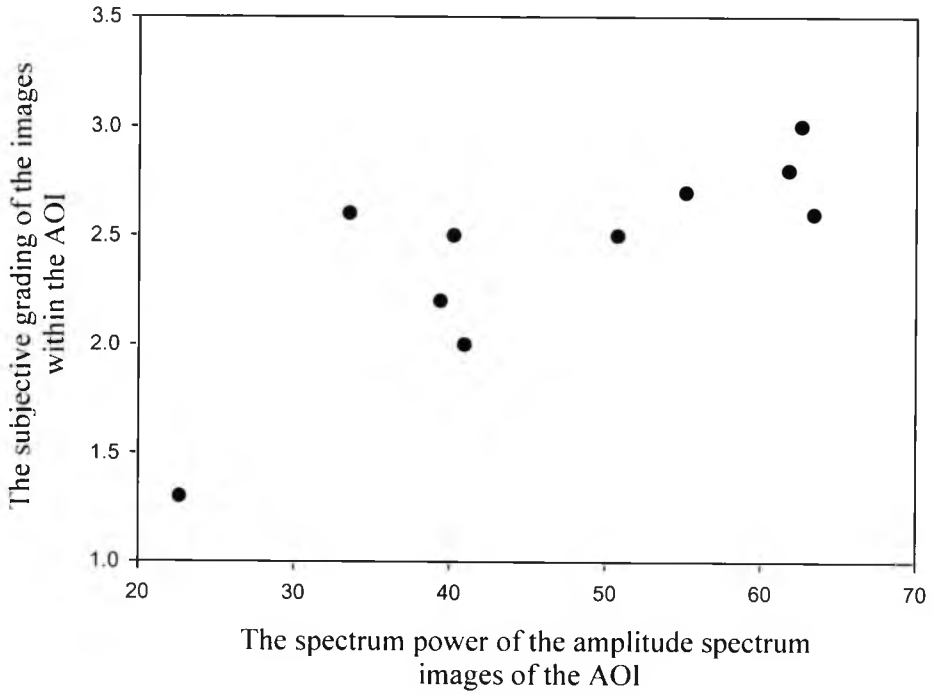

Figure 6.12 Subjective grading of mixed PCO of the AOI images plotted against the spectral power. This shows no linear relationship between the two variables.

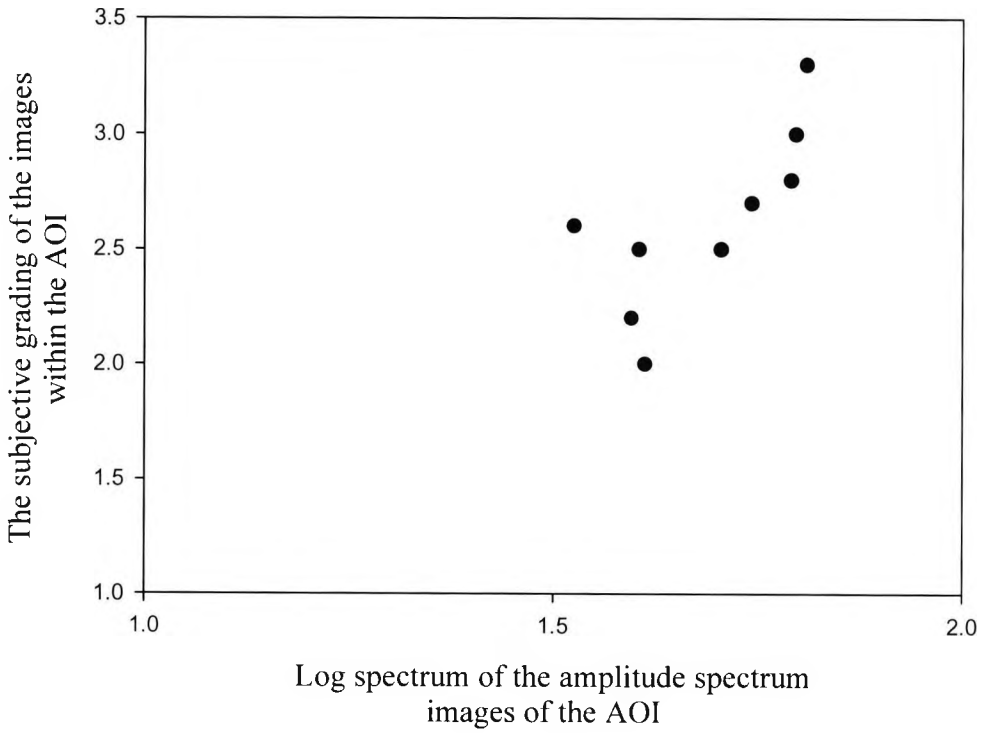

Figure 6.13 Subjective grading of mixed PCO plotted against the Log spectral power. There is linear relationship between the two variables.

6.6 Discussion

Various systems have been developed yet none have provided an ideal technique to quantify PCO objectively. Therefore, it is important to work towards developing an objective technique to measure PCO severity so that it can be used to evaluate clinical trials that seek to reduce PCO. We believe that an objective measurement of PCO severity has been established in this study using the spectral power of the amplitude spectrum image.

The developed technique is objective because the back scattered light, which represents the opacified areas, is shown as peaks in the amplitude spectrum image. This technique does not use subjective user interference to identify or outline the boundaries of the different levels of PCO of the digital images on computer and the software calculates a value of PCO. An advantage is that the FFT option is present in most image processing and analysis software hence the technique does not require the purchasing of further expensive software or need extensive image manipulation. We believe that once the area of interest image is obtained then there are three straightforward steps needed to obtain the spectral power value that provides an estimate of the PCO severity, as explained in figures 6.6 and 6.7. Furthermore, this technique provides an absolute value that estimates PCO severity, because it does not set or fix a threshold value that may not be suitable for use with images having different luminance.

This study demonstrates that this objective technique to quantify PCO severity provides valid results that have a strong association between the subjective grading of PCO within the AOI images and Log of spectral power for the three types of PCO. Although the value of the Spearman's rank correlation coefficient for mixed PCO is slightly less than fibrotic and pearl this might be due to the mixed PCO sample size in this group (n=10).

Chapter Seven

7. Objective classification of posterior capsule opacification

7.1 Introduction

As technology improves, the number of digital images created in all medical fields for the purposes of both patient care and research correspondingly increases. There is current interest in developing practical systems for classifying and diagnosing these images, especially where medically significant content such as shape, geometry, colour and texture can be clearly defined. An example of such a system is the structured analysis of the retina system (STARE) (Goldbaum et al. 2000).

Currently there are various techniques to classify and recognise images. These include (1) expert systems where human expert knowledge provides the rules and the system searches through these images to locate the relevant rule to match the data; (2) Supervised classification, a technique developed to identify a number of classes specified by a human; (3) Unsupervised classification where prototypes of various classes and class variation are identified and placed into class regions in order to maximize the similarity of objects within each cluster and the difference between groups (Russ, 2000). In this study we decided to classify our images using an expert system due to the facilities and options provided by Image Pro+. This software allows fast handling of collected data without the need to use additional software.

An *Expert system* is a computer program specifically designed to solve any problem in a domain that relies on human expertise. In this study the expert system comprises of three major modules: the *knowledge base,* which stores the expertise required to solve the problem, the *working memory,* which contains data that triggers or hinders certain rules, and the *inference engine,* which provides the answers using the *knowledge base and working memory* (fig. 7.1). The knowledge base and inference engine are separate modules to add or subtract rules without modifying the inference engine. An expert system program differs from a conventional computer program by putting together the knowledge base with the working memory to reach conclusions or decide what actions should be taken next (Luger, 2002).

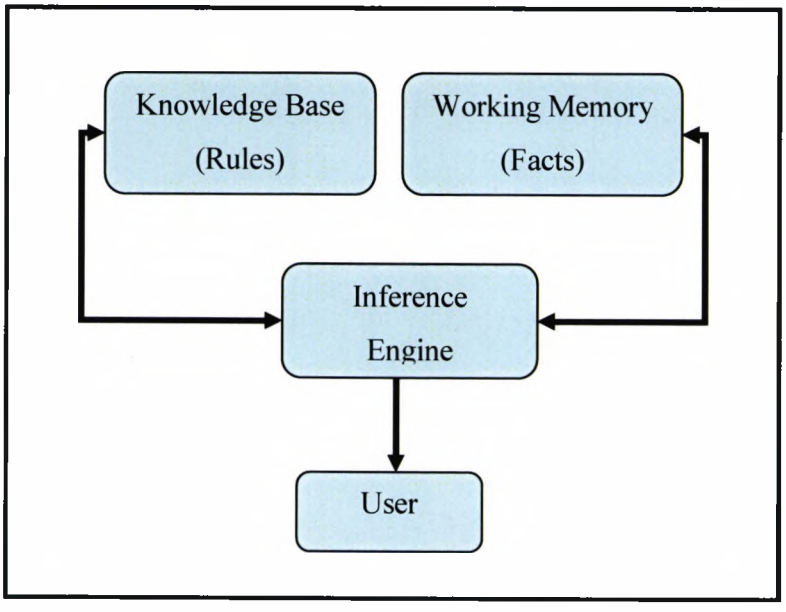

Figure 7.1 Expert System Architecture.

The main aim of this section of the study was to develop an objective method of classifying posterior capsule opacification into is three main morphological groups fibrotic, pearl or mixed, by creating a smaller version of the expert system described above.

7.2 Classification criteria

Often ophthalmologists tend to describe PCO using high level descriptors. For example, pearl-type PCO is often described as "clumps" or "bubbly structure". However, this level of description has no meaning to a computer therefore it is necessary to generate equivalent computer representations at a lower level. The representation method used in this study is the 'if – then' rule, where the rule is a statement or set of statements. In these statements *If* represents the conditions and *then* represents a conclusion or an appropriate next step.

Our approach has been to use the definitions of the PCO types provided by ophthalmologists to set the rules of identification. Objects within the area of interest (AOI) are then selected, measured, and interpreted to distinguish between the three types of PCO with the assistance of subjective classification. Finally, the results of objective classification were compared with subjective morphological classification performed by an experienced ophthalmologist.

Classification is established by creating a set of measurement criteria for the objects of interest within the image. These can then be used to identify or distinguish between PCO types. The selection of these measurement criteria is based on the ophthalmologist's description and definition of PCO morphological types. For example, in the case of pearl PCO, a clump of cell mass generally starts at the centre of the posterior capsule (fig. 7.3), suggesting very small areas of opacity, large in number and with a small distance between them. Fibrotic PCO is normally viewed as a sheet or bundle of tissues, dependent on the severity, and usually extending from the periphery toward the centre of the posterior capsule. This suggests the objects of interest are large areas, which are small in number (fig. 7.2). Mixed PCO, a combination of both pearl and fibrotic, may suggest that there are two classes of objects of interest with different sizes, the smaller ones often located centrally representing pearling and larger peripheral objects that represent the extension of fibrotic PCO (fig. 7.4).

For the purpose of computer recognition, the criteria chosen in this study are the size, number and distance between objects of interest within the AOI. The size of the objects of interest within the AOI is crucial, because it plays a key role in distinguishing between pearl and fibrotic PCO. The number of objects of interest within the AOI can help to distinguish between fibrotic and mixed PCO because it was apparent that the number of small areas of opacity are less with fibrotic than mixed PCO. The distance between objects of interest can also be used to distinguish pearl from other PCO types due to the small distances between areas of opacity.

7.3 Image segmentation and outlying the objects of interest

Image segmentation or thresholding is a crucial step in image analysis. This process produces a pixel-based representation of the image that assigns each pixel either to the object of interest or to the surroundings. Classification criteria then concentrate on the pixels of the objects of interest and discard the rest.

Thresholding is achieved either manually or automatically. Threshold levels can be set interactively by a user watching the image. However, the result is not consistent from one user to another or even with the same user. Automatic thresholding, on the other hand, is usually implemented using algorithms. For example, in Image Pro+, auto-thresholding is a method that offers consistency as its main advantage. It assumes that the grey level histogram is the sum of two normal intensity distributions (two classes): foreground and background pixels. The threshold is usually not obvious because the two distributions overlap. Using this model, finding the threshold is equivalent to finding where the two distributions intersect (which is not necessarily at the bottom of the valley that, in the best case, separates the two distributions). For each grey level (t) along the histogram h(t), the algorithm calculates the variance of the two portions of the histogram lying on each side of t, V_1 (t) and V_2 (t). It picks the grey level (threshold) that minimises the sum of the two normalised variances.

Although it is recognised that many different thresholding techniques exist, the method described above provides an objective approach that will be shown to work well for this application. It may be worth exploring other methods in the future.

The second step, following thresholding, is to outline the objects of interest for measurement. Manually outlining the objects of interest is performed using a mouse. However, it relies on subjective assessment to locate boundaries of the objects of interest. Automatic outlining can be achieved using image processing software and is particularly useful especially where the size of the objects of interest is very small or where they have a low intensity. It is therefore possible to improve the objectivity and consistency of the measurement results.

In PCO, the areas of opacification appear as bright areas within the AOI. Figures 7.2 to 7.4 show that the Image Pro+ software is capable of automatically segmenting and outlining the three types of PCO with various levels of severity where the selected measurement criteria are size, number and distance between objects of interest within the AOI image.

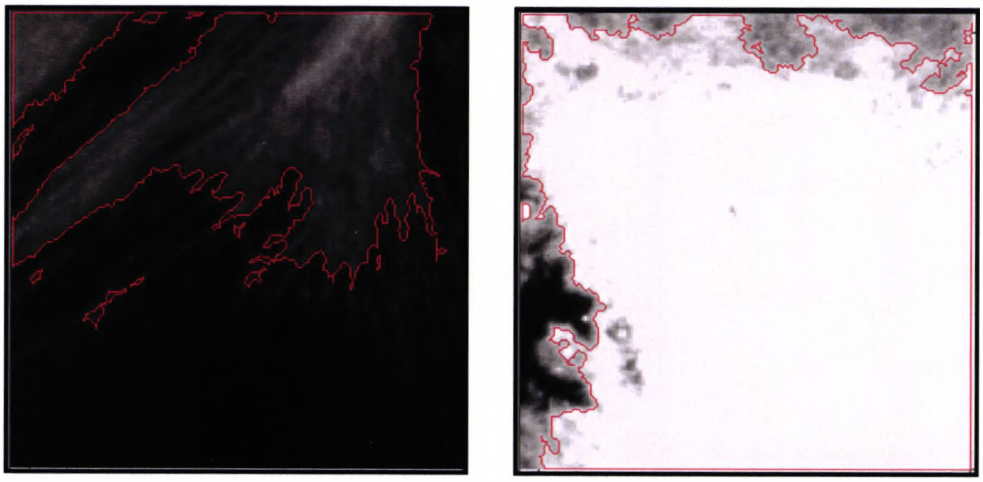

Figure 7.2 Images from subjects 30 and 21 subjectively classified as fibrotic PCO with severity grading of 3.5 and 4.5, and morphological confidence levels of 4.0 and 4.5 respectively. These images have been automatically segmented and outlined using Image Pro+ software (count and size option).

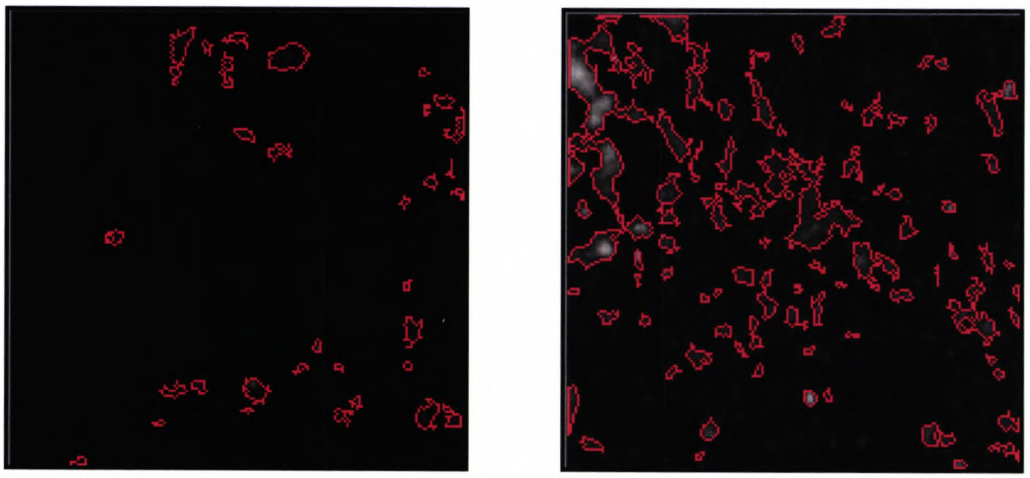

Figure 7.3 Images from subjects 35 and 13 subjectively classified as pearl PCO with severity grading of 2.3 and 3.0, and morphological confidence levels of 3.0 and 4.0 respectively. These images have been automatically segmented and outlined using Image Pro+ software (count and size option).

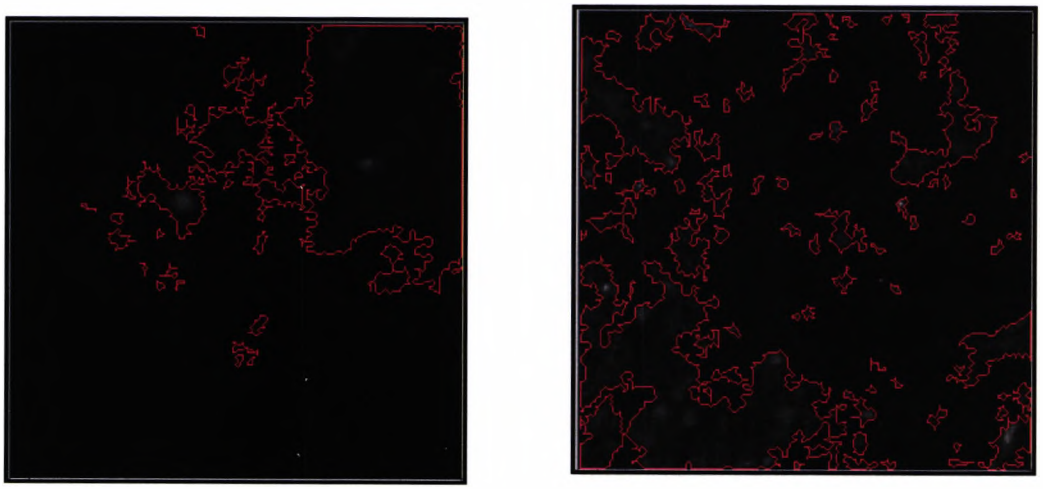

Figure 7.4 Images from subjects 41 and 45 subjectively classified as mixed PCO with severity gradings of 2.0 and 2.6 respectively and morphological confidence levels of 2.5 for both. These images have been automatically segmented and outlined using Image Pro+ software (count and size option).

7.4 Implementation of image classification using Image Pro+

Subjective classification of PCO images is based on the definitions and descriptions of PCO types linked to the size and location of the area of opacity. However, subjective classification does not provide an estimation or actual measurement of the size, number and distance between areas of opacity. In order to create the rules for the computer to identify and distinguish between the three types of PCO an estimation of these measurements must be specified.

To do this, 45 images were divided into three categories: fibrotic, pearl and mixed according to the subjective morphological classification. The images in each category were arranged into ascending order according to their severity. Finally data on the size, number and distance between areas of opacity were collected for all images in each category.

The method described above permits the study of changes in the area of the opacity and the number and distance between these areas as severity progresses. For the area measurements, it was apparent that fibrotic PCO at an early stage tended to progress as bundles of tissue that spread horizontally and cover an increasingly a large area. As the severity increases, the opacity manifests as thick white sheets of tissue. In the case of pearl PCO, the opacity manifests as small areas of opacity often located centrally. As the severity increases the density and number of these regions increases rather than the area of the opacities. Therefore, comparing the area of both fibrotic and pearl data would provide an estimation of the area threshold which could then be used to distinguish between fibrotic and pearl PCO.

The number of small areas of opacity is high in case of pearl PCO. The number of opaque regions increase and the distance between them becomes less as the severity increases. Mixed PCO combines features of two main classes of pearl and fibrotic PCO. Yet, counting the number of small areas which represent pearl PCO might distinguish fibrotic from mixed PCO since pearl PCO is distinguished by a larger number of small areas compared to fibrotic PCO. Also the presence of larger areas of opacity may distinguish between mixed and pearl PCO since the latter comprises small areas. Therefore, comparing the number of small areas of opacity for fibrotic and mixed PCO could be used to distinguish between them.

The distances between the centres of the objects of interest were calculated using Pythagoras' theorem, where the centre is the centroid of the object weighted by its intensity distribution. Examining the results of these distances may provide a threshold that could be used to distinguish between pearl and other types of PCO.

For instance, it was apparent that fibrotic PCO often covers larger areas and is seen as sheets or bundles, dependent on its severity. According to the data, these bright areas may start from 0.60mm^2 and tend to grow larger in size as the severity increases. Also, these areas of fibrosis tend to extend from the periphery toward the centre of the posterior capsule.

In the case of pearl PCO, the bright areas representing opacity are smaller in size. Increase in severity of pearl PCO often manifests itself as an increase in the density of the opacity thus the size of the bright areas maybe less than 0.60mm^2. Also, the result of counting the bright areas of opacity revealed that there are a large number of objects. For example, the number of opacified areas may reach 3000 within the AOI. Therefore, a loop was introduced to reduce the number of areas for analysis to 1000. It contains a sequence of functions that are repeated until the specified numbers of areas are obtained. Initially the auto range is set to segment the pixels of the objects of interest from the background by adding 5 steps to the starting point of the range of the minimum intensity value until a reasonable number of objects of interest are obtained. This loop is triggered if the number of objects is more than 1000. This was considered sufficient to identify and distinguish between all types of PCO since fibrotic and mixed PCO tend to have a smaller number of areas than pearl. The loop accelerates data collection and analysis. Furthermore, the result shows that the actual distance between the centres of nearest bright areas are often less than 0.25mm.

A minimum area size is also defined since there is no point in analysing very tiny areas (such as 0.0001mm²) as they were shown to not affect the classification result. Examining the data reveals that an appropriate threshold area would be 0.002mm².

In cases of mixed PCO, the data show a combination of fibrotic and pearl characteristics, such as the presence of larger and smaller areas within the AOI. However, it was apparent that with mixed PCO the number of small areas was larger than fibrotic PCO, hence the estimation of the number of small areas threshold is set to 35.

The rules and conditions of identification of PCO types implanted in this macro represent the knowledge base and are applied until one rule matches the image. The rules applied to classify PCO morphologically are summarised as follows:

Rule 1: *If there are bright objects of area larger than 0.60*mm² within the AOI, AND *also bright objects of area between 0.60*mm² *and 0.002*mm², *count the number of smaller objects. If the number of smaller objects of interest is:*

Less than 35= fibrotic

More than 35=mixed

Rule 2: *If there are no bright objects of interest larger than 0.60* mm², *AND if there are bright objects of interest smaller than 0.60* mm² *and larger than 0.002* mm², *then calculate the distance between the centres of pairs of objects of interest. If the distance between the nearest objects of interest is:*

Less *than 0.25mm = pearl*

More *than 0.25mm = mixed*

Finally, once the data of the bright objects within the AOI image triggers all the conditions of either of the two main rules, a classification result is obtained and printed in the Image Pro+ output window.

7.5 Method and materials

This pilot study comprised 45 eyes of 45 subjects. The images of the posterior capsule of the eyes were taken using a Nikon FS-2 slit lamp with the modified fixation stimulus, and with the following settings: slit beam width 3.5mm, 45° angle of illumination, film speed (ISO) for camera was 1600 and DSU 800, exposure compensation 0, flash intensity 2, and magnification 25X. In addition, retroillumination images were taken for some of the subjects. All the images were obtained at the same session for each subject and with the same observer. The subjects were all volunteers recruited from the Royal Eye Unit at Kingston Hospital. They had all received uncomplicated cataract surgery with posterior chamber intraocular lens implants due to age related cataract. They were attending a clinic prior to Nd:YAG laser capsulotomy. The images of PCO were captured through a dilated pupil (one drop of tropicamide 1%). All the procedures used to capture the images were the same as described in § 5.4.

7.6 Results

Subject demographic details according to posterior capsule opacification morphological classification types of intraocular lens the subject had received, and the time interval between cataract surgery and Nd:YAG laser capsulotomy according to implanted IOL types can be found in § 6.5.1.

Although there are two main types of PCO (pearl and fibrotic), a third type is a combination of both. However this does not imply that the two main forms manifest as pure types. Therefore, a proforma was given to an experienced ophthalmologist that contained one visual analogue scale (VAS) (5cm long) for each presented image of PCO shown on the computer screen. The ophthalmologist was asked to grade these images on the basis of how confident he was of his morphological classification result. For example, if the subjective classification is fibrotic then the visual analogue scale provides an estimate of the confidence of the classification. Table 4.2 shows the subjective classification of PCO morphology, confidence and objective classification for each subject.

Subjects	Subjective morphological classification	Objective morphological classification	morphological Confidence subjective grading (1-5)
1	Fibrotic	Fibrotic	3.4
2	Fibrotic	Fibrotic	2.0
3	Fibrotic	Fibrotic	1.5
4	Mixed	Pearl	2.5
5	Fibrotic	Fibrotic	3.6
6	Mixed	Fibrotic	2.5
7	Pearl	Pearl	3.0
8	Pearl	Pearl	3.0
9	Fibrotic	Fibrotic	3.5
10	Fibrotic	Fibrotic	3.0
11	Fibrotic	Pearl	2.7
12	Fibrotic	Fibrotic	3.0
13	Pearl	Pearl	4.0
14	Pearl	Pearl	3.3
15	Fibrotic	Fibrotic	3.5
16	Pearl	Fibrotic	4.0
17	Fibrotic	Fibrotic	3.3
18	Pearl	Pearl	3.7
19	Pearl	Mixed	3.5
20	Fibrotic	Pearl	4.0
21	Fibrotic	Fibrotic	4.5
22	Pearl	Pearl	3.6
23	Pearl	Mixed	4.0
24	pearl	Pearl	2.7
25	Pearl	Pearl	3.0
26	Fibrotic	Fibrotic	3.0
27	Mixed	Pearl	2.5
28	Mixed	Fibrotic	2.5
29	Fibrotic	Fibrotic	2.4
30	Fibrotic	Fibrotic	4.0
31	Mixed	Pearl	2.5
32	Pearl	Mixed	3.0
33	Mixed	Pearl	2.6

34	Fibrotic	Fibrotic	3.2
35	Pearl	Pearl	3.0
36	Pearl	Pearl	2.8
37	Pearl	Pearl	3.3
38	Pearl	Mixed	3.1
39	Pearl	Pearl	3.5
40	Pearl	Pearl	3.1
41	Mixed	Mixed	2.5
42	Mixed	Fibrotic	2.5
43	Fibrotic	Fibrotic	3.5
44	Mixed	Mixed	2.5
45	Mixed	Mixed	2.5

Table 7.1 Subjective classification of PCO morphology, objective classification by the expert system and the confidence factor for the subjective grading.

The results of the objective morphological classifier revealed that out of 45 images of the 45 subjects, only 31 images matched the subjective classification. Table 7.2 shows the 45 images classified into fibrotic, pearl and mixed PCO where the subjective classification performed by an experienced ophthalmologist was tabulated against the objective classification obtained from the expert system.

The cross diagonal shaded cells of table 7.2 represent the matches between subjective classification and objective classification for the three types of PCO, whilst the other cells represent un-matched classifications.

	Subjective classification		
Objective classification	Fibrotic	Mixed	Pearl
Fibrotic	15	3	1
Mixed	0	3	4
Pearl	2	4	13

Table 7.2 Subjective versus objective morphological classification of PCO images. Shadowed cells represent the matches between subjective and objective classification.

Statistical analysis of the results revealed a weighted kappa of 0.61. This indicates that the strength of agreement is "good" according to Altman (1991). Examination of the table (7.2) reveals that there is considerable agreement between the two methods of classification for fibrotic and pearl-type PCO since the number of cases that agree compared to those that disagree is high. For mixed PCO disagreement is considerable since the number of cases of agreement and disagreement are similar.

The mean confidence values and their 95% confidence intervals were calculated for each category in table 7.3. The results reveal that there is good agreement particularly with fibrotic and pearl PCO when the mean confidence value was moderately high (3.16 and 3.23). This may indicate that there is good agreement when severity of PCO is high, because the opacity characteristic is better defined and hence the subjective classifier is confident

of their result.

	Subjective classification			
Objective classification		Fibrotic	Mixed	Pearl
Fibrotic	Mean ± CI	3.16 (4.63, 1.69)	2.5 (2.5, 2.5)	4.0 0
Mixed	Mean ± CI	0 0	2.5 (2.5, 2.5)	3.4 (4.29, 2.51)
Pearl	Mean ± CI	3.35 (5.15, 1.55)	2.5 (2.5, 2.5)	3.23 (3.97, 2.49)

Table 7.3 Mean confidence values for subjective grading with associated 95% confidence intervals shown in parenthesis for each category.

However, the results that do not agree for fibrotic and pearl PCO show that the mean confidence values are also high. For example, in the case of fibrotic images classified as pearl the mean confidence level was 3.35. This could be explained due to a limitation of subjective classification and the presence of folds or wrinkles in the posterior capsule. In the case of pearl PCO that was classified as mixed, the confidence level was 3.34 due to presence of classes of fibrotic and pearl PCO.

In the case of pearl PCO that was classified as fibrotic, the confidence level was 4.0. However, this result was from a single case where there was a unique morphological structure; the pearl opacity covered a large area, which was engulfed by thin bundles of fibrotic tissue, thus the system identified the opacity as one area and classified it as fibrotic. This case can therefore be considered as an outlier compared to the other 44 cases.

The results for mixed PCO, which are confused with fibrotic or pearl, show that the mean confidence value was 2.5 in both cases. This could be explained due to various factors: in the case of fibrotic PCO it may be due its early development making it difficult to classify, or the fact that fibrotic PCO usually progresses faster than pearling hence it can engulf pearl PCO. In the case of mixed PCO confused with pearl PCO, this could be due to the early development of the PCO where pearling is predominant in the central AOI.

In order to form a better understanding of why the objective morphological classifier did not produce the same results as a subjective classifier in 14 cases, re-examination of the images was performed based on dividing them into five categories: (1) fibrotic-pearl, (2) pearl-fibrotic, (3) mixed–pearl, (4) pearl-mixed and (5) mixed-fibrotic. In these categories, the first represents the subjective classification and the second represents the objective classification.

In the first category (fibrotic-pearl), the subjective classification for subjects 11 and 20 was fibrotic whilst the objective classification was pearl PCO. Examination of the retroillumination image for subject 11 reveals that the subject has pearl PCO as seen in figure (7.5. B) which supports the objective result. This may be due to an error in subjective classification for this subject; figure (7.5. A) illustrates how this might have arise.

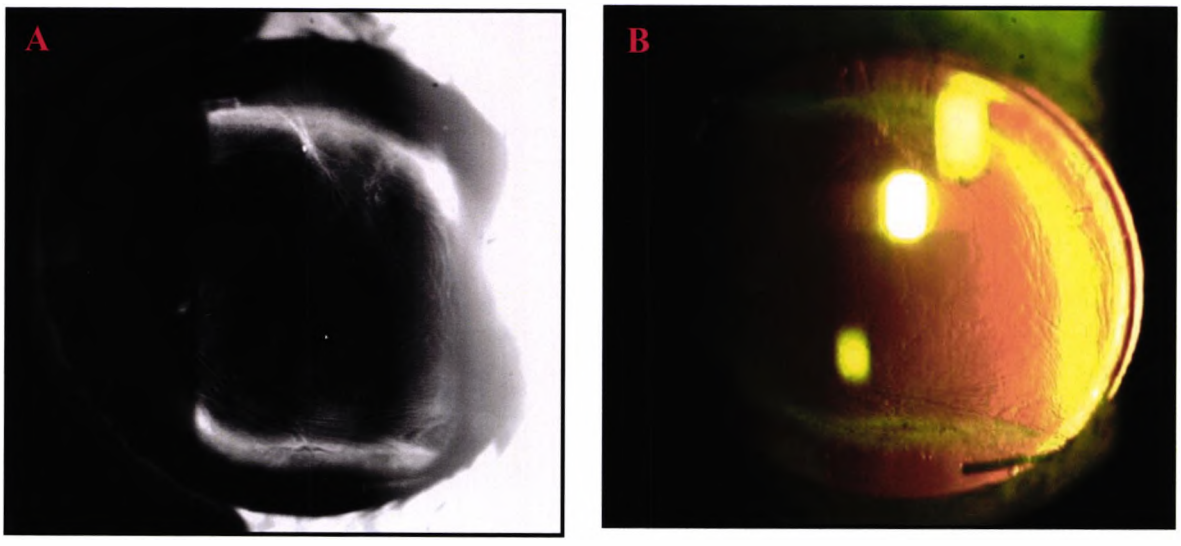

Figure 7.5 Images for subject 11, (A) reflected light image, and (B) retroillumination image. The confidence level for subjective morphological classification was 2.7.

As discussed in chapter 3, wrinkling of the posterior capsule occurs because of the contractile nature of the newly formed fibrocytes (Apple et al. 1989). Examination of subject 20's image, which was produced by a surface plot that creates a three dimensional representation of the intensity of an image; revealed that there were folds or wrinkles through which the LECs migrate and proliferate as pearl and fibrotic PCO (fig. 7.6.B). The objective morphologic classifier recognises the presence of pearl PCO but did not recognise the fibrotic PCO because the fibrotic PCO had developed along these long folds (fig. 7.6.A). Consequently the objective morphological classifier classified this as pearl PCO.

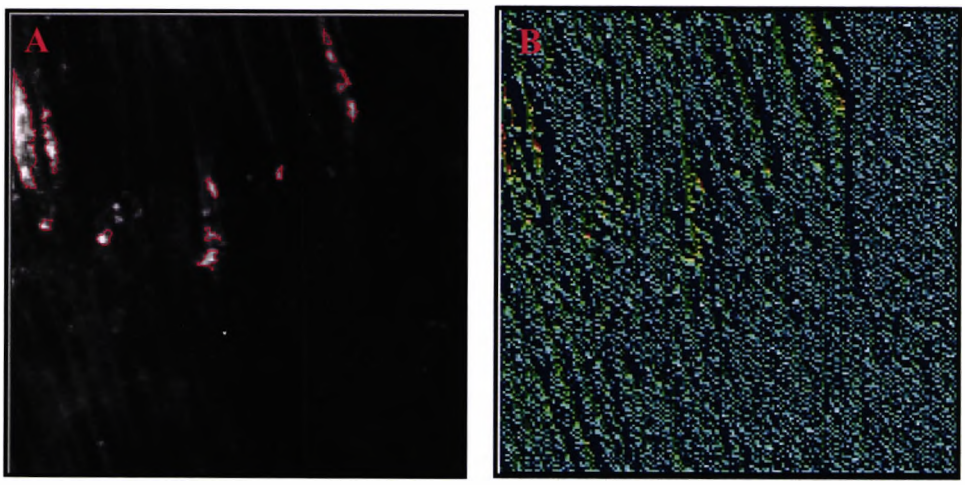

Figure 7.6 Images for subject 20: (A) is a reflected light image with the object of interest outlined and (B) is a surface plot image to show the folds in the posterior capsule. These grooves are either empty or filled with fibrocytes, which are able to manifest as either fibrotic or pearl tissue.

In the second category (pearl-fibrotic), the subjective classification for subject 16, as taken from table (7.3), was pearl PCO whilst the objective classification was fibrotic PCO. Examination of the images for subject 16 revealed that the main reason for disagreement was that pearl PCO had spread over a large area of the capsule and had been engulfed by bundles of fibrotic tissue thus the system recognised one area hence the classification was fibrotic. The initial subjective classification was pearling yet a second classification by the same subjective classifier reported it as mixed PCO. It would seem reasonable to consider this case as an outlier due to its unique morphological texture and structure compared with the other 44 cases. It appears that the current objective morphological classifier is not able to separate or well-define classes in the posterior capsule. Thus, more sophisticated techniques are required to separate these two classes.

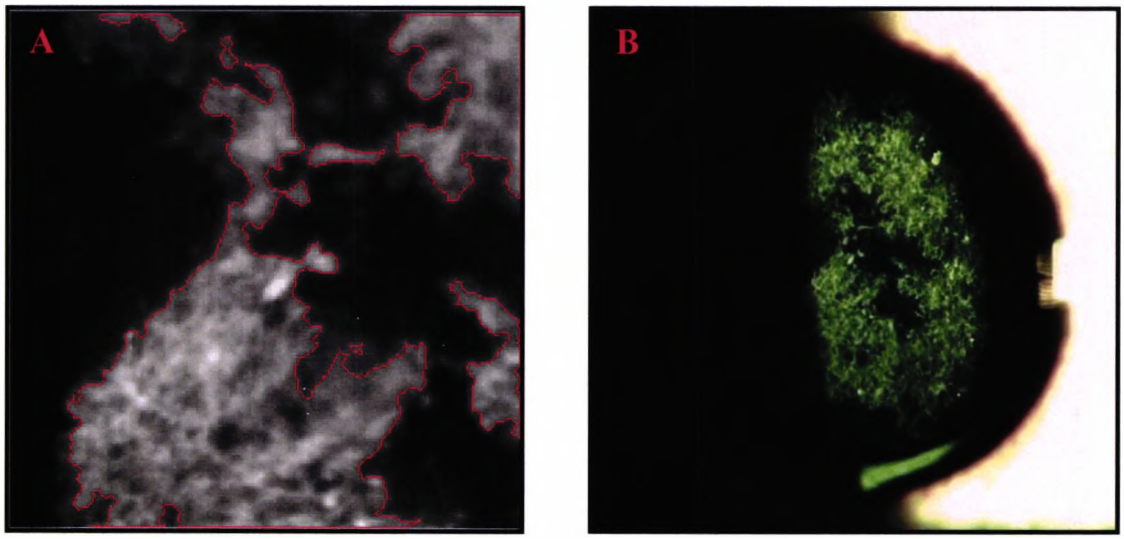

Figure 7.7 Images for subject 16: (A) the reflected light image of the AOI with the objects of interest outlined, and (B) the whole image of the posterior capsule. The confidence level for subjective morphological classification was 4.

In the third category (mixed-pearl), the subjective classification for subjects 4, 27, 31, and 33 was mixed PCO whilst the objective classification was pearl PCO. Examination of the images for subjects 4 and 31 shows that there is an early development of pearl PCO as seen in figures (7.8.A and 7.9.A), since pearling often starts at the centre of the posterior capsule and progresses more slowly than fibrotic PCO. Also, the negative images of the posterior capsule (7.8.B and 7.9.B) conform that there is early progress. In the cases of subjects 27 and 33 (7.10.A and 7.11.A) the classification criteria data of the AOI for both subjects reveals that all the conditions of the classification rules are fulfilled for pearl PCO. These cases of disagreement may be due to the fact that the subjective classification was performed by presenting the whole image to the subjective classifier whereas the objective system classifies images by concentrating only on the AOI. It may have been more appropriate to present AOI images to the subjective classifier.

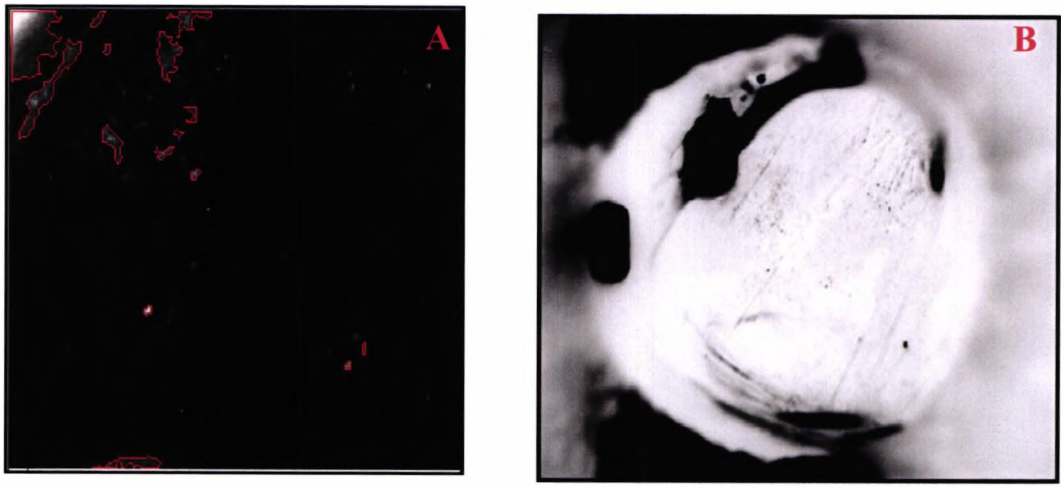

Figure 7.8 (A) Image of subject 4 captured with the reflected light technique and the objects of interest outlined. (B) Shows the negative image of the whole posterior capsule. The confidence level for subjective morphological classification was 2.5.

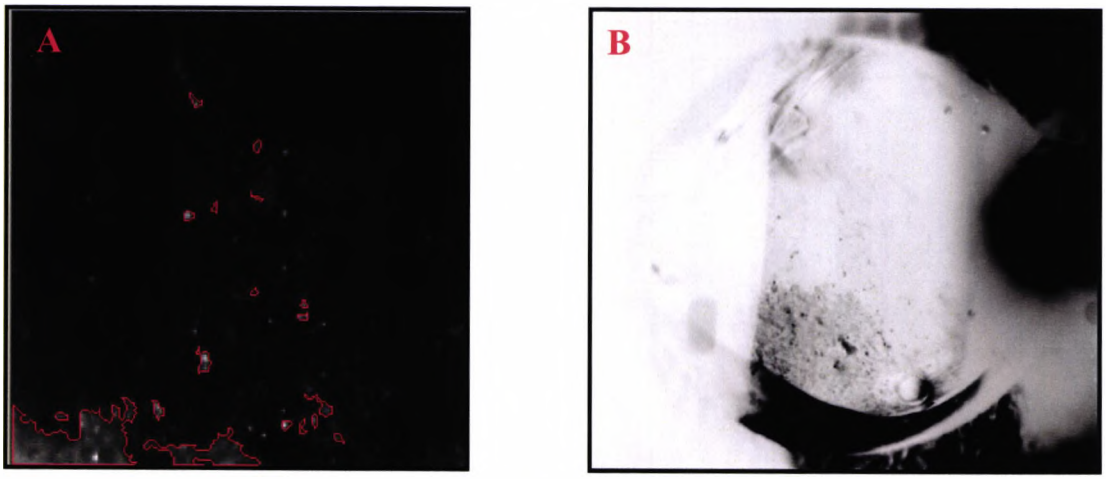

Figure 7.9 (A) Image of subject 31 captured with the reflected light technique and the objects of interest outlined. (B) Shows the negative image of the whole posterior capsule. The confidence level for subjective morphological classification was 2.5.

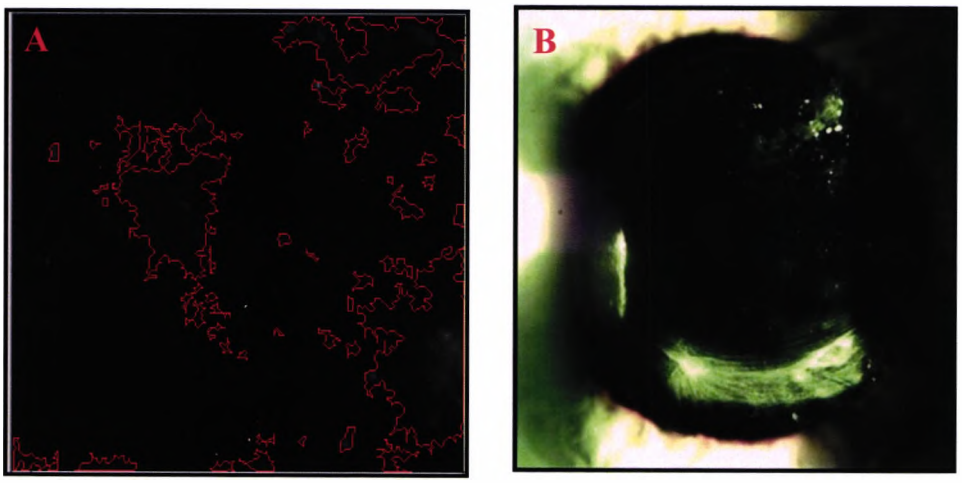

Figure 7.10 (A) Image of subject 27's AOI with the objects of interest outlined, and (B) the whole of the posterior capsule. The confidence level for subjective morphological classification was 2.6.

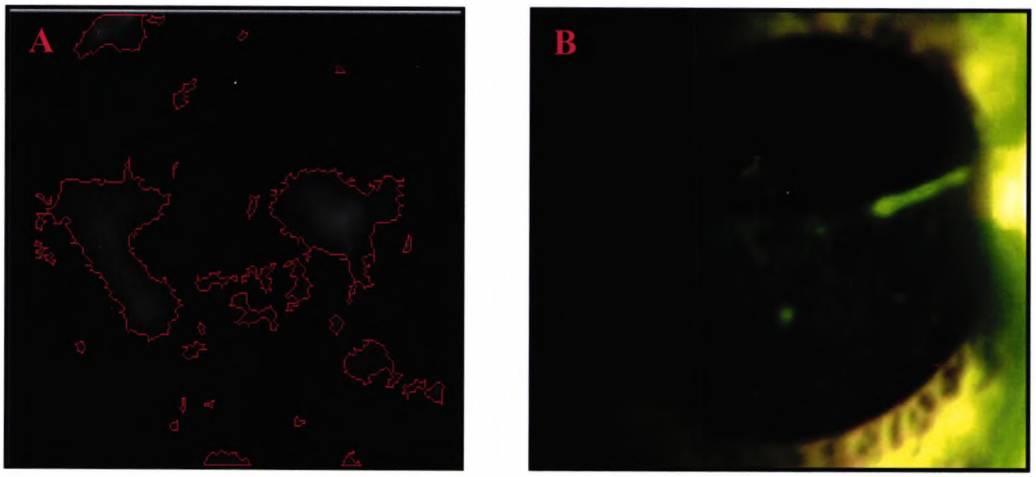

Figure 7.11 (A) Image of subject 33's AOI with the objects of interest outlined, and (B) the whole image of the posterior capsule. The confidence level for subjective morphological classification was 2.6.

In the fourth category (pearl-mixed), subjective classification for subjects 19, 23, 32 and 38 was pearl PCO whilst the objective classification was mixed. Examination of the images for subjects 19, 23, and 32 revealed that the main reason for disagreement was due to the fact that there was a clear combination of the main features of both fibrotic and pearl PCO. In the case of subject 38, the images show a clearly mixed PCO with the fibrotic PCO extending from the periphery whilst the pearl PCO manifests itself at the centre of the posterior capsule. As discussed earlier to resolve this disagreement it would be appropriate in the future is to represent AOI images to the subjective classifier instead of presenting the whole image.

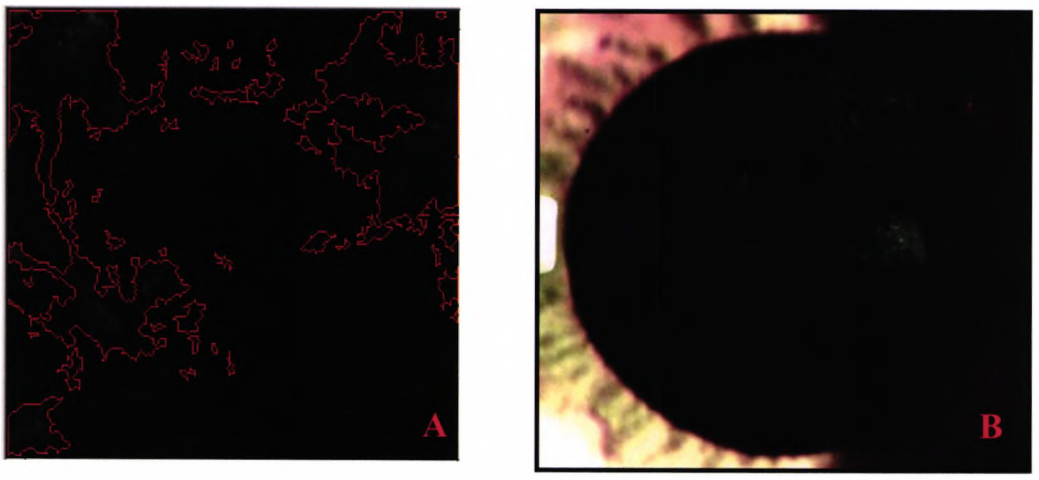

Figure 7.12 (A) Reflected light image of the AOI of subject 19 with the objects of interest outlined, and (B) showing the whole of the posterior capsule. The confidence level for subjective morphological classification was 3.5.

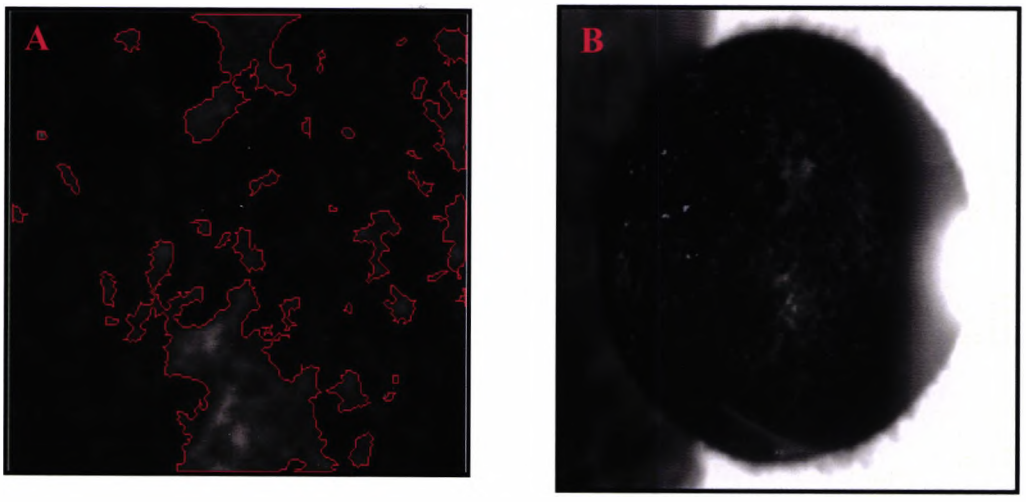

Figure 7.13 (A) Reflected light image of the AOI of subject 23 with the objects of interest outlined, and (B) showing the whole image of the posterior capsule. The confidence level fore subjective morphological classification was 4.

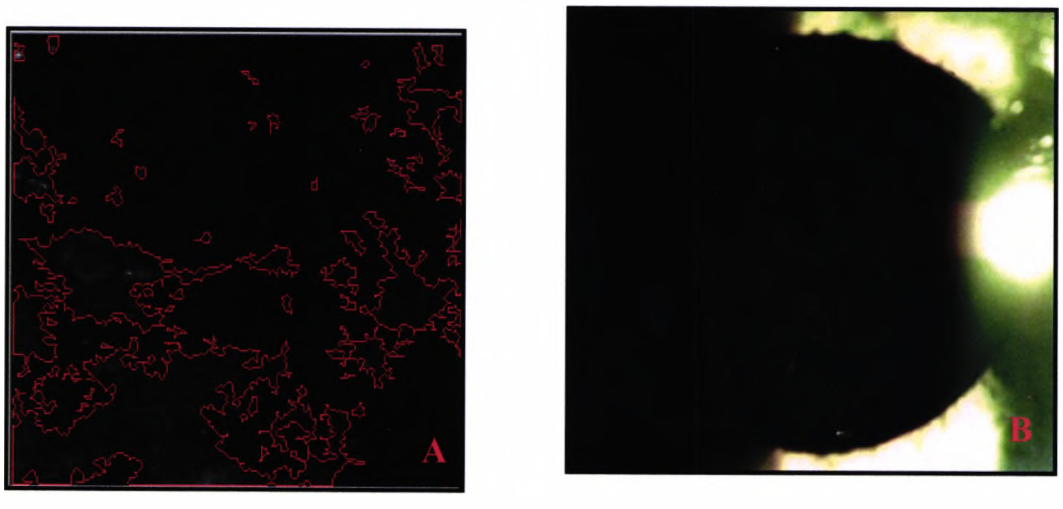

Figure 7.14 (A) Reflected light image of the AOI of subject 32 with the objects of interest outlined, and (B) showing the whole of the posterior capsule. The confidence level for subjective morphological classification was 3.

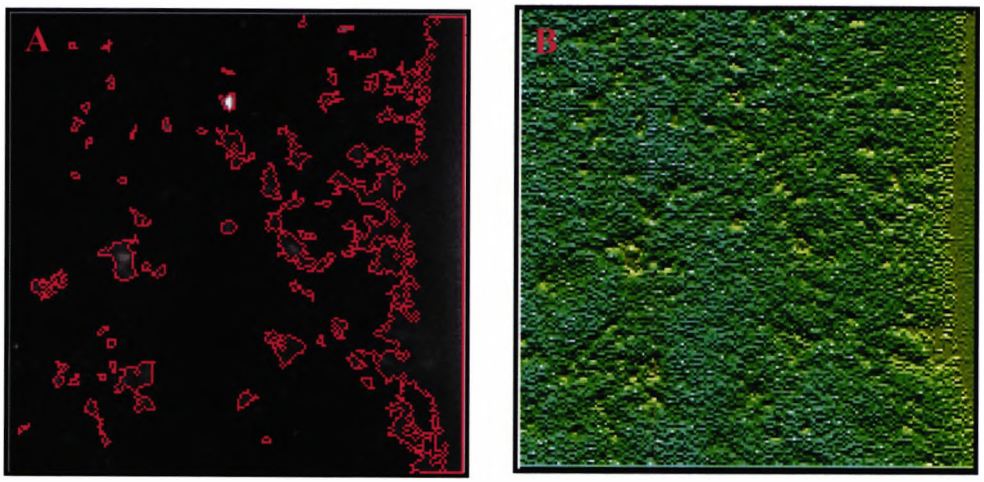

Figure 7.15 (A) Reflected light image of the AOI of subject 38 with the objects of interest outlined. (B) A surface plot image shows presence of both fibrotic and pearl PCO. The confidence level for subjective morphological classification was 3.1.

In the fifth category (mixed-fibrotic), the subjective classification for subjects 6, 28 and 42 was mixed, whilst the objective classification was fibrotic PCO. In the case of subject 42, the images revealed an early development of fibrotic PCO (fig. 7.16.A). Also the negative image clearly showed early manifestation of opacity. Examination of the images for subjects 6 and 28 revealed that the main reason for conflict was that fibrotic PCO is progressing towards the centre of the posterior capsule and engulfing the pearl PCO. This could be explained if the fibrotic PCO was progressing faster than the pearl PCO.

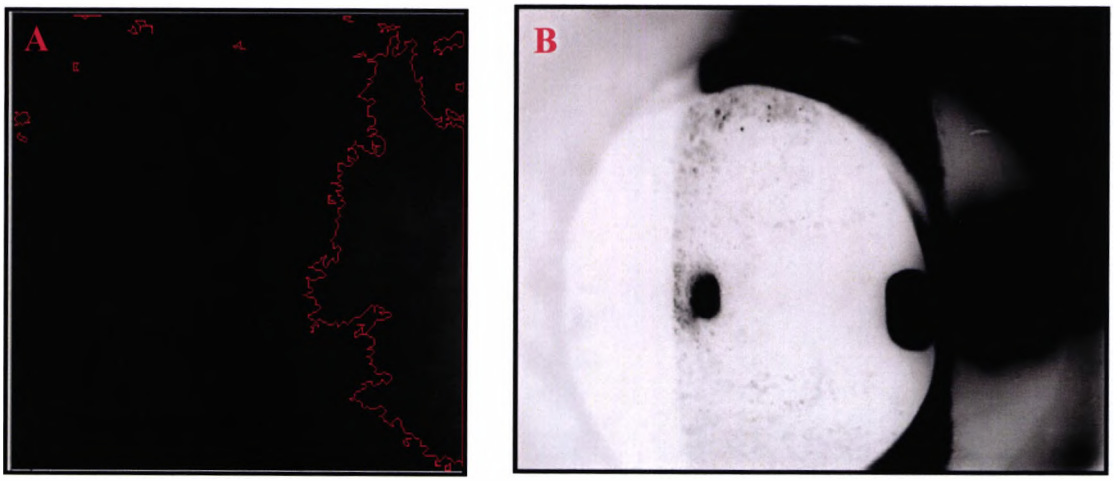

Figure 7.16 (A) Reflected light images of subject 42 with the objects of interest outlined. (B) The negative image of the entire posterior capsule. The confidence level for subjective morphological classification was 2.5.

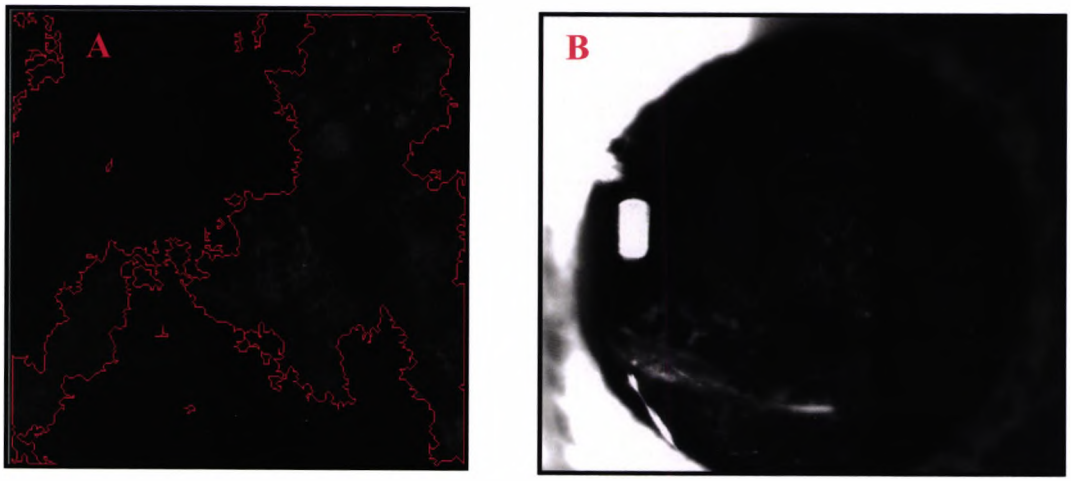

Figure 7.17 (A) Reflected light image of subject 6 with the objects of interest outlined. (B) Image of the entire posterior capsule. The confidence level for subjective morphological classification was 2.5.

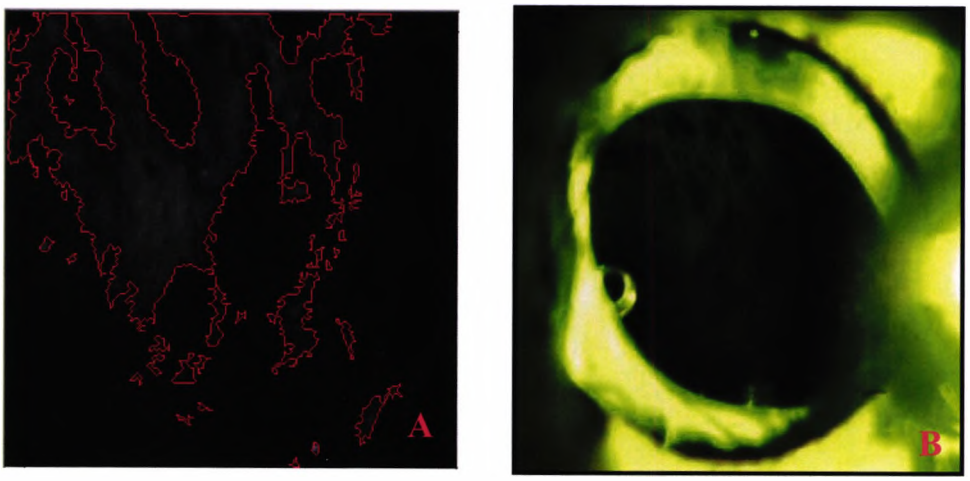

Figure 7.18 (A) Reflected light image of subject 28 with the objects of interest outlined. (B) A corresponding retroillumination image. The confidence level for subjective morphological classification was 2.5.

7.8 Summary

An attempt has been made to develop an objective morphological classifier using the auto-Pro option in Image Pro+ software to write a macro that could implement the three major modules of the expert system.

The results of the objective morphological classifier revealed that there are 31 satisfactory matches out of the 45 subjective classifications. The result show 15 out of 17 matches were found for fibrotic PCO, 13 out of 18 matches for pearl PCO, and 3 out of 10 matches for mixed PCO. The weighted kappa result indicated that there was good agreement between the objective morphological classifier results and subjective classification for the 45 images.

In conclusion, the 14 mis-matched cases were due to various factors such as the presence of folds or wrinkles in the posterior capsule. This hinders the usual manifestations of PCO because the LECs migrate and proliferate along these folds, and there is a faster progression of fibrotic PCO towards the centre of the posterior capsule potentially engulfing pearl PCO. In these cases there is confusion between the correct classes making it impossible for the objective morphological classifier to deliver the correct classification. More specialised techniques and rules are needed to separate between these classes and to deliver the correct classification. Other factors such as early development of PCO, and images of the AOI show that all the conditions of the classification rules were fulfilled. The conflict in these cases may be due to the fact that the subjective classification was performed by presenting the whole image to the ophthalmologist whereas the objective system concentrates only on the centre of the posterior capsule. It may have been more appropriate to present the AOI image to the subjective classifier.

Chapter Eight

8. Discussion and conclusion

8.1 Discussion and summary of results

In February 2000, the Good Practice Guidance "Action on Cataracts" report was published with the aim of modernising and helping local eye services. The Government backed up this strategy by allocating £20 million (£12 million in 2000-01 and £8 million in 2001-02) to support innovative service developments with a view to increasing efficiency in this area of the National Health Service (NHS). Section 3.6.5 of the report proposed that general practitioners (GPs) and optometrists should refer their patients who need Nd:YAG laser capsulotomy straight to the dedicated laser clinics without waiting for a consultant appointment in a general ophthalmology clinic. The proposal also sought to utilise trained nurses in these clinics to carry out laser treatment. The benefits of this proposal were to enhance nurses professional contribution to the NHS, free up consultants' time, reduce waiting times, allow more patients to be treated and streamline the patient's treatment pathway (http://www.doh.gov.uk).

We believe that the digital imaging system developed in this study is able to contribute to the primary care eye service by: (1) Supporting the decision of patient's referral and priority for Nd:YAG laser capsulotomy treatment based on objective assessment of PCO severity and (2) Producing a practical database that can contribute towards prevention methods thereby indicating which of these methods is more effective in reducing PCO. Apple et al. (2001) documented that implementing prevention methods such as phacoemulsification with CCC or choice of intraocular lens design or

material did in fact reduce the number of patients that required laser treatment. Furthermore, this system is ideal for use in a primary care environment due to the fact that it is easy to setup (as explained in chapter 4), and straightforward to operate (as explained in the chapter 6 and 7).

Experiments were undertaken with the parameters of the digital imaging system in order to obtain high quality images. The results reveal that the optimal parameters were found to be a 3.50mm beam width, a 45° angle of illumination, a film speed of 1600 for the camera and 800 for the DSU, a flash intensity of 2, an exposure compensation of 0, and a magnification of 25x. These findings are supported by other studies (Brown et al. 1972, 1988, Kawara et al. 1980, AREDS 2001b, Camparini et al. 2000). Images produced with these parameters were of optimal quality, helping to provide reliable objective measurements of PCO severity and morphological classification. Furthermore, these images are capable of recording the presence of the three main types of PCO at different levels of severity.

There are factors that affect the quality of the images, such as uveitis subsequent to diabetes mellitus, corneal scarring, vitreous clouding, glaucoma and dislocated or tilted IOLs. Subjects with such complications were excluded from this study; similar exclusion criteria have been documented in previous studies (Pande et al. 1997, Camparini et al. 2000, Barman et al. 2000).

One inevitable problem that all developers of imaging systems encounter is maintaining patient fixation to avoid Purkinje reflections. The solution was to develop a fixation stimulus that is compatible with the system, an approach that has been reported in many other studies (Hayashi et al. 1998 a, Wang et al. 2000, Saika et al. 2001, Camparini et al. 2000, Pande et al. 1997). Chapter

5 introduces fixation stimulus version (1), a modified fixation stimulus (version 2), and details of the tests performed to examine their reliability.

Results showed that Fixation stimulus version (1) may help to maintain subject fixation because 66% of the displacement values (distance between the pupil centre and Purkinje reflex of the fixation stimulus, which should be constant) lie on average within ± 0.22mm. The standard deviation of each subject was relatively low indicating that the stimulus did contribute towards maintaining fixation therefore eliminating Purkinje reflections caused by poor fixation. The intra-observer repeatability demonstrated that there was good agreement between the first and second images with a coefficient of variation of 1.1% indicating that there is only a small variability within any subject.

A modified fixation stimulus was developed. it comprised a glass reinforced plastic copper laminated printed circuit board, five red LEDs modified by flattening their convex heads and a control box with a switch that allowed all LEDs to stay on until the examiner pressed the camera shutter, pressing the shutter release caused the central LED to be turned off. The purpose of the design alteration was to rectify limitations found in the first version, in particular time taken to acquire images and patient fatigue. This is a difficult task especially with older subjects who are experiencing blurred vision in one eye whilst the other is occluded to avoid diplopia.

The standard deviation of the total spectral power for the images of subjects with the modified fixation stimulus was 1.63 compared to the standard deviation without a fixation stimulus of 2.33. This suggests that the modified version is helpful in reducing variations in the results. However Levene's test demonstrated that this reduction was not statistically significant.

The intra-observer repeatability for the modified fixation stimulus revealed that there was genuine variation in the total spectral power within-subjects, thus the pooled within-subject SD was used as an indication of the typical variability. The within-subject variability was 1.26, and the within-subject coefficient of variation was 1.5%. Spearman's correlation coefficient was 0.273 (P = 0.446) indicating that the variability was unrelated to the magnitude of the measurement. The residual plot demonstrated that the normal distribution was reasonable, although there were two specious values for subjects 3 and 10. These specious values were more than three standard deviations away from the mean value. Excluding these two values decreased the within-subject standard deviation and the within-subject coefficient of variation to 0.743 and 0.93% respectively.

The inter-observer repeatability results for the three pairs of observers; optometrist and ophthalmologist, optometrist and non-clinician, ophthalmologist and non-clinician, revealed that there was good agreement between optometrist and ophthalmologist. However, the agreement between optometrist and non-clinician, and ophthalmologist and non-clinician was poor. The limits of agreements between optometrist and ophthalmologist, optometrist and non-clinician, and ophthalmologist and non-clinician were 1.86 to -1.1, 13.1 to -6.02 and 12.54 to -6.24 respectively. This indicates that it would be inappropriate for an untrained non-clinician to capture images with the system. Variation could also be due to other factors such as patient fixation and observer focusing techniques as documented in previous studies (Barman et al. 2000).

Comparison of the results produced by the various digital imaging systems reported in the literature is not possible. This is due to many factors such as the variety of photographic techniques and parameters, experiment details, methods of statistical analysis, and the technique used to quantify PCO. However, we will highlight the results of inter and intra-observer repeatability of these systems to emphasize whether the standard of the developed system in this study is comparable with previous systems. The retroillumination system developed by Barman et al. (2000), had a bias and standard deviation of the difference of -0.33% and 4.7% respectively for intra-observer variation; and the limits of agreement were +9.1% and -9.8%. The inter-observer repeatability result showed that the Pearson correlation coefficient was 0.99. Similarly, for the retroillumination system developed by Friedman et al. (2000), the intra-observer repeatability results revealed that the bias and standard deviation of difference for the percent coverage of opacity were 0.73% and ± 0.53 respectively, whilst the bias and standard deviation of the difference for the density of opacity were 0.06% and ± 0.06 respectively.

Our system results for inter and intra-observer repeatability with the modified fixation stimulus show there is a slightly higher variability compared to the results of the systems described above. This may be due to increased variability in reflected light images with eye movement and alignment causing relatively large changes in the specular reflection off the opacity. In contrast, retroillumination images would be less sensitive to this effect. However, retroillumination images are affected by low contrast, with complex features and indistinct and incomplete boundaries. As a result sophisticated approaches have to be used to analyses these images (Barman et al. 2000). Also, the central area of retroillumination images are affected by the corneal reflex thus the peripheral area is used to study early development

of PCO. Conversely, reflected light images allow examination of the central area of the posterior capsule as clearly demonstrated in this study.

The only reflected light system that has been documented recently was developed by Camparini et al. (2000). It resembles our digital system, although there are differences such as the use of photographic film instead of digital imaging. Photographic images are often affected by variation in the film and its development. This is not the case with digital images (Harris et al. 1993). Currently, there is an increase in accessibility to technology due to practicality, accuracy, consistency, and speed of image processing and analysis. Furthermore, the Camparini study relied purely on subjective grading using the AREDS cataract grading system for cortical and posterior capsular opacities; they did not establish objective measures of PCO. In addition, there is no published study of inter or intra-observer repeatability of the Camparini system to compare our results with.

The first goal of this study, following system validation, was to establish an objective technique to quantify PCO severity. The rank correlation coefficients for fibrotic, pearl and mixed PCO were 0.909, 0.864, and 0.713 respectively. This demonstrates that there is good correlation between the subjective grading of PCO within the AOI images and log of the spectral power of the amplitude spectrum images. Although the value of the coefficient for mixed PCO was slightly less this may be due to the sample size of the three types of PCO which were 18, 17 and 10 respectively. Barman et al. (2000) suggested it would be helpful if a measure of PCO severity could be found that correlated with visual function. However the relationship between forward light scatter, which affects visual function, and backscatter is not straightforward. Until this problem is understood we believe that these systems are best used to aid referral and monitor techniques

used to inhibit PCO.

The advantages of the methods described in this thesis are that they are objective and do not rely on subjective methods to identify or outline the area of opacity. Systems developed by Bender (2001) and Tetz et al. (1997) are not fully objective since they require user interaction to identify or outline the boundaries covered by opacity of the posterior capsule. In addition our system provides an absolute value that estimates PCO severity, since it is affected by both the area and density of the opacity simultaneously. Previous systems have relied on the area and density as separate measurements (Friedman et al. 1999, Bender, 2001, Tetz et al. 1997). Even when both are considered, no overall value is computed. Our technique does not require the purchasing of expensive software because the FFT option is present in most image processing and analysis packages. Conversely, the most recently developed retroillumination system (Barman et al. 2000) relies significantly on specialised software and requires a high level of computational effort and knowledge making it impractical to use in a primary care setting.

The second goal of this study was to develop an objective technique to classify PCO morphologically into three classes: fibrotic, pearl and mixed. The results of the objective morphological classifier show that 31 out of the 45 cases agree with subjective classification. The weighted inter-rater kappa between the subjective morphological classification and objective morphological classifier was 0.61 indicating that the strength of agreement is good.

The 14 cases where there was no agreement between subjective classification and objective classification could be explained by various reasons. For example, a faster progression of fibrotic PCO towards the centre of the posterior capsule could engulf the pearl PCO. Similarly the presence of folds and wrinkles in the posterior capsule can hinder the usual manifestations of PCO because the LECs migrate and proliferate along these long folds, making it impossible for the objective morphological classifier to separate the two main classes and deliver the correct classification. This indicates that more specialised techniques are needed to separate between these classes in order to deliver a correct classification. Some incorrect classifications could be rectified by presenting a 3mm x 3mm AOI image to the subjective classifier instead of the whole image.

8.2 Future work

There are several ways in which this study could be extended. For example a large trial in a primary care environment could include a larger sample of patients with various degrees of PCO, ranging from early to severe. In addition, several experienced ophthalmologists could be used to classify the images for better confirmation of severity grading and optimization of the rules of the objective morphological classifier. Such a trial should also involve several non-clinicians, such as nurses, to determine the level of training needed for a non-clinician to operate the system. A prospective trial involving several users in a primary care environment could be set up to conduct a comparative study on the effect of various techniques used to prevent PCO or monitor the progression of PCO.

Recently the Royal College of Ophthalmologist introduced a proposal to create an electronic cataract national dataset. The dataset comprises two parts: process output (referral method, waiting time, admission type, etc) and clinical output (age, gender, operation type, postoperative complications) (Johnston, 2003). The benefits of the system include providing data on individual clinician performance, setting standards for all aspects of cataract surgery, and monitoring complications following cataract surgery. As mentioned earlier our system could be used with a database such as the electronic cataract national dataset. This database if combined with digital images obtained by our system, would open up large area for investigation such as prospective studies to investigate the effect of surgeons experience on the cataract surgery outcomes. Such a study should also involve several regions since already 12 of the electronic cataract national dataset systems have been purchased by different departments in the UK. This also allows investigation of the effect of the standard of cataract surgery provided by different regions.

8.3 conclusion

This study has demonstrated the development of a digital imaging system that provides an objective and reproducible technique to quantify the severity of PCO and classify it morphologically. It may provide the evidence to facilitate a clinical decision and perhaps encourage research that develops best practice to ultimately reduce the occurrence of PCO.

Reference

1. Abela-Formanek C, Amon M, Schild G, Schauersberger J, Heinze G, Kruger A.(2002). Uveal and capsular biocompatibility of hydrophilic acrylic, hydrophobic acrylic, and silicone intraocular lenses. J.Cataract Refract.Surg. 28, 50-61.

2. Age-related Eye Disease Study (AREDS). (2001b). Lens Grading Protocol. http://eyephoto.ophth.wisc.edu/ResearchAreas.html

3. Age-related Eye Disease Study (AREDS).(2001a). Risk factors associated with age-related nuclear and cortical cataract: a case-control study in the Age-Related Eye Disease Study, AREDS Report No. 5. Ophthalmology. 108,1400-1408.

4. Albert DM, Clayman H et al. 1999. Ophthamlic Surgery: principle and techniques. Blackwell Science, Inc. USA. Chapter 21, 23, 24, 25, 27.

5. Alio JL, Sayans JA, Chipont E.(1996). Laser flare-cell measurement of inflammation after uneventful extracapsular cataract extraction and intraocular lens implantation. J.Cataract Refract.Surg. 22, Suppl 1, 775-779.

6. Alio JL, Sayans JA, Chipont E.(1997). Flare-cell meter measurement of inflammation after uneventful cataract surgery with intraocular lens implantation. J.Cataract Refract.Surg. 23, 935-939.

7. Allarakhia L, Knoll RL, Lindstrom RL.(1987). Soft intraocular lenses. J.Cataract Refract.Surg. 13, 607-620.

8. Ambler JS, Constable IJ.(1988). Retinal detachment following Nd:YAG capsulotomy. Aust.N.Z.J.Ophthalmol. 16, 337-341.

9. Amon M, Menapace R, Radax U, Freyler H.(1996). In vivo study of cell reactions on poly(methyl methacrylate) intraocular lenses with different surface properties. J.Cataract Refract.Surg. 22, Suppl 1, 825-829.

10. Amon M, Menapace R.(1994). In vivo documentation of cellular reactions on lens surfaces for assessing the biocompatibility of different intraocular implants. Eye. 8, 649-656.

11. Anjou C et al. (1960). A photographic method for measuring the aqueous flare of the eye in normal and pathological conditions. Acta Ophthalmol. 38, 178-224.

12. Apple D.J, Peng Q, Arthur SN, Werner L, Merritt JH, Vargas LG, Hoddinott DS, Escobar-Gomez M, and Schmidbauer JM.(2002) Snowflake degeneration of polymethyl methacrylate posterior chamber intraocular lens optic material: a newly described clinical condition caused by unexpected late opacification of polymethyl methacrylate. Ophthalmology. 109, 1666-1675.

13. Apple DJ & Rabb MF (1998). Lens and pathology of intraocular lenses. In: Apple DJ & Rabb MF (eds) Ocular Pathology. Mosby, St. Louis, Missouri, pp 175.

14. Apple DJ et al (2000a). Posterior capsule opacification (Sacandary Catarat). Surv Ophthalmol. 45, Suppl1, 100-125.

15. Apple DJ et al (2000c). Cataract surgery with rigid and fgoldable posterior chamber IOLs, ECCE and phacoemulsification. Surv Ophthalmol. 45, Suppl1, 70-99.

16. Apple DJ et al (2000d). Evolution of cataract surgery and intraocular lenses (IOLs): IOL Quality. Surv Ophthalmol. 45, Suppl1, 53-69.

17. Apple DJ et al.(2000b). Cataract surgery with intraocular cataract extraction and spectacles). Surv Ophthalmol. 45, Suppl1, 45 -52.

18. Apple DJ et al.(2000e). Anterior chamber intraocular lenses. Surv Ophthalmol. 45, Suppl1, 131-149.

19. Apple DJ et al.(2000g). Refractive surgery in the developing world. Surv Ophthalmol. 45, Suppl1, 169-176.

20. Apple DJ, Auffarth GU, Peng Q, Visessook N.(2000h). Foldable intraocular lenses: evolution, clinicopathologic correlations and complications. Thorofare, NJ, Slack. Chapter 4.

21. Apple DJ, Kincaid M C et al. (1989). Intraocular lenses: evolution, designs, complications, and pathology. Williams & Wilkins. London. Chapter 7, 12.

22. Apple DJ, Peng Q, Visessook N, Werner L, Pandey SK, Escobar-Gomez M, Ram J, Auffarth GU. (2001). Eradication of posterior capsule opacification: documentation of a marked decrease in Nd:YAG laser posterior capsulotomy rates noted in an analysis of 5416 pseudophakic human eyes obtained postmortem. Ophthalmology. 108, 505-518.

23. Apple DJ, Solomon KD, Tetz MR, Assia EI, Holland EY, Legler UF, Tsai JC, Castaneda VE, Hoggatt JP, Kostick AM. (1992). Posterior capsule opacification. Surv.Ophthalmol. 37, 73-116.

24. Apple,DJ, Peng Q, Visessook N, Werner L, Pandey SK, Escobar-Gomez M, Ram J, Whiteside SB, Schoderbeck R, Ready EL, Guindi A. (2000f). Surgical prevention of posterior capsule opacification. Part 1: Progress in eliminating this complication of cataract surgery. J.Cataract Refract.Surg. 26, 180-187.

25. Argento C, Nunez E, Wainsztein R. (1992). Incidence of postoperative posterior capsular opacification with types of senile cataracts. J.Cataract Refract.Surg. 18, 586-588.

26. Aron-Rosa D. (1981). Use of a pulsed neodymium-Yag laser for anterior capsulotomy before extracapsular cataract extraction. J.Am.Intraocul.Implant.Soc. 7, 332-333.

27. Aslam TM, Dhillon B, Werghi N, Taguri A, and Wadood A. (2002) Systems of analysis of posterior capsule opacification. Br.J.Ophthalmol. 86, 1181-1186.

28. Assia EI, Apple DJ, Barden A, Tsai JC, Castaneda VE, Hoggatt JS. (1991). An experimental study comparing various anterior capsulotomy techniques. Arch.Ophthalmol. 109, 642-647.

29. Assia EI, Apple DJ. (1992). Side-view analysis of the lens. II. Positioning of intraocular lenses. Arch.Ophthalmol. 110, 94-97.

30. Assia EI, Legler UF, Apple DJ. (1995). The capsular bag after short- and long-term fixation of intraocular lenses. Ophthalmology. 102, 1151-1157.

31. Auffarth GU. (2001). Personal communication / presentations. ASCRS 2001.

32. Barman SA, Hollick EJ, Boyce JF, Spalton DJ, Uyyanonvara B, Sanguinetti G, Meacock W. (2000). Quantification of posterior capsular opacification in digital images after cataract surgery. Invest Ophthalmol.Vis.Sci. 41, 3882-3892.

33. Bellucci R, Pucci V, Morselli S, Bonomi L. (1996). Secondary implantation of angle-supported anterior chamber and scleral-fixated posterior chamber intraocular lenses. J.Cataract Refract.Surg. 22, 247-252.

34. Beltrame G, Salvetat ML, Chizzolini M, Driussi GB, Busatto P, Di Giorgio G, Barosco F. (2002). Posterior capsule opacification and Nd:YAG capsulotomy rates after implantation of silicone, hydrogel and soft acrylic intraocular lenses: a two-year follow-up study. Eur.J.Ophthalmol. 12, 388-394.

35. Benliner M L (1943). Biomicroscopy of the eye. 1943. pp 64-123.

36. Bernd Jahne. (2002). Digital Image Processing: Concepts, Algorithms, and Scientific Applications. Springer Verlag Berlin Heidelberg; 5th edition. Chapter2.

37. Bertelmann E, Kojetinsky C. (2001). Posterior capsule opacification and anterior capsule opacification. Curr.Opin.Ophthalmol. 12, 35-40.

38. Bhermi GS, Spalton DJ, El Osta AA., and Marshall J. (2002) Failure of a discontinuous bend to prevent lens epithelial cell migration in vitro. J.Cataract Refract.Surg. 28, 1256-1261.

39. Binkhorst C et al. (1959). Iris-supported artificial pseudophakia.A new development in intraocular artificial lens surgery (iris clip lens). Trans.Ophthalmol.Soc.Uk. 79: 469-584.

40. Birinci H, Kuruoglu S, Oge I, Oge F, Acar E. (1999). Effect of intraocular lens and anterior capsule opening type on posterior capsule opacification. J.Cataract Refract.Surg. 25, 1140-1146.

41. Bland JM & Altman DG. (1999). Measuring agreement in method comparison studies. *Statistical Methods in Medical Research.* 8, 135-160.

42. Bloemendal H, Benedetti EL, DunialI. (1996). Transgenic mice: models for the study of cataractogenesis. A minireview. Ophthalmic Res. 28, Suppl 1, 1-7.

43. Borgioli M, Coster DJ, Fan RF, Henderson J, Jacobi KW, Kirkby GR, LaiY K, Menezo JL, Montard M, Strobel J. (1992). Effect of heparin surface modification of polymethylmethacrylate intraocular lenses on signs of postoperative inflammation after extracapsular cataract extraction. One-year results of a double-masked multicenter study. Ophthalmology. 99, 1248-1254.

44. Born CP, Ryan DK. (1990). Effect of intraocular lens optic design on posterior capsular opacification. J.Cataract Refract.Surg. 16, 188-192.

45. Brian G, Taylor H. (2001). Cataract blindness--challenges for the 21st century. Bull.World Health Organ 79, 249-256.

46. Bron AJ, Tripathi Brenda J, Tripathi Ramesh C. (1997). Wolff's anatomy of the eye and orbit. Chapman. & Hall.Medical. London; 8th ed.

47. Brown N. A. P. (1972). Quantitaive slit-image photography of the lens. Trans Ophthalmol.SocUK.92:303-17.

48. Brown NA, Bron AJ, Sparrow JM. (1988). Methods for evaluation of lens changes. Int.Ophthalmol. 12, 229-235.

49. Buchen SY, Richards SC, Solomon KD, Apple DJ, Knight PM., Christ R, Pham LT, Nelson DL, Clayman HM, KarpinskiLG. (1989). Evaluation of the biocompatibility and fixation of a new silicone intraocular lens in the feline model. J.Cataract Refract.Surg. 15, 545-553.

50. Buehl W, Findl O, Menapace R, Georgopoulos M, Rainer G, Wirtitsch M, Siegl H, and Pinz A. (2002). Reproducibility of standardized retroillumination photography for quantification of posterior capsule opacification. J.Cataract Refract.Surg. 28,265-270.

51. Burton M, Fergusson E, Hart A, Knight K, Lary D, Liu C. (1997). The prevalence of cataract in two villages of northern Pakistan with different levels of ultraviolet radiation. Eye 11 (1), 95-101.

52. Caballero A, Lopez MC, Losada M , Perez FD, Salinas M. (1995). Long-term decentration of intraocular lenses implanted with envelope capsulotomy and continuous curvilinear capsulotomy: a comparative study. J.Cataract Refract.Surg. 21, 287-292.

53. Caballero A, Salinas M, Marin JM. (1997). Spontaneous disappearance of Elschnig pearls after neodymium:YAG laser posterior capsulotomy. J.Cataract Refract.Surg. 23, 1590-1594.

54. Caird FI. (1973). Problem of cataract epidemiology with special reference to diabetes. Ciba Foundation Symp. 19:281-301.

55. Camparini M, Macaluso C, Reggiani L, Maraini G. (2000). Retroillumination versus reflected-light images in the photographic assessment of posterior capsule opacification. Invest Ophthalmol.Vis.Sci. 41, 3074-3079.

56. Caporossi A, Casprini F, Tosi GM, Baiocchi S. (2002). Preliminary results of cataract extraction with implantation of a single-piece AcrySof intraocular lens. J.Cataract Refract.Surg. 28, 652-655.

57. Chee SP, Ti,S E, Sivakumar M, Tan DT. (1999). Postoperative inflammation: extracapsular cataract extraction versus phacoemulsification. J.Cataract Refract.Surg. 25, 1280-1285.

58. Chehade M, Elder MJ. (1997). Intraocular lens materials and styles: a review. Aust.N.Z.J.Ophthalmol. 25, 255-263.

59. Chitkara DK, Smerdon DL. (1997). Risk factors, complications, and results in extracapsular cataract extraction. J.Cataract Refract.Surg. 23, 570-574.

60. Christ FR, Buchen SY, Deacon J. et al. (1995). Biomaterials used for intraocular lens. In: Wise DL, Trantolo DJ, Altobelli DE, rt al, eds. Encyclopedic handbook of Biomaterials and Bioengineering. Part B: applications. Vol 2. New York, Marcel Dekker, Inc, 1261-1313.

61. Christ FR, Fencil DA., Van Gent S, Knight PM. (1989). Evaluation of the chemical, optical, and mechanical properties of elastomeric intraocular lens materials and their clinical significance. J.Cataract Refract.Surg. 15, 176-184.

62. Christiansen G, Durcan FJ, Olson RJ, and Christiansen K. (2001) Glistenings in the AcrySof intraocular lens: pilot study. J.Cataract Refract.Surg., 27,728-733.

63. Chung HS, Lim SJ, Kim HB. (2000). Effect of mitomycin-C on posterior capsule opacification in rabbit eyes. J.Cataract Refract.Surg. 26, 1537-1542.

64. Chylack LT, Rosner B, Cheng HM., McCarthy D, Pennett M. (1987). Sources of variance in the objective documentation of human cataractous change with Topcon SL-45 and Neitz-CTR retroillumination photography and computerized image analysis. Curr.Eye Res. 6, 1381-1390.

65. Clemente P. (1999). Langzeivertraglichekeit einer neuen VKL SP 525 Clemente Optift 3-Punkt-Fization Ohne Positionierunglosch, Kongress der Deutschsprachigen Gesselschaft fur Intraokularlinsen-Implantation und refractive Chirurgie, Herausgegeben vo, Kohnen T, Ohrloff C, and Wenzel M, Biermann.

66. Cortina P, Gomez-Lechon MJ, Navea A, Menezo JL, Terencio MC, Diaz-Llopis M. (1997). Diclofenac sodium and cyclosporin A inhibit human lens epithelial cell proliferation in culture. Graefes Arch.Clin.Exp.Ophthalmol. 235, 180-185.

67. Courtney P. (1992). The National Cataract Surgery Survey: I. Method and descriptive features. Eye 6 (5), 487-492.

68. Cunanan CM, Tarbaux NM, Knight PM. (1991). Surface properties of intraocular lens materials and their influence on in vitro cell adhesion. J.Cataract Refract.Surg. 17, 767-773.

69. Dahan E, Allarakhia L. (1991). Irrigation, aspiration, and polishing cannula. J.Cataract Refract.Surg. 17, 97-98.

70. Dahlhauser KF, Wroblewski KJ, Mader TH. (1998). Anterior capsule contraction with foldable silicone intraocular lenses. J.Cataract Refract.Surg. 24, 1216-1219.

71. Dana MR, Chatzistefanou K, Schaumberg DA, Foster CS. (1997). Posterior capsule opacification after cataract surgery in patients with uveitis. Ophthalmology 104, 1387-1393.

72. Dardenne MU, Gerten GJ, Kokkas K, KermaniO. (1989). Retrospective study of retinal detachment following neodymium:YAG laser posterior capsulotomy. J.Cataract Refract.Surg. 15, 676-680.

73. Davidson MG, Morgan DK, McGahan MC. (2000). Effect of surgical technique on in vitro posterior capsule opacification. J.Cataract Refract.Surg. 26, 1550-1554.

74. Daviel J. (1967). On a new method to cure cataract by extraction of the lens. Br.J.Ophthalmol. 51, 449-458.

75. Desai P, Minassian DC, Reidy A. (1999). National cataract surgery survey 1997-8: a report of the results of the clinical outcomes. Br.J.Ophthalmol. 83, 1336-1340.

76. Dick B, Schwenn O, Pfeiffer N. (1997). [Extent of damage to different intraocular lenses by neodymium:YAG laser treatment--an experimental study]. Klin.Monatsbl.Augenheilkd. 211, 263-271.

77. Dick B, Schwenn O, Stoffelns B, Pfeiffer N. (1998). [Late dislocation of a plate haptic silicone lens into the vitreous body after Nd:YAG capsulotomy. A case report]. Ophthalmologe. 95, 181-185.

78. Dick HB, Schwenn O, Krummenauer F, Krist R, Pfeiffer N. (2000). Inflammation after sclerocorneal versus clear corneal tunnel phacoemulsification. Ophthalmology. 107, 241-247.

79. Doan KT, Olson RJ, Mamalis N. (2002). Survey of intraocular lens material and design. Curr.Opin.Ophthalmol. 13, 24-29.

80. Dowler JG, Hykin PG, Hamilton A.M. (2000). Phacoemulsification versus extracapsular cataract extraction in patients with diabetes. Ophthalmology 107, 457-462.

81. Downing JE. (1986). Long-term discission rate after placing posterior chamber lenses with the convex surface posterior. J.Cataract Refract.Surg. 12, 651-654.

82. Dragomirescu V, Hockwin O. et al. (1978). Development of new equipment for rotating slit image photography according to Scheimpflug's principle. In: Van Hahn HP, ed. Interdisciplinary Toics in Gerontology. Basel: S. Karger; 1978:118-130.

83. Drews DC. (1964). Depth of field in slit lamp photography. New York, Ophthalmolofica.148:143-150.

84. Drews RC. (2000). Five year study of astigmatic stability after cataract surgery with intraocular lens implantation: comparison of wound sizes. J.Cataract Refract.Surg. 26, 250-253.

85. Duck-Elder. (1969). Diseases of the lens and vitreous: glaucoma and hypotony. pp 289-291

86. Ederer F, Hiller R, Taylor HR. (1981). Senile lens changes and diabetes in two population studies. Am.J.Ophthalmol. 91, 381-395.

87. Edwards PA, Datiles MB, Green SB. (1988). Reproducibility study on the Scheimpflug Cataract Video Camera. Curr.Eye Res. 7, 955-960.

88. Edwards PA, Datiles MB, Unser M, Trus BL, Freidlin V, Kashima K. (1990). Computerized cataract detection and classification. Curr.Eye Res. 9, 517-524.

89. Ernest P, Tipperman R, Eagle R, Kardasis C, Lavery K, Sensoli A., Rhem M. (1998). Is there a difference in incision healing based on location? J.Cataract Refract.Surg. 24, 482-486.

90. Ficker LA, Steele AD. (1985). Complications of Nd:YAG laser posterior capsulotomy. Trans.Ophthalmol.Soc.U.K. 104 (5), 529-532.

91. Findl O, Buehl W, Menapace R, Georgopoulos M, Rainer G, Siegl H, Kaider A, and Pinz A. (2003) Comparison of 4 methods for quantifying posterior capsule opacification. J.Cataract Refract.Surg. 29,106-111.

92. FindlO, Drexler W, Menapace R, Georgopoulos M, Rainer G, Hitzenberger CK, Fercher AF. (1999). Changes in intraocular lens position after neodymium:YAG capsulotomy. J.Cataract Refract.Surg. 25, 659-662.

93. Fine IH, Lewis JS, Hoffman RS. (1998). New techniques and instruments for lens implantation. Curr.Opin.Ophthalmol. 9, 20-25.

94. Fisher R. (1969). The elastic constant of the human lens capsule. J Physiol. 201,1.

95. Fisher R. (1971). The elastic constant of the human lens. J Physio. 212, 147

96. Fourman S, Apisson J. (1991). Late-onset elevation in intraocular pressure after neodymium-YAG laser posterior capsulotomy. Arch.Ophthalmol. 109, 511-513.

97. Frezzotti R, Caporossi A. (1990). Pathogenesis of posterior capsular opacification. Part I. Epidemiological and clinico-statistical data. J.Cataract Refract.Surg. 16, 347-352.

98. Friedman DS, Duncan DD, Munoz B, West SK, Schein OD. (1999). Digital image capture and automated analysis of posterior capsular opacification. Invest Ophthalmol.Vis.Sci. 40, 1715-1726.

99. Frohn A, Dick HB, Augustin AJ, and Grus FH. (2001). Late opacification of the foldable hydrophilic acrylic lens SC60B-OUV. Ophthalmology. 108,1999-2004.

100. Gallenga PE, Mastropasqua L. (1990). Heparin in pseudophakia. Eur J Implant Refract Surg. 2, 203-207.

101. Gallenga PE, Mastropasqua L. et al. (1986). [Heparin in pseudophakia- presented at the 4th Congress of the European Society of Cataract and Refractuive Surgeons, Jerusalem, June].

102. Gatinel D, Lebrun T, Le Toumelin P, Chaine G. (2001). Aqueous flare induced by heparin-surface-modified poly (methyl methacrylate) and acrylic lenses implanted through the same-size incision in patients with diabetes. J.Cataract Refract.Surg. 27, 855-860.

103. Gillies M, Brian,G, La Nauze J, Le Mesurier R, Moran D, Taylor H, Ruit S. (1998). Modern surgery for global cataract blindness: preliminary considerations. Arch.Ophthalmol. 116, 90-92.

104. Gills JP, Sanders DR. (1991) Use of small incisions to control induced astigmatism and inflammation following cataract surgery. J.Cataract Refract.Surg. 17, Suppl, 740-744.

105. Gimbel HV, Neuhann T. (1990). Development, advantages, and methods of the continuous circular capsulorhexis technique. J.Cataract Refract.Surg. 16, 31-37.

106. Gimbel HV. (1994). Hydrodissection and hydrodelineation. Int.Ophthalmol.Clin. 34, 73-90.

107. Goble RR, O'Brart DP, Lohmann CP, Fitzke F, and Marshall J. (1994) The role of light scatter in the degradation of visual performance before and after Nd:YAG capsulotomy. Eye. 8 (5), 530-534.

108. Goins KM, Ortiz JR, Fulcher SF, Handa JT, Jaffe GJ, Foulks GN, Cobo LM. (1994). Inhibition of proliferating lens epithelium with antitransferrin receptor immunotoxin. J.Cataract Refract.Surg. 20, 513-516.

109. Goldmann H. (1939). Spaltlampenphotographic und photometric. Ophthalmica. 98, 257-270.

110. Gonzalez, R.C. and R.E. Woods. (1992). Digital Image Processing. Reading, Massachusetts: Addison-Wesley. 2nd edn.

111. Hansen TE, Otland N, Corydon L. (1988). Posterior capsule fibrosis and intraocular lens design. J.Cataract Refract.Surg. 14, 383-386.

112. Hara T, Hara T (1984). Subcapsular phacoemulsification and aspiration. J.Am.Intraocul.Implant.Soc. 10, 333-337.

113. Hara T, Hara T, Sakanishi K, Yamada Y. (1995). Efficacy of equator rings in an experimental rabbit study. Arch.Ophthalmol. 113, 1060-1065.

114. Härfstrand A. et al. (1990). Evidence for an increased biocompatibility of heparin surface modificatied (HSM) PMMA intraocular lenses. Implants.Ophthalmology. 4, 35-39.

115. Harris ML, Hanna KJ, Shun-Shin GA., Holden R, Brown NA. (1993). Analysis of retro-illumination photographs for use in longitudinal studies of cataract. Eye. 7 (4), 572-577.

116. Hashizoe M, Hara T, Ogura Y, Sakanishi K, Honda T, Hara T. (1998). Equator ring efficacy in maintaining capsular bag integrity and transparency after cataract removal in monkey eyes. Graefes Arch.Clin.Exp.Ophthalmol. 236, 375-379.

117. Hassan TS, Soong HK, Sugar A, Meyer RF. (1991). Implantation of Kelman-style, open-loop anterior chamber lenses during keratoplasty for aphakic and pseudophakic bullous keratopathy. A comparison with iris-sutured posterior chamber lenses. Ophthalmology. 98, 875-880.

118. Hayashi H, Hayashi K, Nakao F, Hayashi F. (1998b). Quantitative comparison of posterior capsule opacification after polymethylmethacrylate, silicone, and soft acrylic intraocular lens implantation. Arch.Ophthalmol. 116, 1579-1582.

119. Hayashi K, Hayashi H, Nakao F, and Hayashi F. (1998a). In vivo quantitative measurement of posterior capsule opacification after extracapsular cataract surgery. Am.J.Ophthalmol. 125,837-843.

120. Hayashi K, Hayashi H, Nakao F, Hayashi F. (1998c). Reproducibility of posterior capsule opacification measurement using Scheimpflug videophotography. J.Cataract Refract.Surg. 24, 1632-1635.

121. He W, L P, Zhang X, et al. (2000). [A clinical investigation on cataract surgery with 2.8 mm incision]. Chung Hua Yen Ko Tsa Chih. 36, 282-284.

122. Hecht E. (1998). Optics. Addison-Wesley, 3rd edn, p520

123. Hiller R, Sperduto RD, Podgor MJ, Wilson PW, Ferris FL, III, Colton T, D'Agostino RB, Roseman MJ, Stockman ME, Milton RC. (1997). Cigarette smoking and the risk of development of lens opacities. The Framingham studies. Arch.Ophthalmol. 115, 1113-1118.

124. Hockwin O., Poonawalla N. et al. (1973). Durchlässigkeit der isolierten Rinderlinsenkapsel für Aminosä uren und wasserlosliche. Gref. Arch Ophthalmol: 188,175.

125. Hollick EJ, Spalton DJ, Ursell PG, Meacock WR, Barman SA., Boyce JF. (2000). Posterior capsular opacification with hydrogel, polymethylmethacrylate, and silicone intraocular lenses: two-year results of a randomized prospective trial. Am.J.Ophthalmol. 129, 577-584.

126. Hollick EJ, Spalton DJ, Ursell PG, Pande MV, Barman SA, Boyce JF, Tilling K. (1999). The effect of polymethylmethacrylate, silicone, and polyacrylic intraocular lenses on posterior capsular opacification 3 years after cataract surgery. Ophthalmology 106, 49-54.

127. Hollows F, Moran D. (1981). Cataract--the ultraviolet risk factor. Lancet. 2, 1249-1250.

128. http://www.akh-wien.ac.at/iol

129. http://www.ophtec.com.

130. Ishibashi T, Hatae T, Inomata H. (1994). Collagen types in human posterior capsule opacification. J.Cataract Refract.Surg. 20, 643-646.

131. Ismail MM, Alio JL, Ruiz Moreno JM. (1996). Prevention of secondary cataract by antimitotic drugs: experimental study. Ophthalmic Res. 28, 64-69.

132. Jaffe NS, Jaffe MS, Jaffe GF. (1997). Cataract Surgery and it complications. Mosby.USA. sith Edition. Chapter6

133. Jahn CE, Emke M. (1996). Long-term elevation of intraocular pressure after neodymium: YAG laser posterior capsulotomy. Ophthalmologica. 210, 85-89.

134. Jamal SA, Solomon LD. (1993). Risk factors for posterior capsular pearling after uncomplicated extracapsular cataract extraction and plano-convex posterior chamber lens implantation. J.Cataract Refract.Surg. 19, 333-338.

135. Javdani SM, Huygens MM, Callebaut F. (2002). Neodymium: YAG capsulotomy rates after phacoemulsification with hydrophobic and hydrophilic acrylic intraocular lenses. Bull.Soc.Belge Ophtalmol. 13-17.

136. Johnston Rob. (2003). Electronic clinical system, cataract audit and national cataract dataset. Refractive eye news.1 (6), 6-7.

137. Kato K, Nishida M, Yamane H, Nakamae K, Tagami Y, and Tetsumoto K. (2001) Glistening formation in an AcrySof lens initiated by spinodal decomposition of the polymer network by temperature change. J.Cataract Refract.Surg. 27,1493-1498.

138. Kawara T, Obazawa H. (1980). A new method for retroillumination photography of cataractous lens opacities. Am.J.Ophthalmol. 90, 186-189.

139. Kelman CD. (1967). Phaco-emulsification and aspiration. A new technique of cataract removal. A preliminary report. Am.J.Ophthalmol. 64, 23-35.

140. Khalifa MA. (1992). Polishing the posterior capsule after extracapsular extraction of senile cataract. J.Cataract Refract.Surg. 18, 170-173.

141. Khan AJ, Percival SP. (1999). 12 year results of a prospective trial comparing poly(methyl methacrylate) and poly(hydroxyethyl methacrylate) intraocular lenses. J.Cataract Refract.Surg. 25, 1404-1407.

142. Kim MJ, Lee HY, Joo CK. (1999). Posterior capsule opacification in eyes with a silicone or poly(methyl methacrylate) intraocular lens. J.Cataract Refract.Surg. 25, 251-255.

143. Klein BE, Klein R, Lee KE. (1998). Diabetes, cardiovascular disease, selected cardiovascular disease risk factors, and the 5-year incidence of age-related cataract and progression of lens opacities: the Beaver Dam Eye Study. Am.J.Ophthalmol. 126, 782-790.

144. Kohnen T, Magdowski G, Koch DD. (1996). Scanning electron microscopic analysis of foldable acrylic and hydrogel intraocular lenses. J.Cataract Refract.Surg. 22, Suppl 2, 1342-1350.

145. Kohnen T. (1996). The variety of foldable intraocular lens materials. J.Cataract Refract.Surg. 22, Suppl 2, 1255-1258.

146. Kruger A.J, Schauersberger J, Abela C, Schild G, and Amon M. (2000). Two year results: sharp versus rounded optic edges on silicone lenses. J.Cataract Refract.Surg. 26,566-570.

147. Kruger AJ, Schauersberger J, Abela-Formanek C, Schild G, Kellner C, Kolodjaschna J, Amon M. (2001). [Effect of duration of phacoemulsification on postoperative inflammation--a retrospective study] Einfluss der Dauer der Phakoemulsifikation auf die postoperative Inflammation--eine retrospektive Studie. Klin.Monatsbl.Augenheilkd. 218, 204-208.

148. Kurosaka D, Kato K, Kurosaka H, Yoshino M, Nakamura K, Negishi K. (2002). Elschnig pearl formation along the neodymium:YAG laser posterior capsulotomy margin. Long-term follow-up. J.Cataract Refract.Surg. 28, 1809-1813.

149. Kuszak JR, Ennesser CA, Bertram BA, Imherr-McMannis S, Jones-Rufer LS, Weinstein RS. (1989). The contribution of cell-to-cell fusion to the ordered structure of the crystalline lens. Lens Eye Toxic.Res. 6, 639-673.

150. Landau IM, Laurell CG. (1999). Ultrasound biomicroscopy examination of intraocular lens haptic position after phacoemulsification with continuous curvilinear capsulorhexis and extracapsular cataract extraction with linear capsulotomy. Acta Ophthalmol.Scand. 77, 394-396.

151. Lasa MS, Datiles MB, III, Magno BV, Mahurkar A. (1995). Scheimpflug photography and postcataract surgery posterior capsule opacification. Ophthalmic Surg. 26, 110-113.

152. Laurell CG, Zetterstrom C, Lundgren B, Torngren L, Andersson K. (1997). Inflammatory response in the rabbit after phacoemulsification and intraocular lens implantation using a 5.2 or 11.0 mm incision. J.Cataract Refract.Surg. 23, 126-131.

153. Leaming DV. (1987). Practice styles and preferences of ASCRS members--1986 survey.J Cataract Refract Surg. 13(5):561-7.

154. Leaming DV. (1988). Practice styles and preferences of ASCRS members--1987 survey. J.Cataract Refract.Surg. 14, 552-559.

155. Leaming DV. (1999). Practice styles and preferences of ASCRS members--1998 survey. J.Cataract Refract.Surg. 25, 851-859.

156. Leaming DV. (2000). Practice styles and preferences of ASCRS members-1999 survey. J.Cataract Refract.Surg. 26, 913-921.

157. Lee CP. (1990). Capsulorhexis- a 5-years experience. Eur J Implant Refract Surg.2:27-31.

158. Legeais JM, Werner LP, Legeay G, Briat B, Renard G. (1998). In vivo study of a fluorocarbon polymer-coated intraocular lens in a rabbit model. J.Cataract Refract.Surg. 24, 371-379.

159. Legler UF, Apple DJ., Assia EI, Bluestein EC, Castaneda VE, Mowbray SL. (1993). Inhibition of posterior capsule opacification: the effect of colchicine in a sustained drug delivery system. J.Cataract Refract.Surg. 19, 462-470.

160. Levy JH, Pisacano A.M, Chadwick K. (1994). Astigmatic changes after cataract surgery with 5.1 mm and 3.5 mm sutureless incisions. J.Cataract Refract.Surg. 20, 630-633.

161. Lim SJ, Kang SJ, Kim HB, Apple DJ. (1998). Ideal size of an intraocular lens for capsular bag fixation. J.Cataract Refract.Surg. 24, 397-402.

162. Lindstrom RL, Harris WS. (1980). Management of the posterior capsule following posterior chamber lens implantation. J.Am.Intraocul.Implant.Soc. 6, 255-258.

163. Linebarger EJ, Hardten DR, Shah GK, Lindstrom RL. (1999). Phacoemulsification and modern cataract surgery. Surv.Ophthalmol. 44, 123-147.

164. Lois N, Cohen EJ, Rapuano CJ, Laibson PR. (1997). Long-term graft survival in patients with flexible open-loop anterior-chamber intraocular lenses. Cornea 16, 387-392.

165. Mackool RJ, Chhatiawala H. (1991). Pediatric cataract surgery and intraocular lens implantation: a new technique for preventing or excising postoperative secondary membranes. J.Cataract Refract.Surg. 17, 62-66.

166. Macky TA, Trivedi RH, Werner L, Pandey SK, Izak AM, and Apple DJ. (2001) Degeneration of ultraviolet absorber material and calcium deposits within the optic of a hydrophilic intraocular lens. Int.Ophthalmol.Clin. 41, 79-90.

167. Magno BV, Freidlin V, Datiles MB, III (1994). Reproducibility of the NEI Scheimpflug Cataract Imaging System. Invest Ophthalmol.Vis.Sci. 35, 3078-3084.

168. Majima K. (1996). An evaluation of the biocompatibility of intraocular lenses. Ophthalmic Surg.Lasers. 27, 946-951.

169. Mamalis N, Crandall AS, Linebarger E, Sheffield WK., Leidenix MJ. (1995). Effect of intraocular lens size on posterior capsule opacification after phacoemulsification. J.Cataract Refract.Surg. 21, 99-102.

170. Mamalis N, Phillips B, Kopp CH, Crandall AS, Olson RJ. (1996). Neodymium: YAG capsulotomy rates after phacoemulsification with silicone posterior chamber intraocular lenses. J.Cataract Refract.Surg. 22, Suppl 2, 1296-1302.

171. Martin RD, Gills JP, Sanders D R. (1993). Foldable intraocular lenses. Thorofare, New Jersey: SLACK. Pp 55-72. 161-177.

172. Martin RG, Sanders DR, Souchek J, Raanan MG, DeLuca M. (1992). Effect of posterior chamber intraocular lens design and surgical placement on postoperative outcome. J.Cataract Refract.Surg. 18, 333-341.

173. Masket S, Crandall A. (1999). Atlas of caratact surgery. Martin Dunitz Ltd.London. Chapter 21.

174. Masket S, Geraghty E, Crandall AS, Davison JA, Johnson S H, Koch DD, Lane SS. (1993b). Undesired light images associated with ovoid intraocular lenses. J.Cataract Refract.Surg. 19, 690-694.

175. Masket S. (1993a). Postoperative complications of capsulorhexis. J.Cataract Refract.Surg. 19, 721-724.

176. Mastropasqua L, Lobefalo L, Ciancaglini M, Ballone E, Gallenga PE. (1997). Heparin eyedrops to prevent posterior capsule opacification. J.Cataract Refract.Surg. 23, 440-446.

177. Mathey CF, Kohnen TB, Ensikat HJ, Koch HR. (1994). Polishing methods for the lens capsule: histology and scanning electron microscopy. J.Cataract Refract.Surg. 20, 64-69.

178. McDonnell PJ, Krause W, Glaser BM. (1988). In vitro inhibition of lens epithelial cell proliferation and migration. Ophthalmic Surg. 19, 25-30.

179. McDonnell PJ, Zarbin MA, Green WR. (1983). Posterior capsule opacification in pseudophakic eyes. Ophthalmology. 90, 1548-1553.

180. McPherson RJ, Govan JA. (1995). Posterior capsule reopacification after neodymium:YAG laser capsulotomy. J.Cataract Refract.Surg. 21, 351-352.

181. Meacock WR, Spalton DJ, Boyce JF, Jose RM. (2001a). Effect of optic size on posterior capsule opacification: 5.5mm versus 6.0mm AcrySof intraocular lenses. J.Cataract Refract.Surg. 27, 1194-1198.

182. Meacock WR, Spalton DJ, Hollick EJ, Barman S, Boyce JF. (2001 b). The effect of polymethylmethacrylate and acrysof intraocular lenses on the posterior capsule in patients with a large capsulorrhexis. Jpn.J.Ophthalmol. 45, 348-354.

183. Menapace R. (1996). Posterior capsule opacification and capsulotomy rates with taco-style hydrogel intraocular lenses. J.Cataract Refract.Surg. 22, Suppl 2, 1318-1330.

184. Mester U, Strauss M, Grewing R. (1998). Biocompatibility and blood-aqueous barrier impairment in at-risk eyes with heparin-surface-modified or unmodified lenses. J.Cataract Refract.Surg. 24, 380-384.

185. Michelson MA..(1991). Endocapsular phacoemulsification with minicapsulorhexis. In: Koch P.s, Davison J. A, eds, Textbook of advanced Phacoemulsification techniques. Thorofare, NJ, Slack. Pp 275-309.

186. Milazzo S, Turut P, Blin H. (1996). Alterations to the AcrySof intraocular lens during folding. J.Cataract Refract.Surg. 22, Suppl 2, 1351-1354.

187. Minassian DC, Rosen P, Dart JK, Reidy A, Desai P, Sidhu M, Kaushal S, Wingate N. (2001). Extracapsular cataract extraction compared with small incision surgery by phacoemulsification: a randomised trial. Br.J.Ophthalmol. 85, 822-829.

188. Miyake et al (1991). Collagen IOL: a suggestion for intraocular lens biocompatibility. Eur J.implant Refract.Surg. 3, 99-102.

189. Miyake K, Mibu H, Horiguchi M, and Shirasawa E. (1990) Inflammatory mediators in postoperative aphakic and pseudophakic baboon eyes. Arch.Ophthalmol. 108, 1764-1767.

190. Miyake K, Mibu H. et al. (1990). Inflammatory mediators in post operative aphakic and pseudophakic baboon eye. Arch Ophthalmol.108, 164-1767.

191. Miyauchi A., Mukai S, Sakamoto Y. (1990). A new analysis method for cataractous images taken by retroillumination photography. Ophthalmic Res. 22, Suppl 1, 74-77.

192. Mullner-Eidenbock A, Amon M, Schauersberger J, Kruger A, Abela C, Petternel V, Zidek T. (2001). Cellular reaction on the anterior surface of 4 types of intraocular lenses. J.Cataract Refract.Surg. 27, 734-740.

193. Nagamoto T, Eguchi G. (1997). Effect of intraocular lens design on migration of lens epithelial cells onto the posterior capsule. J.Cataract Refract.Surg. 23, 866-872.

194. Nagamoto T, Hara E, Kurosaka D. (1996). Lens epithelial cell proliferation onto the intraocular lens optic in vitro. J.Cataract Refract.Surg. 22, Suppl 1, 847-851.

195. Nagata T, Machida K & Shigemori S. (1993). Effect of intraocular lens optic design on posterior capsular opacification.Nihon Ganka Kiyo (Folia Ophthalmol Jpn).44, 1248-1253.

196. Nagata T, Watanabe I. (1996). Optic sharp edge or convexity: comparison of effects on posterior capsular opacification. Jpn.J.Ophthalmol. 40, 397-403.

197. Nakaizumi H, Sasaki K, Sakamoto Y. (1992). In vivo observation of the axial movement of intraocular lenses through an anterior eye segment analysis system. Ophthalmic Res. 24, Suppl 1, 21-25.

198. Natchiar GN, Thulasiraj RD, Negrel AD, Bangdiwala S, Rahmathallah R, Prajna NV, Ellwein LB, Kupfer C. (1998). The Madurai Intraocular Lens Study. I: A randomized clinical trial comparing complications and vision outcomes of intracapsular cataract extraction and extracapsular cataract extraction with posterior chamber intraocular lens. Am.J.Ophthalmol. 125, 1-13.

199. Naumann GOHIE. (1980). Pathologie des Auges. A2 - In: Naumann GOH ADe. 144-146.

200. Newland TJ, Auffarth GU, Wesendahl TA, Apple DJ. (1994). Neodymium:YAG laser damage on silicone intraocular lenses. A comparison of lesions on explanted lenses and experimentally produced lesions. J.Cataract Refract.Surg. 20, 527-533.

201. Niesel P, Bachmann E. (1974). [First disjunction zone of the lens in glaucoma patients (author's transl)] Beobachtungen am Abspaltungsstreifen der Linse bei Glaukomkranken. Albrecht.Von.Graefes Arch.Klin.Exp.Ophthalmol. 189, 211-217.

202. Ninn-Pedersen K, Bauer B. (1997). Cataract patients in a defined Swedish population 1986-1990. VI. YAG laser capsulotomies in relation to preoperative and surgical conditions. Acta Ophthalmol.Scand. 75, 551-557.

203. Nishi O, Nishi K, Hikida M. (1993). Removal of lens epithelial cells following loosening of the junctional complex. J.Cataract Refract.Surg. 19, 56-61.

204. Nishi O, Nishi K, Hikita M. (1991 b). A new approach to lens epithelial cell removal: dispersion aspiration. Dev.Ophthalmol. 22, 101-105.

205. Nishi O, Nishi K, Imanishi M, Mano C, Yamada Y, Tada Y, Shirasawa E, Harfstrand A. (1996). Decreased prostaglandin E2 synthesis by lens epithelial cells cultured on heparin-surface-modified poly(methyl methacrylate). J.Cataract Refract.Surg. 22, Suppl 1, 859-862.

206. Nishi O, Nishi K, Imanishi M. (1992). Synthesis of interleukin-1 and prostaglandin E2 by lens epithelial cells of human cataracts. Br.J.Ophthalmol. 76, 338-341.

207. Nishi O, Nishi K, Mano C, Ichihara M, Honda T, Saitoh I. (1997). Inhibition of migrating lens epithelial cells by blocking the adhesion molecule integrin: a preliminary report. J.Cataract Refract.Surg. 23, 860-865.

208. Nishi O, Nishi K, Mano C, Ichihara M, Honda T. (1998c). The inhibition of lens epithelial cell migration by a discontinuous capsular bend created by a band-shaped circular loop or a capsule-bending ring. Ophthalmic Surg.Lasers. 29, 119-125.

209. Nishi O, Nishi K, Menapace R, Akura J. (2001). Capsular bending ring to prevent posterior capsule opacification: 2 year follow-up. J.Cataract Refract.Surg. 27, 1359-1365.

210. Nishi O, Nishi K, Menapace R. (1998a). Capsule-bending ring for the prevention of capsular opacification: a preliminary report. Ophthalmic Surg.Lasers. 29, 749-753.

211. Nishi O, Nishi K, Morita T, Tada Y, Shirasawa E, Sakanishi K. (1996b). Effect of intraocular sustained release of indomethacin on postoperative inflammation and posterior capsule opacification. J.Cataract Refract.Surg. 22, Suppl 1, 806-810.

212. Nishi O, Nishi K, Saitoh I, Sakanishi K. (1996a). Inhibition of migrating lens epithelial cells by sustained release of ethylenediaminetetraacetic acid. J.Cataract Refract.Surg. 22, Suppl 1, 863-868.

213. Nishi O, Nishi K, Sakanishi K. (1998b). Inhibition of migrating lens epithelial cells at the capsular bend created by the rectangular optic edge of a posterior chamber intraocular lens. Ophthalmic Surg.Lasers. 29, 587-594.

214. Nishi O, Nishi K, Yamada Y, Mizumoto Y. (1995). Effect of indomethacin-coated posterior chamber intraocular lenses on postoperative inflammation and posterior capsule opacification. J.Cataract Refract.Surg. 21, 574-578.

215. Nishi O, Nishi K. (1991a). Intercapsular cataract surgery with lens epithelial cell removal. Part III: Long-term follow-up of posterior capsular opacification. J.Cataract Refract.Surg. 17, 218-220.

216. Nishi O, Nishi K. (1999). Preventing posterior capsule opacification by creating a discontinuous sharp bend in the capsule. J.Cataract Refract.Surg. 25, 521-526.

217. Nishi O. (1988). Fibrinous membrane formation on the posterior chamber lens during the early postoperative period. J.Cataract Refract.Surg. 14, 73-77.

218. Odrich MG, Hall SJ, Worgul BV, Trokel SL, and Rini FJ. (1985) Posterior capsule opacification: experimental analyses. Ophthalmic Res. 17, 75-84.

219. O'Keefe M, Mulvihill A, Yeoh PL. (2000). Visual outcome and complications of bilateral intraocular lens implantation in children. J.Cataract Refract.Surg. 26, 1758-1764.

220. Olsen G & Olson RJ. (2000). Update on a long-term, prospective study of capsulotomy and retinal detachment rates after cataract surgery. J Cataract Refract Surg. 26, 1017-1021.

221. Olson RJ, Crandall AS. (1998). Silicone versus polymethylmethacrylate intraocular lenses with regard to capsular opacification. Ophthalmic Surg.Lasers. 29, 55-58.

222. Omar O, Pirayesh A, Mamalis N, and Olson RJ. (1998) In vitro analysis of AcrySof intraocular lens glistenings in AcryPak and Wagon Wheel packaging. J.Cataract Refract.Surg. 24,107-113.

223. Oshika T, Nagata T, Ishii Y. (1998). Adhesion of lens capsule to intraocular lenses of polymethylmethacrylate, silicone, and acrylic foldable materials: an experimental study. Br.J.Ophthalmol. 82, 549-553.

224. Oshika T, Shiokawa Y. (1996). Effect of folding on the optical quality of soft acrylic intraocular lenses. J.Cataract Refract.Surg. 22, Suppl 2, 1360-1364.

225. Oshika T, Suzuki Y, Kizaki H, Yaguchi S. (1996). Two year clinical study of a soft acrylic intraocular lens. J.Cataract Refract.Surg. 22, 104-109.

226. Oshika T, Tsuboi S, Yaguchi S, Yoshitomi F, Nagamoto T, Nagahara K, Emi K. (1994). Comparative study of intraocular lens implantation through 3.2- and 5.5-mm incisions. Ophthalmology. 101, 1183-1190.

227. Oshika T, Yoshimura K, Miyata N. (1992). Postsurgical inflammation after phacoemulsification and extracapsular extraction with soft or conventional intraocular lens implantation. J.Cataract Refract.Surg. 18, 356-361.

228. Owen CG (1998). Quantitative Analysis of Conjunctival Vasculature. PhD Thesis, City University, London.

229. Pande M, Spalton DJ, Marshall J. (1996b). Continuous curvilinear capsulorhexis and intraocular lens biocompatibility. J.Cataract Refract.Surg. 22, 89-97.

230. Pande MV, Spalton DJ, Kerr-Muir MG, Marshall J. (1996a). Postoperative inflammatory response to phacoemulsification and extracapsular cataract surgery: aqueous flare and cells. J.Cataract Refract.Surg. 22, Suppl 1, 770-774.

231. Pande MV, Ursell PG, Spalton DJ, Heath G, Kundaiker S. (1997). High-resolution digital retroillumination imaging of the posterior capsule after cataract surgery. J.Cataract Refract.Surg. 23, 1521-1527.

232. Pandey SK, Cochener B, Apple DJ, Colin J, Werner L, Bougaran R, Trivedi RH, Macky TA, Izak AM. (2002). Intracapsular ring sustained 5-fluorouracil delivery system for the prevention of posterior capsule opacification in rabbits: a histological study. J.Cataract Refract.Surg. 28, 139-148.

233. Pandey SK, Werner L, Escobar-Gomez M, Roig-Melo EA, Apple DJ. (2000). Dye-enhanced cataract surgery. Part 1: anterior capsule staining for capsulorhexis in advanced/white cataract.J Cataract Refract Surg. 26(7):1052-9.

234. Paplinski AP, Boyce JF.(1997). Segmentation of a class of ophthalmological images using a directional variance operator and co-occurrence arrays. Opt Eng. 36, 3140-3147.

235. Pearce JL. (1984). The Pearce tripod posterior chamber lenses, in RosenES, Haining WM, Arontt EJ (eds): intraocular lens implantation. St. Louis, CV Mosby. pp 376-82.

236. Peng Q, Apple DJ, Visessook N, Werner L, Pandey SK, Escobar-Gomez M, Schoderbek R, Guindi A. (2000). Surgical prevention of posterior capsule opacification. Part 2: Enhancement of cortical cleanup by focusing on hydrodissection. J.Cataract Refract.Surg. 26, 188-197.

237. Peng Q, Visessook N, Apple DJ, Pandey SK., Werner L, Escobar-Gomez M, Schoderbek R, Solomon KD, Guindi. (2000). Surgical prevention of posterior capsule opacification. Part 3: Intraocular lens optic barrier effect as a second line of defense. J.Cataract Refract.Surg. 26, 198-213.

238. Powell SK, Olson RJ. (1995). Incidence of retinal detachment after cataract surgery and neodymium: YAG laser capsulotomy. J.Cataract Refract.Surg. 21, 132-135.

239. Prajna NV, Ellwein LB, Selvaraj S, Manjula K, and Kupfer C. (2000) The madurai intraocular lens study IV: posterior capsule opacification. Am.J.Ophthalmol. 130,304-309.

240. Press WH et al. (1992). Numerical Recipes in C, C.U.P., 2nd edn, Chapter 12.

241. Quinlan M, Wormstone IM., Duncan G, Davies PD. (1997). Phacoemulsification versus extracapsular cataract extraction: a comparative study of cell survival and growth on the human capsular bag in vitro. Br.J.Ophthalmol. 81, 907-910.

242. Rafferty NS, Goosens W. (1978). Cytopasmic filaments in the crystalline lens of various species: functional correlations. Exp eye Res.26:177.

243. Ram J, Apple DJ, Peng Q, Visessook N, Auffarth GU, Schoderbek RJ, Jr, Ready EL. (1999a). Update on fixation of rigid and foldable posterior chamber intraocular lenses. Part II: Choosing the correct haptic fixation and intraocular lens design to help eradicate posterior capsule opacification. Ophthalmology. 106, 891-900.

244. Ram J, Apple DJ, Peng Q, Visessook N, Auffarth GU, Schoderbek RJ, Jr, Ready EL. (1999b). Update on fixation of rigid and foldable posterior chamber intraocular lenses. Part I: Elimination of fixation-induced decentration to achieve precise optical correction and visual rehabilitation. Ophthalmology. 106, 883-890.

245. Ram J, Pandey SK, Apple DJ, Werner L, Brar GS, Singh R, Chaudhary KP, Gupta A. (2001). Effect of in-the-bag intraocular lens fixation on the prevention of posterior capsule opacification. J.Cataract Refract.Surg. 27, 1039-1046.

246. Ravalico G, Baccara F, Lovisato A, Tognetto D. (1997). Postoperative cellular reaction on various intraocular lens materials. Ophthalmology. 104, 1084-1091.

247. Ravalico G, Tognetto D, Palomba M, Busatto P, Baccara F. (1996). Capsulorhexis size and posterior capsule opacification. J.Cataract Refract.Surg. 22, 98-103.

248. Ridley F. (1956). Laser surgical results of use of the intraocular acrylic lenses after cataract extraction. J.Int.Coll.Surg. 26, 225-241.

249. Ruiz JM, Medrano M, Alio JL. (1990). Inhibition of posterior capsule opacification by 5-fluorouracil in rabbits. Ophthalmic Res. 22, 201-208.

250. Russ J C. (2000). The image processing handbook. Forth ed. CRC press, London. Chapter 5, 6, 9, 10.

251. Saika S, Miyamoto T, Ishida I, Tanaka T, Okada Y, Nagane Y, Shirai K, and Ohnishi Y. (2001) Comparison of Scheimpflug images of posterior capsule opacification and histological findings in rabbits and humans. J.Cataract Refract.Surg. 27, 1088-1092.

252. Saika S, Ohmi S, Kanagawa R, Tanaka S, Ohnishi Y, Ooshima A, Yamanaka A. (1996). Lens epithelial cell outgrowth and matrix formation on intraocular lenses in rabbit eyes. J.Cataract Refract.Surg. 22, Suppl 1, 835-840.

253. Saika S, Yamanaka A, Tanaka S, Ohmi S, Ohnishi Y, Ooshima A. (1995). Extracellular matrix on intraocular lenses. Exp.Eye Res. 61, 713-721.

254. Sakamoto Y, Nakaizumi K, Nakamura Y, Watanabe N. (1992). Reproducibility of data obtained by a newly developed anterior eye segment analysis system, EAS-1000. Ophthalmic Res. 24, Suppl 1, 10-20.

255. Santos BA, Pastora R, DelMonte MA, O'Donnell FE, Jr. (1986). Lens epithelial inhibition by PMMA optic: implications for lens design. J.Cataract Refract.Surg. 12, 23-26.

256. Santos BA, Pastora R, DelMonte MA, O'Donnell FE, Jr. (1987). Comparative study of the effects of optic design on lens epithelium in vitro. J.Cataract Refract.Surg. 13, 127-130.

257. Sasaki K, Shibata T, Obazawa H, Fujiwara T, Kogure F, Obara Y, Itoi M, Katou K, Akiyama K, Okuyama S. (1990). Classification system for cataracts. Application by the Japanese Cooperative Cataract Epidemiology Study Group. Ophthalmic Res. 22, Suppl 1, 46-50.

258. Scaramuzza A, Fernando GT, Crayford BB. (2001). Posterior capsule opacification and lens epithelial cell layer formation: Hydroview hydrogel versus AcrySof acrylic intraocular lenses. J.Cataract Refract.Surg. 27, 1047-1054.

259. Schauersberger J, Amon M, Kruger A, Abela C, Schild G, Kolodjaschna J. (2001). Comparison of the biocompatibility of 2 foldable intraocular lenses with sharp optic edges. J.Cataract Refract.Surg. 27, 1579-1585.

260. Schauersberger J, Kruger A, Abela C, Mullner-Eidenbock A, Petternel V, Svolba G, Amon M. (1999). Course of postoperative inflammation after implantation of 4 types of foldable intraocular lenses. J.Cataract Refract.Surg. 25, 1116-1120.

261. Schaumberg DA, Dana MR, Christen WG, Glynn RJ. (1998). A systematic overview of the incidence of posterior capsule opacification. Ophthalmology. 105, 1213-1221.

262. Schmidbauer JM, Escobar-Gomez M, Apple DJ, Peng Q, Arthur SN, and Vargas LG. (2002). Effect of haptic angulation on posterior capsule opacification in modern foldable lenses with a square, truncated optic edge. J.Cataract Refract.Surg. 28, 1251-1255.

263. Schneiderman TE, Johnson MW, Smiddy WE, Flynn HW, Jr, Bennett SR, Cantrill HL. (1997). Surgical management of posteriorly dislocated silicone plate haptic intraocular lenses. Am.J.Ophthalmol. 123, 629-635.

264. Sellman TR, Lindstrom RL. (1988). Effect of a plano-convex posterior chamber lens on capsular opacification from Elschnig pearl formation. J.Cataract Refract.Surg. 14, 68-72.

265. Shah GR, Gills JP, Durham DG, Ausmus WH. (1986). Three thousand YAG lasers in posterior capsulotomies: an analysis of complications and comparison to polishing and surgical discission.

Ophthalmic Surg. 17, 473-477.

266. Shearing SP. (1984). Evolution of the posterior chamber intraocular lens. J.Am.Intraocul.Implant.Soc. 10, 343-346.

267. Shepherd JR. (1994). Small incisions and foldable intraocular lenses. Int.Ophthalmol.Clin. 34, 103-112.

268. Shimizu K, Sakai H. (1987). Physical characteristics of various intraocular lenses. J.Cataract Refract.Surg. 13, 151-156.

269. Shugar JK, Lewis C, Lee A. (1996). Implantation of multiple foldable acrylic posterior chamber lenses in the capsular bag for high hyperopia. J.Cataract Refract.Surg. 22, Suppl 2, 1368-1372.

270. Simcoe CW. (1978). An ounce of prevention. J.Am.Intraocul.Implant.Soc. 4, 39-44.

271. Smith H. (1903). Extraction of cataract in the capsule. Br.J.Ophthalmol. 2, 719.

272. Smith H. (1926). A new technique for expression of the Cataractous lens inits capsule. Arch Ophthalmology. 55:213-23.

273. Snellingen T, Shrestha JK, Huq F, Husain R, Koirala S, Rao GN, Pokhrel RP, Kolstad A, Upadhyay MP., Apple DJ, Arnesen E, Cheng H, Olsen EG, Vogel M. (2000). The South Asian cataract management study: complications, vision outcomes, and corneal endothelial cell loss in a randomized multicenter clinical trial comparing intracapsular cataract extraction with and without anterior chamber intraocular lens implantation. Ophthalmology. 107, 231-240.

274. Sparrow JM, Brown NA, Shun-Shin GA, Bron AJ. (1990). The Oxford modular cataract image analysis system. Eye. 4, 638-648.

275. Steinert RF, Brint SF, White SM, Fine IH. (1991a). Astigmatism after small incision cataract surgery. A prospective, randomized, multicenter comparison of 4- and 6.5-mm incisions. Ophthalmology. 98, 417-423.

276. Steinert RF, Giamporcaro JE, Tasso VA. (1997). Clinical assessment of long-term safety and efficacy of a widely implanted silicone intraocular lens material. Am.J.Ophthalmol. 123, 17-23.

277. Steinert RF, Puliafito CA, Kumar SR, Dudak SD, Patel S. (1991b). Cystoid macular edema, retinal detachment, and glaucoma after Nd:YAG laser posterior capsulotomy. Am.J.Ophthalmol. 112, 373-380.

278. Sterling S, Wood TO. (1986). Effect of intraocular lens convexity on posterior capsule opacification. J.Cataract Refract.Surg. 12, 655-657.

279. Sundelin K, Friberg-Riad Y, Ostberg A, Sjostrand J. (2001). Posterior capsule opacification with AcrySof and poly(methyl methacrylate) intraocular lenses. Comparative study with a 3-year follow-up. J.Cataract Refract.Surg. 27, 1586-1590.

280. Sundelin K, Sjostrand J. (1999). Posterior capsule opacification 5 years after extracapsular cataract extraction. J.Cataract Refract.Surg. 25, 246-250.

281. Tabbara KF, Al Kaff AS, Al Rajhi AA, Al Mansouri SM, Badr IA, Chavis PS, Al Omar OM. (1998). Heparin surface-modified intraocular lenses in patients with inactive uveitis or diabetes. Ophthalmology. 105, 843-845.

282. Talamo JH, Stark WJ, Gottsch JD, Goodman DF, Pratzer K, Cravy TV, Enger C. (1991). Natural history of corneal astigmatism after cataract surgery. J.Cataract Refract.Surg. 17, 313-318.

283. Tamura M, Kanagawa R, Saika S, Ohmi S, Nakao T, Kinoshita C, Uenoyama K. (1990). Comparison of the cellular response on intraocular lenses implanted in rabbit eyes with and without extracapsular lens extraction. J.Cataract Refract.Surg. 16, 746-750.

284. Tan DT, Chee SP. (1993). Early central posterior capsular fibrosis in sulcus-fixated biconvex intraocular lenses. J.Cataract Refract.Surg. 19, 471-480.

285. Tana P, Belmonte J. (1996). Experimental study of different intraocular lens designs implanted in the bag after capsulorhexis. J.Cataract Refract.Surg. 22, 1211-1221.

286. Tassignon MJ, De G, Vrensen GF. (2002) Bag-in-the-lens implantation of intraocular lenses. J.Cataract Refract.Surg. 28, 1182-1188.

287. Tawab BM, Tassignon MJ. (1995). Ocular and systemic factors associated with posterior capsule opacification. Bull.Soc.Belge Ophtalmol. 259, 21-25.

288. Tetz M, Imkamp E, Hansen SO, Solomon KD, Apple DJ. (1988). [Experimental study of posterior capsule opacification and optic decentering of various posterior chamber lenses following intercapsular implantation]. Fortschr.Ophthalmol. 85, 682-688.

289. Tetz M. (1994). Die cataract secundaria hach hinterkammer linsenimplantatiom: Klinik, pathologie und moglichkeiten der pravention. Habilitation sschrift.

290. Tetz MR, Auffarth GU, Sperker M, Blum M, Volcker HE. (1997). Photographic image analysis system of posterior capsule opacification. J.Cataract Refract.Surg. 23, 1515-1520.

291. Tognetto D, Ravalico G. (2001). Inflammatory cell adhesion and surface defects on heparin-surface-modified poly(methyl methacrylate) intraocular lenses in diabetic patients. J.Cataract Refract.Surg. 27, 239-244.

292. Tognetto D, Toto L, Sanguinetti G, and Ravalico G. (2002). Glistenings in foldable intraocular lenses. J.Cataract Refract.Surg. 28, 1211-1216.

293. Trivedi RH, Werner L, Apple DJ, Pandey SK, and Izak AM. (2002). Post cataract-intraocular lens (IOL) surgery opacification. Eye. 16,217-241.

294. Ursell PG, Spalton DJ, Pande MV, Hollick EJ, Barman S, Boyce J, and Tilling K. (1998) Relationship between intraocular lens biomaterials and posterior capsule opacification. J.Cataract Refract.Surg. 24,352-360.

295. Ursell PG, Spalton DJ, Pande MV, Hollick EJ, Barman S, Boyce J, and Tilling K. (1998). Relationship between intraocular lens biomaterials and posterior capsule opacification. J.Cataract Refract.Surg. 24,352-360.

296. Ursell PG, Spalton DJ, Pande MV. (1997). Anterior capsule stability in eyes with intraocular lenses made of poly(methyl methacrylate), silicone, and AcrySof. J.Cataract Refract.Surg. 23, 1532-1538.

297. Versura P, Torreggiani A, Cellini M, Caramazza R. (1999). Adhesion mechanisms of human lens epithelial cells on 4 intraocular lens materials. J.Cataract Refract.Surg. 25, 527-533.

298. Vivino MA, Mahurkar A, Trus B, Lopez ML, Datiles M. (1995). Quantitative analysis of retroillumination images. Eye. 9, 77-84.

299. Vivino MA., Chintalagiri S, Trus B, Datiles M. (1993). Development of a Scheimpflug slit lamp camera system for quantitative densitometric analysis. Eye. 7 (6), 791-798.

300. Wang MC, Woung LC. (2000). Digital retroilluminated photography to analyze posterior capsule opacification in eyes with intraocular lenses. J.Cataract Refract.Surg. 26, 56-61.

301. Weale RA. (1982). A biography of the eye: Development, Growth, age. H. K. Lewis, London.

302. Wenzel M, Reim M, Heinze M, Bocking A. (1988). Cellular invasion on the surface of intraocular lenses. In vivo cytological observations following lens implantation. Graefes Arch.Clin.Exp.Ophthalmol. 226, 449-454.

303. Werner L, Apple DJ, Kaskaloglu M, and Pandey SK. (2001). Dense opacification of the optical component of a hydrophilic acrylic intraocular lens: a clinicopathological analysis of 9 explanted lenses. J.Cataract Refract.Surg. 27, 1485-1492.

304. Werner LP, Legeais JM, Durand J, Savoldelli M, Legeay G, Renard G. (1997). Endothelial damage caused by uncoated and fluorocarbon-coated poly(methyl methacrylate) intraocular lenses. J.Cataract Refract.Surg. 23, 1013-1019.

305. West S, Munoz B, Schein OD, Vitale S, Maguire M, Taylor HR, Bressler NM. (1995). Cigarette smoking and risk for progression of nuclear opacities. Arch.Ophthalmol. 113, 1377-1380.

306. Westheimer G, Liang J. (1994) Evaluating diffusion of light in the eye by objective means. Invest Ophthalmol.Vis.Sci. 35,2652-2657.

307. Westling AK, Calissendorff BM. (1991). Factors influencing the formation of posterior capsular opacities after extracapsular cataract extraction with posterior chamber lens implant. Acta Ophthalmol (Copenh). 69, 315-320.

308. WHO. (1997). Fact sheet N143. Blindness and visual disability. Part II of VII: Major causes world wide. Geneva: World Health organization.

309. Wormstone IM, Liu CS, Rakic JM, Marcantonio JM, Vrensen GF, Duncan G. (1997). Human lens epithelial cell proliferation in a protein-free medium. Invest Ophthalmol.Vis.Sci. 38, 396-404.

310. Yanoff M, Fine M. (1996). Ocular pathology, 4th ed. London, Baltimore, MD, Mosby-Wolfe.

311. Yun B, ShiY. (2001). [Pediatric phacoemulsification with Acrysof intraocular lens implantation]. Chung Hua Yen Ko Tsa Chih. 37, 111-114.